UNIVERSITÀ DEGLI STUDI DI TORINO

Doctoral School of the University of Torino
PhD Programme in Chemical and Materials Sciences 33rd Cycle

Development and Implementation of Novel ab initio Methods for the Quantum Mechanical Study of Crystalline Solids

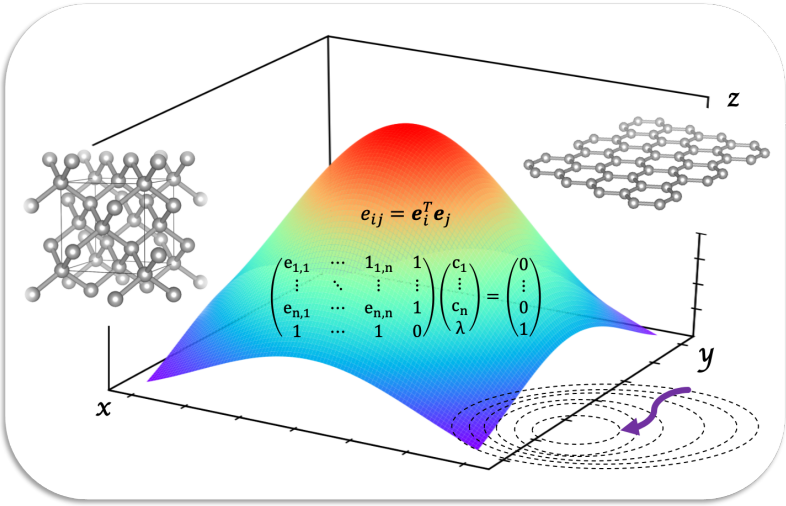

Loredana Edith Daga

Supervisor:
Prof. Lorenzo Maschio

UNIVERSITÀ DEGLI STUDI DI TORINO

Doctoral School of the University of Torino
PhD Programme in Chemical and Materials Sciences 33rd Cycle

Development and Implementation of Novel ab initio Methods for the Quantum Mechanical Study of Crystalline Solids

Candidate: Loredana Edith Daga

Supervisor: Prof. Lorenzo Maschio

Jury Members:

Prof. Nicholas Harrison
Imperial College, London, UK
Chemistry Department

Prof. Susi Lehtola
Helsinki, Finland
University of Helsinki

Prof. Silvia Casassa
University of Turin, Italy
Chemistry Department

Head of the Doctoral School: Prof. Alberto Rizzuti
PhD Programme Coordinator: Prof. Bartolomeo Civalleri

Torino, 2021

Contents

Preface

My PhD project is focused on the implementation of new algorithms in the field of quantum chemistry and the related application in the field of thermoelectric materials. The project was carried out within the Theoretical Chemistry Group of University of Turin whose main interest is the maintenance and development of the CRYSTAL program.[1]

Regarding the code development, two main algorithms have been implemented in this work: a basis set optimizer and a tool to perform excited states in solids.

The basis set optimizer is a technique for the optimization of basis set exponents and contraction coefficients, that is based on the Direct Inversion in the Iterative Subspace (DIIS) technique[2, 3, 4] and actually quite similar to its geometry optimization variant GDIIS.[5]. The algorithm was implemented in the CRYSTAL code and a detailed description of the method and some applications on prototypical solids are presented in this thesis and in the paper *"Gaussian Basis Sets for Crystalline Solids: All Purpose Basis Set Libraries vs System Specific Optimizations"*.[6]

Once the algorithm was fully tested, we decided to apply it to a more extended set of tests. In 2016 Lejaeghere, Kurt, et al. (*Reproducibility in density functional theory calculations of solids.* Science 351,6280)[7] presented a work focused on density functional theory and the definition of a method to demonstrate the reproducibility among many of the most widely used DFT codes. In particular, in this work equations of state (EOS) parameters are used by means of comparison and they report results of a community-wide effort that compared, 15 solid-state codes, using 40 different potentials or basis set types, to assess the quality of the Perdew-Burke-Ernzerhof (PBE) functional for 71 elemental crystals. We tried to reproduce this work by using CRYSTAL and the gaussian basis sets optimizer.

In the field of the DIIS-methods, we also tried to implement in the CRYSTAL code the GDIIS method, thus the geometry-optimization variant. In order to verify the efficiency of the implementation many tests were performed on both molecular and crystalline structures. The efficiency of the algorithm is presented with respect to the regular optimizer commonly used in the CRYSTAL code.

The second algorithm implemented in the CRYSTAL code regards the study of excited states in the field of quantum chemical modelling. In fact, while for ground states calculations a wide variety of methods have been implemented throughout the years, excited states are still under investigation in many ways. In this work we present the implementation in the CRYSTAL code of the Maximum Overlap Method (MOM).[8] The technique is rather simple: orbital occupations are enforced in a specific configuration against the Aufbau principle. In this way excited states can be easily studied at the Hartree-Fock or DFT level with the same computational cost as a ground state. The features and performance of the method are presented through its application to prototypical solids such as bulk silicon and diamond. General considerations and results about the method are reported in this thesis and in the submitted article "Electronic Excitations in Crystalline Solids through the Maximum Overlap Method" reported in Appendix 12.3.

Besides code developments, during my PhD I had the possibility to study the thermoelectricity of new generation materials. In fact, thermoelectricity has become an important aspect for the promotion of the sustainable development, since the possibility to directly convert waste heat into electricity. Moreover, simulations play an important role in predicting new materials and in particular CRYSTAL can perform directly thermoelectric properties without any external program [9]. Even if the calculation is rather simple to be implemented, the basis set quality has an important impact on the properties evaluation, above all on thermoelectrics since strictly dependent on the quality of the electronic structure. In this regard, a study on a specific family of thermoelectric materials has been done: Half Heusler (HH) alloys starting from the most known TiNiSn compound and extending the study to TiPtSn, TiPdSn and Ta based compounds as well. Results and discussions about Ti based HH and the role of defects in these systems are summarized in this thesis and can be found in the published paper *"Key Role of Defects in Thermoelectric Performance of TiMSn (M=Ni, Pd, and Pt) Half-Heusler Alloys"*.[10] This paper is the result of a collaboration with Prof. Antti Karttunen of the Department of Chemistry and Materials Science at the Aalto University in Helsinki, Finland. In fact, in 2019 I won CSC grants resources for travel-accomodation and 100,000 CPU hours with the HPC-Europa3 Transnational Access programme. Thanks to this project I had the possibility to visit Finland and I spent around one month abroad at the Aalto University.

Finally, a preliminary overview about a new family of materials that are predicting to be particularly interesting from the point of view of thermoelectricity is presented: the ullmannites. In this regard, four compounds are studied: NiSbS, NiSbSe, PdSbS and PdSbSe. Thermodynamic stability, electronic structures and thermoelectric properties are presented as well.

In more details, this thesis is characterized by two main parts structured as

follows:

PART I - Code Development

- Chapter 2: general overview about the CRYSTAL program
- Chapter 3: Basis Set Optimization Implementation
- Chapter 4: Basis Set Optimization Benchmark on Elemental Solids
- Chapter 5: Direct Inversion of the Iterative Subspace for Geometry Optimization
- Chapter 6: Maximum Overlap Method

PART II - Thermoelectrics Materials

- Chapter 7: Half Heusler Alloys
- Chapter 8: Ullmannites

Appendices

- Appendix A: technical and detailed description of the Basis Set Optimization algorithm.
- Appendix B: technical details about Maximum Overlap Method algorithm.
- Appendix C: papers published, submitted and in prerараtion.

Bibliography

[1] Roberto Dovesi, Alessandro Erba, Roberto Orlando, Claudio M Zicovich-Wilson, Bartolomeo Civalleri, Lorenzo Maschio, Michel Rérat, Silvia Casassa, Jacopo Baima, Simone Salustro, et al. Quantum-mechanical condensed matter simulations with CRYSTAL. *Wiley Interdisciplinary Reviews: Computational Molecular Science*, 8(4):e1360, 2018.

[2] Péter Pulay. Convergence acceleration of iterative sequences. the case of SCF iteration. *Chemical Physics Letters*, 73(2):393–398, 1980.

[3] Peter Pulay. Improved SCF convergence acceleration. *Journal of Computational Chemistry*, 3(4):556–560, 1982.

[4] Lorenzo Maschio. Direct inversion of the iterative subspace (DIIS) convergence accelerator for crystalline solids employing Gaussian basis sets. *Theoretical Chemistry Accounts*, 137(4):60, 2018.

[5] Pál Császár and Péter Pulay. Geometry optimization by direct inversion in the iterative subspace. *Journal of Molecular Structure*, 114:31–34, 1984.

[6] Loredana Edith Daga, Bartolomeo Civalleri, and Lorenzo Maschio. Gaussian basis sets for crystalline solids: all-purpose basis set libraries vs system-specific optimizations. *Journal of Chemical Theory and Computation*, 16(4):2192–2201, 2020.

[7] Kurt Lejaeghere, Gustav Bihlmayer, Torbjörn Björkman, Peter Blaha, Stefan Blügel, Volker Blum, Damien Caliste, Ivano E Castelli, Stewart J Clark, Andrea Dal Corso, et al. Reproducibility in density functional theory calculations of solids. *Science*, 351(6280), 2016.

[8] Andrew TB Gilbert, Nicholas A Besley, and Peter MW Gill. Self-consistent field calculations of excited states using the maximum overlap method (MOM). *The Journal of Physical Chemistry A*, 112(50):13164–13171, 2008.

[9] Giuseppe Sansone, Andrea Ferretti, and Lorenzo Maschio. Ab initio electronic transport and thermoelectric properties of solids from full and range-separated hybrid functionals. *The Journal of Chemical Physics*, 147(11):114101, 2017.

[10] Atreyi Dasmahapatra, Loredana Edith Daga, Antti J Karttunen, Lorenzo Maschio, and Silvia Casassa. Key role of defects in thermoelectric performance of TiMSn (M= Ni, Pd, and Pt) half-heusler alloys. *The Journal of Physical Chemistry C*, 124(28):14997–15006, 2020.

Chapter 1

Introduction

Computational materials science a branch of materials science showing an increasing success nowadays. In fact, the development of efficient tools and the enhancement of the computer capacities result in a growing interest about this field. In particular, the increasing availability of very fast computers and the development of efficient algorithms allows for the evolution of *in silico* simulations in many research fields. Fast High Performance Computing (HPC) systems allow for solving complex problems impossible in the past, paving the way to an exploratory research that in a laboratory and under common physical conditions are usually not feasible. This rather new approach established an interdisciplinary research bringing together such diverse fields as physics, mathematics, chemistry, biology, engineering and medicine. Evidence of this is the increasing number of scientific publications that testifies the important impact of this approach.

Regarding the computational resources, HPC, performed through supercomputers heading towards hexascale, is at the moment the best option for running quantum-mechanical simulations. It refers to computing systems with extremely high computational power that are able to solve demanding and hugely complex problems. Besides HPC, GPU (graphics processing unit) computing is also a rather new tool for computational materials science. A GPU is usually used as a co-processor and proved to be an efficient accelerator for CPUs usual performance.

Concerning the state-of-art of quantum chemistry and solid-state programs, many codes have been developed (either open source or commercial), each one with different features and strong points. The programming language usually adopted is Fortan or C++, but in more recent years even Python has been used as well (PySCF[1]). Moreover, one of the main distinguishing characteristic among these programs is the basis set adopted. For solid-state calculations[2],

plane waves[3, 4, 5], atom-centered Gaussians[6] (or their combinations[7]), and numerical basis sets[8, 9], are all popular choices as basis sets. Plane waves and gaussian functions are the most known ones, and depending on the choice, the code will have specific strong points and limitations.

In the field of quantum chemical modelling, CRYSTAL is a well-known ab initio code for solid-state simulations [6]; it is suited to evaluate not only energy and equilibrium geometry, but also many other essential properties for the material characterization: vibrational properties, thermal properties, linear and nonlinear optical properties, strain properties, electron transport properties and X-ray.

During my PhD, carried out within the Theoretical Chemistry Group of University of Turin, I was involved in many projects regarding the development and improvement of this software along with application on new generation materials in the thermoelectric field.
The peculiarity of the CRYSTAL program is that Gaussian Type Functions (GTF) are used as basis sets. Although Gaussian type basis sets are less commonly adopted for the quantum chemical treatment of solids, with respect to plane waves, Gaussian functions have the great advantage of allowing to transfer to the solid state a large part of the technology and knowledge that is the legacy of several decades of advances in molecular quantum chemistry and to retain the chemical intuition when looking at the electronic charge partition of the investigated system. The local nature of gaussian functions and the strict dependence on the atomic positions, allows an easy chemical interpretation of the results. Moreover, they are rather suitable to the description of 3D, 2D and 1D systems as well as an easy and relatively cheap use of hybrid functionals. The price to pay is the mandatory definition of a basis set for each atomic species, that is ultimately left in the hands of the end user. Thereafter, when dealing with the quantum chemical modeling of crystalline solids, the existence of various types of chemical bonding is clearly evident and this variety reflects the choice of the type and quality of the basis set adopted in the mathematical form of the wave function when solving the Schrödinger equation within periodic boundary conditions (i.e., Bloch functions)[10, 11, 2]. This situation calls for a different approach to the choice of basis sets, namely a system–specific optimization of the basis set that requires a practical algorithm that could be used on a routine basis. To this purpose we developed a technique called BDIIS (Basis Set Direct Inversion of the Iterative Subspace) to automatize the calibration of exponents and coefficients in a basis set. This kind of approach is absolutely new and it has never been attempted before.

Another important aspect that will be discussed in this work of thesis it is the excitation in solids. Whereas ground state calculations and equilibrium properties are widespread methods (HF and DFT[12, 13]), the study of excited states is not a straightforward. Many attempts have been developed: Multi Reference

Configuration Interaction (MRCI)[14], Multi Reference Møller - Plesset Perturbation theory (MRMP)[15], Configuration Interaction Single-excitation (CIS) and with perturbative treatment of doubles (CIS(D))[16], Time Dependent DFT (TD-DFT)[17], many - body Green's functions methods (GW)[18] and many others. Nevertheless, the methods available are rather expensive computationally and their application is usually limited to atoms, molecules or small clusters[17, 15]. Thereafter, very few or even absent implementations on solid-state are nowadays available. In this work of thesis we have implemented in the CRYSTAL code a simple technique to enforce orbital occupations, bypassing the "natural" occupation dictated by the Aufbau principle. The method is not new in its fundamentals and is commonly called called Maximum Overlap Method (MOM); a recent discussion can be found in Gilbert et al.[19]. However, the application of the method to periodic systems is scarce in the literature, and we were not able to find a reference reporting details of its periodic implementation or results on crystalline solids. From a technical point of view, the algorithm tries to maximize the overlap between the occupied orbitals with those of the preceding iteration or of a reference state during the SCF iterations. This procedure leads the SCF towards excited state solutions instead of ground state ones, or can be useful in order to stabilize the ground state solution preventing the intrusion of numerical instabilites in the density matrix. Promoting an electron from an occupied to a virtual orbital is then a sufficient guess to start an SCF calculation with MOM. In fact, the algorithm will keep the excited configuration.

The last topic that will be discussed in this work of thesis regards thermoelectricity, thus the direct conversion of heat into electricity. As mentioned above, ab initio or first principles methods, such as provided by the Density Functional Theory (DFT), are widely accepted as the best compromise between cost and accuracy above all in materials characterization. Moreover, *in silico* simulations are important in designing new and high-performance thermoelectric (TE) materials. Among the properties that can be simulated[20], obtaining an estimate of conductivity and thermoelectric power of materials has become of primary interest for the technological development. In fact, in recent years, thermoelectrics has made remarkable progress for its potentially broad applications in refrigeration, waste heat recovery, solar energy conversion, etc [21, 22, 23]. Thermoelectric energy generation (TEG) might be the alternative way to fight against global warming as this method does not require fossil-fuels and it is environmental friendly and extremely reliable. Since the electrical transport properties are directly determined by the band structures, a proper understanding and description of the band structure is suggested. In this regard, the quality of the basis sets used for the simulations is extremely important to optimize and design novel functional materials, hence the BDIIS algorithm was key to a successful study of these materials.

Bibliography

[1] Qiming Sun, Timothy C. Berkelbach, Nick S. Blunt, George H. Booth, Sheng Guo, Zhendong Li, Junzi Liu, James D. McClain, Elvira R. Sayfutyarova, Sandeep Sharma, Sebastian Wouters, and Garnet Kin-Lic Chan. PySCF: the Python-based simulations of chemistry framework, 2017.

[2] Richard M Martin. *Electronic structure: basic theory and practical methods*. Cambridge University Press, 2020.

[3] Georg Kresse and Jürgen Furthmüller. Efficient iterative schemes for ab initio total-energy calculations using a plane-wave basis set. *Physical Review B*, 54(16):11169, 1996.

[4] Stewart J Clark, Matthew D Segall, Chris J Pickard, Phil J Hasnip, Matt IJ Probert, Keith Refson, and Mike C Payne. First principles methods using CASTEP. *Zeitschrift für Kristallographie-Crystalline Materials*, 220(5-6):567–570, 2005.

[5] Paolo Giannozzi, Stefano Baroni, Nicola Bonini, Matteo Calandra, Roberto Car, Carlo Cavazzoni, Davide Ceresoli, Guido L Chiarotti, Matteo Cococcioni, Ismaila Dabo, et al. QUANTUM ESPRESSO: a modular and open-source software project for quantum simulations of materials. *Journal of Physics: Condensed Matter*, 21(39):395502, 2009.

[6] Roberto Dovesi, Alessandro Erba, Roberto Orlando, Claudio M Zicovich-Wilson, Bartolomeo Civalleri, Lorenzo Maschio, Michel Rérat, Silvia Casassa, Jacopo Baima, Simone Salustro, et al. Quantum-mechanical condensed matter simulations with CRYSTAL. *Wiley Interdisciplinary Reviews: Computational Molecular Science*, 8(4):e1360, 2018.

[7] By Gerald Lippert, Jurg Hutter Parrinello, and Michele. A hybrid gaussian and plane wave density functional scheme. *Molecular Physics*, 92(3):477–488, 1997.

[8] Bernard Delley. From molecules to solids with the DMol 3 approach. *The Journal of Chemical Physics*, 113(18):7756–7764, 2000.

[9] Sergey V Levchenko, Xinguo Ren, Jürgen Wieferink, Rainer Johanni, Patrick Rinke, Volker Blum, and Matthias Scheffler. Hybrid functionals for large periodic systems in an all-electron, numeric atom-centered basis framework. *Computer Physics Communications*, 192:60–69, 2015.

[10] Cesare Pisani. *Quantum-mechanical ab-initio calculation of the properties of crystalline materials*, volume 67. Springer Science & Business Media, 2012.

[11] Roberto Dovesi, Bartolomeo Civalleri, Roberto Orlando, Carla Roetti, and Victor R Saunders. Ab initio quantum simulation in solid state chemistry. *Reviews in Computational Chemistry*, 21:1, 2005.

[12] Pierre Hohenberg and Walter Kohn. Inhomogeneous electron gas. *Physical Review*, 136(3B):B864, 1964.

[13] Walter Kohn and Lu Jeu Sham. Self-consistent equations including exchange and correlation effects. *Physical Review*, 140(4A):A1133, 1965.

[14] Trygve Helgaker, Poul Jorgensen, and Jeppe Olsen. *Molecular electronic-structure theory*. John Wiley & Sons, 2014.

[15] K Hirao. Multireference Møller—Plesset method. *Chemical Physics Letters*, 190(3-4):374–380, 1992.

[16] James B Foresman, Martin Head-Gordon, John A Pople, and Michael J Frisch. Toward a systematic molecular orbital theory for excited states. *The Journal of Physical Chemistry*, 96(1):135–149, 1992.

[17] Erich Runge and Eberhard KU Gross. Density-functional theory for time-dependent systems. *Physical Review Letters*, 52(12):997, 1984.

[18] Lars Hedin. New method for calculating the one-particle Green's function with application to the electron-gas problem. *Physical Review*, 139(3A):A796, 1965.

[19] Andrew TB Gilbert, Nicholas A Besley, and Peter MW Gill. Self-consistent field calculations of excited states using the maximum overlap method (MOM). *The Journal of Physical Chemistry A*, 112(50):13164–13171, 2008.

[20] Giuseppe Sansone, Andrea Ferretti, and Lorenzo Maschio. Ab initio electronic transport and thermoelectric properties of solids from full and range-separated hybrid functionals. *The Journal of Chemical Physics*, 147(11):114101, 2017.

[21] HJ Goldsmid and RW Douglas. The use of semiconductors in thermoelectric refrigeration. *British Journal of Applied Physics*, 5(11):386, 1954.

[22] Lon E Bell. Cooling, heating, generating power, and recovering waste heat with thermoelectric systems. *Science*, 321(5895):1457–1461, 2008.

[23] Daniel Kraemer, Bed Poudel, Hsien-Ping Feng, J Christopher Caylor, Bo Yu, Xiao Yan, Yi Ma, Xiaowei Wang, Dezhi Wang, Andrew Muto, et al. High-performance flat-panel solar thermoelectric generators with high thermal concentration. *Nature Materials*, 10(7):532–538, 2011.

Part I

Method Development and Implementation

Chapter 2

The CRYSTAL program

CRYSTAL is a program for solid-state quantum-mechanical ab initio simulations. Historically speaking CRYSTAL was one of the first codes devoted to periodic systems and to be distributed publicly in 1988 through the Quantum Chemistry Program Exchange. [1, 2]. Since then, other releases have followed (1992, 1995, 1998, 2003, 2006, 2009, 2014, 2017) till today. It adopts atom-centered Gaussian-type functions as a basis set, which makes possible all-electron and pseudopotential calculations. Systems of different periodicity can be studied: 0D molecules, clusters and nanocrystals, 1D polymers, helices, nanorods, and nanotubes, 2D monolayers and slab models for surfaces and 3D bulk crystals.[3, 4] Hartree Fock and density functional theory calculations can be performed with a variety of functionals available: local-density (LDA), generalized-gradient (GGA), meta-GGA, global hybrid, range-separated hybrid, and self-consistent system-specific hybrid. The efficient implementation of exact nonlocal Fock exchange enables to use hybrid functionals with a modest computational cost. A rather wide variety of properties can be computed including open-shell systems: geometry optimization, vibrational properties, thermal properties, linear and nonlinear optical properties, strain properties, electron transport properties and X-ray.

2.1 CRYSTAL in the framework of ab initio simulation: a Gaussian Based Code

While many ab initio solid state codes are based on plane waves, CRYSTAL uses a Gaussian-Type basis set, thus local functions expressed as linear combination of a certain number of Gaussian type functions (GTF).

In mathematical terms, in the linear combinations of atomic orbitals (LCAO) framework, the crystalline orbitals ψ are treated as linear combinations of Bloch functions (BF) ϕ that are, in turn, defined in terms of local atom-centered functions (AO) φ:

$$\psi_i(\mathbf{r};\mathbf{k}) = \sum_{\mu} a_{\mu,i}(\mathbf{k})\,\phi_\mu(\mathbf{r};\mathbf{k}) \tag{2.1}$$

$$\phi_\mu(\mathbf{r};\mathbf{k}) = \sum_{\mathbf{g}} \varphi_\mu(\mathbf{r}-\mathbf{A}_\mu-\mathbf{g})\,e^{i\mathbf{k}\cdot\mathbf{g}} \tag{2.2}$$

in which $\mathbf{g}$ is a direct space lattice vector, $\mathbf{k}$ is the lattice vector defining a point in the reciprocal lattice, $\mathbf{A}$ are the coordinates of the atom in the reference cell on which the AO φ is centered, a are the variational coefficients. The sum over μ is limited to the number of basis functions in the unit cell. Thus $\mathbf{A}_\mu$ is the centroid of the orbital μ on the atom at position $\mathbf{A}$. The sum over $\mathbf{g}$ is, in principle, extended to all the (infinite) lattice vectors of the direct lattice, therefore suitable screening techniques have to be adopted.[1, 5, 6]

As usual, the AOs can be defined as a contraction of a number n of primitive Gaussian–Type Functions (GTF) G centered on the same atom,

$$\varphi_\mu(\mathbf{r}-\mathbf{A}_\mu-\mathbf{g}) = \sum_{j}^{nG} d_j G(\alpha_j;\mathbf{r}-\mathbf{A}_\mu-\mathbf{g}) \tag{2.3}$$

in which d_j are the contraction coefficients and α_j the exponents of the radial component of the function. The number, type and contraction scheme of the Gaussian basis set define its quality. The flexibility of Gaussian functions allows for an accurate description of the system chemistry and a relatively good speed of two-electron integral evaluation.[7]

While in molecular quantum chemistry Gaussian Type Fuctions (GTF) are almost unanimously accepted as the best choice, it is not so for solids. Just to name a few, Gaussians, plane waves (PW), eventually projector-augmented (PAW), and numerical basis sets are all more or less popular choices, alongside their possible combinations. It goes beyond the scopes of this discussion to thoroughly address all the pros and cons of each of them, therefore in the following only the features of GTF used in CRYSTAL and plane waves PW are briefly compared.

- *Local Nature of Gaussian Functions*
  In CRYSTAL periodic boundary conditions can be easily applied in all directions (1D, 2D, 3D) and the true dimensionality of the system is always kept, without any spurious effects. They depend on atomic positions,

similarity with quantum chemical codes and allow for an easy chemical interpretation of the results. On the other hand, plane waves are intrinsically periodic in three dimensions. In fact, in any case a 3D box is defined filled with plane waves uniformly. This implies the mandatory expansion of the aforementioned box along a specific direction when dealing with lower dimensionality than 3D one, creating in this way sufficient void space around the system.[8] Moreover, although PW permit a less demanding description to metals (3D) and of delocalized electrons, PW are completely independent of atomic positions.

- *Completeness and Quality of Gaussian Functions*
  For PW the mathematics is relatively easy, since the overall quality is due to the definition of a single parameter called cut-off energy: higher is this parameter, better is the quality. For GTF it is more complicated. Although a wide choice of gaussian basis sets is available for molecules, that is not true for periodic systems. In fact, a direct transfer of basis set from molecule to periodic system is not recommended due to the most diffused functions that can be very critical in systems with high density. In fact, the Bloch functions constructed from diffuse Gaussians tend to be very similar, leading to a nearly singular overlap matrix that in turn creates serious numerical problems in the basis functions orthogonalization. To avoid these linear dependencies, an appropriate definition of the gaussian basis set is mandatory, but it is not a straightforward and many times requires experience.[9] Over the years specific basis sets have been implemented for periodic systems and some of them are available in the CRYSTAL website (`https://www.crystal.unito.it`).

- *Hybrid Functionals*
  With GTF it is relatively cheap and easy the use of hybrid functionals (e.g. B3LYP, PBE0 and HSE06). These functionals are known to improve the description of electronic properties and usually be much closer to what should be considered the correct result. PW instead have extremely high computational cost in this respect.

- *Pseudopotentials*
  Both Gaussians and PW based codes allow for an implicit description of core electrons by using pseudopotential. This turns out to play a fundamental role in the description of heavy atoms, because the pseudopotentials include relativistic effects. A more detailed discussion on these aspects is beyond the purpose of this comparison and we redirect the reader to more specialized textbooks.

2.2 Main Features of the Code

In this section some remarks about the basic structure of the CRYSTAL code are briefly summarized with some hints to the new features available.

- *Symmetry*
  One of the peculiar aspects of the CRYSTAL code is the use of symmetry that is exploited in many steps of the calculation. Most importantly, the construction of Symmetry Adapted Crystalline Orbitals (SACOs) lead to the factorization of the Fock matrix that consequently reduce the allocation memory, and only symmetry-irreducible integrals are computed.

- *Self-Consistent Field*
  In the SCF calculation (self-consistent field), Coulomb, exchange and monoelectronic integrals are evaluated in the direct space and once the Fock or Kohn–Sham matrix is built, it is Fourier transformed to the reciprocal space and diagonalized. The obtained density matrix is transformed back to the real space before the next self-consistent field iteration. In particular, in DFT calculation exchange–correlation contribution to the Fock matrix is evaluated over the unit cell volume by numerical integration.

- *Restricted and Unrestricted Hartree–Fock*
  Both restricted (RHF) and unrestricted Hartree–Fock (UHF) option were implemented allowing for a good description of transition metal compounds.

- *Gradients*
  For the geometry optimization analytical gradients with respect to atomic coordinates and cell parameters are implemented, while for the vibrational frequencies and second order elastic constants gradients are computed semi analytically (numerical derivatives of the analytical gradients).

- *Vibrational spectroscopy*
  CRYSTAL can perform harmonic frequencies (numerical Hessian), infrared intensities (numerical and analytical), Raman Intensities (analytical), phonon dispersion and since 2017 (CRYSTAL17) phonon density of states and inelastic neutron scattering.

- *One-electron Properties*
  Electronic band structure, density of states, electron charge density (2D maps and 3D plots), X-ray structure factors, X-ray diffraction spectrum and transport properties like thermoelectrics are some examples. Many of these properties can also be easily visualized by a new tool called CRYSPLOT. CRYSPLOT is a web oriented tool (`http://crysplot.crystalsolutions.`

`eu`) to visualize computed properties of periodic systems, along with plotting, it also permits the modification and customization of plots to meet the standards required for scientific graphics.[10]

- *DFT and Dispersion Correction*
  Density Functional Theory and dispersion correction are implemented in CRYSTAL. In particular, Local-density (LDA), Generalized-gradient (PBE, BLYP,...), Meta-GGA (M06,...), Global hybrid (B3LYP, PBE0,...), Range-separated hybrid (HSE06,...), Grimme's D2 Correction for Dispersive Interactions are available. Moreover, since CRYSTAL17, Grimme's D3 Correction, Self-consistent global hybrids and Composite methods for molecular crystals (HF-3c, PBEh-3c) are implemented.

Recently in the public CRYSTAL program an extension to g-type basis functions has been implemented for quantum-chemical simulations of n-dimensional periodic systems ($n = 0, 1, 2, 3$).[11]. Moreover, the code has been generalized in many respects to allow for the use of g-type functions for: Hartree–Fock energy and forces; density functional theory energy and forces (in either a local density, generalized gradient, meta-GGA or various hybrid approximations); all-electron and pseudo-potential basis sets; spin-restricted and unrestricted calculations; coupled-perturbed Hartree–Fock/Kohn–Sham (hyper)-polarizability calculations; projected density-of-states. This extension has an important role in the description of the electronic structure of heavy elements like lanthanides and actinides with occupied 4f and 5f bands.

More recently a two-component relativistic DFT calculations with the simultaneous self-consistent treatment of spin-orbit coupling (SOC) and non-local Fock exchange in periodic systems have been implemented in a development version of the code [12, 13]. In particular, the SOC refers to the coupling of the spin of an electron with its orbital motion. This coupling not only shifts the electronic levels of the system but also changes the symmetry of the electronic states. This means that in heavy element systems, where the SOC is strong, it can be necessary to include it in calculations even for a qualitatively correct description of the electronic structure.

Among the available features that have been implemented in the code recently, the Direct Inversion of Iterative Subspace (DIIS) convergence accelerator is strictly correlated with the topic of this thesis. In particular, in the actual public version of the CRYSTAL code the DIIS has been implemented for the self-consistent field (SCF) procedure and for first and second-order Coupled-Perturbed-Hartree-Fock/Kohn-Sham (CPHF/KS) self-consistent procedures[14]. The use of such a scheme is found to drastically reduce the required number of iterations to get convergence and it is thus activated by default.

Since part of this Thesis work will be closely related to DIIS, in the following we present a detailed description of this method.

2.2.1 Direct Inversion of Iterative Subspace Algorithm

The DIIS method was firstly proposed by Pulay in 1980 [15] and even today it is the most popular algorithm for the acceleration and stabilization of the SCF iterative procedure.[14]

The aim of this method is to find the minimum of a function of many variables, through the evaluation of the errors in a number of trial solutions (vectors), through interpolation/extrapolation. One of the application is in the SCF (Self-Consistent Field) procedure, thus an iterative method that involves selecting an approximate Hamiltonian, solving the Hartree-Fock/Kohn Sham equations iteratively to obtain a more accurate set of orbitals, till the results converge to predetermined thresholds.[3, 4] A critical point of the DIIS method can be the storage of error vectors and Fock matrices from previous iterations that could be demanding in terms of memory and disk space, and a cost for the DIIS-related linear algebra that grows as the number of iterations grows. But the advantages in terms of a faster time to solution usually compensate for these issues. Even though other variants such as the Energy-DIIS (EDIIS)[16] have been claimed to be able to find more efficiently the lowest energy solution, the original formulation of DIIS remains the most widely diffused and adopted.

Considering the SCF iterative procedure, at each iterative cycle n (in the direct space), instead of the Fock matrix $\mathbf{F}_n$, an averaged effective Fock matrix is defined as a linear combination of the Fock matrices of previous iterations:

$$\bar{\mathbf{F}}_n = \sum_{i=1}^{n} c_i \mathbf{F}_i \tag{2.4}$$

The c_i coefficients are obtained by minimizing a suitable error functional $\mathbf{e}$, subject to the constraint that $\sum_{i=1}^{n} c_i = 1$. This is obtained by solving the linear equation system:

$$\begin{pmatrix} \mathbf{e} & \mathbf{1^T} \\ \mathbf{1} & 0 \end{pmatrix} \begin{pmatrix} \mathbf{c} \\ \lambda \end{pmatrix} = \begin{pmatrix} \mathbf{0} \\ 1 \end{pmatrix} \tag{2.5}$$

where e is an error matrix having the size of the iterative space up to cycle n and λ is a Lagrange multiplier. This corresponds to minimising the off-diagonal elements of the Fock matrix in the basis of crystalline orbitals. To save time, memory and disk, errors are evaluated by default only in $k = 0$. In this k point (Γ) of the Brillouin zone the error matrix is defined through scalar products of suitable error vectors:

$$e_{mn} = \langle \mathbf{e}_n(\Gamma) | \mathbf{e}_m(\Gamma) \rangle \tag{2.6}$$

Other choices are possible (such as considering all k points, either with equal weight or weighted by Kerker factors[17], to avoid charge sloshing) but the above has been identified as the best default choice since it works well in most cases and minimizes the amount of information to be stored on disk [14]. According to Pulay's commutator DIIS (CDIIS) formulation[18], we define the error vector for the SCF procedure as:

$$\mathbf{e}_n(\mathbf{k}) = \mathbf{F}_n(\mathbf{k})\mathbf{D}_n(\mathbf{k})\mathbf{S}(\mathbf{k}) - \mathbf{S}(\mathbf{k})\mathbf{D}_n(\mathbf{k})\mathbf{F}_n(\mathbf{k}) \tag{2.7}$$

where $\mathbf{S}(\mathbf{k})$ is the overlap matrix. Such error vector is better evaluated through a transformation linearly independent basis, i.e. the molecular/crystalline orbital basis, in order to avoid linear dependencies.

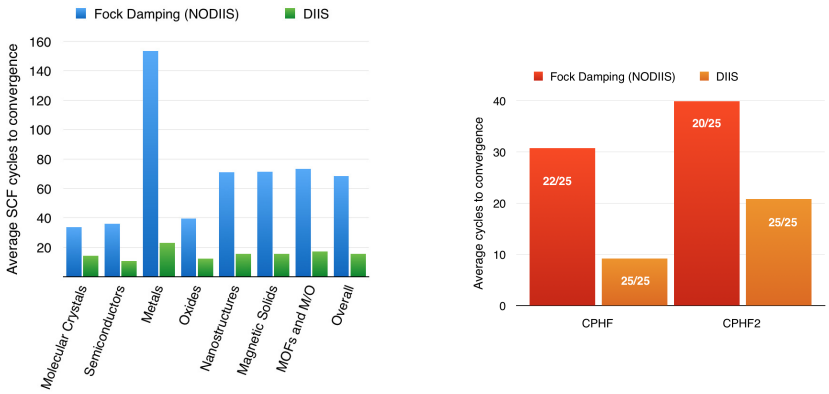

Figure 2.1: Left: Average self-consistent field (SCF) cycles needed to reach convergence with (green bars) and without (blue bars) DIIS convergence accelerator, as benchmarked on a test set of 42 periodic systems, grouped in seven categories. MOF stands for metal-organic frameworks and M/O for metal/oxide interfaces. The rightmost column reports the global average. For more details see the Ref. [14].
Right: Average Coupled-Perturbed-Hartree-Fock (CPHF) and CPHF2 cycles needed to reach convergence with (orange bars) and without (red bars) DIIS convergence accelerator, as benchmarked on a test set of 25 periodic systems. White numbers reported on the bars indicate the number of calculations which reached convergence over the total of 25.[14]

As mentioned above, the DIIS method was implemented in CRYSTAL a few years ago by L. Maschio.[14] The assessment of its performance was done through

a comprehensive test set of 42 systems was designed for benchmarking the performance of DIIS. The set comprises 3D, 2D, and 1D periodic systems, with basis sets ranging from minimal to quadruple zeta, either all electrons or using pseudopotentials. Seven groups of systems have been chosen: molecular crystals, semiconductors, metals, oxides, nanostructures, magnetic solids and metal-organic frameworks, and metal-oxide interfaces. HF and five different functionals were adopted. In Fig 2.1 the effect of the accelerator compared with the old default is reported. A gain factor of 3 is consistent throughout the test set with the DIIS method above all in metallic systems, nanostructures and magnetic systems.

As regard the CPHF/KS iterative procedure for the response to an external electric field E is similar to the SCF one above described, except that a density matrix perturbed by a field along Cartesian direction t is obtained at each cycle, $\mathbf{D}_n^{E_t}(\mathbf{k})$. Even in this case there is a gain factor of 3-4 by using the DIIS method, as outline in Fig 2.1

In general, the DIIS algorithm shows impressive efficiency in terms of rate of convergence even in complex chemical systems. For this reason in recent time the algorithm was implemented in many molecular codes and it is universally recognized. In the CRYSTAL code it is a default option of the calculation.

Bibliography

[1] C Pisani, R Dovesi, and C Roetti. Lecture notes in chemistry. In *Hartree—Fock ab initio treatment of crystalline systems*, volume 48. Springer Berlin, 1988.

[2] R Dovesi, C Pisani, C Roetti, M Causa, and VR Saunders. CRYSTAL88, QCPE Program No 577. *Indiana University, Bloomington, IN*, 1988.

[3] Roberto Dovesi, Alessandro Erba, Roberto Orlando, Claudio M Zicovich-Wilson, Bartolomeo Civalleri, Lorenzo Maschio, Michel Rérat, Silvia Casassa, Jacopo Baima, Simone Salustro, et al. Quantum-mechanical condensed matter simulations with CRYSTAL. *Wiley Interdisciplinary Reviews: Computational Molecular Science*, 8(4):e1360, 2018.

[4] Roberto Dovesi, Fabien Pascale, Bartolomeo Civalleri, Klaus Doll, Nicholas M Harrison, Ian Bush, Philippe D'arco, Yves Noël, Michel Rérat, Philippe Carbonniere, et al. The CRYSTAL code, 1976–2020 and beyond, a long story. *The Journal of Chemical Physics*, 152(20):204111, 2020.

[5] Cesare Pisani. *Quantum-mechanical ab-initio calculation of the properties of crystalline materials*, volume 67. Springer Science & Business Media, 2012.

[6] VR Saunders, C Freyria-Fava, R Dovesi, L Salasco, and C Roetti. On the electrostatic potential in crystalline systems where the charge density is expanded in gaussian functions. *Molecular Physics*, 77(4):629–665, 1992.

[7] Attila Szabo and Neil S Ostlund. *Modern quantum chemistry: introduction to advanced electronic structure theory*. Courier Corporation, 2012.

[8] PE Blöchl. Electrostatic decoupling of periodic images of plane-wave-expanded densities and derived atomic point charges. *The Journal of chemical physics*, 103(17):7422–7428, 1995.

[9] R Dovesi, B Civalleri, R Orlando, C Roetti, and VR Saunders. Reviews in computational chemistry. *Wiley, New York*, 21:1–11, 2005.

[10] Giorgia Beata, Gianpaolo Perego, and Bartolomeo Civalleri. CRYSPLOT: a new tool to visualize physical and chemical properties of molecules, polymers, surfaces, and crystalline solids. *Journal of Computational Chemistry*, 40(26):2329–2338, 2019.

[11] Jacques Kontak Desmarais, A Erba, and R Dovesi. Generalization of the periodic LCAO approach in the CRYSTAL code to g-type orbitals. *Theoretical Chemistry Accounts*, 137(2):1–11, 2018.

[12] Jacques K Desmarais, Jean-Pierre Flament, and Alessandro Erba. Spin-orbit coupling from a two-component self-consistent approach. I. Generalized Hartree-Fock theory. *The Journal of Chemical Physics*, 151(7):074107, 2019.

[13] Jacques K Desmarais, Jean-Pierre Flament, and Alessandro Erba. Spin-orbit coupling from a two-component self-consistent approach. II. non-collinear density functional theories. *The Journal of chemical Physics*, 151(7):074108, 2019.

[14] Lorenzo Maschio. Direct inversion of the iterative subspace (DIIS) convergence accelerator for crystalline solids employing Gaussian basis sets. *Theoretical Chemistry Accounts*, 137(4):60, 2018.

[15] Péter Pulay. Convergence acceleration of iterative sequences. the case of SCF iteration. *Chemical Physics Letters*, 73(2):393–398, 1980.

[16] Konstantin N Kudin, Gustavo E Scuseria, and Eric Cances. A black-box self-consistent field convergence algorithm: One step closer. *The Journal of Chemical Physics*, 116(19):8255–8261, 2002.

[17] Georg Kresse and Jürgen Furthmüller. Efficient iterative schemes for ab initio total-energy calculations using a plane-wave basis set. *Physical review B*, 54(16):11169, 1996.

[18] Peter Pulay. Improved SCF convergence acceleration. *Journal of Computational Chemistry*, 3(4):556–560, 1982.

Chapter 3

Basis Set Optimization Implementation

In the field of quantum chemistry plane waves and atom-centered gaussians are generally chosen as suitable function for solid state calculations. The local nature of gaussian functions and the strict dependence on the atomic positions, allows an easy chemical interpretation of the results. Moreover, they are rather suitable to the description of 3D, 2D and 1D systems as well as an easy and relatively cheap use of hybrid functionals. While many ab initio solid state codes are based on plane waves, CRYSTAL [1] uses a Gaussian-Type basis set local functions expressed as linear combination of a certain number of Gaussian type functions (GTF) as shown in Equ.1 and Equ.2 of Ref. [2] and discussed in Section 2.1.

In general it is difficult the calibration-optimization of exponents and contraction coefficients. Furthermore, standardized and well-assessed libraries of basis sets are not available for solids as they are for molecules (different density). Moreover, while with molecules extended basis sets can be easily used without linear dependence problems, in periodic systems it is not the case. In fact, the wide chemical diversity of solids (ionic, covalent, metallic) implies an accurate definition of the basis set. In this thesis a system specific optimization was implemented in the CRYSTAL code and taking inspiration from the DIIS method (see Section 2.2.1) a novel method was considered: BDIIS, Basis set Direct Inversion of Iterative Subspace.

A documentation about the technical aspects of the algorithm is reported in Appendix 10.

-Published paper: "Gaussian Basis Sets for Crystalline Solids: All-Purpose Basis Set Libraries vs System-Specific Optimization" [2], reported along with the supplementary material in Appendix 12.1 of this thesis.

3.1 Basis set Direct Inversion of Iterative Subspace Method

The historical background of the Basis set Direct Inversion of Iterative Subspace (BDIIS) method goes back to the DIIS (self-consistent field accelerator) and to the GDIIS (Geometry version of the DIIS), in which the main procedure is kept, but the parameters involved are exponents and coefficients of the basis set.

The main procedure of the BDIIS algorithm can be summarized as follows:

- construction of a suitable error vector at each iteration n

  Average Error Vector:

$$\mathbf{r} = \sum_{i=1}^{n} c_i \mathbf{e}_i = \bar{\mathbf{e}} \tag{3.1}$$

- n-th step as linear combination of previous trial vectors by solving a simple system of linear equations

  Set of linear equations:

$$\begin{pmatrix} a_{1,1} & \dots & a_{1,n} & 1 \\ \vdots & \ddots & \vdots & \vdots \\ a_{n,1} & \dots & a_{n,n} & 1 \\ 1 & \dots & 1 & 0 \end{pmatrix} \begin{pmatrix} c_1 \\ \vdots \\ c_n \\ \lambda \end{pmatrix} = \begin{pmatrix} 0 \\ \vdots \\ 0 \\ 1 \end{pmatrix} \tag{3.2}$$

  where $a_{ij} = \mathbf{e}_i^T \mathbf{e}_j$, with the constraint $\sum_{i=1}^{n} c_i = 1$. In the following, we will refer to this system of linear equations by using this formalism:

$$AEr \cdot CEr = ZEr \tag{3.3}$$

While for DIIS the error vector is related with the SCF parameters (Fock matrix and Density matrix) and previous geometries (Coordinates) for the GDIIS, in the actual case it is related with previous values of both exponents and coefficients. In fact, the error vector can be defined through the derivative of the total

energy (E_{tot}) with respect to changes in exponents (α) or contraction coefficients (d) in the basis set:

$$e_i^{\alpha} = \frac{\partial E_{tot}}{\partial \alpha} \qquad e_i^{d} = \frac{\partial E_{tot}}{\partial d} \tag{3.4}$$

Technically, the above derivative is evaluated by means of a double-sided numerical derivatives, thus two points were used for the gradient evaluation. In particular, the displacements considered are 1% of the previous exponents and 0.1% of the previous coefficients weighted by the relative exponents. More details are available in Section 3.1.1.

A graphical representation of the overall procedure is reported in Fig. 3.1.

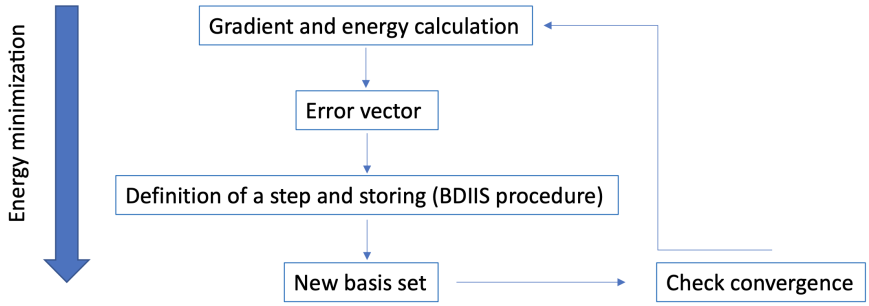

Figure 3.1: Graphical representation of the basis set optimization procedure.

3.1.1 Algorithm details

In this section few supplementary details about the algorithm will be provided:

- *Only exponents, only coefficients or both can be optimized.*
  Since an energy calculation is usually more sensitive to the choice of the exponents instead of the coefficients, the exponents optimization is the default option and the suggested option for the less expert user. Nevertheless, if the aim is the coefficients optimization, that can be activated by a proper *keyword* in input: `COEFFONLY`. Moreover, it is possible to optimize both exponents and coefficients with the keyword `ALLBDIIS`. It is also suggested to optimized just the valence shells and uncontracted if possible. In fact, valence shells are known to be more involved in the bonding.

- *Condition Number*
  The minimization procedure involve a suitable functional Ω that corresponds to the system total energy E_{tot} to which we add a penalty function

including the Overlap matrix condition number:

$$\Omega\left(\{\alpha, d\}\right) = E_{tot}\left(\{\alpha, d\}\right) + \gamma \ln \kappa\left(\{\alpha, d\}\right) \tag{3.5}$$

where γ is set at 0.001 as suggested by [3] and $\kappa(\{\alpha, d\})$ is the condition number. The latter is the ratio between the largest and the smallest eigenvalue of the overlap matrix at the center of the Brillouin zone (Γ-point). The introduction of such penalty function should prevent the onset of harmful linear dependence that can give rise to numerical instabilities and unphysical states. The Ω functional is called *Objective Function* in the following.

- *Two-Sided Numerical Derivative*
  Gradients are performed by using a two-sided numerical derivative method. Which means, for exponents α:

$$e_i^{\alpha} = \frac{\Omega(\alpha_i + \Delta\bar{\alpha}) - \Omega(\alpha_i - \Delta\bar{\alpha})}{2\Delta\bar{\alpha}} \tag{3.6}$$

  and similarly for the coefficients.

  The displacement $\Delta\bar{\alpha}$ is 1% of the exponent value ($\Delta\bar{\alpha} = 0.01 \cdot \alpha$), while for coefficients the step is set to 0.1%, weighted by the relative exponents ($\Delta\bar{d} = 0.001 \cdot \frac{d}{\alpha}$).

  This set up was defined by different trials done during the implementation. In fact, we also tried fixed step (e.g. 0.001 and 0.0005), but proving to be too rough as approximation.

- *Scale factor obtained by a line search method*
  By default a proper scale factor is applied to the optimization step (see Equ.12 in [2]). A suitable discrete point grid is used, sampling the scale factor from 0.05 to 1 (0.05, 0.1, 0.15, 0.2, 0.3, 0.4, 0.6, 0.8, 1.0).

  The idea of introducing a scale factor started from the well known implemented "Trust Radius" strategy already applied in the geometry optimization in CRYSTAL. The basic idea is to limit the displacement that can be too large and sometimes catastrophic for the overall calculation. In fact, many times during the optimization the step obtained from the BDIIS procedure turns out to be too big for a specific exponent-coefficient involved. This step may cause a linear dependence problem in the calculation. Technically for each scale factor f_l in the grid, a suitable step ($f_l\,\Delta\bar{\alpha}_n$) is defined, e.g. for the exponents α:

$$\widetilde{\alpha}_n = \alpha_{n-1} + f_l\,\Delta\bar{\alpha}_n \tag{3.7}$$

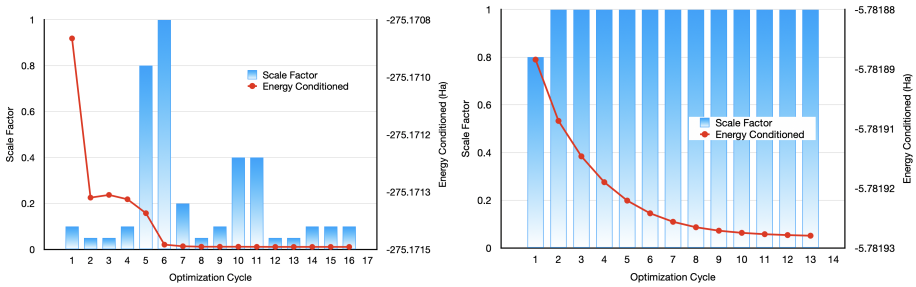

Figure 3.2: Objective Function behaviour during a basis set optimization along with the optimal scale factor adopted at each optimization cycle. On the left MgO system, pob-DZ basis set, optimization of oxygen p-coefficients. On the right He bulk, def-QZ basis set, valence exponents and coefficients optimization.

For each point a SCF (self consistent field) calculation is performed, and the one with the minimum value of Objective Function (Ω) is then retained.

In Figure 3.2 two examples of basis set optimization are reported along with the optimal scale factor adopted at each cycle. On the left picture it is reported the optimization of p-oxygen coefficients in MgO system. On the right picture valence exponents and coefficients optimization of He bulk is shown. In the first case, the scale factor is rather fundamental to get the convergence. In fact, cycle 2 and 3 seem to drive the optimization in the wrong direction (high energy) and the scale factor applied is rather low (smaller step). While from the fourth cycle the weight on the step increases due to the minimization of the energy. In the latter case instead, the scale factor is almost 1 at each cycle, thus the step applied is not limited by the line search at all. This means that the step length was kept unmodified till the end of the optimization, that in this case brings to a rather smooth convergence.

- *Matrix Size Reduction*
  Solving the system of linear equations in 3.2, linear dependencies issues among vectors may occur. In order to prevent this catastrophic behaviour and taking inspiration from the GDIIS implemented in the DALTON code [4, 5] an appropriate size control of the AEr matrix is applied. In particular, a specific condition number is considered:

$$\left|\frac{m}{M}\right| > 10^{-t} \tag{3.8}$$

where t is set to 4 by default. m and M are minimum and maximum

value of the eigenvalues of AEr matrix. If this condition is not satisfied the appropriate size reduction is applied. Further details will be provided in Section 10.4 and a graphical representation of the strategy adopted is reported in Fig. 3.3.

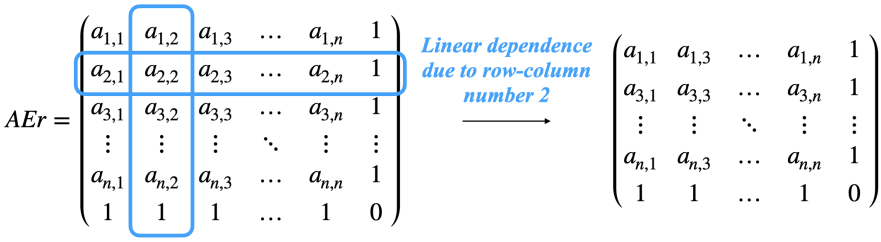

Figure 3.3: Graphical representation of the linear dependence removal method through the matrix size reduction. In the example row-column number 2 are the ones involved in the removal.

- *LBFGS method*
  An alternative to the BDIIS optimization procedure, a LBFGS method (Limited-memory BFGS) has been implemented for exponents. The algorithm is described in "On the limited memory BFGS method for large scale optimization", by D. Liu and J. Nocedal, Mathematical Programming B 45 (1989) 503-528.[6]
  In particular, considering a $f(x)$ function minimization, we can define:

$$s = x_{k+1} - x_k \tag{3.9}$$

and

$$y = \nabla f(x_{k+1}) - \nabla f(x_k) \tag{3.10}$$

While the well known BFGS formula is:

$$H_{k+1} = H_k + \frac{yy^T}{y^T s} - \frac{H_k s s^T H_k}{s^T H_k s} \tag{3.11}$$

the LBFGS method uses the inverse BFGS formula in the form:

$$H_{k+1}^{-1} = \left(1 - \frac{sy^T}{y^T s}\right) H_k^{-1} \left(1 - \frac{ys^T}{y^T s}\right) + \frac{ss^T}{y^T s} \tag{3.12}$$

The LBFGS method can be easily activated in input with the keyword `BFGSBAS`, but only exponents optimization can be performed.

3.2 Validation Tests

As demonstrative systems we have considered simple prototypical solids such as diamond, graphene, sodium chloride, and LiH. In the paper [2] we show how basis set optimizations have certain advantages also towards the use of large (quadruple-ζ) basis sets in solids, both at the DFT and Hartree-Fock level. System-specific optimization of def2-like Gaussian basis sets in solids leads to a significant improvement over the adoption of more general sets, and yields significantly different exponents in the valence part when systems of different chemical bonds are compared. A detailed description of all the results obtained is available in the abovementioned paper [2] in Appendix 12.1 of this thesis.

Bibliography

[1] Roberto Dovesi, Alessandro Erba, Roberto Orlando, Claudio M Zicovich-Wilson, Bartolomeo Civalleri, Lorenzo Maschio, Michel Rérat, Silvia Casassa, Jacopo Baima, Simone Salustro, et al. Quantum-mechanical condensed matter simulations with CRYSTAL. *Wiley Interdisciplinary Reviews: Computational Molecular Science*, 8(4):e1360, 2018.

[2] Loredana Edith Daga, Bartolomeo Civalleri, and Lorenzo Maschio. Gaussian basis sets for crystalline solids: all-purpose basis set libraries vs system-specific optimizations. *Journal of Chemical Theory and Computation*, 16(4):2192–2201, 2020.

[3] Joost VandeVondele and Juerg Hutter. Gaussian basis sets for accurate calculations on molecular systems in gas and condensed phases. *The Journal of Chemical Physics*, 127(11):114105, 2007.

[4] LSDalton, a linear scaling molecular electronic structure program, 2015. http://daltonprogram.org.

[5] Dalton, a molecular electronic structure program, 2015. http://daltonprogram.org.

[6] Dong C Liu and Jorge Nocedal. On the limited memory BFGS method for large scale optimization. *Mathematical Programming*, 45(1):503–528, 1989.

[7] Benjamin P Pritchard, Doaa Altarawy, Brett Didier, Tara D Gibson, and Theresa L Windus. New basis set exchange: An open, up-to-date resource for the molecular sciences community. *Journal of Chemical Information and Modeling*, 59(11):4814–4820, 2019.

Chapter 4

Basis Set Optimization Benchmark on Elemental Solids

In this Chapter an extensive application of the BDIIS Basis Set Optimizer is reported. In fact, we took inspiration from a paper published in 2016 by Lejaeghere et al. [1] where a systematic work to demonstrate DFT reproducibility is well described. In particular, they calculated equation of states data considering 15 solid state codes, using 40 different potentials or basis set types, to assess the PBE (Perdew-Burke-Ernzerhof) quality for 71 elemental crystals. In this work of thesis we tried to reproduce their work for 36 elemental solids, starting from def2-like basis set and optimizing these basis sets by using the BDIIS method. The eos parameters have been evaluated by fitting 7 energy points around the equilibrium volume. Moreover, we extended the PBE calculation to hybrid functional one, specifically using HSE06 functional. This work is still in progress and it will be part of a paper not yet finished. A draft of the paper and a preliminary supplementary material is reported in Appendix 12.4.

4.1 Basis Set Optimization and Simulation Set Up

In order to be competitive with the other codes we preliminary applied the BDIIS method [2] to all the systems to get the best basis sets possible. The basis set are derived from def2-TZVP, optimizing valence and polarization functions

that are the ones relevantly changing in a different chemical environment. In some cases (e.g. noble gases) more extended basis set have been used like def2-QZVP. Behind this, the optimized basis sets are named dcm-TZ or dcm-QZ in the following. As regards geometry and structural parameters they were provided by the Ref. [1], to which we add the FIXINDEX option of CRYSTAL.[3] In fact, when the geometrical and/or the basis set parameters of the system are changed, maintaining the symmetry and the setting, the truncation criteria of the Coulomb and exchange series, based on overlap can lead to the selection of different numbers of bi-electronic integrals. This may be the origin of numerical noise in the optimization curve. When small changes are made on the lattice parameter or on the Gaussian orbital exponents, the indices of the integrals to be calculated can be selected for a reference geometry (or basis set), "frozen", and used to compute the corresponding integrals with the modified geometry (or basis set). The reference geometry considered corresponds to the most compact structure, thus the one with the smallest volume.

Concerning the functional, as mentioned in the introduction, PBE functional has been used and an extension to hybrid functional is proposed. In particular, HSE06 functional.

Other more technical details like energy thresholds and k-mesh grid are reported in the Supplementary Material available in Appendix of this thesis.

Moreover, as outlined at the beginning of this Chapter, an extensive test set was used by taking the ground state crystal structures of elemental solids in their most common symmetry geometries.

In our work the elemental crystals considered range from Hydrogen to Krypton. In Fig. 4.1 a schematic periodic table is reported along with space group and magnetic state for each elemental crystal.

4.2 Equations of States Paramenters as benchmark

As mentioned earlier, the benchmark is performed evaluating the equation of states parameters (EOS in the following).

In this section a brief summary of the mathematical background is reported. Three are the equations of state (EOS) parameters commonly used for accuracy assessments:

- Volume (V)
- Bulk Modulus: resistance to volume changes (B_0)
- Pressure Derivative of the Bulk Modulus: one order higher effects (B_1)

H																	He
194																	194
hP4																	hP2
nm																	nm
Li	Be											B	C	N	O	F	Ne
166	194											166	194	205	12	15	225
hR9	hP2											hR36	hP4	cP8	mS4	mS8	cF4
nm	nm											nm	nm	nm	afm	nm	nm
Na	Mg											Al	Si	P	S	Cl	Ar
166	194											225	227	64	166	64	225
hR9	hP2											cF4	cF8	oS8	hR3	oS8	cF4
nm	nm											nm	nm	nm	nm	nm	nm
K	Ca	Sc	Ti	V	Cr	Mn	Fe	Co	Ni	Cu	Zn	Ga	Ge	As	Se	Br	Kr
229	225	194	194	229	229	225	229	194	225	225	194	64	227	166	152	64	225
cI2	cF4	hP2	hP2	cI2	cI2	cF4	cI2	hP2	cF4	cF4	hP2	oS8	cF8	hR6	hP3	oS8	cF4
nm	nm	nm	nm	nm	afm	afm	fm	fm	fm	nm	nm	nm	nm	nm	nm	nm	nm
Rb	Sr	Y	Zr	Nb	Mo	Tc	Ru	Rh	Pd	Ag	Cd	In	Sn	Sb	Te	I	Xe
229	225	194	194	229	229	194	194	225	225	225	194	139	227	166	152	64	225
cI2	cF4	hP2	hP2	cI2	cI2	hP2	hP2	cF4	cF4	cF4	hP2	tI2	cF8	hR6	hP3	oS8	cF4
nm	nm	nm	nm	nm	nm	nm	nm	nm	nm	nm	nm	nm	nm	nm	nm	nm	nm
Cs	Ba	Lu	Hf	Ta	W	Re	Os	Ir	Pt	Au	Hg	Tl	Pb	Bi	Po	At	Rn
229	229	194	194	229	229	194	194	225	225	225	139	194	225	166	221		225
cI2	cI2	hP2	hP2	cI2	cI2	hP2	hP2	cF4	cF4	cF4	tI2	hP2	cF4	hR6	cP1		cF4
nm	nm	nm	nm	nm	nm	nm	nm	nm	nm	nm	nm	nm	nm	nm	nm		nm

Figure 4.1: In blue elements involved in the basis set optimization and in the DFT benchmark. Elemental crystal structures are represented by their space group number (top) and in the Pearson notation (middle) (with hRx standing for x atoms in the hexagonal setting of the rhombohedral unit cell). The tag on the bottom indicates the magnetic state of each elemental crystal: nm stands for nonmagnetic, fm for ferromagnetic and afm for antiferromagnetic.

The equations of state (EOS) parameters are usually obtained using a common third-order Birch-Murnaghan relation[4]:

$$E(V) = E_0 + \frac{9V_0B_0}{16}\left\{\left[\left(\frac{V_0}{V}\right)^{2/3} - 1\right]^3 B_1 + \left[\left(\frac{V_0}{V}\right)^{2/3} - 1\right]^2 \left[6 - 4\left(\frac{V_0}{V}\right)^{2/3}\right]\right\} \quad (4.1)$$

where E_0 represents the energy per atom of the compound under investigation in its ground state, i.e., at 0 K and without external stress, V is the volume and V_0 represents the equilibrium volume.

The bulk modulus is closely related to the $E(V)$ behaviour as well. It is proportional to the curvature of the equation of state at the equilibrium volume:

$$B_0 = -V\left.\frac{\partial P}{\partial V}\right|_T = V\left.\frac{\partial^2 E}{\partial V^2}\right|_T \quad (4.2)$$

It represents the resistance of the unloaded material to volume change, and hence to uniform pressure (P). Since it is linked to the curvature of the $E(V)$ relation, B_0 is a numerically sensitive quantity. A small deviation at a few data points is already able to change its value noticeably, especially when the bulk modulus is small and a narrow volume range is studied.

Consequently, B_1 can be evaluated at the equilibrium volume in the following way:

$$B_1 = \left.\frac{\partial B_0}{\partial P}\right|_T = \left.\frac{\partial}{\partial P}\left(V\frac{\partial^2 E}{\partial V^2}\right)\right|_T \tag{4.3}$$

It is a third-order derivative of the energy and hence describes effects that are one order higher even than the bulk modulus. It is related to the volume dependence of the $E(V)$ curvature and it is therefore the most sensitive quantity. In general, one can extract the equilibrium energy and EOS parameters by fitting few $E(V)$ data points to an empirical equation of state. In this specific work 7 data points were used for the fitting procedure (Fig. 4.2).

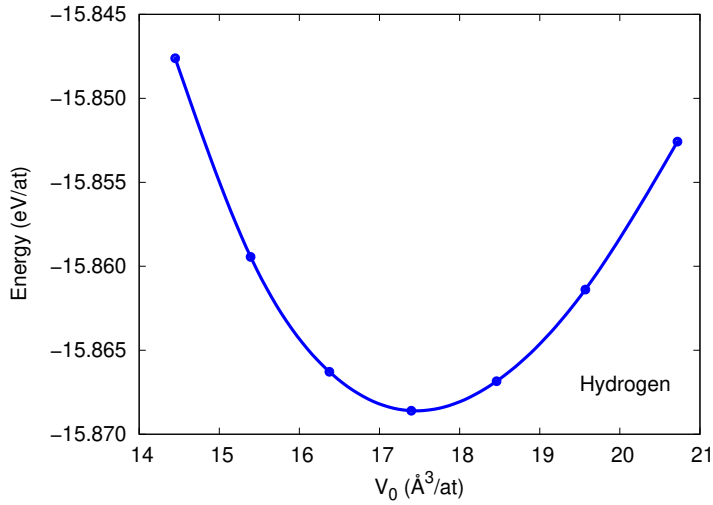

Figure 4.2: Graphical representation of the E(V) curve used for the fitting in the case of Hydrogen Elemental Solid.

In fact, for each elemental solid, 7 different inputs have been prepared, with distinct volume ($0.94 \cdot V$, $0.96 \cdot V$, $0.98 \cdot V$, V, $1.02 \cdot V$, $1.04 \cdot V$ and $1.06 \cdot V$, where V is the volume obtained with the original geometry). In particular, we multiplied the starting lattice parameters by the cubic root of the percentage (e.g. for the 94%, we multiplied the lattice parameters by $\sqrt[3]{0.94} = 0.9796$).

Then we applied the third-order Birch-Murnaghan relation and the fitting procedure described above to get V_0, B_0 and B_1. In particular, for the fitting we used a script provided by Ref. [1].

The comparison between CRYSTAL and the other codes have been performed in terms of Δ gauge. It expresses the root-mean-square difference between the equations of state of two codes a and b, that for each element i is given by the formula:

$$\Delta_i(a,b) = \sqrt{\int_{0.94V_{0,i}}^{1.06V_{0,i}} \frac{(E_{b,i}(V) - E_{a,i}(V))^2}{0.12V_{0,i}} dV} \tag{4.4}$$

where $V_{0,i}$ is the equilibrium volume, $E_{b,i}(V)$ and $E_{a,i}(V)$ are the energies calculated by performing the 7 equidistant $E(V)$ data points abovementioned.

Even in this case a script has been provided by Ref. [1].

A comparison of Δ_i values allows the expression of EOS differences as a single number, and a small Δ_i automatically implies small deviations between equilibrium volumes, bulk moduli, or any other EOS-derived observables. The overall difference Δ between methods a and b is obtained by averaging Δ_i over all elemental crystals in the benchmark set.

4.3 Results and Considerations

Many tests have been performed and three level of accuracy have been obtained at the PBE level:

- *CRYSTAL-TZ*
  Triple-ζ Basis Sets optimized by the BDIIS algorithm are used for all cases. EOS parameters and simulation set up in Table 1 of the Supplementary Material in Appendix.

- *CRYSTAL-TZ/acc*
  Triple-ζ Basis Sets optimized by the BDIIS algorithm for almost all cases excepting some basis sets that have been handly adjusted. In some particular cases (Se, Br, Sc) a full geometry optimization was mandatory to define the reference volume. EOS parameters and simulation set up are reported in Table 2 of the Supplementary Material in Appendix.

- *CRYSTAL/acc*
  Considering the previous point, we adopted larger basis sets in some critical cases (noble gases predominantly). EOS parameters and simulation set up are reported in Table 3 of the Supplementary Material in Appendix.

All the basis sets obtained and used for the calculation are listed in the Supplementary Material in Appendix. Considering the *CRYSTAL/acc* set our Δ gauge values are smaller than 1 with respect to other all electron calculations (see Table

4 in Supplementary Material in Appendix), demonstrating that CRYSTAL can reproduce non-gaussian basis sets results if rather good basis sets are used.

In Fig. 4.3 and 4.4 histograms related with our best set up (*CRYSTAL/acc*) compared with one of the references reported in the Lejaeghere's paper[1] are shown. In particular, the reference is a FP-LAPW code called WIEN2K (*WIEN2K/acc*). The error bars reported are related with the whole set of results available from other codes. Going from V_0 to B_1 we may note an increasing of uncertainty because of the wide range of results available. This implied large error bars (e.g. Fe, Mn) due to the intrinsic formula derivation of the B_0 and B_1. Nevertheless, a good agreement is obtained using the CRYSTAL code with respect with the other code. Special attention has to be taken in the case of noble gases because the model adopted enforces these elements in a condensed phase that is not always well described by solid state codes.

We do not enter here in the details of the benchmark set chosen in the work of Ref. [1]. Some of the systems, such as rare gas crystals, appear to be numerically well-defined as they are in principle not even bound at the pure PBE level. This is reflected also in the reference set by a wide spread of values and a strong dependence on computational parameters in many of the adopted codes, which we also find in our calculations. Nevertheless, we see that our results, thanks to the adoption of optimized basis sets, fits reasonably well within the picture. The optimization of basis sets was key to it, as the POB–type basis sets yielded results much less conformant to the reference data.

Starting from our best set up (*CRYSTAL/acc*), we also extended this work by using Hybrid Functional (HSE06) instead of PBE functional. In fact, with CRYSTAL and in particular with Gaussian Functions, Hybrid Functionals are easy and relatively cheap to be implemented. Even if hybrids usually increase the calculation cost, they improve the chemical accuracy (higher position in the Jacob' ladder for DFT). In Fig. 4.5 and 4.6 EOS parameters evaluated by using CRYSTAL with PBE and HSE06 functional and other codes with PBE functional are reported graphically for all the elemental solids considered. Relative differences between PBE and HSE06 are reported as well in the panel (b) of Fig. 4.6. Looking at the relative differences between functionals, while differences with respect to V_0 and B_1 are less pronounced, in some cases B_0 values deviate more. Again these problems can be traced back to the absence of a proper description of noncovalent interactions.

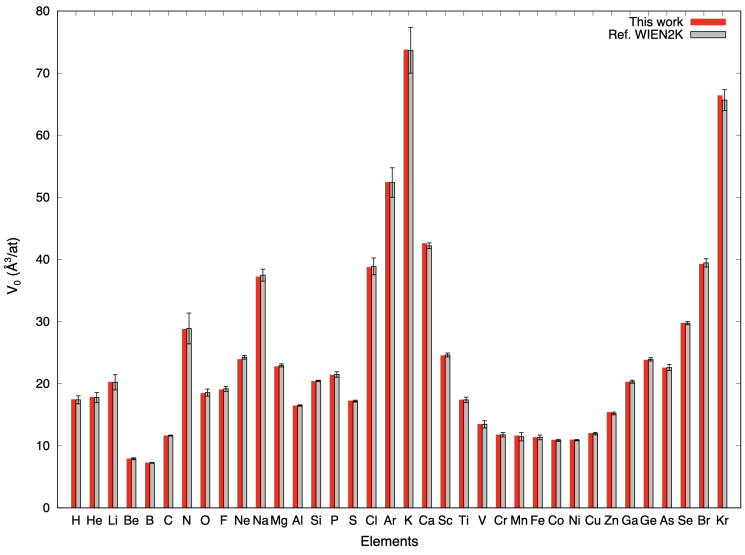

(a)

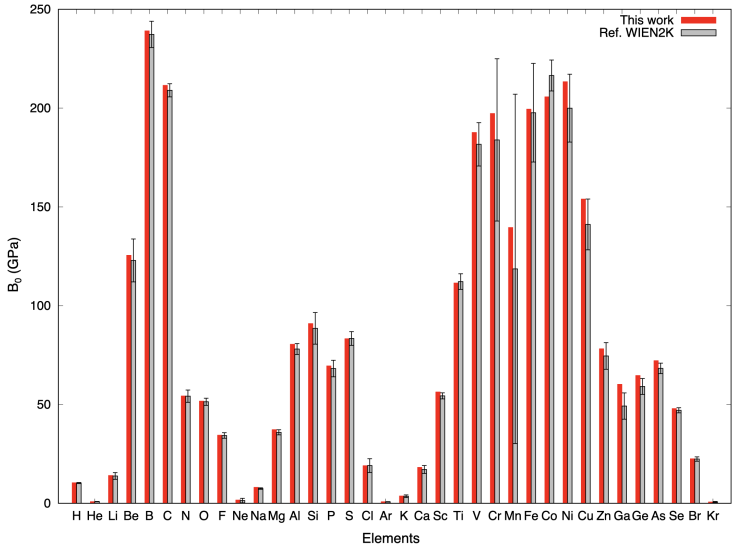

(b)

Figure 4.3: Equilibrium Volume (a), Bulk Modulus (b) and relative Error Distribution between CRYSTAL/acc PBE and WIEN2K/acc PBE from [1].

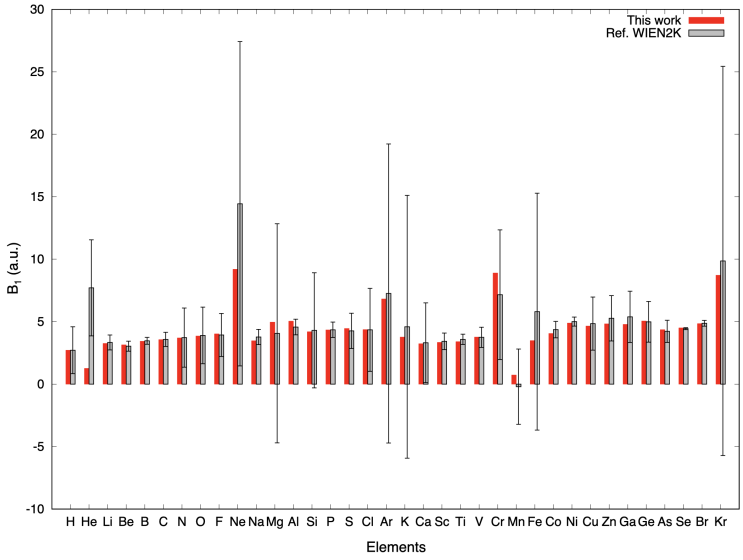

(a)

Figure 4.4: Bulk Modulus Derivative (a) and relative Error Distribution between CRYSTAL/acc PBE and WIEN2K/acc PBE from [1].

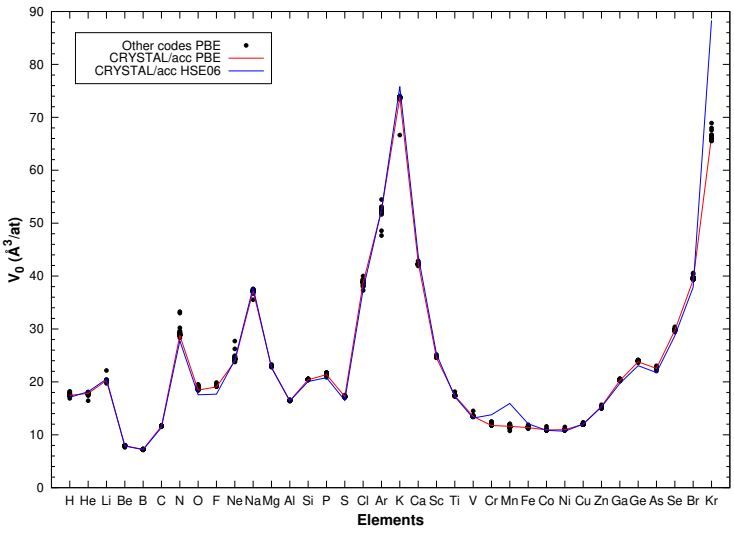

(a)

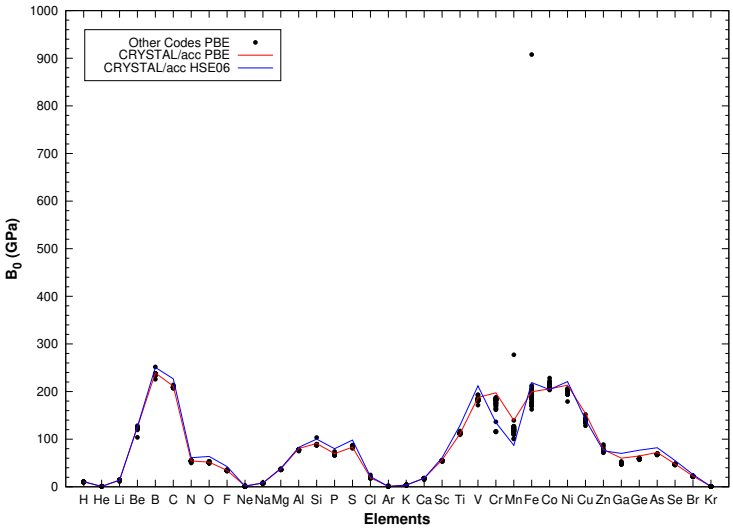

(b)

Figure 4.5: Equilibrium Volume V_0 (a), Bulk Modulus B_0 (b) comparison among CRYSTAL/acc PBE, CRYSTAL/acc HSE06 and other codes with PBE functional from Ref. [1].

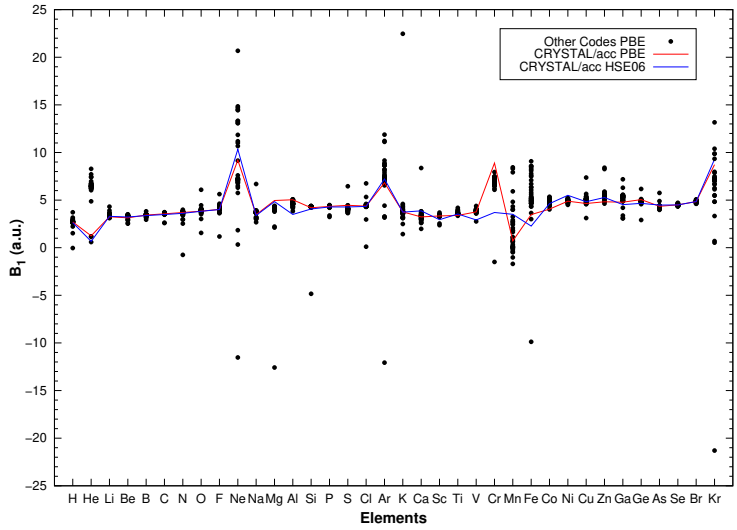

(a)

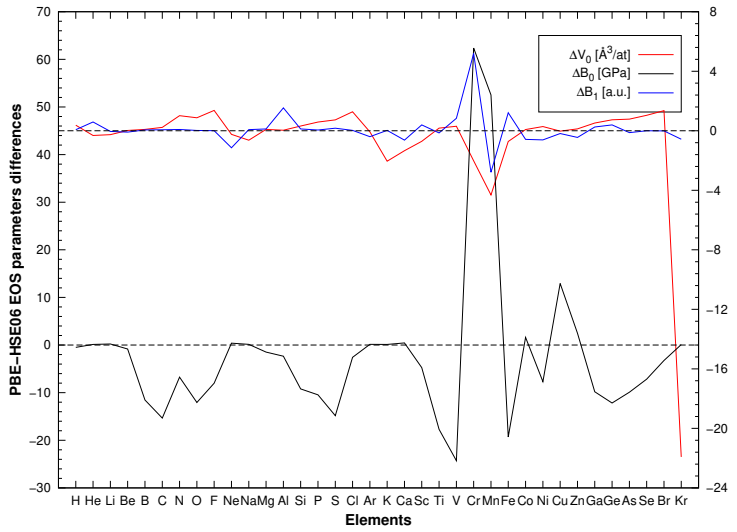

(b)

Figure 4.6: Bulk Modulus Derivative B_1 (a) comparison among CRYSTAL/acc PBE, CRYSTAL/acc HSE06 and other codes with PBE functional from Ref. [1]. A graphical representation of the relative differences between PBE and HSE06 for the set CRYSTAL/acc is reported in panel (b).

Bibliography

[1] Kurt Lejaeghere, Gustav Bihlmayer, Torbjörn Björkman, Peter Blaha, Stefan Blügel, Volker Blum, Damien Caliste, Ivano E Castelli, Stewart J Clark, Andrea Dal Corso, et al. Reproducibility in density functional theory calculations of solids. *Science*, 351(6280), 2016.

[2] Loredana Edith Daga, Bartolomeo Civalleri, and Lorenzo Maschio. Gaussian basis sets for crystalline solids: all-purpose basis set libraries vs system-specific optimizations. *Journal of Chemical Theory and Computation*, 16(4):2192–2201, 2020.

[3] R Dovesi, VR Saunders, C Roetti, R Orlando, CM Zicovich-Wilson, F Pascale, B Civalleri, K Doll, NM Harrison, IJ Bush, et al. CRYSTAL17. 2017.

[4] Kurt Lejaeghere, Veronique Van Speybroeck, Guido Van Oost, and Stefaan Cottenier. Error estimates for solid-state density-functional theory predictions: an overview by means of the ground-state elemental crystals. *Critical Reviews in Solid State and Materials Sciences*, 39(1):1–24, 2014.

Chapter 5

Direct Inversion of the Iterative Subspace for Geometry Optimization

In the first year of my PhD, I worked for a few months on a topic already developed during my master thesis: GDIIS, Direct Inversion of the Iterative Subspace for Geometry optimization. This method is the application of the DIIS (Direct Inversion of the Iterative Subspace) method to the geometry optimization. This work did not lead to a publication, as the method itself did not prove to be more effective than the geometry optimizer already in use, and the implementation did not make it to be included in the Crystal code. Nevertheless, I think it is worth here to report and document the work and efforts made in this project.

As mentioned earlier, the DIIS or Commutator-DIIS is a Self-Consistent-Field (SCF) accelerator and the algorithm itself has been extensively used in many fields. Beside the application developed in the preceding chapters about the basis set optimization, another feasible implementation is in the field of the geometry optimization.

The well known purpose of the geometry optimization is to find an atomic arrangement and the structure that corresponds to a chemically stable species. Many methods and procedures were developed and are available to users.

In CRYSTAL a quasi-Newton optimization scheme is implemented. It computes analytical gradients of the energy with respect to both cell parameters and atom coordinates and the second derivative matrix is updated by means of the BFGS (Broyden–Fletcher–Goldfarb–Shanno) algorithm. This method will be

called Regular Optimizer in the following. Nevertheless, geometry optimization and in particular the search for the absolute minimum is not a straightforward, above all in some critical cases. For this reason in this thesis we decided to study the direct inversion in the iterative subspace algorithm (DIIS) for geometry (GDIIS) and to apply it to the geometry optimization of crystals. In fact, according to available literature, for molecular systems it is quite efficient in the quadratic vicinity of a minimum and the algorithm leads to a decrease of optimization steps needed to reach convergence criteria.[1] The main work of implementation has been done during my master thesis, but throughout my PhD I had the possibility to improve the algorithm.

5.1 GDIIS Method

The DIIS method foresees the construction at each iteration of a suitable error vector and its minimization implicates the SCF convergence. Basically the error vector is related to the gradient of the electronic energy with respect to the SCF parameters. As parameters, it is customary to use the elements of the Fock matrix [2, 3], that represent the electronic gradients in the space of crystalline orbitals. Similarly, the GDIIS constructs the error vectors based on the previous geometries [1]. GDIIS is based on a linear interpolation and extrapolation of the available structures that minimizes the length of an error vector. In fact, for each structure we can construct an error vector by using a quadratic approximation to the potential energy surface. The error vector is the displacement and in a quadratic approximation it is a linear combination of individual error vectors. By solving a proper set of equations we can find all the coefficients that define the new geometry as a linear combination of previous geometries.

In mathematical terms, the method is an interpolation that allows to minimize the length of the "Average Error Vector":

$$\mathbf{r} = \sum_{i=1}^{n} c_i \mathbf{e}_i = \bar{\mathbf{e}} \tag{5.1}$$

for a geometry given by:

$$\bar{\mathbf{x}} = \sum_{i=1}^{n} c_i \mathbf{x}_i \tag{5.2}$$

and considering the following constraint:

$$\sum_{i=1}^{n} c_i = 1 \tag{5.3}$$

in which the index n coincides with the iteration number. This means in specific terms that the coefficients are obtained by the minimization of the term $|\mathbf{r}|^2$.

As for DIIS, also in this case trace is kept of previous iterations: we need to store previous positions. In fact, we can define the error vector by considering a step (Raphson Step, SR) given by:

$$\mathbf{x}_i^{SR} = \mathbf{x}_i + \mathbf{H}^{-1}\mathbf{f}_i \tag{5.4}$$

where $\mathbf{H^{-1}}$ is the inverse of the Hessian and $\mathbf{f_i}$ are gradients with opposite sign, in other words the force acting on the position $\mathbf{x_i}$. In this way the error vector can be defined by:

$$\mathbf{e}_i = \mathbf{x}_i^{SR} - \mathbf{x}_i = \mathbf{H}^{-1}\mathbf{f}_i \tag{5.5}$$

At this point the problem turns into a simple solution of a set of linear equations:

$$\begin{pmatrix} a_{1,1} & \dots & a_{1,n} & 1 \\ \vdots & \ddots & \vdots & \vdots \\ a_{n,1} & \dots & a_{n,n} & 1 \\ 1 & \dots & 1 & 0 \end{pmatrix} \begin{pmatrix} c_1 \\ \vdots \\ c_n \\ \lambda \end{pmatrix} = \begin{pmatrix} 0 \\ \vdots \\ 0 \\ 1 \end{pmatrix} \tag{5.6}$$

in which the elements a_{ij} are defined as a scalar product $e_i^T e_j$ and λ is the Lagrangian multiplier.

Once obtained the coefficients, it is easy to construct $\bar{\mathbf{x}}$ and consequently the new geometry:

$$\mathbf{x}_{n+1} = \bar{\mathbf{x}} + \mathbf{r} = \sum_{i=1}^{n} c_i(\mathbf{x}_i + \mathbf{e}_i) = \sum_{i=1}^{n} c_i \mathbf{x}_i^{SR} \tag{5.7}$$

Again as in DIIS method the new geometry is the result of the linear combination of previous points. In particular, in our work the information that we extrapolated from the equation (5.7) is the step, in other words the difference between the new point and the previous one.

In literature many studies show that the efficiency of GDIIS is similar to, or sometimes better than Newton Raphson method. Therefore, it seems to be very suited for flat PESs, thus when one or more Hessian eigenvalues are small. [4]

5.2 Results and Considerations

In order to verify the efficiency of the implementation many tests were performed on both molecular and crystalline structures. The efficiency of the algorithm was evaluated by using the following criteria:

- Number of steps needed for the minimum identification;
- Identification of the absolute minimum;
- The affinity between the minimum found and the minimum expected.

Concerning the set of *Molecular systems* we used the *Baker's test* [5] that consists in thirty small to medium molecules covering a wide range of symmetries and structural properties. As regards *Periodic systems* we performed a systematic set of tests on the dataset proposed by Civalleri et al. [6] composed by twenty systems (named "C20 set") with the addition of sodium nitrite and five periodic systems based on simple molecules (named "Simple solids"): ammonia, carbon dioxide, urea, benzene and the diamond crystal. In particular, the "C20 set" is characterized by different periodicity: polymers (1D), slabs (2D) and crystals (3D). Moreover, in order to be more systematic each periodic system is characterized by a different structure and symmetry. Finally, three systems of remarkable complexity were tested: Zeolite Silicalite (MFI), Amorphous Silica and a slab model (2D) of an organo-silica material (named "Complex solids").

In all the systems listed above we systematically tried some options of the GDIIS algorithm and the best operative condition for the algorithm was defined:

- Starting cycle for GDIIS computation: 2^{nd};
- Number of previous steps stored: 6;
- Hessian update operative;
- Tolerance change in removing linear dependence in GDIIS matrices (Matrix Size Reduction) with condition number 10^{-3}. (See Section 3.1.1 for details about the method)

In general, GDIIS showed performances similar to the Regular CRYSTAL optimizer and high versatility. The test performed demonstrated the high applicability of the method and the possibility to modify the options in order to get the best results for each chemical system above all in critical cases. In Fig.5.1 is reported a histogram that compares results obtained from different chemical systems.

In order to improve the algorithm implemented, we decided to resume the subject. From a technical point of view, we tried to recode the algorithm from

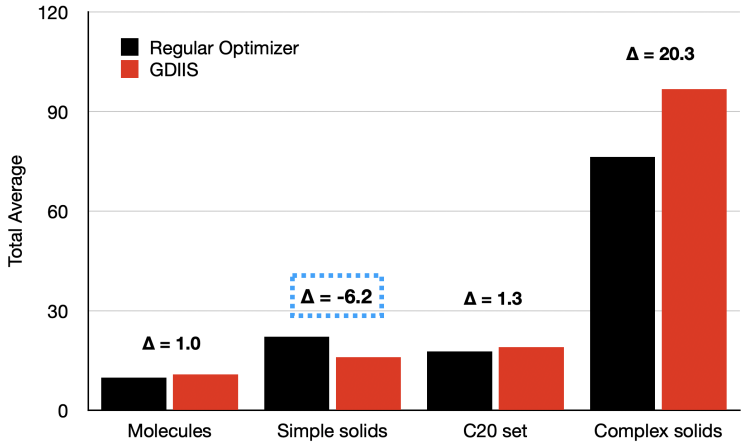

Figure 5.1: Total average comparison among different systems analysed by the regular optimizer and the GDIIS one. The total average is the sum of the overall number of cycles divided by the number of chemical structures studied. In particular, if a chemical system does not converge it is not considered in the evaluation.

scratch. This procedure was for us essential in order to remove some spurious effects. In fact, we tried to minimize the code intervention on the regular optimizer and the last version of the CRYSTAL code was used.

Even if no remarkable enhancement have been found, a better stability of the algorithm can be seen. In the Fig.5.2, a comparison between the old version and the new version of the algorithm is reported. Specifically, the energy is plotted with respect to the number of cycles for a molecular system (ACHTAR10). The new version displays a good behaviour above all at the beginning of the calculation.

Although the GDIIS algorithm demonstrates to be rather competitive with the regular optimizer in CRYSTAL, it does not show better performances except for few cases. It is possible that further improvements of the algorithm can be done, but till now no significant acceleration in terms of time and optimization cycles was observed with respect to the 'standard' geometry optimizer.

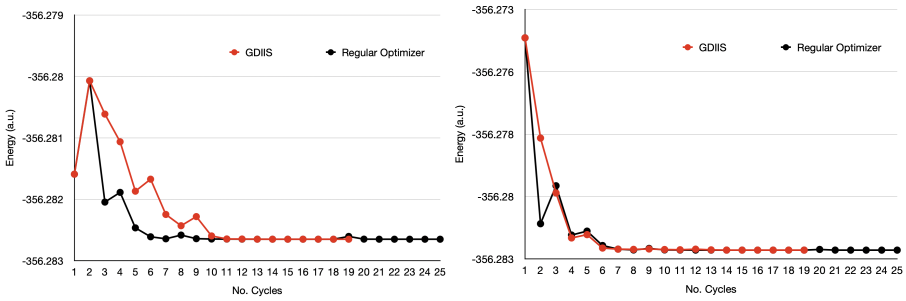

(a) (b)

Figure 5.2: Energy behaviour during regular optimization and GDIIS one for the molecular system ACHTAR10, old (a) and new (b) version.

Bibliography

[1] Pál Császár and Péter Pulay. Geometry optimization by direct inversion in the iterative subspace. *Journal of Molecular Structure*, 114:31–34, 1984.

[2] Péter Pulay. Convergence acceleration of iterative sequences. the case of SCF iteration. *Chemical Physics Letters*, 73(2):393–398, 1980.

[3] Peter Pulay. Improved SCF convergence acceleration. *Journal of Computational Chemistry*, 3(4):556–560, 1982.

[4] Ödön Farkas and H Bernhard Schlegel. Methods for optimizing large molecules. part III. an improved algorithm for geometry optimization using direct inversion in the iterative subspace (GDIIS). *Physical Chemistry Chemical Physics*, 4(1):11–15, 2002.

[5] Jon Baker. Techniques for geometry optimization: a comparison of cartesian and natural internal coordinates. *Journal of Computational Chemistry*, 14(9):1085–1100, 1993.

[6] Bartolomeo Civalleri, Ph D'Arco, Roberto Orlando, VR Saunders, and Roberto Dovesi. Hartree–Fock geometry optimisation of periodic systems with the CRYSTAL code. *Chemical Physics Letters*, 348(1-2):131–138, 2001.

Chapter 6

Maximum Overlap Method

Whereas ground state calculations and equilibrium properties are widespread methods (HF and DFT[1, 2]), the study of excited states is not as straightforward, and this is due to many reasons. First of all, the single-determinant approach is generally not as good as for the ground state, and secondly, a black-box approach is difficult, work and understanding from the side of the researcher are required. Many multi-determinantal approaches have been developed: Multi Reference Configuration Interaction (MRCI)[3], Multi Reference Møller - Plesset Perturbation theory (MRMP)[4], Configuration Interaction Single-excitation (CIS) and with perturbative treatment of doubles (CIS(D))[5], Time Dependent DFT (TD-DFT)[6], many - body Green's functions methods (GW)[7] and many others. The choice can be convoluted and, even if these methods are accurate, computationally they are notably expensive and applications are restricted to atoms, molecules and clusters.

In the search for simpler and more applicable methods, direct generalizations of the ground state method have been developed, such as ΔSCF[8, 9, 10] where, instead of having all electrons in the lowest orbitals, one or more electrons are placed in higher lying Kohn-Sham orbitals, and excitation energies are obtained as the difference between the ground and excited state scf. One of the main drawbacks of this procedure is the possible numerical instability that usually hinders the convergence to a specific excited state, also because of the somewhat intrinsic multideterminantal character of excited states. An attempt to avoid the intrinsic variational collapse of the minimization procedure has been proposed by Gilbert et al.[11] that developed a method to keep track of the occupation during the SCF named Maximum Overlap Method (MOM). The general purpose is to get solutions of the SCF equation with the highest energy considering excited state and ground state with almost the same approach.

In this work of thesis we have implemented in the CRYSTAL code this simple technique to enforce orbital occupations, bypassing the "natural" occupation dictated by the Aufbau principle. In fact, during the SCF iterations the algorithm tries to maximize the overlap between the occupied orbitals with those of the preceding iteration or of a reference state. This procedure leads the SCF towards excited state solutions instead of ground state ones, or can be useful in order to stabilize the ground state solution preventing the intrusion of unphysical states in the density matrix. Promoting an electron from an occupied to a virtual orbital is then a sufficient guess to start an SCF calculation with MOM. In fact, the algorithm will keep the excited configuration. In this way excited states can be studied at the Hartree-Fock (HF) or DFT level at the cost of a ground–state calculation and with the same computational scalability.

The development and implementation of the MOM method is fully described in the attached submitted paper "Electronic Excitations in Crystalline Solids through the Maximum Overlap Method" (Appendix 12.3). In this chapter the basics of the method will be presented in a concise form. Some documentation of the code will be reported along with discussion on the input/output structure in Appendix 11.

6.1 Maximum Overlap Method Implementation

As mentioned in the introduction, the Maximum Overlap Method can be useful in different application:

- study excitation energies
- optimize geometry of excited states (luminescence)
- stabilize the ground state solution, preventing the intrusion of unphysical states (due to numerical issues)

and we tried to implement the algorithm in the CRYSTAL code for solid state calculation. Although in solids more than in the molecular case, there is a large variety of possible electronic excitations, we focus on two types of excitation:

- excitation in Γ-point only
- band to band excitation

The initial guess is obtained by performing a preliminary ground state calculation and then pushing electrons from occupied to virtual orbitals. MOM is used to keep track of a desired state during the SCF procedure.

6.1.1 Details of the Implementation

The MOM method acts on the definition of the occupation matrix $n(\mathbf{k})$ of the density matrix in the Hartree-Fock/Kohn Sham equations. Starting from a reference solution $C^{ref}(\mathbf{k})$, which can be either from the converged ground state, or an initial guess, firstly the eigenvectors are sorted by energy and the code overrides the Aufbau principle by forcing a different occupation pattern $n^{ref}(\mathbf{k})$.

In subsequent iterations, the overlap between the new coefficients and the reference ones C^{ref} is evaluated

$$O(\mathbf{k}) = C^{ref\,\dagger}(\mathbf{k})\, S(\mathbf{k})\, C(\mathbf{k}) \tag{6.1}$$

The projection of the j-th new orbital onto the old occupied space is the expressed by:

$$p_j(\mathbf{k}) = \sum_i^n O_{ij}(\mathbf{k}) = \sum_\nu^N \left[\sum_\mu^N \left(\sum_i^n C_{i\mu}^{ref}(\mathbf{k}) \right)^\dagger S_{\mu\nu}(\mathbf{k})\, C_{\nu j}(\mathbf{k}) \right] \tag{6.2}$$

For each nonzero diagonal element in $n^{ref}(\mathbf{k})$ the largest corresponding projection $p(\mathbf{k})$ locates the position to be filled in the new $n(\mathbf{k})$.

The evaluation of $O(\mathbf{k})$ as in Eq. (6.1) is relatively inexpensive, hence the additional cost of the MOM procedure is virtually negligible with respect to that of the corresponding ground-state method (i.e., HF and DFT), even though convergence can turn out to be more difficult.

Depending on the definition of $n^{ref}(\mathbf{k})$ MOM can then be used to converge the SCF towards solutions different from the ground state. This will be the use of MOM we will focus on in the following.

Two kinds of excitation have been implemented:

- *Excitation from a single k point to another*
  Since the direct space density matrix must keep the translational invariance in the SCF procedure only excitations that are totally symmetric with respect to the group of lattice translation vectors are possible within our approach. Namely, only vertical excitations at the center of the Brillouin zone (Γ-point only) or by constructing a supercell other excitations are possible. In particular, by increasing the size of the periodically repeating unit in the direct space the reciprocal space folds in itself making accessible other transitions. In Fig. 6.1 the abovementioned excitation in the Γ point along with the band structure folding is reported for Bulk Silicon.

- *Band to band excitation*
  A portion of the corresponding valence and conduction bands corresponding to a sphere of radius $\mathbf{r}$ around Γ can be involved in the excitation.

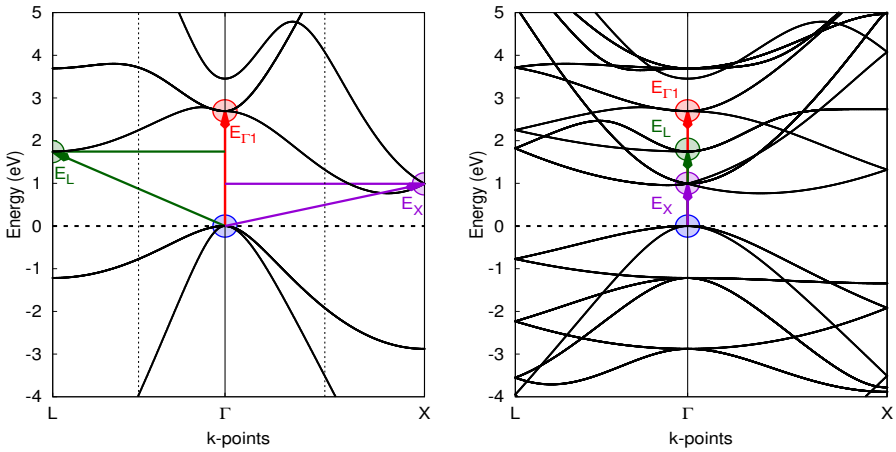

Figure 6.1: A graphical representation of some possible electronic excitations – labeled as $E_{\Gamma 1}$, E_X, E_L, in the electronic structure of bulk silicon (PBE functional). Left panel: primitive unit cell. Right panel: 2x2x2 supercell. Upon folding of the bands in the supercell creation, the excitations $E_{\Gamma 1}$, E_X, E_L become all Γ–point only excitations. The lines along which the band structure is folded are marked by black dashed vertical lines in the left panel.

This process can physically correspond to a light which is not precisely monochromatic used to induce the excitation.

Such approach is graphically described in Figure 6.2.

As a first step, when defining the initial reference excited state we need to trace the involved bands across the Brillouin zone, to cope with possible band crossings and degeneracies. In this regard, we have to evaluate the overlap $O_{\mathbf{k},\mathbf{k}'}$ between the band eigenvectors in two neighbouring points $\mathbf{k}$ and $\mathbf{k}'$, expressed as:

$$O_{\mathbf{k},\mathbf{k}'} = (C(\mathbf{k}'))^{\dagger} S(\mathbf{k}) C(\mathbf{k}) \tag{6.3}$$

The largest overlap elements allow to trace the bands between $\mathbf{k}$ and $\mathbf{k}'$. Since we start from a Γ-point excitation, we follow a path in reciprocal space as depicted in the right panel of Fig. (6.2). Moreover, it is possible to define a sphere where only a number $N_{\mathbf{k}}^{exc}$ of k points are involved in the excitation itself.

The excitation energy in both cases can be evaluated as:

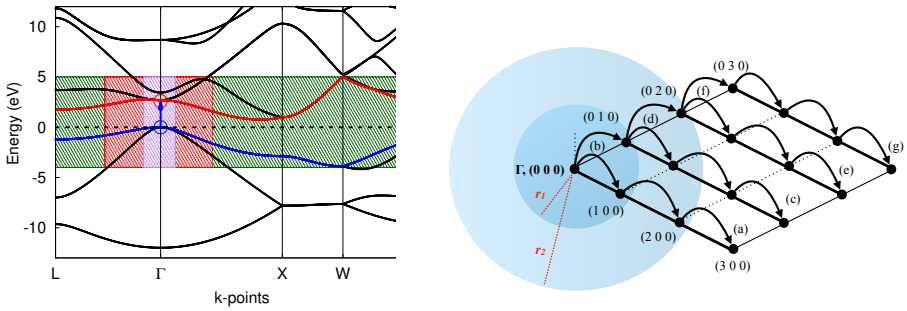

Figure 6.2: On the left an excitation in Si bulk (PBE functional) in which the radial-sphere approach is graphically represented. On the right, the path in a 2D Brillouin zone followed to trace the Γ-point bands and the spheres around Γ are represented.

$$E^{exc} = \frac{N_{\mathbf{k}}}{N_{\mathbf{k}}^{exc}} \left(E_{\uparrow}^{tot} - E_{ground}^{tot} \right) \tag{6.4}$$

where we have denoted as $E_{\uparrow}^{tot}$ the energy obtained through the excitation, E_{ground}^{tot} the ground state energy, $N_{\mathbf{k}}$ and $N_{\mathbf{k}}^{exc}$ are the k points sampling the 1^{st} Brillouin zone and the k points involved in the excitation respectively ($N_{\mathbf{k}}^{exc} = 1$ for k to k excitation, $N_{\mathbf{k}}^{exc} \neq 1$ for the band to band excitation). A more detailed description of the theory is available in the paper in Appendix 12.3.

Energy Gradients and Geometry Optimization

The energy gradients must be computed, in the $\Gamma-$only excitation scheme, by summing back the energy of the ground state to the excitation energy of Eq. (6.4) and then taking the derivative with respect to atomic displacements

$$\frac{\partial E_{\uparrow}}{\partial \mathcal{R}_a^A} = \frac{\partial E_{\uparrow}^{tot}}{\partial \mathcal{R}_a^A} N_{\mathbf{k}} - \frac{\partial E_{ground}^{tot}}{\partial \mathcal{R}_a^A} \left(N_{\mathbf{k}} - 1 \right) \tag{6.5}$$

where $\mathcal{R}_a^A$ is the coordinate of atom A along a general cartesian direction a. Analogous equations hold for cell gradients. Moreover, during a geometry optimization procedure, at each geometry the ground and excited state gradients are required for the evaluation of Eq. (6.5), thus requiring a double SCF procedure.

For a more detailed description of the mathematical approach and the validation tests performed the reader should refer to the paper reported in Appendix.

6.2 Results and Considerations

In the paper in Appendix validation tests and results are reported in details. In fact, the features and performance of the method are presented through its application to prototypical solids such as bulk silicon, diamond and lithium fluoride, and comparing the results to available experimental data. Moreover, two demonstrative applications to nickel oxide and solid CuI(piperazine) highlight the promising potential of the MOM method in solid state quantum chemistry. The first was used as a prototypical system that lends itself well to the validation of our geometry optimization algorithm. In Figure 6.3 we compare the result of the optimization with the potential energy curves obtained through single point calculations, which clearly shows that our MOM algorithm correctly finds the right minimum of the excited state curve.

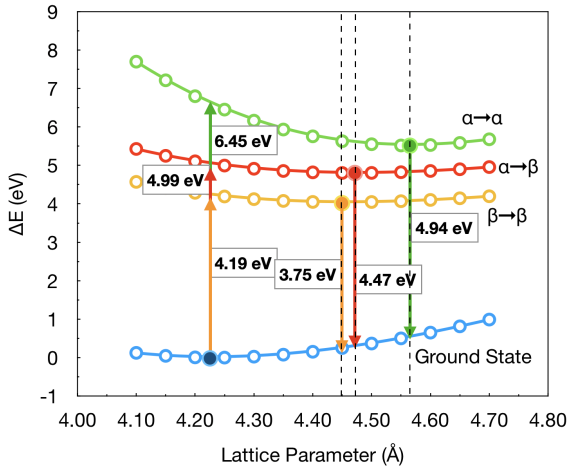

Figure 6.3: Energy of the ground and first excited states of bulk ferromagnetic NiO as a function of lattice parameter. The ground state minimum is taken as a reference ($\Delta E = 0$). B3LYP Functional was used. The full bullets mark the results of the geometry optimizations using analytical gradients as in Eq. (6.5).

Among the luminescent copper(I) halides, CuI(piperazine) is a peculiar compound that exhibits a dual luminescence, a feature that is of potential relevance in technological applications. We were able to reproduce this effect applying our MOM geometry optimizer to this structure. We considered two excitations around the Fermi level, namely HOMO→LUMO and HOMO-1→LUMO+1, in Γ-point only (HOMO (highest occupied molecular orbital) and LUMO (lowest

unoccupied molecular orbital)). In Figure 6.4 energy levels and atomic structure optimized after electronic excitation are reported.

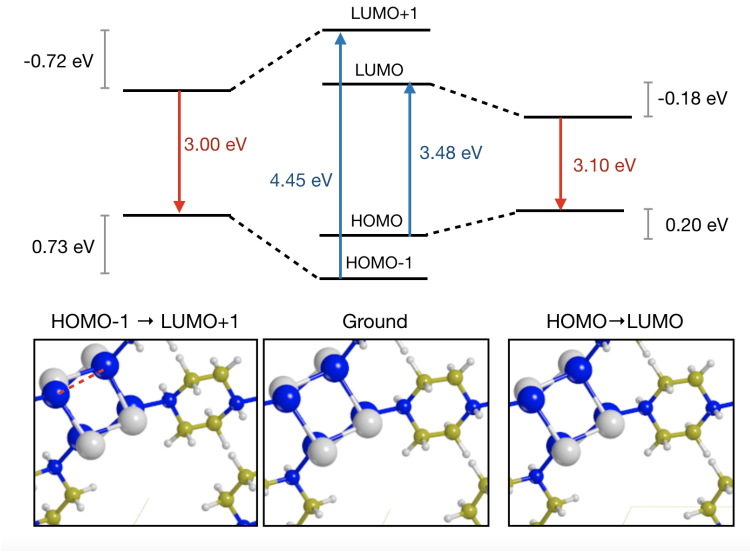

Figure 6.4: Energy levels and atomic structure of solid CuI-piperazine around the Fermi level at the ground state geometry (center), and at the geometries optimized after an HOMO→LUMO (right) and HOMO-1→LUMO+1 (left) electronic excitation.

A more detailed description of the results is available in the paper in Appendix.

6.3 Maximum Overlap Method Code Development

The MOM method has been imported in the CRYSTAL code exploiting the current SCF implementation. Due to the wide scattered intervention of the method in the code, a flowchart regarding the SCF calculation and the files involved is reported in Fig. 6.5. In fact, beside the common SCF procedure, in the MOM method two additional steps are present: the eigenvectors storage that is essential for the O matrix construction (see Equ. 6.1) and the change in the occupation to actually perform the excitation.

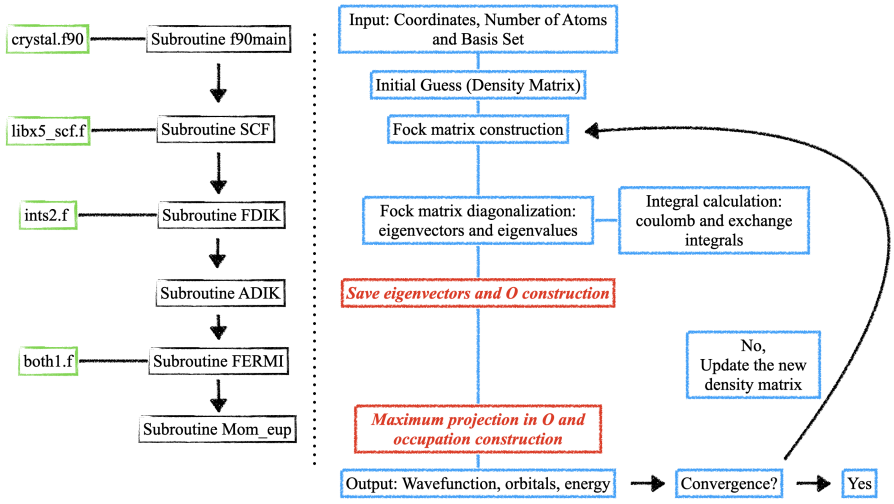

Figure 6.5: Flowchart reporting SCF main steps (blue boxes) and MOM interventions (red boxes) along with the files (green boxes) and routines names involved (black boxes). Variables and many parameters are saved in the `Module mom_module` in `mom_module.f90` file.

Bibliography

[1] Pierre Hohenberg and Walter Kohn. Inhomogeneous electron gas. *Physical Review*, 136(3B):B864, 1964.

[2] Walter Kohn and Lu Jeu Sham. Self-consistent equations including exchange and correlation effects. *Physical Review*, 140(4A):A1133, 1965.

[3] Trygve Helgaker, Poul Jorgensen, and Jeppe Olsen. *Molecular electronic-structure theory*. John Wiley & Sons, 2014.

[4] K Hirao. Multireference Møller—Plesset method. *Chemical Physics Letters*, 190(3-4):374–380, 1992.

[5] James B Foresman, Martin Head-Gordon, John A Pople, and Michael J Frisch. Toward a systematic molecular orbital theory for excited states. *The Journal of Physical Chemistry*, 96(1):135–149, 1992.

[6] Erich Runge and Eberhard KU Gross. Density-functional theory for time-dependent systems. *Physical Review Letters*, 52(12):997, 1984.

[7] Lars Hedin. New method for calculating the one-particle Green's function with application to the electron-gas problem. *Physical Review*, 139(3A):A796, 1965.

[8] Robert O Jones and Olle Gunnarsson. The density functional formalism, its applications and prospects. *Reviews of Modern Physics*, 61(3):689, 1989.

[9] Anders Hellman, Behrooz Razaznejad, and Bengt I Lundqvist. Potential-energy surfaces for excited states in extended systems. *The Journal of Chemical Physics*, 120(10):4593–4602, 2004.

[10] Jeppe Gavnholt, Thomas Olsen, Mads Engelund, and Jakob Schiøtz. δ self-consistent field method to obtain potential energy surfaces of excited molecules on surfaces. *Physical Review B*, 78(7):075441, 2008.

[11] Andrew TB Gilbert, Nicholas A Besley, and Peter MW Gill. Self-consistent field calculations of excited states using the maximum overlap method (MOM). *The Journal of Physical Chemistry A*, 112(50):13164–13171, 2008.

Part II

Thermoelectric Materials

Chapter 7

Defects and Electron Transport in Half Heusler Alloys

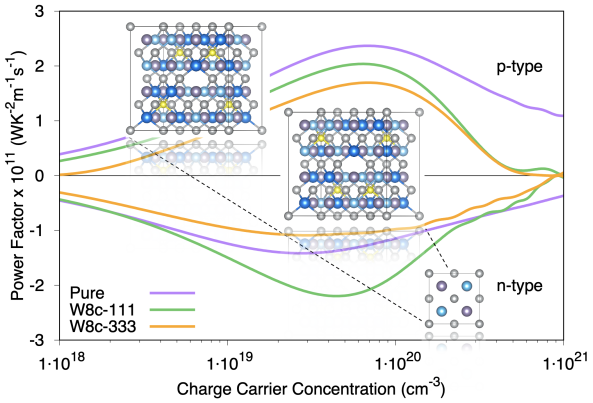

The modern world sees an ever-increasing demand for energy due to population growth and industrial advancements. The majority of our energy still comes from fossil fuel combustion that is converted to electricity. A secondary product of any combustion process is the generation of waste heat: finding ways to harvest the waste heat has become a major challenge and an answer is found by use of technologies like thermoelectrics (TE) energy conversion.

TE materials can convert waste heat directly to electricity and pave a way

to reduce greenhouse gas emissions and promote sustainable development. In the current scientific discussions about TE materials, the role of defects is a key aspect in defining their TE efficiency. Defects are present in significant concentration in real samples; a deep understanding of their role in altering the electronic properties of a material is fundamental to tailor new and more efficient TE materials.

Commercial TE devices are currently based on $(Bi,Sb)_2Te_3$, skutterudites (e.g. $CoAs_3$) and silicides. However, all these materials have a major drawback. $(Bi,Sb)_2Te_3$ works in a temperature range 300 - 500 K, which is too low for heat harvesting in high temperature applications (e.g. automotive, steel plants). The use of tellurium TE is environmentally critical. Skutterudites and silicides work at higher temperature with respect to $(Bi,Sb)_2Te_3$, but show low resistance to oxidation so that they need to be encapsulated in inert atmosphere for long lasting applications. Thus, one of the most promising TE system is represented by the Half Heusler (HH) compounds because of their chemical and mechanical stability, easy processing and tunable transport properties.

In this view, ab initio calculations can play a fundamental role in understanding and decoupling the many effects such diverse types of structure can have on the underlying physics of the materials, as well as providing a mean for predicting behaviour of new compounds. In particular, thermoelectric properties can be simulated and nowadays it is a fundamental tool. Of course, obtaining a rather good description of the thermoelectric properties is obtained if the electronic structure is good as well. In this regards, the basis set optimization implemented played a fundamental role.

Our scientific challenges of the problem was to explore TE properties of some HH alloys (ABX crystal structure , $F\bar{4}3m$ (No.216)) – TiMSn (M=Ni,Pd,Pt); TaM'Sn (M'=Co,Rh,Ir) - and the influence of interstitial atoms and vacancies in the HH structure. In general, the crystal structure can be thought to be composed as a fusion of rock-salt type and zinc-blende forms (see Figure 7.1).

The TE performance is based on their Seebeck (S) coefficient, electrical conductivity (σ), electrical contribution to the total thermal conductivity (κ_{el}) and, consequently, the power factor (product of electrical conductivity and Seebeck coefficient squared, PF). Moreover, we considered some examples of point defect that is expected to enhance the TE performance. In fact, point defects in HH alloys have a strong impact on the whole band structure and consequently on transport properties.

Usually the alliance of theoretical modelling and the experimental characterization is not easy: in fact, experimentally is extremely difficult to fully characterize types and amount of defects in real systems, while computationally, realistic models that integrate defects are difficult to mimic. Thus good reproducibility is possible only with a realistic model. However, these models imply the in-

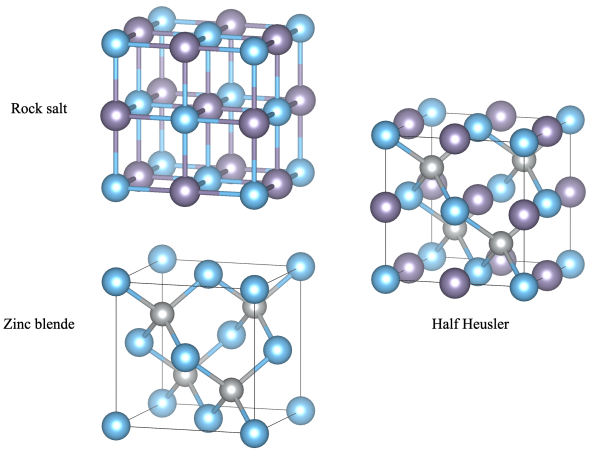

Figure 7.1: Crystal structure of a typical HH alloy as a fusion of rock-salt type and zinc-blende forms. Blue, purple and grey spheres denote Ti, Sn and Ni atoms respectively.

troduction of supercell, which required significant amount of CPU-hours, would was feasible with the use of high performance computing, obtained by the HPC-Europe project in Finland.

-Published paper: "Key Role of Defects in Thermoelectric Performance of TiMSn (M=Ni, Pd, and Pt) Half-Heusler Alloys" [1], reported along with the supplementary material in Appendix 12.2 of this thesis.

7.1 Transport Properties in CRYSTAL

Most existing solid state ab initio codes available today do not possess a comprehensive set of tools for the study of TEs, and rely on external programs such as BoltzTrap[2] and BoltzWann[3]. As a consequence, quantities such as band velocities or third-order force constants (which involve derivatives of electronic and phonon bands, respectively) can be computed only numerically within that approach, with high computational costs and evident accuracy-stability problems. In addition, many studies found in literature not even adopt such approaches, but just analyze band structures and density of states, to yield qualitative or semi-quantitative considerations with limited validity. In particular, BoltzTrap[2] relies on a Fourier expansion of the band energies and differentiates numerically. BoltzWann[3] exploits a maximally localized Wannier function basis and, after lo-

calization, the band derivatives are evaluated analytically at each k point. Moreover, hybrid functionals (that contain a fraction of Hartree-Fock exact exchange) are known to outperform other functionals in the description of band-gap related quantities, as well as phononic bands. Nevertheless, the use of such functionals in the most commonly used plane-wave codes is prohibitive, due to the very high computational costs. The atomic-centered local basis used in CRYSTAL allows for an easy use of hybrid functionals.

Thus the advantages of our approach are:

- *CRYSTAL performs directly the thermoelectric properties*
  It is possible to perform calculations in a single ab initio code without transferability issues and without using external programs for properties. The current benchmark is to use a plane-wave code like VASP/Quantum Espresso/etc for electronic structure calculations, BoltzTrap[2]/BoltzWann[3] for TE properties and Phonopy[4]/Phono3py[5] for computation of force constants.

- *Hybrid Functionals*
  Implementation of hybrid functionals that are free of self-interaction errors and define the physics of these HH semiconductors better.

considering few drawbacks:

- *No spin orbit coupling available*
  The band gap of some the HH alloys to be investigated might depend on the spin-orbit coupling (SOC) due to relativistic effects. SOC is still not implemented in CRYSTAL.

- *Frozen Band Approximation and Constant Relaxation Time Approximation*
  Two are the main approximation for the solution of the Boltzmann Transport Equation: Frozen Band Approximation and Constant Relaxation Time Approximation (RTA). The first approximation implies no changes or variation in the band structure in relation to temperature changes. The latter implies a lifetime τ to be not dependent on k. For a more accurate description of carrier lifetimes, the electron-phonon coupling and phonon-phonon coupling is necessary. Unfortunately these aspects are still under development within the CRYSTAL code.

7.1.1 Transport Properties: semi-classical Boltzmann theory

A meaningful quantity in the thermoelectric field that can be evaluated by the CRYSTAL code is the *Figure of Merit*:

$$ZT = \frac{\sigma S^2 T}{\kappa} \tag{7.1}$$

where T is the Temperature, σ is the electrical conductivity, S is the Seebeck coefficient (charge average entropy, $\Delta V = S\Delta T$), σS^2 is commonly named as the Power Factor (PF) and κ is the thermal conductivity ($\kappa_p + \kappa_{el}$ = phononic+ electronic contribution).

When the Power Factor is large there is an efficient conversion of heat into electricity and a small κ keeps a temperature gradient and reduces conduction heat losses. A desirable ZT value is at least 1 and ideally $ZT > 2$. In fact, high S, high σ but low κ can give an ideal thermoelectric material.

Historically the thermoelectric processes were studied by Onsager and Callen[6, 7] in the first half of the XXth century, in the framework of the thermodynamics of dissipative system. In their model, current densities can be expressed as

$$\begin{bmatrix} \mathbf{J}_E \\ \mathbf{J}_Q \end{bmatrix} = \begin{bmatrix} \boldsymbol{\sigma} & \boldsymbol{\sigma}\mathbf{S} \\ \mathbf{T}\boldsymbol{\sigma}\mathbf{S} & \boldsymbol{\kappa}_{el} \end{bmatrix} \begin{bmatrix} -\boldsymbol{\nabla} V \\ -\boldsymbol{\nabla} T \end{bmatrix} \tag{7.2}$$

where
J_E = electrical current density
J_Q = heat current density
σ = electrical conductivity
S = Seebeck coefficient
T = Temperature
V = Electric potential
κ_{el}= Electronic contribution to the thermal conductivity

in which the first vector is related with the current density, the second matrix is correlated with the transport coefficients and the last one represents the forces.

This equation can provide the expressions of the three so-called *Transport Coefficients*:

Electrical Conductivity

$$[\sigma]_{qr}(\mu, T) = \int dE \left(-\frac{\partial\, f_0}{\partial E} \right) \Xi_{qr}(E) \tag{7.3}$$

Seebeck Coefficient

$$[\sigma\mathbf{S}]_{qr}(\mu, T) = \frac{1}{T} \int dE \left(-\frac{\partial\, f_0}{\partial E} \right) (E - \mu) \Xi_{qr}(E) \tag{7.4}$$

and Thermal Conductivity

$$[\kappa_{el}]_{qr}(\mu, T) = \frac{1}{T}\int dE \left(-\frac{\partial\ f_0}{\partial E}\right)(E-\mu)^2 \Xi_{qr}(E) \tag{7.5}$$

considering μ as the chemical potential, E as the energy and f_0 as the Fermi-Dirac distribution. $\Xi_{qr}(E)$ is the transport distribution function (TDF), the core of the transport coefficients and it is defined as

$$\Xi_{qr}(E) = \tau \sum_{\mathbf{k}} \frac{1}{N_{\mathbf{k}}} \sum_{i} \nu_{i,q}(\mathbf{k})\nu_{i,r}(\mathbf{k})\delta(E - E_i(\mathbf{k})) \tag{7.6}$$

where $\nu_{i,q}$ is the velocity of the i-th band calculated along the direction q and τ is the lifetime which is not dependent on k according to the constant relaxation time approximation.

The expression of the band velocities is

$$\nu_{i,q}(\mathbf{k}) = \frac{\partial E_i(\mathbf{k})}{\partial k_q} \tag{7.7}$$

and since CRYSTAL uses Gaussian-Type basis set, thus local functions as linear combination of Gaussian type functions (GTF), it is rather trivial to obtain the k-vector derivative of both the Fock (F) and overlap (S) matrices:

$$\mathbf{F}(\mathbf{k}) = \sum_{\mathbf{g}} \mathbf{F}(\mathbf{g}) e^{i\mathbf{k}\cdot\mathbf{g}}, \frac{\partial \mathbf{F}(\mathbf{k})}{\partial k_q} = \sum_{\mathbf{g}} i g_q \mathbf{F}(\mathbf{g}) e^{i\mathbf{k}\cdot\mathbf{g}} \tag{7.8}$$

$$\mathbf{S}(\mathbf{k}) = \sum_{\mathbf{g}} \mathbf{S}(\mathbf{g}) e^{i\mathbf{k}\cdot\mathbf{g}}, \frac{\partial \mathbf{S}(\mathbf{k})}{\partial k_q} = \sum_{\mathbf{g}} i g_q \mathbf{S}(\mathbf{g}) e^{i\mathbf{k}\cdot\mathbf{g}} \tag{7.9}$$

where g is the direct lattice vector, k is the reciprocal lattice vector.

With this knowledge it is possible to write the band velocities as

$$\frac{\partial E_i(\mathbf{k})}{\partial k_q} = \left[\mathbf{C}^{\dagger}(\mathbf{k})\frac{\partial \mathbf{F}(\mathbf{k})}{\partial k_q}\mathbf{C}(\mathbf{k})\right]_{ii} - \left[\mathbf{C}^{\dagger}(\mathbf{k})\frac{\partial \mathbf{S}(\mathbf{k})}{\partial k_q}\mathbf{C}(\mathbf{k})\mathbf{E}(\mathbf{k})\right]_{ii} = \nu_{i,q}(\mathbf{k}) \tag{7.10}$$

where C is the expansion coefficient matrix.

For a detailed description of the implementation in the CRYSTAL code the reader is redirected to [8].

In general, a thermoelectric material can be defined as p-type or n-type depending on which are the predominant carriers in the material itself: holes and electrons respectively. Theoretically speaking, it is just a different sign in the carrier concentration ("+" if holes, "−" if electrons) and in the Seebeck coefficient obtained ("+" if p-type predominant, "−" if n-type predominant). In Fig. 7.2 a schematic representation of the transport properties is reported.

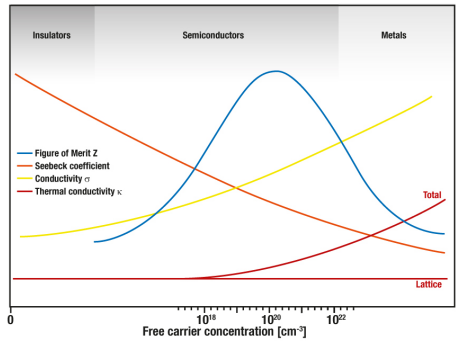

Figure 7.2: The scheme shows the behavior of insulators, metals and semiconductors. The carrier concentration, Seebeck coefficient and thermal conductivity give the characteristic value ZT or figure of merit that describes the thermoelectric behavior of any material with one value. Ref. [https://www.linseis.com/en/properties/seebeck-coefficient/.]

7.2 Results and Considerations

Our fist work on thermoelectric materials involves the study of the thermoelectric properties of TiMSn (M = Ni, Pd, and Pt) alloys with space group $F\bar{4}3m$ using the CRYSTAL code[1]. A systematic study of these alloys has never been attempted using local Gaussian type orbitals (GTOs) and hybrid density functional theory methods within a periodic approach. Our benchmark was TiNiSn by comparing our data to existing literature values of Seebeck coefficient, power-factor, and thermoelectric *figure of merit*. Then, we extended these calculations to TiPdSn and TiPtSn, for which consistent previous data are limited. TiMSn (M=Ni,Pd,Pt) alloys are predicted to favor p-type transport. In addition, we aim to explain the low band gap of TiNiSn by modeling defects in the pure system. Our defect model proves to have a smaller band-gap, and its power factor is found to be almost twice of the pure TiNiSn. All the details of this work are reported in [1].

7.2.1 TiNiSn, a general overview

HH alloys are originated from Full-Heusler alloys (FH) and they have a space group $F\bar{4}3m$ (No. 216) instead of $Fm\bar{3}m$ (No. 225) (Figure 7.3). HH are made up of 4 distinct face-centred cubic (fcc) sub-lattices. The primitive cell has 3 atoms while the conventional cell has 12 atoms. We perform Density Functional Theory (DFT) for all our computations as implemented in the CRYSTAL code.

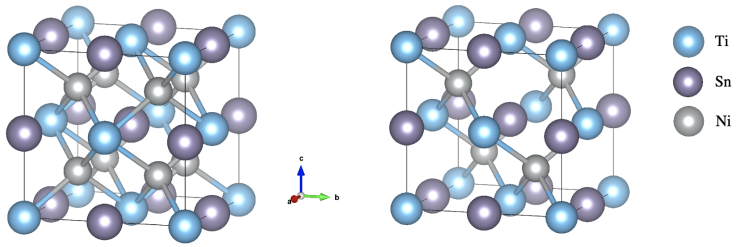

Figure 7.3: Left: Crystal structure of a typical FH (Fm-3m (No. 225)). Right: Crystal structure of a typical HH alloy (F-43m (No. 216)).

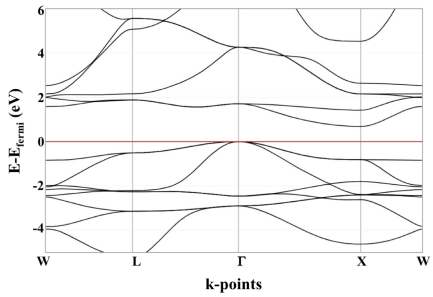

	a (Å)	E_g(eV)
This work	5.94	0.48
Reference	5.92 [9]	0.45[10] (0.12[11])

Figure 7.4: Left: Band structure of TiNiSn with PBE functional. Right: Lattice Parameter (a) and Band Gap (E_g) with references at the PBE level.

HH alloys are generally characterized by an indirect band gap between Γ and X k point.

In Figure 7.4 the band structure, lattice parameter and band gap data are reported at the PBE level. Although the agreement regarding the lattice parameter is rather good, the main discrepancy is observed in the band gap. In fact, even if in agreement with other simulation ([10]), a huge difference is seen with respect to the experimental result (0.12 eV[11]). Many considerations can be done regarding this experimental band gap. In fact, very few information is available on this sample both on the synthesis and on the measurements. The only assumption is that the sample was particularly rich in defects and unfortunately this is the reference to which everybody refer.

Considering the thermoelectrics, the defect-free TiNiSn shown a p-type behaviour predominant, in good agreement with existing theoretical literature at specified charge carrier concentration but not with experimental data. Experimentally an n-type material was expected.

In order to understand this peculiar behaviour, point defects have been introduced in the model: in particular a 2x2x2 supercell 24 atoms was used for the defect dilution. In fact, defects introduce localized levels in the vicinity of the Fermi level within the "forbidden region".

Among all the possible defect we displaced a Ni atom from an Half Heusler (HH) position to a vacant Full Heusler (FH) site. We preserved in this way the space group and it was beneficial in terms of computing time. Figure 7.5 shows a representative model of the defect.

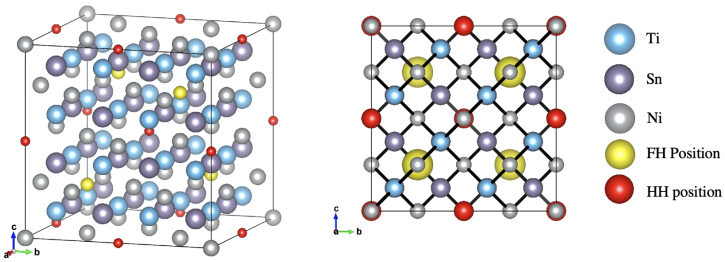

Figure 7.5: Representative model of the crystallographic cell for defect in TiNiSn. Blue, purple and grey spheres denote Ti, Sn and Ni atoms respectively. The yellow spheres (enlarged for better visualization) are Ni positions that were originally unoccupied in the pure system. The red spheres denote vacant sites.

Moreover, the choice of the defect was driven by the experimental data: no change in stoichiometry was expected. In particular, two defective systems have been found: *W8c-111* and *W8c-333*. They differ in the band gap values (0.26 eV and 0.19 eV respectively - PBE10 level) that are narrow than the pure system (0.69 eV - PBE10 level) and in the coordination patterns. All the details of these models are described in [1].

We reached the agreement with experiment with the *W8c-111* defect system that prefers n-type carriers and has an higher Power Factor compared to pure TiNiSn.

Moreover, Half Heusler alloys are extremely sensitive to the choice of functionals above all at high temperature. For this reason all the calculation have been carried out by using hybrid functionals that are known to improve the accuracy for crystal computations. In fact, band gaps using PBE functional, are predicted to be conducting in the defect systems, thus hybrid functional are suggested. In particular, PBE10 - Hybrid Functional with 10% of Hartree Fock (HF) exchange was used.

In Figure 7.6 we show the band structure and the density of state (DOS)

for the pure TiNiSn by using PBE10 hybrid functional. Our computed indirect band gap for TiNiSn is 0.69 eV which is 6 times the experimental value of 0.12 eV. However, we think that the experimental measurements were performed on a sample with high concentration of defects.

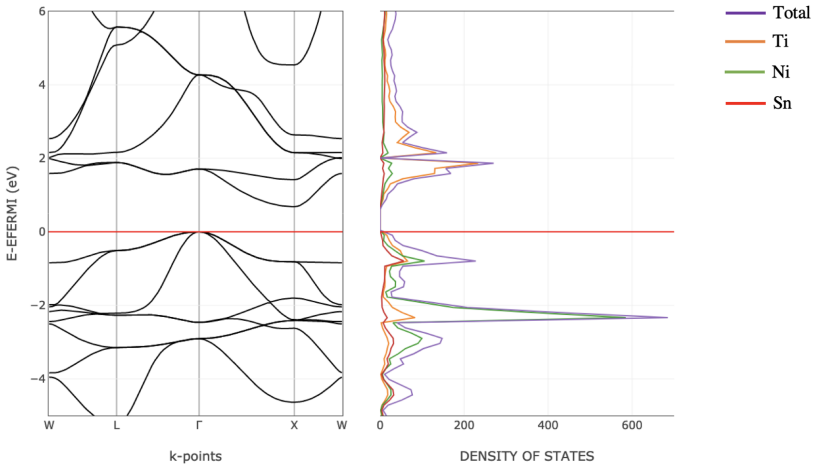

Figure 7.6: Band structure and DOS for TiNiSn with an indirect band gap of 0.69 eV.

Another important aspect to consider while studying HH alloys is the quality of the basis set. In fact, the influence of the basis set quality in the evaluation of the electronic structure and consequently in the thermoelectrics is rather high. A bad quality basis set may describe imprecisely the curvatures of the band structures affecting the band velocity evaluation and therefore all the thermoelectric coefficients. A graphical representation of the basis set influence in the band structure and in the thermoelectric properties is reported in Figure 7.7, where a significant discrepancy is shown in the evaluation of the PF for the TiPtSn compound.

7.2.2 Experimental Comparison

Our results have been compared with the experiments run by the Castellero group in our Chemistry Department. In this regard they shared with us data about the carrier concentration and the thermoelectrics of their sample TiNiSn. Regarding the carrier concentration, in Figure 7.8 a general trend is reported. As shown in the picture the scattering of data is rather huge: the maximum value of

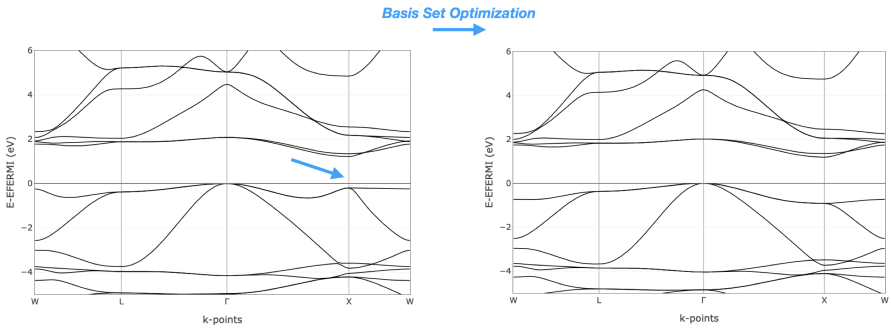

	CC (cm^{-3})	C-type	Temp (K)	PF x10^{11}($WK^{-2}m^{-1}s^{-1}$)	ZT
UNOPT	1E+20	n-type	300	2.25E-01	3.22E-03
OPT				1.10	0.02

Figure 7.7: Top: Influence of the basis set in the band gap structure in TiPtSn. Bottom: Influence of the basis set in the thermoelectric properties (Power Factor, PF) at a specific Carrier Concentration (CC) and Temperature (T). Functional: PBE10. Basis Set Reference: def2-TZVP. UNOPT: unoptimized basis set. OPT: optimized basis set.

carrier concentration is around $3.650 \cdot 10^{19} cm^{-3}$, the minimum is $3.281 \cdot 10^{18} cm^{-3}$ and the arithmetic average is $1.473 \cdot 10^{19} cm^{-3}$.

Comparing our data with the experimental ones with a carrier concentration around $1 \cdot 10^{19} cm^{-3}$, we may observe a slight divergence, but reducing the carrier concentration to $3.81 \cdot 10^{18} cm^{-3}$ the discrepancies are smaller, above all at high temperature. All the details are in Table 7.1.

We reach the experimental value of Seebeck (S = -314.324 μV/K) around $\sim 4E18 cm^{-3}$ at 300K.

In order to give a more general overview of the actual state of art regarding TiNiSn compound, in Figure 7.9, some results regarding Seebeck coefficient and electrical resistivity available in literature are reported. As shown in the pictures we have reported our Seebeck and resistivity data of the defect model *W8c-111*. While for the Seebeck we obtained a rather good agreement with respect to the experimental results of our collaborators, the resistivity shows a slight divergence. Nevertheless, our value is in line with the other references. This discrepancy can justify our slight deviation in the Power Factor with respect to the experimental data reported in Table 7.1.

The overall comparison with the experimental group is still a work in progress, but general prospects are rather good.

$\mathbf{cc = 1 \cdot 10^{19} cm^{-3}}$						
	$\mathbf{S(\mu V/K)}$			$\boldsymbol{\sigma(\Omega^{-1}m^{-1})}$		
	Theo Pure	Theo Defect	Exp.	Theo Pure	Theo Defect	Exp.
300K						
p-type	313.039	346.202		1.436E+04	9.612E+03	
n-type	-216.714	-249.762	-314.730	2.597E+04	2.328E+04	3.442E+03
700K						
p-type	408.499	-78.040		1.369E+04	2.261E+04	
n-type	-323.125	-241.063	-250.267	2.334E+04	3.763E+04	2.999E+04
	$\boldsymbol{\rho(\Omega m)}$			$\mathbf{PF(mWm^{-1}K^{-2})}$		
	Theo Pure	Theo Defect	Exp.	Theo Pure	Theo Defect	Exp.
300K						
p-type	6.963E-05	1.040E-04		1.407	1.152	
n-type	3.851E-05	4.296E-05	2.906E-04	1.219	1.452	0.363
700K						
p-type	7.304E-05	4.424E-05		2.285	0.138	
n-type	4.285E-05	2.657E-05	3.334E-05	2.436	2.187	1.920
$\mathbf{cc = 3.81 \cdot 10^{18} cm^{-3}}$						
	$\mathbf{S(\mu V/K)}$			$\boldsymbol{\sigma(\Omega^{-1}m^{-1})}$		
	Theo Pure	Theo Defect	Exp.	Theo Pure	Theo Defect	Exp.
300K						
p-type	390.138	421.084		5.822E+03	3.943E+03	
n-type	-290.416	-314.324	-314.730	1.052E+04	9.533E+03	3.442E+03
700K						
p-type	479.136	-101.012		5.640E+03	2.464E+04	
n-type	-264.354	-218.766	-250.267	9.631E+03	3.067E+04	2.999E+04
	$\boldsymbol{\rho(\Omega m)}$			$\mathbf{PF\ (mWm^{-1}K^{-2})}$		
	Theo Pure	Theo Defect	Exp.	Theo Pure	Theo Defect	Exp.
300K						
p-type	1.718E-04	2.536E-04		0.886	0.699	
n-type	9.502E-05	1.049E-04	2.906E-04	0.888	0.942	0.363
700K						
p-type	1.773E-04	4.059E-05		1.295	0.251	
n-type	1.038E-04	3.260E-05	3.334E-05	0.673	1.468	1.920

Table 7.1: Seebeck (S), Electrical Conductivity (σ), Electrical Resistivity (ρ) and Power Factor (PF) of the theoretical pure system (Theo Pure), theoretical defect system *W8c-111* (Theo Defect) and the experimental results (Exp.) at 300K and 700K. The carrier concentration (cc) p-type and n-type considered are $1 \cdot 10^{19} cm^{-3}$ and $3.81 \cdot 10^{18} cm^{-3}$.

7.3 Ta-Based half Heusler

Recently, researchers reported some previously unknown Half-Heusler compounds, such as ScPtBi, TiPdSn, ZrNbPb, etc. and TaCoSn [12] was reported to be a semiconductor with high thermoelectric performance. Bhattacharya et al. calculated the optimal ZT of TaCoSn by assuming the lattice part of thermal conductivity $\kappa_{ph}/\tau \sim 10^{14} W/mKs$ and found to be 1.73 [13]. While Haque et al. reported a calculated maximum thermoelectric figure of merit (ZT) of 0.731 at 600 K [14].

Therefore, it was reasonable to study the details of transport properties along with the electronic nature of TaCoSn.

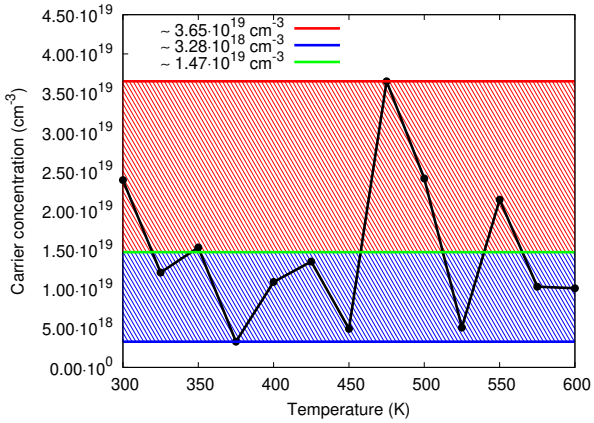

Figure 7.8: Carrier concentration measured by the experimental group. The maximum, the minimum and the arithmetic average are reported in red, blue and green respectively.

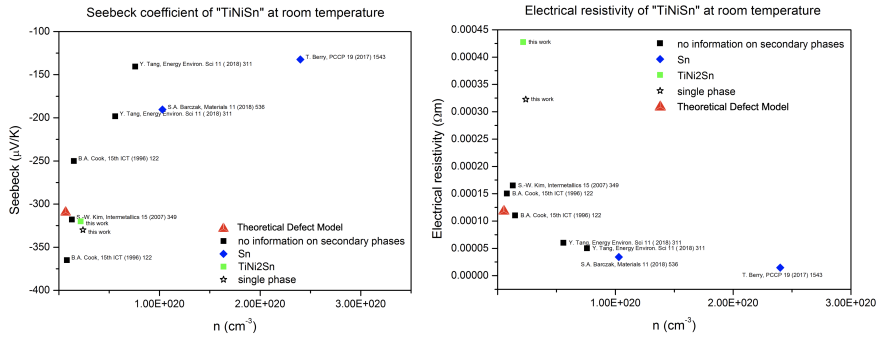

Figure 7.9: General overview of the Seebeck parameter (left) and of the electrical resistivity (right) of TiNiSn available in literature. The label "This work" regard the experimental sample studied by our collaborators.

The computational set up is rather similar to the one adopted for the Ti-based alloys: PBE10 functional and as basis set def2-TZVP like. As regard the basis set, a BDIIS procedure was performed for the basis set optimization. The basis sets adopted are reported in Appendix 12.5.

7.3.1 Defect Free TaCoSn

Crystal Structure and Elastic Properties

As regard the pure system the lattice constant a obtained is 5.9410 Å, comparable with the experimental value of 5.94 Å[15].

The equilibrium Bulk modulus B_0, elastic constants c_{11}, c_{12}, c_{44}, Poisson ratio ν, and Young's modulus Y, are obtained with CRYSTAL by solving the third-order Birch-Murnaghan isothermal equation of state[16] and riported in Tables 7.2 and 7.3.

	B_0	G_V	G_R	G_H	Y	ν
This work	184.57	95.28	92.94	94.11	241.32	0.282
Ref.	226.2[14]	100.1[14]	98.3[14]	99.2[14]	259.6[14]	0.3[14]

Table 7.2: The calculated elasticity moduli in GPa according to Voigt-Reuss-Hill. B_0 is the bulk modulus, G is the shear modulus, Y is the Young's modulus and ν is the Poisson ratio. References are reported when available.

	c_{11}	c_{12}	c_{44}
This work	336.791	108.462	82.692
Ref.	382.2[14]	148[14]	88.8[14]
	303.78[17]	95.97[17]	75.38[17]

Table 7.3: The calculated elastic constants in GPa according to Voigt-Reuss-Hill. c_{11}, c_{12} and c_{44} are the elastic constants. References are reported when available.

The Poisson ratio and the Young modulus are very close to the references, while a slight discrepancy is shown for the bulk and the shear moduli.

Looking at the elastic constants we may states that TaCoSn is elastically stable. Moreover, considering the Pugh ratio as (B/G), we evaluate a value of 1.961, which is greater than 1.75. This result means that our material is ductile as expected from literature ($B/G = 2.2$ for Haque et al. [14]).

In order to evaluate the percentage of elastic anisotropy we used the following expression:

$$A_G = \frac{(G_V - G_R)}{(G_V + G_R)} \tag{7.11}$$

which in our case corresponds to 1.243% that is close to the reference (0.9% for Haque et al.[14]).

The shear elastic anisotropy can be calculated by using the equation:

$$A = \frac{2c_{44}}{(c_{11} - c_{12})} \tag{7.12}$$

that in our specific case is 0.724 with respect to 0.76 of Haque et al. [14]. This indicates that our compound is anisotropic.

The hardness is calculated by the Vickers empirical formula:

$$H_V = 2\left(\left(\frac{G}{B}\right)^2 G\right)^{0.585} - 3 \tag{7.13}$$

which in our case is $H_V = 9.982$ GPa (8.22 GPa for Haque et al. [14]) and it indicates a hard material.

In order to be as much as possible exhaustive about the description of the bulk modulus, we listed in Table 7.4 bulk modulus and first order derivative obtained using different equations of state fitting.

Equation of State	V(Å^3)	E(AU)	B_0(GPa)	B_1(a.u.)
Voigt-Reuss-Hill			184.57	
Murnaghan 1944	52.4622	-1654.155142	183.72	4.02
Birch-Murnaghan 1947	52.4616	-1654.155144	184.11	4.04
Poirier-Tarantola 1998	52.4612	-1654.155145	184.45	4.05
Vinet 1987	52.4613	-1654.155144	184.28	4.05
Polynomial Fitting	V(Å^3)	E(AU)	B_0(GPa)	
Third Order Polynomial	52.4598	-1654.155153	186.86	
Fourth Order Polynomial	52.4608	-1654.155143	184.08	
Fifth Order Polynomial	52.4619	-1654.155144	184.08	
Ref.			186.2674[17]	4.11[17]
			165.4[18]	4.48[18]
			226.2[14]	

Table 7.4: Bulk moduli (B_0) and the first order derivative (B_1) of TaCoSn with the corresponding molar volume (V) and references when available.

Regarding both bulk modulus and the first order derivative a rather good agreement is shown, even if for the bulk modulus huge discrepancies can be seen among the references available.

Band Structures and Density of States

In the following, a general overview about the electronic structure is shown.

In Figure 7.10 both band structure and density of states plots are reported. The calculated energy bands indicate that TaCoSn is an indirect band gap semiconductor and the value of gap is 1.4945 eV which in agreement with references

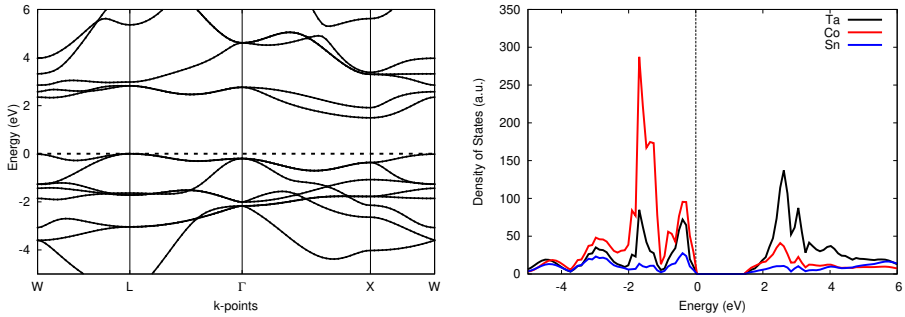

Figure 7.10: Band Structure (Right) and Density of States (Left) of TaCoSn pure system (PBE10 level).

(PBE level: 1.107-1.153 eV [14], 1.09 eV [19], 1.04 eV [20]; PBEsol level: 1.148 eV [17]; HSE06 level: 1.3 eV [15]; LDA level: 1.32 eV [13]).

The total atomic and projected density of states demonstrate a predominat influence of the tantalum orbitals above the Fermi level, while at lower energy cobalt seems to have the paramount influence. On the other hand, tin does not have a dominant contributions. Nevertheless, it seems that the cobalt orbitals have a preponderant behaviour to the density of states at the Fermi level.

The preceding comments and the dense electronic states of this compound at the vicinity of Fermi level play a significant role in the transport properties of TaCoSn. Thus, TaCoSn is expected to be a p-type doping predominant and to possess a large Seebeck coefficient and large power factor.

7.3.2 Point Defects in TaCoSn

As already deeply studied for the TiNiSn alloy, we decided to introduce point defects in the TaCoSn compound as well. We started by using the same kind of model *W8c-111* and *W8c-333*, then an extrinsic defect has been introduced.

Band Structures and Density of States

Starting from the well known *W8c-111* and *W8c-333*, in Figure 7.11 the band structures are reported, in comparison with the pure system as well with the same supercell adopted.

Even in this case, the inclusion of defects in the system implies the introduction of levels in the "forbidden region" of the band gap, narrowing in this way the overall band gap. In fact, while in the pure system we obtain 1.4946 eV, with *W8c-111* we have 0.1859 eV and 0.1606 eV for the *W8c-333* model.

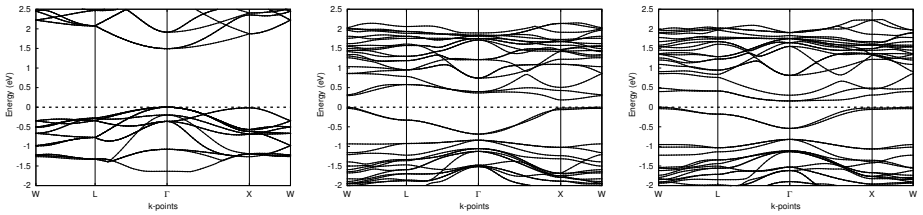

Figure 7.11: From the right Band Structure of TaCoSn pure system, *W8c-111* and *W8c-333* defect models.

As regard the density of states plots in Figure 7.12 the atom projected density of states for the defect models are reported. While for the *W8c-333* model at high energy the tantalum still has a predominant behaviour as for the pure system, for the *W8c-111* model the displaced cobalt atom (named Co(24) in the following) seems to deeply modify the conduction region, and to reverse the original order. At low energy the *W8c-333* shows a huge increasing of the cobalt influence, while *W8c-111* model keeps almost the same relative influence as in the pure system.

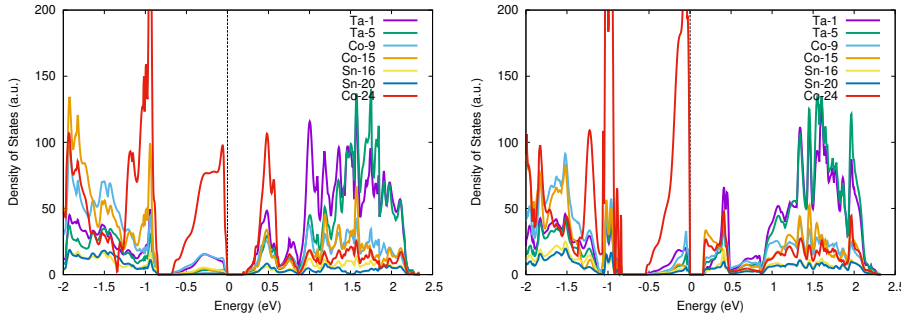

Figure 7.12: Density of States of TaCoSn defect systems. Left: *W8c-111*. Right *W8c-333*.

In Figure 7.13 a comparison of the density of states of the cobalt atom involved in the defect formation is shown. While in the *W8c-111* model the cobalt seems to contribute equally in the valence and in the conduction region, the *W8c-333* keeps the original behaviour of the pure system, with an enhancement in the valence region.

Neighbours analysis of the defect systems is reported in Table 7.5. In fact, as the Co atom is displaced from its HH to a FH position, symmetry related atoms within the $2 \times 2 \times 2$ supercell are no longer equivalent on the basis of different coordination patterns. Before performing the geometry optimization in

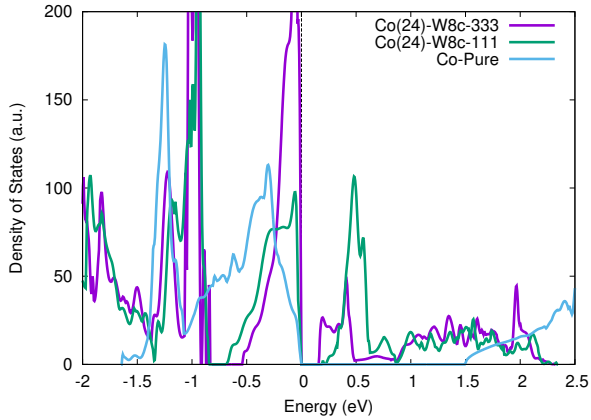

Figure 7.13: PDOS on the defect TaCoSn alloys on the Co(24), thus the displaced atom.

W8c-111, Ti(1) and Ti(5) have 3 and 5 Co atoms in the first neighboring shell. While in *W8c-333* Ti(1) and Ti(5), both have four Co as first neighbors. Similar behaviour is noted for Sn atoms. After the geometry optimization, both the defect alloys seem to rearrange the atoms to restore its 4-Ti and 4-Sn octahedral coordination. This can be seen from the stretching in the distances of the fifth Co neighbour of Ti(5) and Sn(20) in *W8c-111* and *W8c-333* (2.5837 and 2.5977 Å, respectively).

Regarding the relative stability: *W8c-111* is more stable than *W8c-333* of about 0.74 eV. Considering the difference $(E_{defect} - E_{pure})$ (3.115 eV for *W8c-111* and 3.852 eV and for *W8c-333*) and dividing this quantity by 3 (24 atoms in the unit cell and 8 in the asymmetry unit) we get 1.038 eV for the *W8c-111* and 1.284 eV for the *W8c-333* model.

Thermoelectrics

In this section a brief overview about thermoelectric properties is presented along with the available literature. In Fig. 7.14 Seebeck coefficient, electrical conductivity and power factor at room temperature are reported graphically. From the predominant band in the p-type region of the power factor, we can state that our material (defective or not) has a p-type behaviour as expected by other theoretical simulations available in literature.

Below a schematic summary of the result obtained with CRYSTAL and a comparison with literature when available are presented.

	W8c-333				W8c-111			
	no opt	d	opt	d	no opt	d	opt	d
Ti(1)	4Co	2.5665	3Co	2.5932	3Co	2.5665	3Co	2.5892
			1Co	2.6553				
Ti(5)	4Co	2.5665	3Co	2.5561	5Co	2.5665	1Co	2.5239
			1Co	2.5962			3Co	2.5542
							1Co	2.5837
Sn(16)	3Co	2.5665	3Co	2.5877	4Co	2.5665	3Co	2.5983
							1Co	2.7032
Sn(20)	5Co	2.5665	1Co	2.5302	4Co	2.5665	3Co	2.5476
			3Co	2.5727			1Co	2.6042
			1Co	2.5977				

Table 7.5: Neighbours of the non-equivalent atoms in the defect model *W8c-333* and *W8c-111*. "no opt" and "opt" labels regard the defect models before and after geometry optimization respectively. Distances d are in Å.

- *Seebeck, S*

  At 300K plane waves and BoltzTrap predict $S = 252\mu VK^{-1}$[17] and $S = 243\mu VK^{-1}$[14] that we reproduce at a carrier concentration of almost $5 \cdot 10^{19}cm^{-3}$, in particular:

  Pure: $S = 250\mu VK^{-1}$
  W8c-111: $S = 175\mu VK^{-1}$
  W8c-333: $S = 265\mu VK^{-1}$

  At 800 K at a carrier concentration around $1.0 \cdot 10^{19}cm^{-3}$ Wei et al. obtained $S = 680\mu VK^{-1}$ [19] that we reach at a bit lower carrier concentration ($1.0 \cdot 10^{18}cm^{-3}$) with $S = 700\mu VK^{-1}$ with the pure system.

  At 900K we observe an even higher Seebeck coefficient ($S = 650\mu VK^{-1}$ at a carrier concentration of $2.0 \cdot 10^{18}cm^{-3}$) and at 1200K a slight decreasing is shown ($S = 520\mu VK^{-1}$ at a carrier concentration $1.0 \cdot 10^{19}cm^{-3}$) as expected from literature.[19]

- *Electrical Conductivity*

  At 300K theoretically the electrical conductivity is expected to be around $\sigma = 0.728\mu\Omega^{-1}m^{-1}$[14] that we reach at $5.0 \cdot 10^{20}cm^{-3}$ of carrier concen-

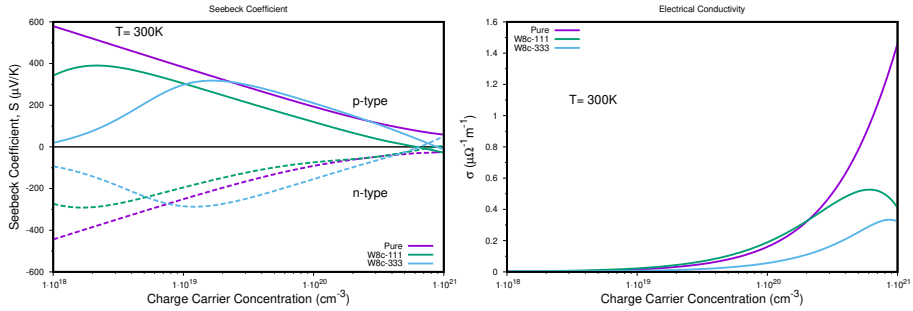

(a) (b)

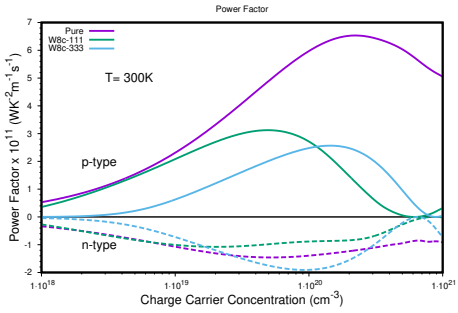

(c)

Figure 7.14: Seebeck (a), electrical conductivity (b) and power factor (c) at room temperature (300K) of TaCoSn pure system, *W8c-111* and *W8c-333* defect models.

tration. The following values of electrical conductivity are obtained:

Pure: $\sigma = 0.78\mu\Omega^{-1}m^{-1}$
W8c-111: $\sigma = 0.52\mu\Omega^{-1}m^{-1}$
W8c-333: $\sigma = 0.25\mu\Omega^{-1}m^{-1}$

Instead experimentally $\sigma = 0.031\mu\Omega^{-1}m^{-1}$[20] and $\sigma = 0.1\mu\Omega^{-1}m^{-1}$[15] are expected. At $5.0 \cdot 10^{19} cm^{-3}$ of carrier concentration the following values of electrical conductivity are obtained for our models:

Pure: $\sigma = 0.08\mu\Omega^{-1}m^{-1}$

W8c-111: $\sigma = 0.11\mu\Omega^{-1}m^{-1}$
W8c-333: $\sigma = 0.03\mu\Omega^{-1}m^{-1}$

Even at high temperature our results are in good agreement with references available[19] (at 800K, Pure: $\sigma = 0.15\mu\Omega^{-1}m^{-1}$ at $1.0 \cdot 10^{20}cm^{-3}$ of carrier concentration).

- *Power Factor*

At 300K at $3 \cdot 10^{19}cm^{-3}$ of carrier concentration we obtain rather high power factors that are comparable with references[14]:

p-type doping
Pure: $PF = 4 \cdot 10^{11}W/msK^2$
W8c-111: $PF = 3 \cdot 10^{11}W/msK^2$
W8c-333: $PF = 1.6 \cdot 10^{11}W/msK^2$
while for the *n-type doping*
Pure: $PF = -1.4 \cdot 10^{11}W/msK^2$
W8c-111: $PF = -1 \cdot 10^{11}W/msK^2$
W8c-333: $PF = -1.4 \cdot 10^{11}W/msK^2$

For sake of completeness the Power Factor of the pure system at different temperature is reported in Fig. 7.15.

Although theoretically our results are in good agreement with available literature at specific carrier concentration, experimentally n-type material is expected with a very low Seebeck coefficient ($S = -4\mu VK^{-1}$[20], $S = -5\mu VK^{-1}$[15]). This discrepancy can be justified by the presence of defects in the samples that are not exactly reproduced by our models. Moreover, it is well known that the synthesis of the TaCoSn is itself very complicated, due to the easy tin loss and the unavoidable porosity of the system.

Considering the preceeding results both defect models adopted (*W8c-111* and *W8c-333*), that were interesting in TiNiSn, are not performant in TaCoSn. In fact, the pure system seems to keep the highest power factor.

7.3.3 Extension to other defect models: Nb substitution

In order to understand the discrepancy with the experimental data, we tried to model also other kind of defect, like extrinsic defect in the TaCoSn.

In particular, we substitute a Ta with a Nb in a supercell 2x2x2. The Nb introduction and Ta substitution in the system is a rather common defect. In

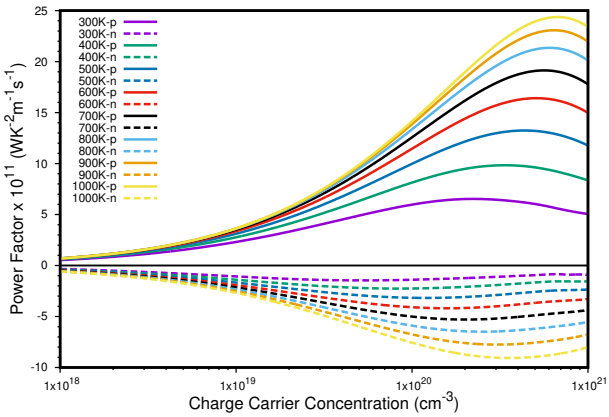

Figure 7.15: Power Factor of the pure system TaCoSn at different temperatures.

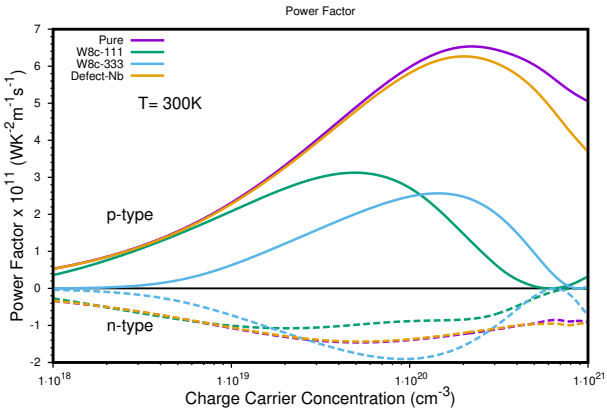

Figure 7.16: Power Factor comparison among pure system and defect models: *W8c-111*, *W8c-333* and extrinsic Nb defect.

fact, experimentally Nb is a common impurity in the TaCoSn.
As regards thermoelectricity (see Fig. 7.16), no enhancing in the power factor is seen in this case, but a rather similar behaviour to the pure system is shown. This result states that a stoichiometric defect is preferred instead of the antisite defect in order to enhance the thermoelectric properties of TaCoSn. Of course, the work is still in process and further investigations are needed. In fact, next possible defect model to study can be the tin loss and the change in cobalt content

that are defects rather common in real sample.

7.3.4 Extension to TaRhSn and TaIrSn

We also extended our discussion to other two Ta-based compound: TaRhSn and TaIrSn in which theoretical and experimental data are rather sparse. Even in this case the basis sets have been optimized by the BDIIS optimizer (basis sets in Appendix 12.5). The SCF setup is the same as before: PBE10 functional and def2-TZVP optimized basis sets.

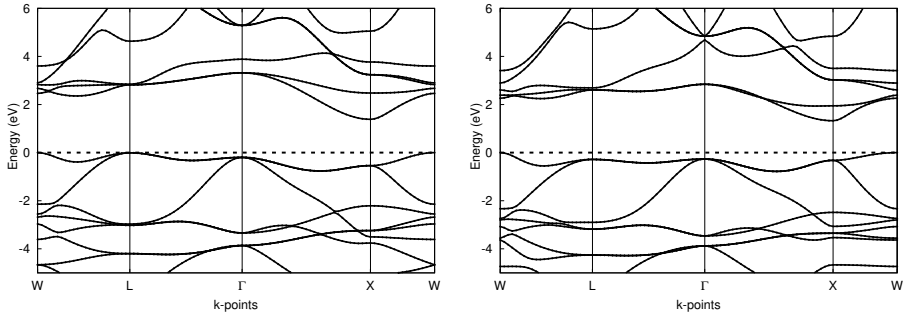

Figure 7.17: Band Structure of TaIrSn (Right) and TaRhSn (Left).

As regards the crystalline structure, TaIrSn has a lattice constant a of about 6.210 Å, while TaRhSn of about 6.120 Å. Very few are the reference data: TaIrSn 6.236 Å(PBE level)[18], 6.23 Å[17] (PBEsol level) and 6.175 Å[15] (experimental); TaRhSn 6.127 Å[17] (PBEsol level) and no experimental data available.

Band Structure and Density of States

As already seen in the previous sections the band structures are characterized by an indirect band gap between the Γ and the X point. In Figure 7.17 the band structures are reported. As regard the band gaps, TaIrSn shown a gap of 1.3852 eV, while TaRhSn a gap of 1.3249 eV. From literature we can find: for TaIrSn 1.3 eV[15] (GGA+U) and 1.331 eV[17] (PBEsol), for TaRhSn 1.2 eV[15] (GGA+U) and 1.160 eV[17] (PBEsol).

As regards the density of states, we decided to compare the atomic projections of the TaCoSn, TaIrSn and TaRhSn (Figure 7.18). While the Sn and Ta show a rather similar behaviour in the three compounds, Co, Ir and Rh seems to modify the valence region. In particular, cobalt orbitals are rather predominant

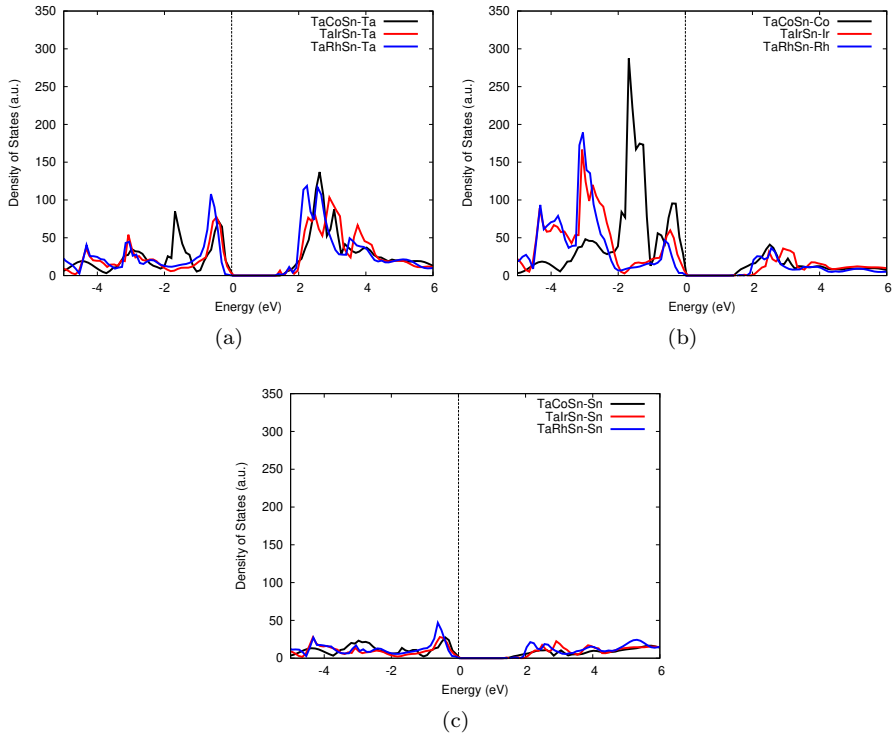

Figure 7.18: Computed PDOS on the atomic orbitals of (a) Ta, (b) Co/Ir/Rh, and (c) Sn, at the PBE10/def2-TZVP level. Dotted line corresponds to the Fermi energy.

in the vicinity of the Fermi level.

Thermoelectrics

In this section thermoelectric properties of TaCoSn, TaIrSn and TaRhSn are reported. In all the systems a p-type predominant behaviour is shown, in fact at almost all the carrier concentration the highest Seebeck value is in the p-type region (see Fig. 7.19 left). While the Seebeck ranking is TaCoSn>TaIrSn>TaRhSn, for the electrical conductivity an opposite behaviour is shown. These results foresee a power factor ranking like TaCoSn>TaIrSn>TaRhSn.

Of course these results are rather preliminary and further investigations are needed, such as the introduction of defects in the abovementioned compounds.

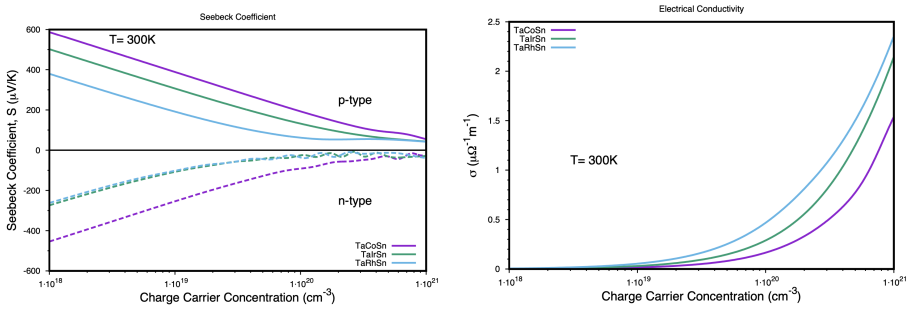

Figure 7.19: Comparison Seebeck and Electrical Conductivity of TaCoSn, TaIrSn and TaRhSn at 300K.

Bibliography

[1] Atreyi Dasmahapatra, Loredana Edith Daga, Antti J Karttunen, Lorenzo Maschio, and Silvia Casassa. Key role of defects in thermoelectric performance of TiMSn (M= Ni, Pd, and Pt) half-heusler alloys. *The Journal of Physical Chemistry C*, 124(28):14997–15006, 2020.

[2] Georg KH Madsen and David J Singh. BoltzTraP. a code for calculating band-structure dependent quantities. *Computer Physics Communications*, 175(1):67–71, 2006.

[3] Giovanni Pizzi, Dmitri Volja, Boris Kozinsky, Marco Fornari, and Nicola Marzari. BoltzWann: A code for the evaluation of thermoelectric and electronic transport properties with a maximally-localized wannier functions basis. *Computer Physics Communications*, 185(1):422–429, 2014.

[4] Atsushi Togo and Isao Tanaka. First principles phonon calculations in materials science. *Scripta Materialia*, 108:1–5, 2015.

[5] Atsushi Togo, Laurent Chaput, and Isao Tanaka. Distributions of phonon lifetimes in Brillouin zones. *Physical Review B*, 91(9):094306, 2015.

[6] Lars Onsager. Reciprocal relations in irreversible processes. I. *Physical Review*, 37(4):405, 1931.

[7] Herbert B Callen. The application of Onsager's reciprocal relations to thermoelectric, thermomagnetic, and galvanomagnetic effects. *Physical Review*, 73(11):1349, 1948.

[8] Giuseppe Sansone, Andrea Ferretti, and Lorenzo Maschio. Ab initio electronic transport and thermoelectric properties of solids from full and range-separated hybrid functionals. *The Journal of Chemical Physics*, 147(11):114101, 2017.

[9] Serdar Öğüt and Karin M Rabe. Band gap and stability in the ternary intermetallic compounds NiSnM (M= Ti, Zr, Hf): a first-principles study. *Physical Review B*, 51(16):10443, 1995.

[10] LL Wang, L Miao, ZY Wang, W Wei, R Xiong, HJ Liu, J Shi, and XF Tang. Thermoelectric performance of half-heusler compounds TiNiSn and TiCoSb. *Journal of Applied Physics*, 105(1):013709, 2009.

[11] FG Aliev, VVl Kozyrkov, VV Moshchalkov, RV Scolozdra, and K Durczewski. Narrow band in the intermetallic compounds MNiSn (M= Ti, Zr, Hf). *Zeitschrift für Physik B Condensed Matter*, 80(3):353–357, 1990.

[12] Romain Gautier, Xiuwen Zhang, Linhua Hu, Liping Yu, Yuyuan Lin, Tor OL Sunde, Danbee Chon, Kenneth R Poeppelmeier, and Alex Zunger. Prediction and accelerated laboratory discovery of previously unknown 18-electron ABX compounds. *Nature Chemistry*, 7(4):308, 2015.

[13] Sandip Bhattacharya and Georg KH Madsen. A novel p-type half-heusler from high-throughput transport and defect calculations. *Journal of Materials Chemistry C*, 4(47):11261–11268, 2016.

[14] Enamul Haque and M Anwar Hossain. First-principles study of elastic, electronic, thermodynamic, and thermoelectric transport properties of TaCoSn. *Results in Physics*, 10:458–465, 2018.

[15] Andriy Zakutayev, Xiuwen Zhang, Arpun Nagaraja, Liping Yu, Stephan Lany, Thomas O Mason, David S Ginley, and Alex Zunger. Theoretical prediction and experimental realization of new stable inorganic materials using the inverse design approach. *Journal of the American Chemical Society*, 135(27):10048–10054, 2013.

[16] Alessandro Erba, A Mahmoud, D Belmonte, and Roberto Dovesi. High pressure elastic properties of minerals from ab initio simulations: The case of pyrope, grossular and andradite silicate garnets. *The Journal of Chemical Physics*, 140(12):124703, 2014.

[17] Zaar Almaghbash, O Arbouche, A Dahani, A Cherifi, M Belabbas, A Zenati, H Mebarki, and A Hussain. Thermoelectric and piezoelectric properties in half-heusler compounds TaXSn (X= Co, Rh and Ir) based on ab initio calculations. *International Journal of Thermophysics*, 42(1):1–19, 2021.

[18] Paul O Adebambo, Ridwan O Agbaoye, Abolore A Musari, Bamidele I Adetunji, and Gboyega A Adebayo. Band structure, thermoelectric properties, effective mass and electronic fitness function of two newly discovered 18 valence electrons stable half-heusler TaX (X= Co, Ir) Sn semiconductors: A density functional theory approach. *Solid State Sciences*, 100:106096, 2020.

[19] Junhong Wei and Guangtao Wang. Thermoelectric and optical properties of half-heusler compound TaCoSn: a first-principle study. *Journal of Alloys and Compounds*, 757:118–123, 2018.

[20] Shan Li, Hangtian Zhu, Jun Mao, Zhenzhen Feng, Xiaofang Li, Chen Chen, Feng Cao, Xingjun Liu, David J Singh, Zhifeng Ren, et al. N-type TaCoSn-based half-heuslers as promising thermoelectric materials. *ACS Applied Materials & Interfaces*, 11(44):41321–41329, 2019.

Chapter 8

Ullmannites

Ullmannites are natural mineral ternary compounds of different nominal composition. They are predicted to be very performant as thermoelectric materials and the most common alloy is NiSbS. In this last chapter, a recent work started in collaboration with the experimental group of Prof. Alberto Castellero at the University of Turin is presented. Stability, electronic structure and thermoelectrics are simulated by using CRYSTAL and compared with the available experimental data. Four compounds have been selected for the study: NiSbS, NiSbSe, PdSbS and PdSbSe. These compounds are pretty new in the field of thermoelectrics and very few literature data are available, predominantly on NiSbS. [1, 2, 3, 4] In general, the crystal structure of these compounds is similar to the well-known FeSi-type cubic structure ($P2_13$, No. 198, see Fig. 8.1).

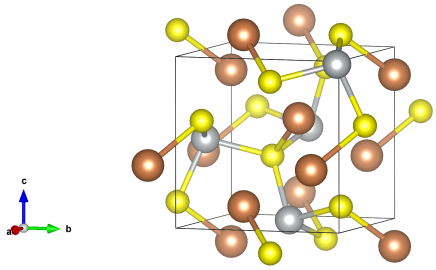

Figure 8.1: Graphical representation of NiSbS; $P2_13$ space group, No. 198. In grey, orange and yellow are reported Ni, Sb and S. The structure is the same for NiSbSe, PdSbS and PdSbSe with the appropriate atoms exchange.

All the CRYSTAL calculations in this chapter have been performed by using

PBE functional and def2-TZVP like basis set. Even in this case the basis sets were optimized with the BDIIS method. The basis sets are fully reported in Appendix 12.6.

8.1 Crystalline Structures and Thermodynamics

We have considered four compounds: NiSbS, NiSbSe, PdSbS and PdSbSe.

Our starting point was the study of relative stability among these compounds looking at the formation reactions given by the experimental group.

Four reactions have been studied:

$$\begin{aligned}
1)\ NiSb_2\ (Pnnm)\ &+ NiS_2\ (Pa\text{-}3) \longrightarrow 2\,NiSbS\ (P2_13)\\
2)\ NiSe_2\ (Pa\text{-}3)\ &+ NiSb_2\ (Pnnm) \longrightarrow 2\,NiSbSe\ (P2_13)\\
3)\ PdSb_2\ (Pa\text{-}3)\ &+ PdSe_2\ (Pbca) \longrightarrow 2\,PdSbSe\ (P2_13)\\
4)\ PdS_2\ (Pbca)\ &+ PdSb_2\ (Pa\text{-}3) \longrightarrow 2\,PdSbS\ (P2_13)
\end{aligned}$$

For each compound the space group is reported in parenthesis. As regards the starting geometries they have been taken from the American Mineralogist Crystal Structure Database [5, 6, 7, 8, 9, 10, 11].

For these four reactions, we obtain a favourable formation enthalpy for the ternary compounds and they are comparable with the data obtained by other theoretical calculations ([12, 13], website: http://oqmd.org/materials/ , label oqmd in the following). The entity is about $-0.1eV/atom$ for almost all the compounds:

$$\begin{aligned}
1)&\Delta H = -0.106eV/atom\ \text{(oqmd:-0.419eV/atom)}\\
2)&\Delta H = -0.097eV/atom\ \text{(oqmd:-0.307eV/atom)}\\
3)&\Delta H = -0.126eV/atom\ \text{(oqmd:-0.421eV/atom)}\\
4)&\Delta H = -0.121eV/atom\ \text{(oqmd:not stable)}
\end{aligned}$$

Experimentally the fourth compound is less stable than the others. In this regards, we tried to change the abovementioned formation reaction to the following one:

$$2\,PdS\ (P42/m)\ + 3\,PdSb\ (P63/mmc)\ + Sb_2S_3(Pnma) \longrightarrow 5\,PdSbS\ (P2_13)$$

where the formation enthalpy is about $-0.036eV/atom$, thus always favourable but less stable.

The ternary diagrams obtained from the oqmd are reported in Figure 8.2 where it is well shown the instability of the PdSbS compound with respect to the others.

Nevertheless, the experimental group with a lot of efforts were capable of synthesizing the PdSbS compound as well.

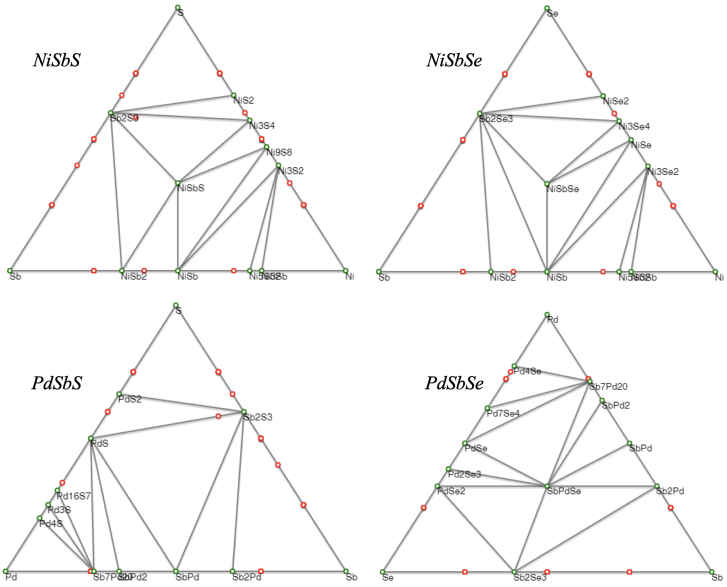

Figure 8.2: Ternary diagram of NiSbSb, NiSbSe, PdSbS and PdSbSe performed by using the oqmd website (http://oqmd.org/materials/). PdSbS is not present in the diagram because it is predicted to be unstable.

8.2 Band Structures and Density of States

From the point of view of the band structures, all these compounds are conductive and the shape obtained is absolutely comparable with the literature data available. In our calculation spin orbit coupling is not considered since not yet available in the CRYSTAL code. In all these band structures, the pudding mold character is present. The "pudding mold" type, consists of a dispersive portion and a somewhat flat portion in the band structure for a range of k points. The important expectation for the pudding mold band is not just the large thermopower, but also a relatively large conductivity and thus a large power factor. Moreover, this band structure shape is usually matched with hole pockets. The combination of these two features are predicted to be rather fundamental for enhancing the thermoelectric properties, and in particular drive large thermopower [14, 15] even if the system is metallic [1].

In Figure 8.3 an overlap of all the band structures is reported along with the density of states.

As regard the density of states, experimental results are available and they

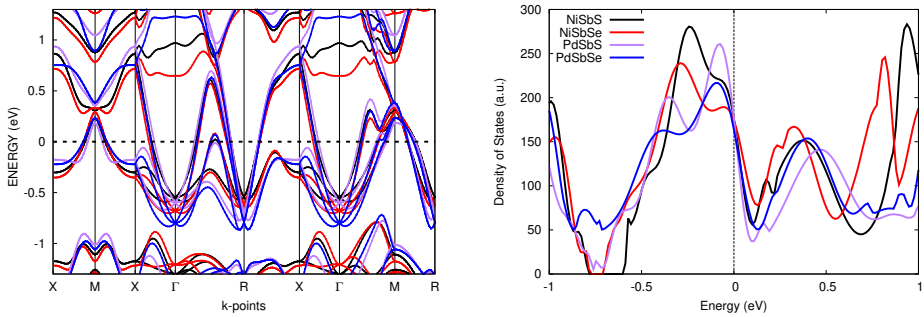

Figure 8.3: Theoretical band structures (left) and density of states (right).

are reported in Figure 8.4 in which a full range and an enlargement are reported. Our calculations are in a good agreement with the expected results. Even if the band structures among the four compounds are rather similar, the density of states demonstrated slight differences at the Fermi level. In fact, the combination Ni and S seems to have a predominant influence around the Fermi level.

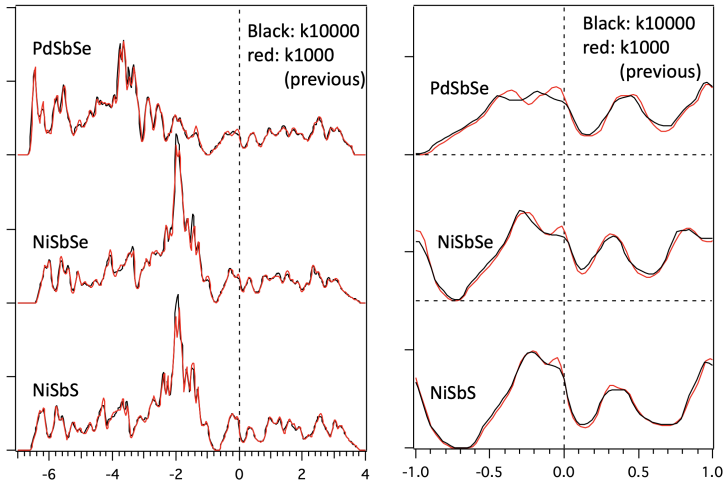

Figure 8.4: Experimental density of states. Two levels of accuracy have been used.

8.3 Thermoelectrics

Thermoelectrics properties of these compounds are very few in literature, but in this work we tried to compared the results obtained with the experimental data given by our collaborators.

In this section we report our data compared with experimental data available.

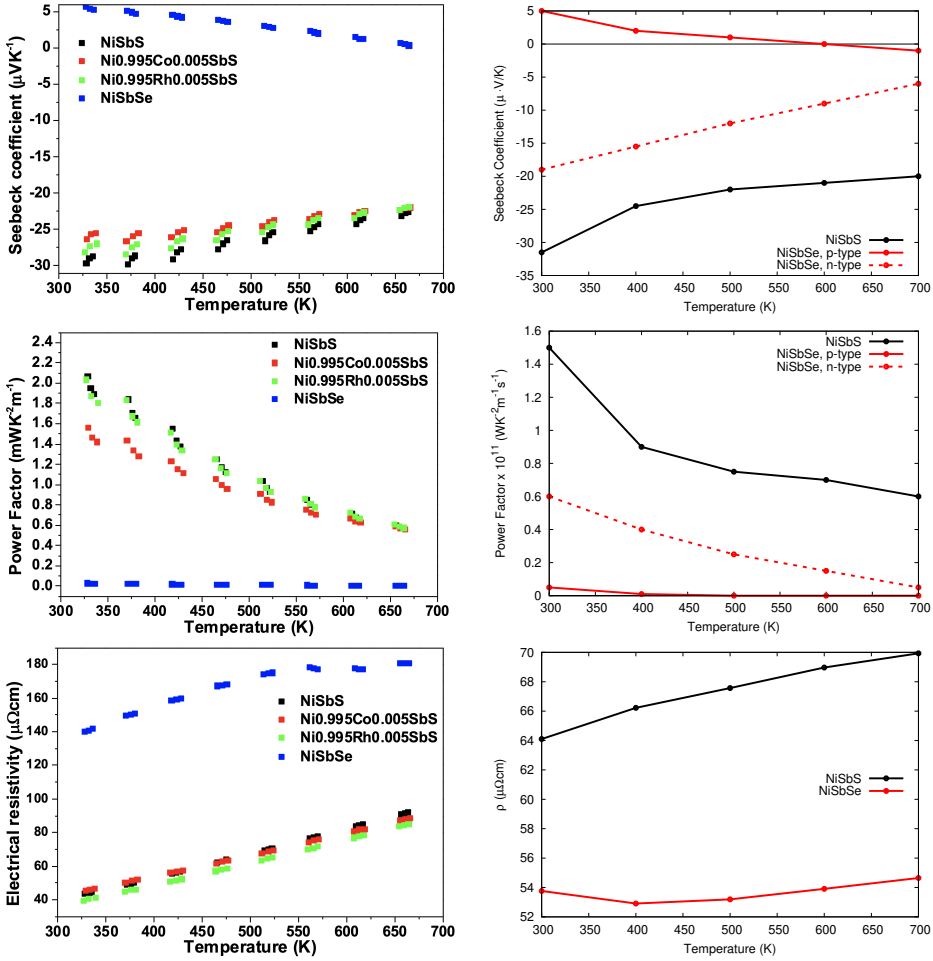

Figure 8.5: NiSbS and NiSbSe thermoelectric properties. On the left experimental results, on the right simulation performed by using CRYSTAL.

Looking at the general trend in Figure 8.5 a good agreement in the evaluation

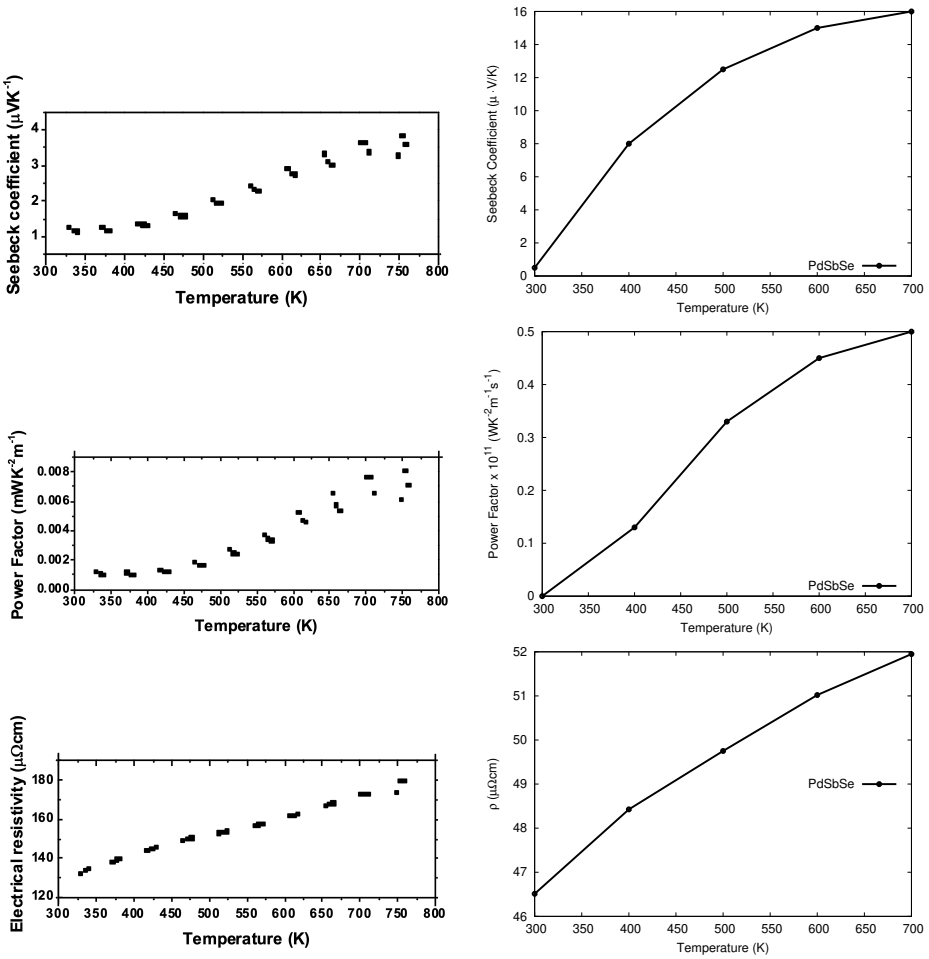

Figure 8.6: PdSbSe thermoelectric properties. On the left experimental results, on the right simulation performed by using CRYSTAL.

of the Seebeck coefficient is obtained, a slight difference in the absolute value of the Power Factor is shown due to an underestimation of the resistivity in the simulation. Theoretical NiSbS is expected to be a n-type material, while NiSbSe shows a predominant n-type instead of a p-type as expected from the experiment. Nevertheless, the calculation on the p carriers is in perfect agreement with the experiment. For sake of completeness p and n type carriers behaviour is reported in all the plots. As regards the carrier concentration, in this case we don't have

any information from the experiment, but due to their conductive nature, high carrier concentration is expected. For this reason the abovementioned plots were performed at a carrier concentration of $6.0 \cdot 10^{20} cm^{-3}$ and $5.5 \cdot 10^{20} cm^{-3}$ for NiSbS and NiSbSe respectively.

As regard the PdSbSe, a comparison experiment and simulation is reported in Figure 8.6. In this case, even if the general trends are rather good among our data and experimental ones, a slight high Seebeck coefficient and a rather low electrical resisitivity increase our power factor not allowing a perfect match between results. Nevertheless, considering that all the calculations were performed without modeling defects, the simulation can be considered rather good, due to the fact that real materials may contain defects and they are fundamental in the evaluation of the thermoelectric properties.

Bibliography

[1] Masanobu Miyata, Taisuke Ozaki, Shunsuke Nishino, and Mikio Koyano. Thermoelectric properties of high power factor sulfide NiSbS and Co substitution system Ni1- x Co x SbS. *Japanese Journal of Applied Physics*, 56(2):021801, 2017.

[2] R Carlini, G Zanicchi, G Borzone, N Parodi, and GA Costa. Synthesis and characterization of the intermetallic compound NiSbS. *Journal of Thermal Analysis and Calorimetry*, 108(2):793–797, 2012.

[3] Masashi Kakihana, Atsushi Teruya, Kengo Nishimura, Ai Nakamura, Tetsuya Takeuchi, Yoshinori Haga, Hisatomo Harima, Masato Hedo, Takao Nakama, and Yoshichika Ōnuki. Split fermi surface properties in ullmannite NiSbS and PdBiSe with the cubic chiral crystal structure. *Journal of the Physical Society of Japan*, 84(9):094711, 2015.

[4] WD Johnston, RC Miller, and DH Damon. Electrical properties of some compounds having the pyrite or marcasite structure. *Journal of the Less Common Metals*, 8(4):272–287, 1965.

[5] Robert T Downs and Michelle Hall-Wallace. The american mineralogist crystal structure database. *American Mineralogist*, 88(1):247–250, 2003.

[6] Arne Kjekshus, Andresen AF, et al. Compounds with the marcasite type crystal structure. IX. structural data for FeAs2, FeSe2, NiAs2, NiSb2, and CuSe2. 1974.

[7] Arne F Andresen. On the magnetic properties of CoSeQ, NiSQ, and NiSe2. *Acta Chemica Scandinavica*, 23(7):2325–2334, 1969.

[8] Aloys J Foecker and Wolfgang Jeitschko. The atomic order of the pnictogen and chalcogen atoms in equiatomic ternary compounds TPnCh (T= Ni, Pd; Pn= P, As, Sb; Ch= S, Se, Te). *Journal of Solid State Chemistry*, 162(1):69–78, 2001.

[9] Sigrid Furuseth, Kari Selte, Arne Kjekshus, PH Nielsen, Berndt Sjöberg, and Erik Larsen. Redetermined crystal structures of PdAs2, PdSb2, PtP2, PtAs2, PtSb2, a-PtBi2, and AuSb2. *Acta Chem Scand*, 19(3):735–741, 1965.

[10] C Soulard, X Rocquefelte, P-E Petit, M Evain, S Jobic, J-P Itié, P Munsch, H-J Koo, and M-H Whangbo. Experimental and theoretical investigation on the relative stability of the PdS2-and pyrite-type structures of PdSe2. *Inorganic Chemistry*, 43(6):1943–1949, 2004.

[11] Werner H Paar, Dan Topa, Emil Makovicky, and Franz J Culetto. Milotaite, PdSbSe, a new palladium mineral species from Předbořice, Czech Republic. *The Canadian Mineralogist*, 43(2):689–694, 2005.

[12] James E Saal, Scott Kirklin, Muratahan Aykol, Bryce Meredig, and Christopher Wolverton. Materials design and discovery with high-throughput density functional theory: the open quantum materials database (OQMD). *Jom*, 65(11):1501–1509, 2013.

[13] Scott Kirklin, James E Saal, Bryce Meredig, Alex Thompson, Jeff W Doak, Muratahan Aykol, Stephan Rühl, and Chris Wolverton. The open quantum materials database (OQMD): assessing the accuracy of DFT formation energies. *npj Computational Materials*, 1(1):1–15, 2015.

[14] Kazuhiko Kuroki and Ryotaro Arita. "pudding mold" band drives large thermopower in NaxCoO2. *Journal of the Physical Society of Japan*, 76(8):083707–083707, 2007.

[15] Hidetomo Usui, Kazuhiko Kuroki, Seiya Nakano, Kazutaka Kudo, and Minoru Nohara. Pudding-mold-type band as an origin of the large Seebeck coefficient coexisting with metallic conductivity in carrier-doped FeAs2 and PtSe2. *Journal of Electronic Materials*, 43(6):1656–1661, 2014.

Chapter 9

Conclusions and Perspectives

In the frame of this PhD thesis work, I had the possibility to investigate different fields by using new and never used methods in solid-state simulations. This three years work can be ideally grouped in two different type of activity: code development and the application of the CRYSTAL code to the study of thermoelectric materials.

Within code development and applications, I have developed a basis set optimizer based on the DIIS algorithm that minimizes the total energy of the system constrained to keep the condition number of the overlap matrix as small as possible in a similar approach as proposed by VandeVondele et al.[1]. The proposed method is quite effective for solid-state calculations and allows for an easy optimization of basis sets with different dimensions. The evidence of the excellent performance of the BDIIS method paves the way for a careful definition of system-specific basis sets, as a viable alternative to all-purpose basis sets. Nevertheless, it could be employed for a more extensive work that would permit the creation of all-purpose basis set families for a larger set of atomic species. This algorithm can be a useful alternative to the usual basis set optimization, commonly performed by hand, allowing for the easy creation of new basis sets or system-specific optimizaton of new ones. A large benchmark on elemental solids demonstrated that the BDIIS method can be used to obtain basis sets for solids of consistent quality as for molecules without pruning the original basis sets. A DIIS-based geometry optimization (GDIIS - Direct Inversion in the Iterative Subspace for the Geometry Optimization) was also implemented in Crystal, with a performance in the results that was not entirely convincing.

Afterwards, the Maximum Overlap Method (MOM) was implemented for the

$\Delta-$SCF excited states calculations. Despite being still in a single-particle picture, the method shows reasonably good ability to describe optical gaps, with the advantages of 1) allowing for cross-spin excitation and 2) allowing for optimization of excited states geometry. Both the Hartree-Fock level and DFT calculations can be performed with the MOM with the same computational cost and in solid states. The gradients expression for excited states was derived, which showed its use in the valuation of luminescence spectra.

Finally, the basis set optimizer denmonstrated to be a key tool for the investigation of the geometry, electronic band structure, and TE properties of HH alloys: starting from TiNiSn, TiPdSn, and TiPtSn to Ta based compounds. P-type doping was obtained from all of these compounds, but an appropriate description of the point defects was fundamental to justify the n-type behaviour predicted experimentally. The ullmannites are the last family of materials that we have just started to study from a thermodynamic point of view and electronically. Till now, good agreement with experimental data available are obtained even if further studies are needed. In terms of thermoelectricity, in both half heusler and ullmannites, many aspects require further investigation: introduction of other kind of defects, increase defect dilution by increasing cell dimension and the extension to other alloys.

Bibliography

[1] Joost VandeVondele and Juerg Hutter. Gaussian basis sets for accurate calculations on molecular systems in gas and condensed phases. *The Journal of Chemical Physics*, 127(11):114105, 2007.

Chapter 10

Appendix A - Basis Set Optimizer, Algorithm Implementation

In this Chapter a brief technical overview about the implementation of the basis set optimizer and the BDIIS method in the CRYSTAL code is reported, following the discussion in the previous chapter. In particular, we describe in detail the code implemented during this thesis and the options available.

It is a rather technical chapter and can be seen as a detailed documentation of the algorithm. It can be rather complicated for non-users of CRYSTAL due to the internal language adopted. Nevertheless, it can be useful for people involved in future CRYSTAL projects. Moreover, it is related with the published paper "Gaussian Basis Sets for Crystalline Solids: All-Purpose Basis Set Libraries vs System-Specific Optimization" [1], reported along with the supplementary material in Appendix 12.1 of this thesis.

CRYSTAL is written in `FORTRAN (77/90/95/03/08)` and it consists today of more than a million lines of code. The program is made up of different subroutines and modules. In general, a subroutine is a unit characterized by a sequence of instructions for a specific task that can be "called" whenever needed. A module is a unit arranged for the storage of variables and parameters. To organize all the information needed in the program, there are many files, each with a specific aim and feasible application and they are controlled by a main file called `crystal.f90`. It contains the `Subroutine f90main` that is the one in which the basis set optimization is invoked. In particular, the subroutine involved in this procedure is the `Subroutine BASIS_OPT_DRIVER` contained in

the file `basis_opt.f`. The BDIIS algorithm has been introduced in a specific module named `Module bdiis_module`. Other variables, matrices definition are reported in a separate module called `Module basis_opt_module`. Both modules are reported in a single file named `basis_opt_module.f90`.

10.1 General Structure of the Optimization

A schematic representation of the work flow during the optimization is here reported in Fig. 10.1 where in black boxes are reported the files involved along with the routines invoked.

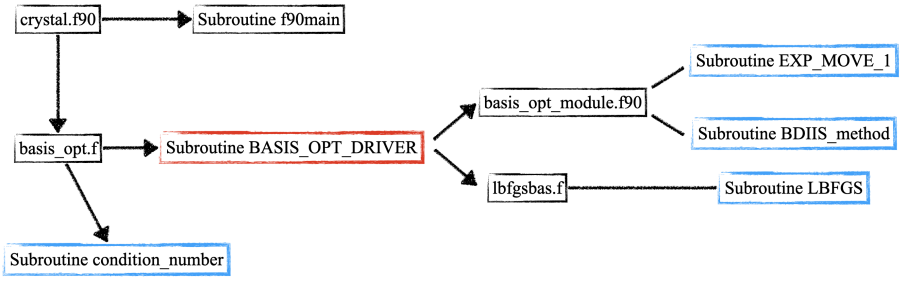

Figure 10.1: Schematic representation of the basis set implementation in CRYSTAL. In black boxes file names are reported, while in red and blue ones the subroutines involved. The `Subroutine BASIS_OPT_DRIVER` is the main routine of the basis set optimization algorithm from which all the others are invoked.

In the following a more detailed description of each section will be provided.

10.2 Basis Opt Driver

File: `basis_opt.f`

This section can be considered as the skeleton of the overall optimization. Here a schematic representation of the file is reported:

- `Subroutine BASIS_OPT_DRIVER`
  - Storing of Data and First SCF
  - Preliminary Step for two-sided Numerical Derivative
  - Gradient Evaluation, two-sided Numerical Derivative

  - BDIIS Algorithm and New Gradients
  - Line Search and Step Application
  - Ultimate SCF and Convergence Checks

- `Subroutine condition_number`

10.2.1 Storing of Data and First SCF

Before the actual starting of the optimization some information regarding the initial basis set must be stored. In particular, two main data are stored:

- *Input Basis Set*
  The exponents are stored in `EXXstore` matrix, while s, p and d-f-g contraction coefficients are stored in the `CX1store`, `CX2store` and `CX3store` matrices respectively. For sp shells two contraction coefficients must be specified, for s and p atomic orbitals, respectively. These matrices are actually vectors of dimension `NPRIMG`, number of primitives. At each optimization cycle (`BASCRYS` in the code) these vectors are stored in matrices named `totEXXstore`, `totCX1store`, `totCX2store` and `totCX3store`.

- *Shells Involved in the Optimization*
  (in input defined by an asterisk, see Section 10.6.1). In this case a checkers-like matrix (named `dama`, dimension
  `{atomic species x max no. of shells}`) is constructed, in which for each atomic species and each shell one number is assigned: 1 corresponds to a "to optimize-shell" and 0 to a "not to optimize" one.

This storing is performed in the `Subroutine INPBAS` where the basis set written in input is read by the CRYSTAL code. This latter routine is invoked at the beginning of any CRYSTAL calculation and it is contained in the `both4.f` file.

Once the `Subroutine BASIS_OPT_DRIVER` is invoked by the `crystal.f90` a first SCF is performed. The calculation has to converge rather smoothly at this stage of the optimization.

The SCF total energy obtained in this first stage of the optimization (`PAR0`) will be the one involved in the minimization. In particular, at this energy a penalty function (`numbcon`) that include the Overlap matrix condition number is added as described in Equ. 3.5 of Section 3.1.1.

The penalty function is performed in `Subroutine condition_number` reported for sake of completeness in Section 10.2.7. This *"Objective Function"* is actually the one involved in the minimization procedure and it is saved in the variable `PAR0`.

```
CALL condition_number
PAR0=PAR0+numbcon
```

10.2.2 Preliminary Step for two-sided Numerical Derivative

Three ingredients related with exponents and coefficients will be necessary in the following:

- *Gradients*
  `FORZEbase_exp`, `FORZEbase_c1`, `FORZEbase_c2` and
  `FORZEbase_c3` vectors of dimension `NPRIMG` number of primitives. At each optimization cycle (`BASCRYS` in the code) these vectors are stored in matrices named `totforze_exp`, `totforze_c1`, `totforze_c2` and `totforze_c3` respectively.

- *Steps*
  `step_exp` , `step_c1`, `step_c2`, `step_c3` vectors of dimension `NPRIMG` number of primitives. The step is 1% of the exponents and 0.1% of the coefficients weighted by the relative exponents.

- *Inverse Steps*
  `INV_step_exp` , `INV_step_c1`, `INV_step_c2`, `INV_step_c3` vectors of dimension `NPRIMG` number of primitives. They are the inverse of the steps abovementioned.

Browsing inside the `dama` matrix we can distinguish which atom species and shells are involved in the optimization and start performing the initial step.

A concatenated series of `DO` loops are involved in order to screen along the basis set.

- loop on optimization steps (`BASCRYS` defines the cycle number)
- loop on atomic species
- loop on shells
- loop on primitives (`IPRIMM_att` is the loop index).

Then a preliminary step is performed and it corresponds to 1% for the exponents and 0.1% for the coefficients (`step_exp`, `step_c1`, `step_c2`, `step_c3`). Moreover, this last step is weighted by the relative exponent. Some other alternatives have been used during the implementation (e.g. fixed steps values like 0.001 and 0.0005), but in the end 1% and 0.1% have proved to be effective for the optimization. Finally, the inverse of these steps are actually used in the following (`INV_step_exp`, `INV_step_c1`, `INV_step_c2`, `INV_step_c3`).

Preliminary step contruction

```
!!!! for exponents
                  step_exp(IPRIMM_att)=EXXstore(IPRIMM_att)*0.01_float

                  step_att_exp=step_exp(IPRIMM_att)

                  INV_step_exp(IPRIMM_att)=1._float/step_att_exp

!!!! for c1 coefficients

                  step_c1(IPRIMM_att)=CX1store(IPRIMM_att)*0.001_float
     >                    /EXXstore(IPRIMM_att)

                  step_att_c1=step_c1(IPRIMM_att)

                  INV_step_c1(IPRIMM_att)=
     >1._float/(step_att_c1*EXXstore(IPRIMM_att))

!!!! for c2 coefficients

                  step_c2(IPRIMM_att)=CX2store(IPRIMM_att)*0.001_float
     >                    /EXXstore(IPRIMM_att)

                  step_att_c2=step_c2(IPRIMM_att)

                  INV_step_c2(IPRIMM_att)=
     >1._float/(step_att_c2*EXXstore(IPRIMM_att))

!!!! for c3 coefficients

                  step_c3(IPRIMM_att)=CX3store(IPRIMM_att)*0.001_float
     >                    /EXXstore(IPRIMM_att)

                  step_att_c3=step_c3(IPRIMM_att)

                  INV_step_c3(IPRIMM_att)=
     >1._float/(step_att_c3*EXXstore(IPRIMM_att))
```

The effective step "ahead" (positive step) is applied subsequently in a routine called `EXP_MOVE_1` in the `basis_opt_module.f90` file:

Positive Step

```
       DO i=1,NPRIMG
          step_att_exp=step_exp(i)
          step_att_c1=step_c1(i)
          step_att_c2=step_c2(i)
          step_att_c3=step_c3(i)
        If(what_ami_doing.eq.1)then
          CALL EXP_MOVE_1(i,1,step_att_exp)
        elseif(what_ami_doing.eq.2)then
          CALL EXP_MOVE_1(i,2,step_att_c1)
        elseif(what_ami_doing.eq.3)then
          CALL EXP_MOVE_1(i,3,step_att_c2)
        elseif(what_ami_doing.eq.4)then
          CALL EXP_MOVE_1(i,4,step_att_c3)
        endif
       ENDDO
```

In which the variable `what_ami_doing` defines the kind of the optimization performed (`what_ami_doing=1` only exponents, `what_ami_doing=2,3,4` for s,p and d-f-g coefficients). Once done, another SCF is performed and the energy saved in the variable `PAR1`.

```
     CALL condition_number
     PAR1=PAR1+numbcon
```

The effective step "backwards" (negative step) is applied subsequently in the same routine called `EXP_MOVE_1` in the `basis_opt_module.f90`:

Negative Step

```
exx=EXXstore
 c1 =cx1store
 c2 =cx2store
 c3 =cx3store
DO i=1,NPRIMG
   step_att_exp=-step_exp(i)
   step_att_c1=-step_c1(i)
   step_att_c2=-step_c2(i)
   step_att_c3=-step_c3(i)
 If(what_ami_doing.eq.1)then
   CALL EXP_MOVE_1(i,1,step_att_exp)
 elseif(what_ami_doing.eq.2)then
   CALL EXP_MOVE_1(i,2,step_att_c1)
 elseif(what_ami_doing.eq.3)then
   CALL EXP_MOVE_1(i,3,step_att_c2)
 elseif(what_ami_doing.eq.4)then
   CALL EXP_MOVE_1(i,4,step_att_c3)
 endif
```

The `Subroutine EXP_MOVE_1` is reported in the Section 10.3. Then the third SCF is performed and the energy saved in the variable `PAR2`.

```
CALL condition_number
PAR2=PAR2+numbcon
```

10.2.3 Gradients Evaluation, two-sided Numerical Derivative

In this work we compute the derivatives by means of a two-sided numerical derivative as reported in Equ. 3.6 of Section 3.1.1. Which means the gradients (`FORZEbase_exp` and `FORZEbase_cx(x=1,2,3)`) are evaluated as half of the difference between `PAR2` and `PAR1` multiplied by the inverse of the step.

Two-sided Numerical Derivative

```
   DO IPRIMM=1,NPRIMG!.......Gradient definition.............
   FORZEbase_exp(IPRIMM)=FORZEbase_exp(IPRIMM)-
>                  (PAR2-PAR1)*INV_step_exp(IPRIMM)*0.5_float
   FORZEbase_c1(IPRIMM)=FORZEbase_c1(IPRIMM)-
>                (PAR2-PAR1)*INV_step_c1(IPRIMM)*0.5_float
   FORZEbase_c2(IPRIMM)=FORZEbase_c2(IPRIMM)-
>                (PAR2-PAR1)*INV_step_c2(IPRIMM)*0.5_float
   FORZEbase_c3(IPRIMM)=FORZEbase_c3(IPRIMM)-
>                 (PAR2-PAR1)*INV_step_c3(IPRIMM)*0.5_float
   ENDDO
```

At this stage we also save the maximum value in absolute terms of those gradients (`maxforze_exp` and `maxforze_cx(x=1,2,3)`) that will be involved in the convergence tests.

Gradients Absolute Maximum Value

```
maxforze_exp=maxval(abs(forzebase_exp(1:NPRIMG)))
maxforze_c1=maxval(abs(forzebase_c1(1:NPRIMG)))
maxforze_c2=maxval(abs(forzebase_c2(1:NPRIMG)))
maxforze_c3=maxval(abs(forzebase_c3(1:NPRIMG)))
```

Moreover, for each optimization cycle `BASCRYS`, gradients, exponents and coefficients are stored into `totforze_exp`, `totforze_cx(x=1,2,3)`, `totEXXstore` and `totCXMstore(M=1,2,3)`.

Gradients, Exponents and Coefficients Storing

```
        totforze_exp(1:NPRIMG,BASCRYS)=FORZEbase_exp(1:NPRIMG)
        totforze_c1(1:NPRIMG,BASCRYS)=FORZEbase_c1(1:NPRIMG)
        totforze_c2(1:NPRIMG,BASCRYS)=FORZEbase_c2(1:NPRIMG)
        totforze_c3(1:NPRIMG,BASCRYS)=FORZEbase_c3(1:NPRIMG)

        totEXXstore(1:NPRIMG,BASCRYS)=EXXstore(1:NPRIMG)
        totCX1store(1:NPRIMG,BASCRYS)=CX1store(1:NPRIMG)
        totCX2store(1:NPRIMG,BASCRYS)=CX2store(1:NPRIMG)
        totCX3store(1:NPRIMG,BASCRYS)=CX3store(1:NPRIMG)
```

These matrices are fundamental for the next section.

10.2.4 BDIIS Algorithm and New Gradients

The BDIIS algorithm and the corresponding gradients are performed in the routine named "`BDIIS_method`" available in the file `basis_opt_module.f90`. This specific routine is invoked when the optimization cycle `BASCRYS` is greater than a variable named `STARTIT` that is set by default to 1. It can be modified by the user in input by using the keyword `WAITIT`. A detailed description of the `Subroutine BDIIS_method` will be reported in Section 10.4.

BDIIS call

```
 if(BDIIS.and.(BASCRYS.gt.STARTIT))then
        totforze_exp=-totforze_exp
        totforze_c1=-totforze_c1
        totforze_c2=-totforze_c2
        totforze_c3=-totforze_c3
        CALL BDIIS_method(totEXXstore,
    >            totcx1store,totcx2store,totcx3store,
    >            totforze_exp,totforze_c1,totforze_c2,totforze_c3,
    >            BASCRYS,NPRIMG,
    >            forzebase_exp,FORZEbase_c1,FORZEbase_c2,FORZEbase_c3,
    >            MAX_HISTORY_GDIIS)
        totforze_exp=-totforze_exp
        totforze_c1=-totforze_c1
        totforze_c2=-totforze_c2
        totforze_c3=-totforze_c3
   endif
```

From this routine the new gradients (steps to applied) are performed (`FORZEBASE_exp, FORZEbase_c1, FORZEbase_c2 and FORZEbase_c3`).

10.2.5 Line Search and Step Application

In order to avoid large steps, a screening of a step multiplier is performed, scaling it from 0.05 to 1.0. (9 different step name `scale_try` are considered). This method is usually known as *Line Search Method* as described in Equ. 3.7 of Section 3.1.1. At each point a SCF calculation is performed and the point with the minimum value of total energy is then retained.

Line Search Method

```
   step_shorter=(/0.05_float,0.1_float,0.15_float,0.2_float,
&              0.3_float,0.4_float,0.6_float,0.8_float,1.0_float/)

   enemin=par0
   scale_factor=0.1_float

   scale_try_index=0

   do scale_try_index=1,9!Scale factor line search
    scale_try=step_shorter(scale_try_index)

   DO IPRIMM=1,NPRIMG

     exponent_try=EXXstore(IPRIMM)-FORZEbase_exp(IPRIMM)*
&                                  scale_try
    if(exponent_try.lt.delta_exp)then
    exx(IPRIMM)=EXXstore(IPRIMM)*0.5_float!1_float!
    else
    EXX(IPRIMM)=EXXstore(IPRIMM)-FORZEbase_exp(IPRIMM)*
&                                  scale_try!_exp
    endif

    C1(IPRIMM)=CX1store(IPRIMM)-FORZEbase_c1(IPRIMM)*
&                                  scale_try!_c1
    C2(IPRIMM)=CX2store(IPRIMM)-FORZEbase_c2(IPRIMM)*
&                                  scale_try!_c2
    C3(IPRIMM)=CX3store(IPRIMM)-FORZEbase_c3(IPRIMM)*
&                                  scale_try!_c3
    exponent_try=0._float
   ENDDO
```

At each step multiplier (`scale_try`) a SCF is performed and the energy saved as `PAR(6)`.

```
   CALL condition_number
   PAR(6)=PAR(6)+numbcon
```

If the convergence is not reached or the energy obtained is higher, the previous step multiplier is taken. If the total SCF energy is lower than the initial total energy (`enemin=PAR0`), the relative scale factor is applied (`scale_factor=scale_try`), otherwise a `scale_factor =0.1` is applied.

Scale Factor Definition

```
   if((INF(35) .eq. 1).or.(ABS(PAR(6)-PAR0).gt.ABS(PAR0))) then!SCF not convergence
     if(scale_factor.eq.0.05_float)then
        scale_factor=0.01_float
elseif((scale_factor.gt.0.05_float).and.(scale_factor.le.0.2))then
        scale_factor=scale_factor-0.05_float
elseif((scale_factor.gt.0.2_float).and.(scale_factor.le.0.4))then
        scale_factor=scale_factor-0.1_float
elseif((scale_factor.gt.0.4_float).and.(scale_factor.le.1.0))then
        scale_factor=scale_factor-0.2_float
     endif

   if(par(6).lt.enemin) Then
    ii=1
    enemin=par(6)
    scale_factor=scale_try
   else
    exit
   endif

   enddo!Scale factor line search
```

Once that the optimal step is found, we compute and apply the step and we create a new `EXXstore` and `CXMstore(M=1,2,3)`. In other words exponents and coefficients involved in the optimization are actually moved. An additional check is performed in the exponent case: since negative exponents cannot be present,

if the resultant exponent is lower than zero (`delta_exp=0._float`), half of the actual exponent is applied.

```
      exponent_low(:)=0
      DO IPRIMM=1,NPRIMG

        exponent_try=EXXstore(IPRIMM)-FORZEbase_exp(IPRIMM)*
     &                                scale_factor
       if(exponent_try.lt.delta_exp)then
       EXXstore(IPRIMM)=EXXstore(IPRIMM)*0.5_float!
       exponent_low(IPRIMM)=1
       else
       EXXstore(IPRIMM)=EXXstore(IPRIMM)-FORZEbase_exp(IPRIMM)*
     &                                scale_factor!_exp
       endif

       CX1store(IPRIMM)=CX1store(IPRIMM)-FORZEbase_c1(IPRIMM)*
     &                                scale_factor!_c1
       CX2store(IPRIMM)=CX2store(IPRIMM)-FORZEbase_c2(IPRIMM)*
     &                                scale_factor!_c2
       CX3store(IPRIMM)=CX3store(IPRIMM)-FORZEbase_c3(IPRIMM)*
     &                                scale_factor!_c3
       FORZEbase_exp(IPRIMM)=0._float
       FORZEbase_c1(IPRIMM)=0._float
       FORZEbase_c2(IPRIMM)=0._float
       FORZEbase_c3(IPRIMM)=0._float
       exponent_try=0._float
      ENDDO
```

10.2.6 Ultimate SCF and Convergence Checks

In this last section an ultimate SCF is then performed (total energy named `PAR3=PAR6`) and checks on convergence are then evaluated. The convergence of the iterative optimization procedure is verified by checking the absolute value of the largest component of both the gradients and the penalty function. The optimization is complete when the absolute value of the difference in the penalty function (`diff=par(6)-par0`) is less than $1.0 \cdot 10^{-5}$ (`toll_bas_e`) and the absolute value of the largest component of gradient converges to $3.0 \cdot 10^{-3}$ (`toll_bas_grad_exp` and `toll_bas_grad_cx(x=1,2,3)`). To avoid numerical noise in the optimization curve, if the convergence criteria are satisfied, one last SCF calculation with a new classification of integrals (`call int_screen(1)`) is performed (total energy named `PAR(6)`). At this stage if `par3-par(6)` is greater than `toll_bas_e` a supplementary optimization cycle is performed (`goto 20` option allows the restarting of the whole optimization).

```
      CALL condition_number
      PAR(6)=PAR(6)+numbcon

              diff=par(6)-par0

            if ((abs(diff).lt.toll_bas_e).and.                          &
     & (maxforze_exp.lt.toll_bas_grad_exp).and.
     & (maxforze_c1.lt.toll_bas_grad_c1).and.
     & (maxforze_c2.lt.toll_bas_grad_c2).and.
     & (maxforze_c3.lt.toll_bas_grad_c3))then

          PAR3=par(6)!fixindex
         call int_screen(1)
        CALL INT_CALC
        IF(ALLOCATED(PG_IRR))DEALLOCATE(PG_IRR)
        IF(ALLOCATED(FG_IRR))DEALLOCATE(FG_IRR)
        CALL SCF

        CALL OUTO3B(IUNIT(20))

        CALL FINE2
        CALL tidy_memory

      CALL condition_number
      PAR(6)=PAR(6)+numbcon

            if(abs(par3-par(6)).gt.toll_bas_e)then!fixindex
               par0=par(6)
               goto 20!fixindex
            endif!fixindex

           exit
```

With this last section the optimization cycle (ultimate or not) is then accomplished.

10.2.7 Condition Number

As mentioned earlier, an additional routine is present in the `basis_opt.f` file named `condition_number` in which the actual condition number is performed. For sake of completeness is here reported.

As reported in Section 3.1.1 in Eq. 3.5, the minimization involved the system total energy to which we add a penalty function including the overlap matrix condition number. In the code below reported, once the overlap matrix (`SK`) is constructed (`CALL SDIG`), through the routine `REIGN` we evaluated both eigenvectors and eigenvalues (`SKevec` and `SKeval` respectively). Then the largest and the smallest eigenvalue of the overlap matrix are evaluated (`EMAX` and `EMIN` respectively). Considering a value $\gamma = 0.001$ (`gammacon`) as suggested in [2] and the base-e logarithm of the ratio between them at the center of the Brillouin zone (Γ-point), we define `numbcon` that is our penalty function.

The purpose of such penalty function is to prevent the onset of harmful linear dependence. Linear dependence issues can give rise to numerical instabilities and, as a consequence of that, the appearance of unphysical states. Such unphysical states generally lead to a catastrophic behaviour of the total energy that can drop to a value that is orders of magnitude larger, in absolute value, than the proper one.

Subroutine condition_number

```
 Subroutine condition_number

  Call cryalloc(sg_irr,isize_sg_irr,znamz,'sg_irr')
  Call cryalloc(sg_red,isize_sg_red,znamz,'sg_red')
  ndf=inf(7)
  Call cryalloc(ex,2,inf(79),znamz,'ex')
  Call cryalloc(exvrs,inf(79),2,znamz,'exvrs')
CALL CRYALLOC(SK    ,ndf*ndf,ZNAMZ,'SK    ')
CALL CRYALLOC(SKevec,ndf,ndf,ZNAMZ,'SKevec')
SKevec(:,:)=0._float
CALL CRYALLOC(SKeval,ndf,ZNAMZ,'SKeval')
SKeval(:)=0._float
  Call Allocate_jacobi(ndf)
  CALL SDIG
  Call expt(0,0,0)

  CALL TRAFN(SG_RED,SK,IDMCOU)
  Call Symheq(sk,ndf)

  CALL REIGN(SK,SKevec,SKeval,ndf,0,0)

  Call crydealloc(ex,znamz,'ex')
  Call crydealloc(exvrs,znamz,'exvrs')
  Call Free_jacobi
CALL CRYDEALLOC(SK    ,ZNAMZ,'SK    ')
  Call crydealloc(sg_irr,znamz,'sg_irr')
  Call crydealloc(sg_red,znamz,'sg_red')
EMIN=100000._float
DO j_numbc=1,ndf
 if (abs(SKeval(j_numbc)) .LT. EMIN) then
   EMIN = abs(SKeval(j_numbc))
   IMIN =j_numbc
 end if
ENDDO
EMAX=0._float
DO j_numbc=1,ndf
 if (j_numbc.eq.imin) cycle
 if (ABS(SKeval(j_numbc)) .GT. EMAX) then
   EMAX = ABS(SKeval(j_numbc))
 end if
ENDDO
CALL CRYDEALLOC(SKevec,ZNAMZ,'SKevec')
CALL CRYDEALLOC(SKeval,ZNAMZ,'SKeval')

numbcon=gammacon*LOG(EMAX/EMIN)
numbcon=numbcon
numbcon_eff=EMAX/EMIN

End Subroutine condition_number
```

10.3 Basis opt Module

File: `basis_opt_module.f90`

Many variables, general definitions and the keywords available are included in the `basis_opt_module.f90` file.

Moreover, in this file the aforementioned `Subroutine EXP_MOVE_1` is included. For sake of completeness is here reported.

In this routine the step is effectively applied. This is fundamental to get the gradients for the optimization.

Subroutine EXP_MOVE_1

```
Subroutine EXP_MOVE_1(iprimm,info,step)
      use numbers
      use memory_use
      use PARAL1_MODULE
      use basato_module
      USE MEMORY_G

implicit none
character(len=10), parameter :: znamz='EXP_MOVE_1'
integer     , intent(in) :: iprimm, info
real(float) , intent(in) :: step
integer::i

NPRIMG=INF(75)

If(info.eq.1) Then
  EXX(iprimm)=EXXstore(iprimm) + step
  C1(iprimm) =CX1store(iprimm)
  C2(iprimm) =CX2store(iprimm)
  C3(iprimm) =CX3store(iprimm)
Else if (info.eq.2) Then
  EXX(iprimm)=EXXstore(iprimm)
  C1(iprimm) =CX1store(iprimm) + step
  C2(iprimm) =CX2store(iprimm)
  C3(iprimm) =CX3store(iprimm)
Else if (info.eq.3) Then
  EXX(iprimm)=EXXstore(iprimm)
  C1(iprimm) =CX1store(iprimm)
  C2(iprimm) =CX2store(iprimm) + step
  C3(iprimm) =CX3store(iprimm)
Else if (info.eq.4) Then
  EXX(iprimm)=EXXstore(iprimm)
  C1(iprimm) =CX1store(iprimm)
  C2(iprimm) =CX2store(iprimm)
  C3(iprimm) =CX3store(iprimm) + step
EndIf

1134  FORMAT('EXX_expmove_1',40X,1P,4E21.13)
1135  FORMAT(35('~.~'))

End Subroutine EXP_MOVE_1
```

The variable `info` it is related with the kind of optimization performed: `info=1` only exponents, while `info=2,3,4` for s, p and d-f-g coefficients.

10.4 BDIIS Module

File: `basis_opt_module.f90`

The core of the BDIIS algorithm is implemented in this module, in particular here the `Subroutine BDIIS_method` is included.

Before starting the actual algorithm, it can be useful to describe the arguments required for the subroutine calling.

```
SUBROUTINE BDIIS_method(Posix,Posix1,Posix2,Posix3,Er,Er1,Er2,Er3,NCRYS,NPRIMG,EXPCOO,EXPCOO1,EXPCOO2,EXPCOO3, &
                        MAX_HISTORY_GDIIS)
```

- `Posix` and `PosixM(M=1,2,3)` correspond to `totEXXstore` and `totcxMstore(M=1,2,3)`; they are the matrices that store at each optimization cycle `BASCRYS` exponents and coefficients.

- `Er` and `ErM(M=1,2,3)` correspond to `totforze_exp` and `totforze_cM(M=1,2,3)`; they are the matrices that store at each optimization cycle `BASCRYS` exponents and coefficients gradients.
- `NCRYS`, it is an integer that corresponds to the iteration number (named `BASCRYS` elsewhere).
- `NPRIMG`, it is an integer that corresponds to the number of primitives in the basis set.
- `EXPCOO` and `EXPCOOM(M=1,2,3)` corresponds to `FORZEbase_exp` and `FORZEbase_cM(M=1,2,3)`; they are the vectors related with the exponents and coefficients gradients.
- `MAX_HISTORY_GDIIS`, number of steps considered in the BDIIS calculation. By default, `MAX_HISTORY_GDIIS=14`. It can be modified by the keyword `TAKEONLY` in input.

Posix and Er are the main information that comes from the preceding part of the code. Once each matrix used in this subroutine is allocated and properly defined, it is possible to build up `AEr` and `ZEr` matrices needed for the BDIIS equations. In fact, as described in the Equ. 3.2 of Section 3.1, we want to solve a matrix equation simply expressed by:

$$AEr \cdot CEr = ZEr \tag{10.1}$$

where

$$AEr : \begin{pmatrix} a_{1,1} & \dots & a_{1,n} & 1 \\ \vdots & \ddots & \vdots & \vdots \\ a_{n,1} & \dots & a_{n,n} & 1 \\ 1 & \dots & 1 & 0 \end{pmatrix}, \; ZEr : \begin{pmatrix} 0 \\ \vdots \\ 0 \\ 1 \end{pmatrix} \tag{10.2}$$

Care must be taken to the fact that in this context the number of cycles is called `NCRYS`, `NCRYS1` and `NCRYS_SHIFT`. `NCRYS1` is the same number of cycles added by one to get the real dimensions of `AEr` and `ZEr`. `NCRYS_SHIFT` is an integer that modifies the dimension of `AEr`. In fact, the BDIIS method requires the storing of data for a specific number of cycles defined by the variable `MAX_HISTORY_GDIIS`. In particular, the keyword `TAKEONLY`, that reads the variable defined by `MAX_HISTORY_GDIIS` can modify the abovementioned number in input. For instance, if in an input file `TAKEONLY` is set at `5`, the algorithm will take only the last five steps for the evaluation of the new set of exponents or coefficients. In particular, by default we set `TAKEONLY` to `14`, thus only the last 14 steps are always kept throughout the calculation.

```
NCRYS_SHIFT=NCRYS-MIN(NCRYS,MAX_HISTORY_GDIIS)

NCRYS1=NCRYS + 1 - NCRYS_SHIFT
```

In the section reported below `AEr` and `ZEr` matrices are constructed along with another vector needed for the BDIIS algorithm:

- `Order` is a vector that stores the index order, important for the size reduction method.

AEr and ZEr construction

```
DO k=1,NCRYS-NCRYS_SHIFT
  Order(k)=k+NCRYS_SHIFT
 ENDDO

DO i= 1,NCRYS1
  DO j= 1, NCRYS1
     if (i==NCRYS1 .AND. j<=NCRYS-NCRYS_SHIFT) then
       aij=1._float
     elseif (i==NCRYS1 .AND. j==NCRYS1) then
       aij=0._float
     elseif (i<=NCRYS-NCRYS_SHIFT .AND. j==NCRYS1) then
       aij=1._float
     else
       aij = 0._float
      DO k = 1,NPRIMG
       aij=aij + Er(k,i+NCRYS_SHIFT)*Er(k,j+NCRYS_SHIFT)
       aij=aij + Er1(k,i+NCRYS_SHIFT)*Er1(k,j+NCRYS_SHIFT)
       aij=aij + Er2(k,i+NCRYS_SHIFT)*Er2(k,j+NCRYS_SHIFT)
       aij=aij + Er3(k,i+NCRYS_SHIFT)*Er3(k,j+NCRYS_SHIFT)
       ENDDO
     endif
       AEr(i,j)=aij
  ENDDO
ENDDO

DO i=1,NCRYS1
 if (i==NCRYS1) then
  zi=1._float
 Else
  zi=0._float
 endif
 ZEr(i)=zi
ENDDO
```

In the following part a particular kind of cycle is reported. In fact, the first row is labeled by the number 25 and the full procedure restarts when it reaches the row `goto 25`. The strategy used is the following:

- make a copy of the matrices `AEr` and `ZEr` called `AErBIS` and `ZErBIS` respectively;
- call the `Subroutine REIGN` in order to find `AEr` eigenvalues (`AErVAL`) and eigenvectors (`AErVEC`);
- find the minimum (`EMIN`) and the maximum (`EMAX`) value of the eigenvalues in absolute terms;
- if `EMIN` is lower than `EMAX` multiplied by a specific number, the index related with `EMIN` is saved as `LSTZER`. In particular, we set a ratio `EMIN/EMAX`

(condition number) as a threshold to determine the launching or the suspension of `AEr` size reduction. In fact, if the "if" statement is not satisfied the execution exits the loop. As already mentioned the condition number is set to 10^{-4}, thus `tolremuv` is set by default as 4;

- find two largest components of the eigenvectors with indexes `MAX11` and `MAX22` in the column `LSTZER` and take only the one which has the lower value. This index is called `REMUV`;

- Remove `AErBIS` column and row with `REMUV` index just found. The same also for the `ZEr` and `Order` matrices.

The only thing that we have to take care of are the allocations and deallocations of the matrices involved in this reduction and the information related with the column-row removal. In fact, for this reason the vector `Order` was introduced to have memory of the indexes.

Matrix Size Reduction - Part 1

```
!! restart from here after reduction of space size
      q=0
  25  Continue
      q=q+1

      DO i=1, NCRYS1
       DO j=1, NCRYS1
        AErBIS(i,j)=AEr(i,j)
       ENDDO
      ENDDO
      DO i=1, NCRYS1
        ZErBIS(i)=ZEr(i)
      ENDDO

      CALL REIGN(AEr, AErEVEC, AErEVAL, NCRYS1, 0,0)

      EMIN=100000._float
      DO j=1,NCRYS1
       if (abs(AErEVAL(j)) .LT. EMIN) then
         EMIN = abs(AErEVAL(j))
         IMIN =j
       end if
      ENDDO
      EMAX=0._float
      DO j=1,NCRYS1
       if (j.eq.imin) cycle
       if (ABS(AErEVAL(j)) .GT. EMAX) then
         EMAX = ABS(AErEVAL(j))
       end if
      ENDDO

      tolremuv=4
      If(emin.lt.EMAX*0.1_float**tolremuv) Then
         lstzer=imin
         izer=1
      else
         izer=0
      endif
```

Matrix Size Reduction - Part 2

```
      if((IZER.GT.0).AND.(NCRYS1.GT.3).AND.                          &
       (emin.lt.EMAX*0.1_float**tolremuv))then
       CMPMAX=0._float
        DO k=1, NCRYS1-1
          if (ABS(AErEVEC(k,lstzer)) .GT. CMPMAX) then
           CMPMAX=ABS(AErEVEC(k,lstzer))
           MAX11=k
          endif
        ENDDO
       CMPMAX2=0._float
        DO k=1, NCRYS1-1
        if (k .NE. MAX11) then
         if (ABS(AErEVEC(k,lstzer)) .GT. CMPMAX2) then
           CMPMAX2=ABS(AErEVEC(k,lstzer))
           MAX22=k
         end if
        end if
        ENDDO
       REMUV=MIN(MAX11, MAX22)
```

Matrix Size Reduction - Part 3

```
        DO i=REMUV, NCRYS1-1
          DO j=1, NCRYS1
            AErBIS(i,j)=AErBIS(i+1,j)
          ENDDO
        ENDDO
        DO i=REMUV, NCRYS1-1
          DO j=1, NCRYS1
           AErBIS(j,i)=AErBIS(j,i+1)
          ENDDO
        ENDDO

        DO i=REMUV, NCRYS1-1
            ZErBIS(i)=ZErBIS(i+1)
        ENDDO

        DO k=REMUV, NCRYS1-2
         Order(k)=Order(k+1)
        ENDDO

       NCRYS1=NCRYS1-1

      Call CryDealloc(Aer,znamz,'AEr')
      CALL CRYALLOC(AEr,NCRYS1, NCRYS1,ZNAMZ, 'AEr' )
      Call CryDealloc(Zer,znamz,'ZEr')
      CALL CRYALLOC(ZEr,NCRYS1,ZNAMZ, 'ZEr' )

      DO i=1, NCRYS1
       DO j=1, NCRYS1
        AEr(i,j)=AErBIS(i,j)
       ENDDO
      ENDDO
      DO i=1, NCRYS1
        ZEr(i)=ZErBIS(i)
      ENDDO
      Call CryDealloc(AerBIS,znamz,'AErBIS')
      Call CryDealloc(ZerBIS,znamz,'ZErBIS')
      Call CryDealloc(AerEVEC,znamz,'AErEVEC')
      CALL CRYALLOC(AErEVEC, NCRYS1, NCRYS1,ZNAMZ, 'AErEVEC')
      AErEVEC=0._float
      CALL CRYALLOC (AErBIS, NCRYS1, NCRYS1, ZNAMZ, 'AErBIS')
      AErBIS=0._float
      CALL CRYALLOC (ZErBIS, NCRYS1, ZNAMZ, 'ZErBIS')
      ZErBIS=0._float

      goto 25
      EndIf
```

Finally, BDIIS equations are solved by calling a subroutine called `diis_solve` contained in the file `diis_module.f90` in order to obtain the coefficients. In particular, this calculation overwrites the `ZEr` vector. Hereafter, `ZEr` coincides with `CEr`, which is our aim.

Some checks have been introduced regarding the values obtained by this rou-

tine. In fact, the sum of the positive coefficients must be lower than 15, otherwise an error message will appear.

Subsequently, there are two main DO cycles: one allows the construction of the step and the other of `EXPCOO` and `EXPCOOM(M=1,2,3)`. These last corresponds to the exponents and coefficients gradients `FORZEbase_exp` and `FORZEbase_cM(M=1,2,3)` required.

The real variables `pij` and `pijM(M=1,2,3)` contains the new exponents and coefficients ($\mathbf{x}_{n+1}$) of the system:

$$\mathbf{x}_{n+1} = \sum_{i=1}^{n} c_i(\mathbf{x}_i + \mathbf{e}_i) \tag{10.3}$$

in which

- $\mathbf{x}_{n+1}$ corresponds to `pij`;
- c_i corresponds to `ZEr(j)`, thus the coefficients previously related with the vector `CEr`;
- $\mathbf{x}_i$ is related with `Posix(i,k)` elements;
- $\mathbf{e}_i$ is related with `Er(i,k)` elements.

As regards `EXPCOO` and `EXPCOOM(M=1,2,3)`, they are related with the BDIIS step and they are given as the difference between the new exponents-coefficients and the old ones. In mathematical terms:

$$\sum_{i=1}^{n} c_i\mathbf{e}_i = \mathbf{x}_{n+1} - \sum_{i=1}^{n} c_i\mathbf{x}_i \tag{10.4}$$

Exponents and Coefficients Gradients, Steps

```
      CALL diis_solve(AErBIS, ZErBIS, NCRYS1)

!Check: sum of positive coefficients<15
      DO j=1,NCRYS1-1
         k=order(j)
       if (ZErBIS(j) .gt. 0._float) then
         ZERBISpiu(j)=ZERBIS(j)
       endif
      ENDDO

        sumcoeffi=sum(ZErBISpiu(1:NCRYS1-1))

      If (sumcoeffi .gt. 15._float) Call errvrs(2,znamz,'Sum of positive coefficients exceed 15')

!Displacement construction

      DO i=1, NPRIMG
        pij=0._float
        pij1=0._float
        pij2=0._float
        pij3=0._float
       DO j=1, NCRYS1-1!-NCRYS_SHIFT
           k=order(j)

           pij=pij+ZErBIS(j)*(Posix(i,k) + Er(i,k))

           pij1=pij1+ZErBIS(j)*(Posix1(i,k) + Er1(i,k))
           pij2=pij2+ZErBIS(j)*(Posix2(i,k) + Er2(i,k))
           pij3=pij3+ZErBIS(j)*(Posix3(i,k) + Er3(i,k))

        ENDDO
         EXPCOO (i) = Posix (i,ncrys) - pij
         EXPCOO1(i) = Posix1(i,ncrys) - pij1
         EXPCOO2(i) = Posix2(i,ncrys) - pij2
         EXPCOO3(i) = Posix3(i,ncrys) - pij3
      ENDDO
```

10.5 LBFGS Method

File: `lbfgsbas.f`

As regard the LBFGS method an auxiliary file was introduced. The LBFGS algorithm is described in "On the limited memory BFGS method for large scale optimization", by D. Liu and J. Nocedal, Mathematical Programming B 45 (1989) 503-528.[3] The file is named `lbfgsbas.f` in which a `SUBROUTINE LBFGS` is reported. The method was implemented for the exponents optimization. It is not yet available for the coefficients.

This subroutine solves the unconstrained minimization problem

$$minF(x), x = (x_1, x_2, ..., x_N), \tag{10.5}$$

using the Limited Memory BFGS method (LBFGS). The routine is especially effective on problems involving a large number of variables. In a typical iteration of this method an approximation `Hk` to the inverse of the Hessian is obtained by applying `M` BFGS updates to a diagonal matrix `Hk0`, using information from the previous `M` steps. The number `M` has to be specified and it determines the amount of storage required by the routine. The routine requires to calculate the function

value F and its gradient G. The step length is determined at each iteration by means of the line search method.

The calling statement is

```
CALL LBFGS(N,M,X,F,G,DIAGCO,DIAG,IPRINT,EPS,XTOL,W,IFLAG)
```

where

- N is an INTEGER variable that must be set to the number of variables. It is not altered by the routine. The restriction is: N>0. In our case it is the number of primitives (N=NPRIMG).
- M is an INTEGER variable that must be set to the number of corrections used in the BFGS update. It is not altered by the routine. Values of M less than 3 are not recommended; large values of M will result in excessive computing time. 3<= M <=7 is recommended. The restriction is: M>0. In our case M was set to 5.
- X is a DOUBLE PRECISION array of length N. On initial entry it must be set to the values of the initial estimate of the solution vector. On exit, it contains the values of the variables at the best point found (usually a solution). In our case are the exponents collected in the vector EXXstore.
- F is a DOUBLE PRECISION variable. It must be set by the user to contain the value of the function F at the point X. In our case F=PAR0, thus the energy.
- G is a DOUBLE PRECISION array of length N. It must contain the components of the gradient G at the point X. In our case FORZEbase_exp.
- DIAGCO is a LOGICAL variable that must be set to .TRUE. if the user wishes to provide the diagonal matrix Hk0 at each iteration. Otherwise, it should be set to .FALSE., in which case LBFGS will use a default value. In our case DIAGCO= .FALSE. .
- DIAG is a DOUBLE PRECISION array of length N. If DIAGCO=.TRUE., it must contain the values of the diagonal matrix Hk0. The restriction is: all elements of DIAG must be positive.
- IPRINT is an INTEGER array of length two. We set them to PRINT(1)= -1. and IPRINT(2)= 3. These options switch off the default printing option. In particular, we have used our own printing option (customized).
- EPS is a positive DOUBLE PRECISION variable that determines the accuracy with which the solution has to be found. In our case EPS_BAS= 1.0D-5.
- XTOL is a positive DOUBLE PRECISION variable that must be set by the user to an estimate of the machine precision. In our case XTOL= 1.0D-16.

- `W` is a `DOUBLE PRECISION` array of length `N(2M+1)+2M` used as workspace for `LBFGS`. This array must not be altered by the user.
- `IFLAG` is an `INTEGER` variable that must be set to `0` on initial entry to the subroutine. It is related with error detections.

For us these variables are defined in `basis_opt.f` where the call statement is also invoked.

The resultant of the `Subroutine LBFGS` is directly a new set of exponents `exx_bfgs`. The difference between the latter and the previous exponents gives the new step (`step_bfgs`) to apply, in other words the gradient (`FORZEbase_exp`). No line search method is applied (`scale_factor=1._float`) to this final gradient because already performed in `Subroutine LBFGS` internally. `IPRIMM` in the following is the loop index on the primitives.

```
step_bfgs(IPRIMM)=(exx_bfgs(IPRIMM)-EXXstore_red(IPRIMM))

FORZEbase_exp(j_hes)=-step_bfgs(IPRIMM)
```

10.6 How to Activate the Algorithm in CRYSTAL

The activation of the optimization is possible by introducing specific *Keywords* in the input, in particular, soon after the geometry section.

In Table 10.1 there are some options available along with their description, where keywords in bold are always used in input.

The minimal set up to run a basis set optimization for the exponents (default set up) is:

```
OPTBASIS
ENDBO
```

it has to be inserted in the geometry section of the CRYSTAL input.

In this specific block extra options can be inserted as reported in Table 10.1. In particular, `COEFFONLY` if the optimization involved only coefficients, `ALLBDIIS` if both exponents and coefficients have to be optimized.

If LGFGS method is required, this is the minimal set up:

```
OPTBASIS
BFGSBAS
ENDBO
```

In this case only exponents can be involved.

Some thresholds are needed in order to decide when the optimization is converged. Consequently, the convergence is complete if these conditions are all satisfied at the same time. All the default values could be modified by suitable keywords summarized in the Table 10.1. By default, the tolerance on energy is set to 10^{-5} (`TOLOPTE`), while on the gradients is $3 * 10^{-3}$ (`TOLOPTG`). The maximum number of cycle is set to 500 by default, but even in this case, inserting the keyword `MAXBASCYC` it can be modified.

Keyword	*Description*
OPTBASIS	Basis optimization active (Default: Only exponent optimization)
COEFFONLY	Only coefficients optimization
ALLBDIIS	Exponents and coefficients optimization
WAITIT No.	Starting BDIIS cycle. Default: 1st cycle
TAKEONLY No.	Number of cycles stored for BDIIS calculations. Default: 14 cycles
TOLOPTE No.	Tolerance on energy. Default: $5 \rightarrow 10^{-5}$
TOLOPTG No.	Tolerance on gradient. Default: $0.002 \rightarrow 0.002 * 1.5 = 3 * 10^{-3}$
MAXBASCYC No.	Max number of cycles for the basis set optimization. Default: 500 cycles
NUMBC No.	Condition number activated Value of the gamma scalar factor (Default: 0.001)
REFBAS No.	Intscreen at a certain cycle. No. of cycles before INTSCREEN option. Default: 10 Integrals screening based on the new set of basis functions.
BFGSBAS	LBFGS method (only exponents)
ENDBO	Basis Set Optimization END statement

Table 10.1: Summary of the keywords available for the basis set optimization. In bold the keywords mandatory for the activation of the method. This section has to be introduced in the geometry section of the CRYSTAL input.

The shells involved in the optimization must be highlighted by a star * in the input basis set. e.g.:

```
...
0 0 1 0 1 *
      1.2429415962           1.0000000
...
```

Suggestions: since the valence shells are usually the ones involved in the chemical bonding, these are the ones usually to be optimized. For less expert users, it is recommended to optimize only exponents and if possible it is also suggested to uncontract the shells if not already. In order to follow the optimization steps, besides checking the minimization of the *Objective Function*, it can be useful to check the stability of the SCF calculations performed in the meanwhile. This information is available in the `SCFOUT.LOG` file where a storing of all the SCF calculations performed are reported.

In the following sections an example of input and output is described in details.

10.6.1 Input

As mentioned earlier, in order to activate the BDIIS optimization, an auxiliary block has to be inserted in the geometry input section (*filename.d12*). Moreover, an asterisk has to be inserted in the line corresponding to the shell involved in the optimization. An example regarding He bulk (molecular def2-QZVP basis set from the Basis Set Exchange software [4]) is reported. In red the basis set options are highlighted.

Input He bulk. Exponent optimization (Default option)

```
He-crystal
CRYSTAL
0 0 0
194
2.92661 4.77913
1
2    0.333333333333333   -0.333333333333333   0.250000000000000
OPTBASIS
ENDBO
END
  2 10
0 0 5 2 1
   1144.6470809              0.35861578618E-03
    171.64596667             0.27725434466E-02
     39.066056254            0.14241892216E-01
     11.051401989            0.55457352277E-01
      3.5725574473           0.16170511810
0 0 1 0 1 *
      1.2429415962           1.0000000
0 0 1 0 1 *
      0.44807668730          1.0000000
0 0 1 0 1 *
      0.16411579128          1.0000000
0 2 1 0 1 *
      5.99400000             1.0000000
0 2 1 0 1 *
      1.74500000             1.0000000
0 2 1 0 1 *
      0.56000000             1.0000000
0 3 1 0 1 *
      4.29900000             1.0000000
0 3 1 0 1 *
      1.22300000             1.0000000
0 4 1 0 1 *
      2.68000000             1.0000000
99 0
END
DFT
PBE
END
TOLINTEG
8 8 8 8 16
SHRINK
8 8
TOLDEE
8
END
```

In this specific case all the uncontracted shells and only the exponents are involved in the optimization. As regard the thresholds, here the default options are kept.

10.6.2 Output

Essentially three files are generated from the basis set optimization:

- *filename.out*: this is the usual output file generated by CRYSTAL in which the information related with each cycle of optimization is reported.
- *filename.out2*: this is usually called SCFOUT.LOG. This is a file where all the background SCF calculations are printed out.
- *filename.f53*: a fort.53 unit where the optimized basis sets at each optimization cycle are printed out.

For sake of clarity parts of a *filename.out* is below described in details. In particular, this file is the corresponding output file of the He bulk in Section 10.6.1.

Output He bulk. Basis Set Optimization initial set up.

```
== SCF ENDED - CONVERGENCE ON ENERGY      E(AU) -5.7865023495207E+00 CYCLES   5


ENERGY EXPRESSION=HARTREE+FOCK EXCH*0.00000+(PBE       EXCH)*1.00000+PBE       CORR


TOTAL ENERGY(DFT)(AU)(  5) -5.7865023495207E+00 DE-1.4E-13 tester 4.1E-14
TTTTTTTTTTTTTTTTTTTTTTTTTTTTTT EDFT        TELAPSE        3.31 TCPU        3.22

~.~.~.~.~.~.~.~.~.~.~.~.~.~.~.~.~.~.~.~.~.~.~.~.~.~.~.~.~.~.~.~.~.~.~.~.~.~.~.
                        ~. BASIS SET OPTIMIZATION .~
~.~.~.~.~.~.~.~.~.~.~.~.~.~.~.~.~.~.~.~.~.~.~.~.~.~.~.~.~.~.~.~.~.~.~.~.~.~.~.

Energy function minimized: ENERGY COND

     ENERGY COND = TOTAL ENERGY + COND No.
     COND No. = GAMMA*ln(EFF)
     EFF = MAX/MIN OVERLAP EIGENVALUE RATIO

INITIAL ENERGY COND (AU):  -5.7818041648630E+00

GAMMA FACTOR:  1.0000E-03

INITIAL EFF:  1.09748E+02

BDIIS OPERATIVE:
                STARTING CYCLE     1
                CYCLES STORED      14

TWO-SIDED NUMERICAL DERIVATIVE,1% EXPONENTS STEP

INITIAL SHELLS TO OPTIMIZE, ONLY EXPONENTS:

ATOMIC SPECIES:    2 HE

     EXP                 COEF
S    1.24294159620E+00   1.00000000000E+00
S    4.48076687300E-01   1.00000000000E+00
S    1.64115791280E-01   1.00000000000E+00
P    5.99400000000E+00   1.00000000000E+00
P    1.74500000000E+00   1.00000000000E+00
P    5.60000000000E-01   1.00000000000E+00
D    4.29900000000E+00   1.00000000000E+00
D    1.22300000000E+00   1.00000000000E+00
F    2.68000000000E+00   1.00000000000E+00
```

Once the first SCF calculation is performed an initial banner define the beginning of the optimization (`~. BASIS SET OPTIMIZATION .~`). Moreover, the general set up and the formalism used for the calculation are printed out:

- `ENERGY COND`, the *Objective Function* that corresponds to the suitable functional Ω to be minimized. Here we decide to minimize the system total energy to which we add a penalty function including the Overlap matrix condition number, following the proposal of [2]. It is named as Ω in Equ.8 of [1] and in Equ. 3.5 of the Section 3.1.1.

- `COND No.`, it is the actual penalty function. Considering Equ. 3.5 of the Section 3.1.1, it corresponds to:

$$\gamma \cdot ln\kappa \tag{10.6}$$

  where $\gamma = 0.001$ (`GAMMA`) and κ (`EFF`) is the condition number, thus the ratio between the largest and the smallest eigenvalue of the overlap matrix at the center of the Brillouin zone (Γ-point).

- BDIIS algorithm is active by default starting from the first cycle and storing the last 14 cycles (`BDIIS OPERATIVE` in the output).

- The atomic species and the shells to be optimized are also printed out at the beginning.

Output He bulk. First cycle of the Basis Set Optimization. Gradients.

```
~.~.~.~.~. OPT CYC     1    MAX OPT CYC   500

 AT. SH. No.EXP ENERGY COND (AU)    DIFF (AU)    STEP
  2   2     1   -5.78178249353E+00   2.1671E-05   1.2429E-02
  2   2     1   -5.78180706873E+00  -2.9039E-06  -1.2429E-02
  2   3     1   -5.78181995595E+00  -1.5791E-05   4.4808E-03
  2   3     1   -5.78178094677E+00   2.3218E-05  -4.4808E-03
  2   4     1   -5.78178068518E+00   2.3480E-05   1.6412E-03
  2   4     1   -5.78182532723E+00  -2.1162E-05  -1.6412E-03
  2   5     1   -5.78180412857E+00   3.6293E-08   5.9940E-02
  2   5     1   -5.78180420199E+00  -3.7132E-08  -5.9940E-02
  2   6     1   -5.78180405405E+00   1.1081E-07   1.7450E-02
  2   6     1   -5.78180427928E+00  -1.1442E-07  -1.7450E-02
  2   7     1   -5.78180312289E+00   1.0420E-06   5.6000E-03
  2   7     1   -5.78180522236E+00  -1.0575E-06  -5.6000E-03
  2   8     1   -5.78180421399E+00  -4.9123E-08   4.2990E-02
  2   8     1   -5.78180411412E+00   5.0741E-08  -4.2990E-02
  2   9     1   -5.78180443937E+00  -2.7451E-07   1.2230E-02
  2   9     1   -5.78180387769E+00   2.8717E-07  -1.2230E-02
  2  10     1   -5.78180416463E+00   2.3199E-10   2.6800E-02
  2  10     1   -5.78180416510E+00  -2.3714E-10  -2.6800E-02

 AT.  N. SH. GRAD EXP    GRAD COEF
  2   HE
         S   9.8859E-04  0.0000E+00
         S  -4.3530E-03  0.0000E+00
         S   1.3601E-02  0.0000E+00
         P   6.1249E-07  0.0000E+00
         P   6.4536E-06  0.0000E+00
         P   1.8745E-04  0.0000E+00
         D  -1.1615E-06  0.0000E+00
         D  -2.2963E-05  0.0000E+00
         F   8.7523E-09  0.0000E+00
```

Then the first optimization cycle can start, printing out the `ENERGY COND (AU)` and the difference (`DIFF (AU)`) with respect to the initial energy at each SCF calculation.

We compute the derivatives by means of a two-sided numerical derivative as reported in Equ. 3.6. For this reason forwards and backwards SCF energies and the step used are reported for each exponent involved (1% of the exponents as step). Moreover, the respective gradients are printed out.

Output He bulk. First cycle of the Basis Set Optimization. Line Search Method.

```
LINE SEARCH FOR THE BEST SCALE FACTOR

SCALE FACTOR  ENERGY COND (AU)      DIFF (AU)
   0.50E-01   -5.7818235435181E+00  -1.9379E-05
   0.10       -5.7818323857410E+00  -2.8221E-05
   0.15       -5.7818406558173E+00  -3.6491E-05
   0.20       -5.7818554570949E+00  -5.1292E-05
   0.30       -5.7818679022546E+00  -6.3737E-05
   0.40       -5.7818855418218E+00  -8.1377E-05
   0.60       -5.7818932056888E+00  -8.9041E-05
   0.80       -5.7818905189361E+00  -8.6354E-05

OPTIMAL SCALE FACTOR:    0.80     ENERGY COND (AU): -5.7818905189361E+00
```

The line search method is then applied and for each scale factor trial the respective SCF energy (`ENERGY COND (AU)`) and the difference (`DIFF (AU)`) with respect to the initial one are shown. (See Equ. 3.7).

Of course also the optimal scale factor (`0.80` in this case) and the final energy are printed out at the end of the line search.

Output He bulk. First cycle of the Basis Set Optimization. Convergence Tests.

```
MAX DIFF ENERGY COND     8.9040825747E-05 THRESHOLD   1.0000E-05  CONVERGED NO
MAX GRAD EXPONENT        1.3600780688E-02 THRESHOLD   3.0000E-03  CONVERGED NO
MAX GRAD S COEF          0.0000000000E+00 THRESHOLD   3.0000E-03  CONVERGED YES
MAX GRAD P COEF          0.0000000000E+00 THRESHOLD   3.0000E-03  CONVERGED YES
MAX GRAD D/F/G COEF      0.0000000000E+00 THRESHOLD   3.0000E-03  CONVERGED YES

TOTAL ENERGY(DFT)(AU)(  4) -5.7865587426803E+00 DE-2.2E-12 DP 5.2E-13

ENERGY COND (AU) -5.7818932056887E+00  COND No.  4.66554E-03 EFF  1.06223E+02

GAMMA FACTOR:  1.0000E-03

                  *** OPTIMIZED SHELLS AT CYCLE     1 ***

ATOMIC SPECIES:    2 HE

     EXP                 COEF                                  DIFF EXP
S    1.24215072387E+00   1.00000000000E+00                     -7.909E-04
S    4.51559054239E-01   1.00000000000E+00                      3.482E-03
S    1.53235166729E-01   1.00000000000E+00                     -1.088E-02
P    5.99399951001E+00   1.00000000000E+00                     -4.900E-07
P    1.74499483709E+00   1.00000000000E+00                     -5.163E-06
P    5.59850037827E-01   1.00000000000E+00                     -1.500E-04
D    4.29900092918E+00   1.00000000000E+00                      9.292E-07
D    1.22301837068E+00   1.00000000000E+00                      1.837E-05
F    2.67999999300E+00   1.00000000000E+00                     -7.002E-09

Writing optimized basis set to fort.53

~.~.~.~.~. OPT CYC     2    MAX OPT CYC   500
```

Then the tests for convergence are computed: convergence on both energy differences and gradients are performed. The total energy (`TOTAL ENERGY(AU)`), the "Objective Function" (`ENERGY COND (AU)`) and the new exponents/coefficients with the differences with respect to the previous cycle are printed out at the end of each optimization cycle.

When the convergence test are all satisfied, the basis set optimization is done and the final optimized basis set is printed out in the usual out format.

Output He bulk. Last cycle of the Basis Set Optimization. Optimized Basis Set.

```
 MAX DIFF ENERGY COND     7.4338299516E-06 THRESHOLD   1.0000E-05  CONVERGED YES
 MAX GRAD EXPONENT        1.9252979798E-03 THRESHOLD   3.0000E-03  CONVERGED YES
 MAX GRAD S COEF          0.0000000000E+00 THRESHOLD   3.0000E-03  CONVERGED YES
 MAX GRAD P COEF          0.0000000000E+00 THRESHOLD   3.0000E-03  CONVERGED YES
 MAX GRAD D/F/G COEF      0.0000000000E+00 THRESHOLD   3.0000E-03  CONVERGED YES

 TOTAL ENERGY(DFT)(AU)(  2) -5.7865619212185E+00 DE-4.4E-15 DP 1.1E-15

 ENERGY COND (AU) -5.7819107951099E+00  COND No.  4.65113E-03 EFF  1.04703E+02

 GAMMA FACTOR:  1.0000E-03

 CONVERGENCE TESTS SATISFIED AFTER    3 ENERGY AND GRADIENT CALCULATIONS

 CONVERGED ENERGY - E(AU): -5.7819110063857E+00 POINTS    3

 ********************************************************************************
 LOCAL ATOMIC FUNCTIONS BASIS SET OPTIMIZED
 ********************************************************************************
   ATOM   X(AU)   Y(AU)   Z(AU)  N. TYPE  EXPONENT  S COEF   P COEF   D/F/G COEF
 ********************************************************************************
   1 HE  -3.193   0.000   2.258
                                  1 S
                                        1.145E+03 3.586E-04 0.000E+00 0.000E+00
                                        1.716E+02 2.773E-03 0.000E+00 0.000E+00
                                        3.907E+01 1.424E-02 0.000E+00 0.000E+00
                                        1.105E+01 5.546E-02 0.000E+00 0.000E+00
                                        3.573E+00 1.617E-01 0.000E+00 0.000E+00
                                  2 S
                                        1.245E+00 1.000E+00 0.000E+00 0.000E+00
                                  3 S
                                        4.473E-01 1.000E+00 0.000E+00 0.000E+00
                                  4 S
                                        1.499E-01 1.000E+00 0.000E+00 0.000E+00
                             5-     7 P
                                        5.994E+00 0.000E+00 1.000E+00 0.000E+00
                             8-    10 P
                                        1.745E+00 0.000E+00 1.000E+00 0.000E+00
                            11-    13 P
                                        5.597E-01 0.000E+00 1.000E+00 0.000E+00
                            14-    18 D
                                        4.299E+00 0.000E+00 0.000E+00 1.000E+00
                            19-    23 D
                                        1.223E+00 0.000E+00 0.000E+00 1.000E+00
                            24-    30 F
                                        2.680E+00 0.000E+00 0.000E+00 1.000E+00
   2 HE  -1.597  -2.765  -2.258
 ********************************************************************************

WRITING OPTIMIZED BASIS SET TO fort.53

 TTTTTTTTTTTTTTTTTTTTTTTTTTTTTTTT END         TELAPSE      195.52 TCPU      195.07
```

Moreover, during the optimization all the basis sets at each iteration are printed in the *filename.f53*. For sake of completeness we report below the optimized basis set obtained. In this unit the basis sets are printed out by using the input format that makes easy the transfer to a new input if needed.

fort.53 He bulk. Last cycle of the Basis Set Optimization. Basis Set Optimized.

```
 ~.~.~.~.~.~.~.~.~.~.~.~.~.~.~.~.~.~.~.~.~.~.~.~.~.~.~.~.~.~.~.~.~.~.~.~.~.~.~.
 LOCAL ATOMIC FUNCTIONS BASIS SET OPTIMIZED

 ~.~.~.~.~. OPT CYC     3    MAX OPT CYC   500
  2 10
0 0  5  2. 1.
      1.14464708090E+03   3.58615786180E-04
      1.71645966670E+02   2.77254344660E-03
      3.90660562540E+01   1.42418922160E-02
      1.10514019890E+01   5.54573522770E-02
      3.57255744730E+00   1.61705118100E-01
0 0  1  0. 1.
      1.24522535919E+00   1.00000000000E+00
0 0  1  0. 1.
      4.47284793404E-01   1.00000000000E+00
0 0  1  0. 1.
      1.49948526659E-01   1.00000000000E+00
0 2  1  0. 1.
      5.99399912883E+00   1.00000000000E+00
0 2  1  0. 1.
      1.74499283285E+00   1.00000000000E+00
0 2  1  0. 1.
      5.59741098492E-01   1.00000000000E+00
0 3  1  0. 1.
      4.29900357838E+00   1.00000000000E+00
0 3  1  0. 1.
      1.22307371167E+00   1.00000000000E+00
0 4  1  0. 1.
      2.67999999353E+00   1.00000000000E+00
```

Bibliography

[1] Loredana Edith Daga, Bartolomeo Civalleri, and Lorenzo Maschio. Gaussian basis sets for crystalline solids: all-purpose basis set libraries vs system-specific optimizations. *Journal of Chemical Theory and Computation*, 16(4):2192–2201, 2020.

[2] Joost VandeVondele and Juerg Hutter. Gaussian basis sets for accurate calculations on molecular systems in gas and condensed phases. *The Journal of Chemical Physics*, 127(11):114105, 2007.

[3] Dong C Liu and Jorge Nocedal. On the limited memory BFGS method for large scale optimization. *Mathematical Programming*, 45(1):503–528, 1989.

[4] Benjamin P Pritchard, Doaa Altarawy, Brett Didier, Tara D Gibson, and Theresa L Windus. New basis set exchange: An open, up-to-date resource for the molecular sciences community. *Journal of Chemical Information and Modeling*, 59(11):4814–4820, 2019.

Chapter 11

Appendix B - Maximum Overlap Method, Algorithm Implementation

11.1 How to Use the Algorithm in the CRYSTAL code

In order to activate the method few options must be introduced in the CRYSTAL input. In Table 11.1 a summary of the new keywords introduced is reported.

Keyword	*Description*
MOM	Maximum Overlap Method (MOM) active
EUPKTOK	Delocalized Excitation (Γ to Γ)
k_a k_b	Initial K point and final K point (only 1 1 implemented)
n_{eup}	No. excitations
i_a s_a i_b s_b	Initial orbital and spin (occupied), final orbital and spin (empty)
BTOBTrue	Localized Excitation (Band to band)
n_{eup}	No. excitations
i_a s_a i_b s_b	Initial orbital and spin (occupied), final orbital and spin (empty)
	SYMMREMO is suggested
PMOMPRT	Printing Option: Partial Occupation matrix printed
$IPAR_{mom}, J_a, J_b$	K points (columns), initial orbital, final orbital (rows)
RADBTOBT	BTOBTrue applied in sphere around Γ
No.	Radius of the sphere
	BTOBTrue must be active
AMOMPRT	Printing Option: All Occupation matrix printed
ENDMO	Maximum Overlap Method (MOM) END statement

Table 11.1: Summary of the keywords available for the MOM method. In bold the keywords mandatory for the activation of the method. This section has to be introduced in the geometry section of the CRYSTAL input.

The input is constructed as a scf input, inserting few keywords in the geometry section. In particular, all the `MOM` calculations have to be run with the `UHF` keyword, thus open shell Hamiltonian must be defined to allow the excitation to take place. In fact, the constraint of double occupancy must be absent and α electrons are allowed to populate orbitals other than those occupied by the β electrons.

Moreover, the `MOM` method automatically activates `NOSYMADA` option. The symmetry adapted functions are not used in the Hamiltonian matrix diagonalization.

An example of delocalized optimization (`EUPKTOK`) is reported below for the diamond system.

The excitation involved the 6^{th} (empty) and the 7^{th} (full) orbital, thus a vertical excitation in the Γ point. In particular, the print option is added (`PMOMPRT` keyword) and the occupation matrix is partially printed. Specifically, the first 5 k points are printed (columns) from the 2^{nd} to the 11^{th} orbital (rows). In red the keywords mandatory for the MOM activation.

Input Gamma to Gamma Excitation

```
DIAMOND-dcm_TZVP
CRYSTAL
0 0 1
227
3.56679
1
6 0. 0. 0.
MOM
EUPKTOK
1 1
1
6 1 7 1
PMOMPRT
5 2 11
ENDMO
END
6 8
0 0 6 2.0 1.0
  13575.349682      0.00022245814352
  2035.2333680      0.00172327382520
  463.22562359      0.00892557153140
  131.20019598      0.03572798450200
  42.853015891      0.11076259931000
  15.584185766      0.24295627626000
0 0 2 2.0 1.0
  6.2067138508      0.41440263448000
  2.5764896527      0.23744968655000
0 0 1 0.0 1.0
  0.4941102000      1.00000000000000
0 0 1 0.0 1.0
  0.1644071000      1.00000000000000
0 2 4 2.0 1.0
  34.697232244      0.00533336578050
  7.9582622826      0.03586410909200
  2.3780826883      0.14215873329000
  0.8143320818      0.34270471845000
0 2 1 0.0 1.0
  0.5662417100      1.00000000000000
0 2 1 0.0 1.0
  0.1973545000      1.00000000000000
0 3 1 0.0 1.0
  0.5791584200      1.00000000000000
99 0
END
UHF
DFT
PBE
END
TOLINTEG
10 10 10 20 50
TOLDEE
8
SHRINK
8 8
FMIXING
50
END
```

The output is very similar to a classical SCF calculation. In the following, parts of the output related with the diamond input above reported, are shown. As mentioned in the previous parts, the MOM method is applied at the beginning of the SCF calculation (cycle 0), then the excited configuration is kept throughout the whole calculation. Nevertheless, a banner at each cycle is printed reminding the kind of excitation performed. In the specific case the `PMOMPRT` keyword is active, thus an additional printing option is present: the occupation matrix is printed, where the rows are the orbitals, while the columns are the k-points. In this example a Γ to Γ excitation is performed, thus in the first column (Γ point) the electron is moved from the sixth to the seventh orbitals, as decided in input.

Output Gamma to Gamma Excitation

```
...
 CYC   0 ETOT(AU) -7.681414183991E+01 DETOT -7.68E+01 tst  0.00E+00 PX  1.00E+00
 TTTTTTTTTTTTTTTTTTTTTTTTTTTTTTTTTT DIIS        TELAPSE        5.61 TCPU        5.56
 TTTTTTTTTTTTTTTTTTTTTTTTTTTTTTTTTT FDIK        TELAPSE        5.62 TCPU        5.57
 *** MOM *** SHIFT IN THE GROUND OCCUPATION APPLIED
  GAMMA to GAMMA EXCITATION
 1 EXCITATION FROM   6(SPIN   1) TO   7(SPIN   1)

      +++      Occupations      +++

        ************************************************************
   2       0.0019531   0.0156250   0.0156250   0.0156250   0.0078125
   3       0.0019531   0.0156250   0.0156250   0.0156250   0.0078125
   4       0.0019531   0.0156250   0.0156250   0.0156250   0.0078125
   5       0.0019531   0.0156250   0.0156250   0.0156250   0.0078125
   6       0.0000000   0.0156250   0.0156250   0.0156250   0.0078125
   7       0.0019531   0.0000000   0.0000000   0.0000000   0.0000000
   8       0.0000000   0.0000000   0.0000000   0.0000000   0.0000000
   9       0.0000000   0.0000000   0.0000000   0.0000000   0.0000000
  10       0.0000000   0.0000000   0.0000000   0.0000000   0.0000000
  11       0.0000000   0.0000000   0.0000000   0.0000000   0.0000000
...
 CYC   7 ETOT(AU) -7.615422786698E+01 DETOT  2.88E-11 tst  2.68E-13 PX  2.74E-06

 == SCF ENDED - CONVERGENCE ON ENERGY      E(AU) -7.6154227866984E+01 CYCLES   7


 ENERGY EXPRESSION=HARTREE+FOCK EXCH*0.00000+(PBE        EXCH)*1.00000+PBE        CORR


 TOTAL ENERGY(DFT)(AU)(  7) -7.6154227866984E+01 DE 2.9E-11 tester 2.7E-13
 TTTTTTTTTTTTTTTTTTTTTTTTTTTTTTTTTT EDFT        TELAPSE       42.52 TCPU       42.46
```

To get the excitation energy as reported in the Equ. 6.4, a ground state calculation must be performed in addition (single SCF). Once obtained both total energies, ground state E_{ground} and excited state $E_{excited}$, the excitation energy is:

$$E_{excitation} = |E_{ground} - E_{excited}| \cdot 27.2114 \cdot \frac{N_{\mathbf{k}}}{N_{\mathbf{k}}^{exc}} \tag{11.1}$$

where the factor 27.2114 is for the Hartree to electronvolt conversion and the $N_{\mathbf{k}}$ are the k point in the cell and $N_{\mathbf{k}}^{exc}$ are the k point actually involved in the excitation. In this specific case the `SHRINK` factor is `8 8`, thus in a 3D system as the diamond, a $8 \times 8 \times 8 = 512$ number of k points are present in the cell ($N_{\mathbf{k}} = 512$), while just the Γ point is involved ($N_{\mathbf{k}}^{exc} = 1$). In particular in this specific example:

$$5.618eV = |76.154631085036 - 76.154227867015| \cdot 27.2114 \cdot \frac{512}{1} \tag{11.2}$$

Suggestion: to get a stable convergence in the excitation state, run a not-excited calculation and use the wavefunction information (`fort.9`) to start the excitation calculation with a `GUESSP` option. Moreover, till now `MOM` calculation can be performed only on insulating systems. If conductive states are present, if possible try to keep the gap at each SCF calculation. For pure conductive system `MOM` method is not yet implemented.

Chapter 12

Appendix C

12.1 Gaussian Basis Sets for Crystalline Solids: All-Purpose Basis Set Libraries vs System-Specific Optimization-Paper Published

JCTC Journal of Chemical Theory and Computation

pubs.acs.org/JCTC Article

Gaussian Basis Sets for Crystalline Solids: All-Purpose Basis Set Libraries vs System-Specific Optimizations

Loredana Edith Daga, Bartolomeo Civalleri, and Lorenzo Maschio*

Cite This: J. Chem. Theory Comput. 2020, 16, 2192−2201 Read Online

ACCESS | Metrics & More | Article Recommendations | Supporting Information

ABSTRACT: It is customary in molecular quantum chemistry to adopt basis set libraries in which the basis sets are classified according to either their size (triple-ζ, quadruple-ζ, ...) and the method/property they are optimal for (correlation-consistent, linear-response, ...) but not according to the chemistry of the system to be studied. In fact the vast majority of molecules is quite homogeneous in terms of density (i.e., atomic distances) and types of bond involved (covalent or dispersive). The situation is not the same for solids, in which the same chemical element can be found having metallic, ionic, covalent, or dispersively bound character in different crystalline forms or compounds, with different packings. This situation calls for a different approach to the choice of basis sets, namely a system-specific optimization of the basis set that requires a practical algorithm that could be used on a routine basis. In this work we develop a basis set optimization method based on an algorithm−similar to the direct inversion in the iterative subspace−that we name BDIIS. The total energy of the system is minimized together with the condition number of the overlap matrix as proposed by VandeVondele et al. [VandeVondele et al. *J. Chem. Phys.* **2007**, *227*, 114105]. The details of the method are here presented, and its performance in optimizing valence orbitals is shown. As demonstrative systems we consider simple prototypical solids such as diamond, graphene sodium chloride, and LiH, and we show how basis set optimizations have certain advantages also toward the use of large (quadruple-ζ) basis sets in solids, both at the DFT and Hartree−Fock level.

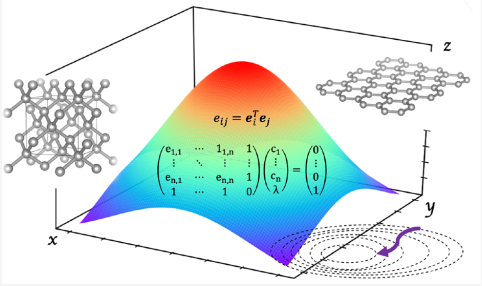

1. INTRODUCTION

When dealing with the quantum chemical modeling of crystalline solids, the existence of various types of chemical bonding is clearly evident. For instance, the polymorphism of carbon in the graphite (or graphene) and diamond allotropes is just one of many examples, in which the profoundly different chemical behavior is manifested by the same chemical element in different crystal packings. Another exemplary case is that of rocksalt NaCl: sodium is by nature metallic as a bulk material, and chlorine is commonly found in the form of a molecular crystal Cl_2. NaCl is a prototypical ionic salt. The chemical differences in those materials can be made evident by looking at their electron density (see Figure 1): the electrons involved in the metallic bond in Na are quite spread out over the whole space, while in Cl_2 the density is somewhat more localized on molecules, with empty space between them. Conversely, the wave function in an ionic system like NaCl is strongly confined in a vicinity of the ions and features nodes in the planes in between neighboring atoms. NaCl is also considerably more densely packed.

This variety of chemical bondings in the solid state then reflects the choice of the type and quality of the basis set adopted in the mathematical form of the wave function when solving the Schrödinger equation within periodic boundary conditions (i.e., Bloch functions).[1−3] The situation in the field of molecular modeling is somewhat simpler as isolated molecules or molecular aggregates have nearly comparable atomic densities, and there are commonly no analogue extended systems featuring metallic, ionic, or covalent bonds. Therefore, in molecular calculations, atom-centered basis sets as Gaussian-type orbitals[4] are almost universally adopted,[5] although other basis sets can be and are eventually used.

On the other hand, for solid-state calculations,[2] plane waves,[6−8] atom-centered Gaussians[9] (or their combinations[10]), and numerical basis sets[11,12] are all popular choices. The plane wave basis, that is naturally suited for nonlocal wave functions such as in the uniform electron gas or in a metal, has the undeniable advantage of a one-knob tuning of accuracy and cost through the kinetic energy cutoff parameter. However, the correct description of local orbitals, core states, or the void can result in a rather high computational cost. Similarly, the inclusion of exact HF exchange in hybrid HF/DFT

Received: October 8, 2019
Published: March 26, 2020

https://dx.doi.org/10.1021/acs.jctc.9b01004
J. Chem. Theory Comput. 2020, 16, 2192−2201

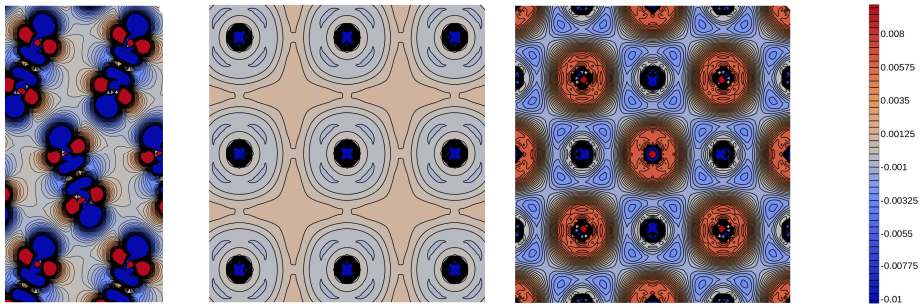

Figure 1. Electron difference density maps (with respect to atomic densities) of molecular solid Cl_2 (panel a), metallic sodium (panel b), and rocksalt ionic NaCl (panel c).[37]

calculations leads to a steep increase in computational time. Gaussian-type basis sets are less commonly adopted for the quantum chemical treatment of solids, with respect to plane waves. Gaussian functions have the great advantage of allowing to transfer to the solid state a large part of the technology and knowledge that is the legacy of several decades of advances in molecular quantum chemistry and to retain the chemical intuition when looking at the electronic charge distribution of the investigated system. The price to pay is the mandatory definition of a basis set for each atomic species, that is ultimately left in the hands of the end user.

Nowadays, standardized basis set libraries are not commonly available for solids as they are for molecules,[13,14] despite recent attempts in that direction being carried out by Bredow and co-workers.[15−17] The reasons are not only to be ascribed to a lesser effort in a systematic construction of all-purpose basis sets but also more specifically to the wide difference in chemical bonding as outlined above. First attempts to understand the role of basis functions in solids were done by Hess and co-workers,[18] but also more recently Jensen[19] compared atomic, molecular, and solid-state basis sets for carbon and silicon to highlight the differences originating from the different chemical environments.

Another aspect related to the adoption of Gaussian-type functions is the basis set incompleteness due to the use of a finite number of basis functions. Basis set incompleteness is an issue in all types of calculations, but most of all in calculations that employ atom-centered basis sets—Gaussians, Slater functions, or numerical orbitals. This is because the atomic basis sets can never be made complete enough in polyatomic systems, as the basis becomes overcomplete—necessitating the removal of variational degrees of freedom—before becoming complete. In molecules it is rather common to adopt a sequence of basis sets of increasing size (e.g., cc-pVXZ (X = D,T,Q,···)[20] and pc-X (X = 1,2,3, ...)[21]), but this is not yet routinely applicable for solids. Therefore, reaching the basis set limit is not trivial—even for such simple systems as lithium hydride[22−26]—and is not just a matter of computational efforts: as basis sets grow larger, exponents tends to become more diffuse, linear dependency problems arise, and the convergence of infinite Coulomb and exchange series is jeopardized.

The problem of linear dependencies with an extended basis set is a matter of active research not only for solids but also for average-sized molecules.[27] While the important role of diffuse functions in solids has been recently highlighted by Kadek et al.,[28] too diffuse functions are often not needed for ground state calculations because of the packing of the atoms in the unit cell. Such very diffuse functions can also be added a posteriori through dual basis set techniques.[29] Seen from another viewpoint, the main conceptual difference in basis sets meant for the solid state as opposite to molecular electronic structure calculations is that the latter have to describe the asymptotic exponential decay of the electron density in a finite system, requiring somewhat diffuse functions, whereas diffuse basis functions are generally thought not to be necessary in solid-state calculations because the density is much more uniform throughout the cell. In this work our aim is to (i) show to what extent the basis sets are different in different chemical environments, by optimizing bases of the def2-TZVP quality[30−32] and (ii) attempt to use suitably optimized quadruple-ζ basis sets, also from the def2- family, to verify whether they can be adopted for solids without significant pruning, and outline possible strategies for reaching such goal.

To this purpose we present a technique for the optimization of basis set exponents and contraction coefficients, that is based on the Direct Inversion in the Iterative Subspace (DIIS) technique[33−35] and actually quite similar to its geometry optimization variant, GDIIS.[36] The algorithm is implemented in the CRYSTAL code.[9] We show how such optimization allows the retaining of the full number of Gaussians letting the algorithm decide about the diffuseness of the exponents.

2. THEORETICAL FRAMEWORK

2.1. Background. In the linear combinations of atomic orbitals (LCAO) framework, the crystalline orbitals ψ are treated as linear combinations of Bloch functions (BF) ϕ that are, in turn, defined in terms of local atom-centered functions (AO) φ

$$\psi_i(\mathbf{r};\mathbf{k}) = \sum_{\mu} a_{\mu,i}(\mathbf{k})\phi_{\mu}(\mathbf{r};\mathbf{k}) \tag{1}$$

$$\phi_{\mu}(\mathbf{r};\mathbf{k}) = \sum_{g} \varphi_{\mu}(\mathbf{r}-\mathbf{A}_{\mu}-\mathbf{g})e^{i\mathbf{k}\cdot\mathbf{g}} \tag{2}$$

in which $\mathbf{g}$ is a direct space lattice vector, $\mathbf{k}$ is the lattice vector defining a point in the reciprocal lattice, $\mathbf{A}$ are the coordinates of the atom in the reference cell on which the AO φ is centered, and a are the variational coefficients. The sum over μ is limited to the number of basis functions in the unit cell. The

https://dx.doi.org/10.1021/acs.jctc.9b01004
J. Chem. Theory Comput. 2020, 16, 2192−2201

sum over **g** is, in principle, extended to all the (infinite) lattice vectors of the direct lattice; therefore, suitable screening techniques have to be adopted.[1,38,39]

As usual, the AOs can be written as a contraction of a number of primitive Gaussian-Type Functions (GTF) G centered on the same atom

$$\varphi_\mu(\mathbf{r} - \mathbf{A}_\mu - \mathbf{g}) = \sum_j^{nG} d_j G(\alpha_j; \mathbf{r} - \mathbf{A}_\mu - \mathbf{g}) \tag{3}$$

in which d_j are the contraction coefficients, and α_j are the exponents of the radial component of the function. The number, type, and contraction scheme of the Gaussian basis set define its quality. Gaussian functions are defined as

$$G(\alpha_j; \mathbf{r} - \mathbf{A}_\mu - \mathbf{g}) = R_l(\mathbf{r} - \mathbf{A}_\mu - \mathbf{g}) Y_{lm}(\theta, \rho) \tag{4}$$

where $R_l(\mathbf{r}) = Ne^{-\alpha \cdot \mathbf{r}^2}$ is the radial part—N being a normalization constant—and $Y_{lm}(\theta, \rho)$ is a spherical harmonic.

2.2. The BDIIS Method. Our goal is to devise a suitable algorithm for a system-specific optimization of the exponents α_j and contraction coefficients d_j as in eq 3. Taking inspiration from the well-known Direct Inversion of Iterative Subspace (DIIS) algorithm of Pulay,[33,34] we describe in the following our Basis-set DIIS (BDIIS) method.

The idea is that of an iterative procedure in which, at each step n, exponents and contraction coefficients are obtained as a linear combination of the trial vectors obtained in previous iterations

$$\bar{\alpha}_{n+1} = \sum_{i=1}^{n} c_i(\alpha_i + e_i^\alpha) \tag{5}$$

$$\bar{d}_{n+1} = \sum_{i=1}^{n} c_i(d_i + e_i^d) \tag{6}$$

In the above, e_i^α and e_i^d are, respectively, the changes in exponents and contraction coefficients, as predicted by a simple Newton–Raphson step. In fact the gradients e_i are defined by

$$e_i^\alpha = \frac{\partial \Omega}{\partial \alpha} \quad e_i^d = \frac{\partial \Omega}{\partial d} \tag{7}$$

where Ω is a suitable functional to be minimized. Here we decide to minimize the system's total energy to which we add a penalty function including the Overlap matrix condition number, following the proposal of VandeVondele and Hutter:[40]

$$\Omega(\{\alpha, d\}) = E_{tot}(\{\alpha, d\}) + \gamma \ln \kappa(\{\alpha, d\}) \tag{8}$$

The value $\gamma = 0.001$ was adopted as suggested in ref 40. In eq 8, $\kappa(\{\alpha, d\})$ is the condition number, i.e., the ratio between the largest and the smallest eigenvalue of the overlap matrix at the center of the Brillouin zone (Γ-point). The purpose of such penalty function is to prevent the onset of harmful linear dependence. Linear dependence issues can give rise to numerical instabilities and, as a consequence of that, the appearance of unphysical states. Such unphysical states generally lead to a catastrophic behavior of the total energy that can drop to a value that is orders of magnitude larger, in absolute value, than the proper one.

Although the first of derivatives in (7) could be in principle computed analytically,[41,42] in the present work we evaluate both e_i^α and e_i^d by means of numerical derivatives (*vide infra*). The length of the estimated Newton steps represented by the $\mathbf{e}^\alpha$ and $\mathbf{e}^d$ can assume the meaning of an estimated distance from the minimum of Ω and thus be utilized as a measure of the "error" at step n.

The DIIS error matrix, that has the size of the iterative space considered, is built from the scalar products

$$e_{ij} = \mathbf{e}_i^T \mathbf{e}_j \tag{9}$$

By imposing the constraint $\sum_{i=1}^{n} c_i = 1$, we can obtain the linear combination coefficients of the BDIIS method to be used in (5) and (6) by solving the linear equation system

$$\begin{pmatrix} e_{1,1} & \cdots & e_{1,n} & 1 \\ \vdots & \ddots & \vdots & \vdots \\ e_{n,1} & \cdots & e_{n,n} & 1 \\ 1 & \cdots & 1 & 0 \end{pmatrix} \begin{pmatrix} c_1 \\ \vdots \\ c_n \\ \lambda \end{pmatrix} = \begin{pmatrix} 0 \\ \vdots \\ 0 \\ 1 \end{pmatrix} \tag{10}$$

where λ is a Lagrange multiplier. Such an approach is, in fact, similar to geometry-optimization DIIS (GDIIS[36]) adopting an identity Hessian.

2.3. Details of the Implementation. The BDIIS procedure outline above has been implemented in a development version of the CRYSTAL17 code.[9] As already mentioned, in this work we compute the derivatives in (7) by means of a two-sided numerical derivative. Which means, for exponents α

$$e_i^\alpha = \frac{\Omega(\alpha_i + \Delta\bar{\alpha}) - \Omega(\alpha_i - \Delta\bar{\alpha})}{2\Delta\bar{\alpha}} \tag{11}$$

and similarly for coefficients d.

The displacement is 1% of the exponent value ($\Delta\bar{\alpha} = 0.01 \cdot \alpha$), while for coefficients the step is set to 0.1%, weighted by the relative exponents ($\Delta\bar{d} = 0.001 \cdot d/\alpha$).

We have also tried to compute a diagonal Hessian using the three points $\alpha_i + \Delta\bar{\alpha}$, α_i and $\alpha_i - \Delta\bar{\alpha}$, so to improve the step (error) as defined in eqs 5 and 6 at the same computational cost. However, such a diagonal Hessian seemed not to improve on the quality of the step, and the overall convergence pattern turned out to be similar or slower in all cases we tested. We surmise that the cause can reside in the insufficient accuracy of a three-point numerical estimate of the second derivative.

Once a suitable step $\Delta\bar{\alpha}_n = \bar{\alpha}_n - \alpha_{n-1}$ is obtained from eq 5, a line search is performed for tuning the optimal parameter f_l

$$\tilde{\alpha}_n = \alpha_{n-1} + f_l \Delta\bar{\alpha}_n \tag{12}$$

by sampling f_l from 0.1 to 1 in a suitable discrete point grid. The point with the minimum value of Ω is then retained.

The convergence of the iterative optimization procedure is verified by checking the absolute value of the largest component of both the gradients and the penalty function. The iterative space used in the BDIIS procedure is set at most to the 14 previous cycles, and the BDIIS step is active since the second basis set optimization step. The optimization is complete when the absolute value of the difference in the penalty function is less than $1.0 \cdot 10^{-5}$ au and the absolute value of the largest component of gradient converges to $3.0 \cdot 10^{-4}$.

3. RESULTS

In this section we first briefly describe the performance of the BDIIS method in minimizing the Ω energy functional as

https://dx.doi.org/10.1021/acs.jctc.9b01004
J. Chem. Theory Comput. 2020, 16, 2192−2201

defined in eq 8. Then we focus on the effect of system-specific basis set optimizations, by showing the differences between optimized exponents of a typical triple-ζ basis in simple systems containing the same atoms but in a different chemical bonding situation. Finally, we analyze how extended basis sets, such as molecular quadruple-ζ quality, can be optimized for dense solids without significant pruning. In the Supporting Information the reader can find full CRYSTAL17[9] inputs for all the calculations presented in the following, including the explicit definition of the atomic basis sets.

All of the optimizations in this work have been carried out starting from molecular def2-TZVP or def2-QZVP basis sets.[30−32] Although the implemented algorithm is general, as described in the previous section, in the following we will focus on the optimization of valence and polarization functions only—the ones relevantly changing in a different chemical environment. Since they are usually uncontracted Gaussian functions, the optimization has been performed solely for the exponents. As a general strategy, we took as a starting point the molecular basis sets, upscaled the exponents of all outermost functions so to avoid small values (<0.1) but without pruning the basis set, and finally optimized the corresponding values by minimizing the function Ω.

For all the calculations the convergence for the self-consistent field (SCF) algorithm is achieved when the energy difference is $1.0 \cdot 10^{-8}$ au ($1.0 \cdot 10^{-10}$ au for LiH) using a Monkhorst−Pack (MP) shrinking factor of 8 (64 for graphene). For triple-ζ basis sets the truncation criteria of Coulomb and Exchange infinite sums are [8,8,8,12,24] for diamond, [8,8,8,15,30] for LiH, and [8,8,8,8,16] for the other systems. Convergence in the case of quadruple-ζ basis sets requires tighter thresholds, up to [10,10,10,35,175] in the case of diamond (Hartree−Fock). In the SI we report all CRYSTAL17 inputs that can be used to reproduce our results.

In many cases, we adopted pure GGA functionals such as PBE[43] and PBEsol[44] in order to have a faster time to solution. In other cases we used PBE0[45] or Hartree−Fock. More generally, we do not regard our basis set optimizations to be much dependent on the chosen method,[46] since we do not deal with the reoptimization of the core. As the focus of our work is on accuracy and numerical stability, we will not present timings.

3.1. Performance of the BDIIS Method. In Figure 2 we report the progress of the Ω functional minimization—cf. eq 8—along with the BDIIS iterations, in two exemplary yet challenging cases for Gaussian-type basis sets: graphene and bulk metallic sodium. In graphene, the basis set optimizer, run with the PBEsol functional, leads to a stable result after a few iterations, which represents a significant energy gain with respect to the starting point and remains stable for long. If the optimization is allowed to continue for hundreds of cycles, a rise in the penalty function $\gamma \ln \kappa(\{\alpha,d\})$ is observed, which evidently prevents the gaussians to become too diffuse. A corresponding decrease of the electronic energy is observed. We remark that such changes are however minimal with respect to the effect of the first iterations, and the optimization is essentially converged after 50 cycles to all practical purposes. In the same figure we have also reported the curve obtained using the Broyden−Fletcher−Goldfarb−Shanno (BFGS) method. It is seen that such a method reaches the same value of the Ω functional, more slowly but also more stably. We will discuss the differences in the solution in the following.

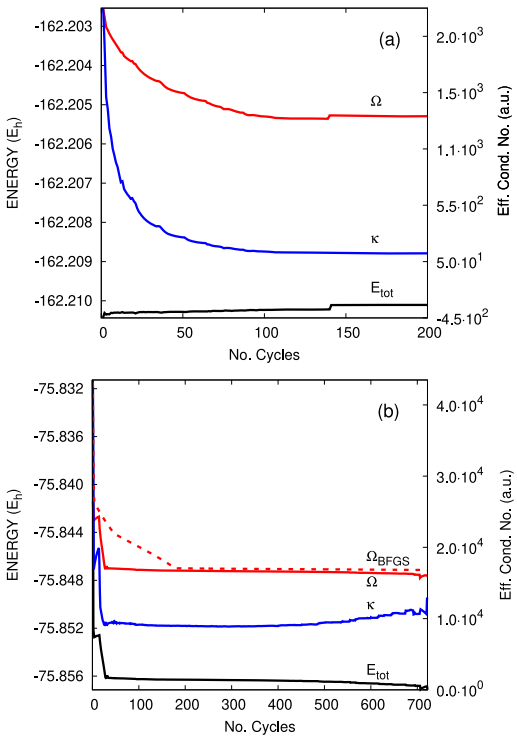

Figure 2. Minimization of the Ω functional of eq 8 as a function of the BDIIS algorithm iteration for two of the systems studied in this work: panel (a) sodium (PBE0), panel (b) graphene (PBEsol). The two components of the functional, E_{tot} and κ, are also reported individually. The dashed line in the bottom panel reports the behavior of the BFGS algorithm.

The case of bulk metallic sodium (Figure 2(a)) is different: the electronic energy varies little (and even increases slightly with respect to the starting point); but the penalty function is much more relevant than in other cases, and about 100 iterations are required to reach a plateau. Notably, in this case the basis set optimization was carried out with a hybrid HF/DFT functional (i.e., PBE0). This level of theory is usually expected to be problematic for metallic systems, but the BDIIS algorithm runs smoothly to convergence.

3.2. Role of the Chemical Environment. We compare here two sets of systems, composed by the same elements: first crystalline diamond, graphene, and carbyne chain and then NaCl with bulk Na and Cl solids. We compare our system-dependent optimized basis sets with the pob-TZVP[15,17] ones. These were also derived from def2-TZVP but differently from ours: (i) the valence exponents were optimized for each system in a comprehensive set of solids with different chemical environments, (ii) for multiple optimization of the same atomic species an averaged value of the exponent was considered, and (iii) most notably, many of the outermost functions were removed, thus reducing the consistent quality of the basis.

We will refer to the basis sets optimized in this work as "dcm-TZVP". Since different basis sets of the same nominal

https://dx.doi.org/10.1021/acs.jctc.9b01004
J. Chem. Theory Comput. 2020, 16, 2192−2201

Table 1. Uncontracted Gaussian Exponents for Different Carbon TZVP Basis Sets[b]

	def2[30]	pob[15]	pob-rev2[17]	dcm[C_{diam}][a]	dcm[C_{graph}][a]	dcm[C_{cby}][a]
s	0.5770	0.4941	0.4941	2.7288	1.0961	1.1383
	0.2297	0.1644	0.1644	0.7083	0.5911	0.6557
	0.0952			0.2754	0.2374	0.2323
p	0.2889	0.5662	0.5662	0.6187	0.3387	0.2857
	0.1006	0.2674	0.1973	0.2713	0.1594	0.0906
d	1.0970	0.8792	0.5792	2.0114	1.2502	1.3095
	0.3180			0.6265	0.7194	0.6132
f	0.7610			1.0624	0.7067	1.1330

[a]Present work. [b]dcm[C_{diam}]-TZVP, dcm[C_{graph}]-TZVP, and dcm[C_{cby}]-TZVP refer to our basis set optimized by BDIIS with the PBE functional in diamond, graphene, and carbyne, respectively.

quality are obtained through optimization on different systems, we will adopt the more detailed notation dcm[···]-TZVP, specifying in square brackets the system used for the optimization (e.g., dcm[NaCl]-TZVP).

3.2.1. Diamond, Graphene, and Carbyne Chain. Diamond and graphene are two allotropes of carbon. Both are covalently bound systems but differ by hybridization (sp^3 and sp^2), as well as crystalline (3D Vs 2D) and electronic (insulator and conductor) structures. Carbyne is a model system with 1D periodicity (polymer), two atoms in the unit cell and alternating bond length.

In Table 1 we compare the exponents of the original def2-TZVP, the original pob-TZVP, the recently revised pob-rev2 basis set, and our dcm-TZVP basis specifically optimized for diamond, graphene, and carbyne with the PBE functional. For brevity, we will refer to the latter two basis sets as dcm[C_{diam}]-TZVP, dcm[C_{graph}]-TZVP, and dcm[C_{cby}]-TZVP, respectively. Figure 3 shows a corresponding graphical representation of the radial component of some of the involved gaussians. The first striking effect observed is the overall contraction of exponents with respect to the molecular basis. This is not unexpected[15,19] and is to be ascribed to the higher density of atoms in the solid-state phase.

The outermost *p*-type function shows probably the most significant difference between diamond and graphene. Such difference is due both to the different chemical bonding (*sp*-hybridization) and atomic density—graphene is a 2D system surrounded by vacuum in the third dimension. This vacuum offers more space for the Gaussian functions to expand and at the same time requires more extended functions to cover that empty space. Such interpretation is corroborated by the example of the 1D carbyne chain basis dcm[C_{cby}]-TZVP, which features an even more diffuse *p*-shell. We take the opportunity here to remind that—conversely to plane-waves—in an atom-centered Gaussian-based approach the true 2D and 1D periodicity is possible, hence the vacuum in the nonperiodic directions is a *true* vacuum. The effect of the reduced dimensionality is, however, partly counterbalanced by a progressively shorter carbon—carbon distance that is 2.92 Å in diamond, 2.69 Å in graphene, and 2.39/2.46 Å in carbyne due to the different hybridization of the carbon atom in the three compounds. The more diffuse *p*-function is responsible for the failed convergence when using the graphene dcm-[C_{graph}]-TZVP basis set in diamond (Table 2). Also *d*- and *f*-type functions have a somewhat different spread in the two systems, showing that quadrupole and octupole interactions act differently in the two allotropes.

In Table 2 we report some total energies obtained at the DFT/PBE level: in addition to dcm-TZVP and pob-TZVP

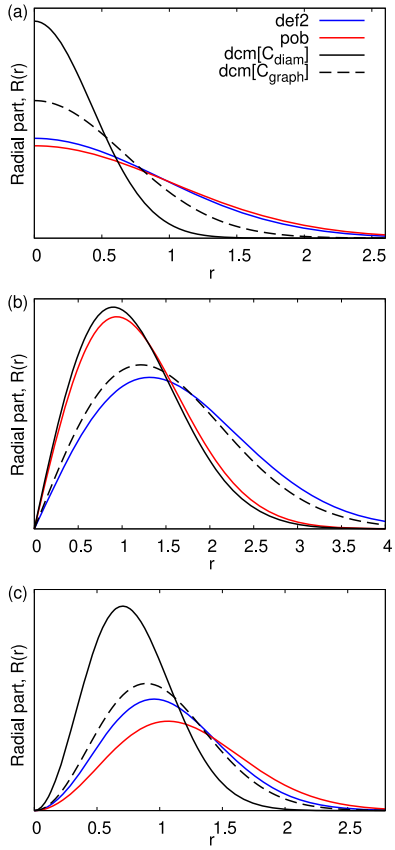

Figure 3. Radial part of some Gaussian functions of carbon from def2-TZVP (def2), pob-TZVP (pob), and two different dcm-TZVP (dcm[C_{diam}] for diamond, dcm[C_{graph}] for graphene) basis sets. Exponents of *s*-, *p*-, and *d*-type functions are reported in panels (a), (b), and (c), respectively.

bases, the dcm[C_{diam}]-TZVP basis was also tested in graphene and the dcm[C_{graph}]-TZVP in diamond. From Table 2, we see that the energies relative to the proper dcm bases are lower by about 0.014 E_h than the pob- ones. On the other hand, swapping the two dcm-TZVP bases led to an energy similar to (though still lower than) that of pob-TZVP[G] while the more diffuse dcm[C_{graph}]-TZVP turned out to be unusable in the

https://dx.doi.org/10.1021/acs.jctc.9b01004
J. Chem. Theory Comput. 2020, 16, 2192−2201

Table 2. Total Energies at the DFT/PBE Level for Diamond and Graphene as Computed with Different Triple-ζ Basis Sets[b]

E_{TOT}^{PBE}	pob[15]	pob-rev2[17]	dcm[C_{diam}][a]	dcm[C_{graph}][a]	dcm[C_{cby}][a]
diamond	−76.157894	−76.154752	**-76.161457**		
graphene	−76.155441	−76.158920	−76.158342	**-76.169383**	
carbyne	−76.072706	−76.086918	−76.073559	−76.096273	**-76.099140**

[a]This work. [b]Energies in E_h. Energies for the consistently optimized basis sets are reported in bold.

more closely packed diamond lattice, leading to linear dependencies, numerical instabilities, and no possible SCF convergence in the end. The same happened when we tried to use the unmodified original molecular def2-TZVP basis sets, with the sole exception of carbyne thanks to its one-dimensional extension. The corresponding energy is −76.098306 E_h, about 1 mE_h higher than our dcm[C_{cby}]-TZVP result.

The optimization carried out with the BFGS algorithm leads to a very similar basis set for graphene, yielding essentially the same energy. For diamond, a significantly different result is obtained with respect to the BDIIS one reported in Table 1 with an energy that is 68 μE_h higher (exponents are 1.0163; 0.6367; 0.2392 for valence *s*-functions, 0.5646; 0.2728 for *p*-functions, 1.0242; 0.5957 for *d*-functions, and 0.8239 for the *f*-function).

3.2.2. Crystalline NaCl, Na, and Cl_2. Let us now compare the optimal basis set obtained with the PBE0 functional for three bulk structures with very different chemical bonding, namely: metallic Na, molecular Cl_2, and ionic rocksalt NaCl, whose electronic charge densities are reported in Figure 1. As discussed in the Introduction, the significantly different features in the electronic structure expectedly require a different support and hence a specific basis set. The geometries adopted are fully reported in the Supporting Information and have been obtained from experimental references in the literature.[47−49]

In Table 3 we see that for the Cl_2 molecular crystal, not unexpectedly, the original def2 basis set undergoes very little

Table 3. Gaussian Exponents for Different Cl TZVP Basis Sets[b]

	def2	pob[15]	pob-rev2[17]	dcm[Cl_2][a]	dcm[NaCl][a]
s	0.5023	0.4499	0.4499	0.5075	0.5724
	0.1796	0.1364	0.1364	0.1831	0.2312
p	2.9433	2.8015	2.8015	2.8983	2.9386
	1.0405	0.7396	0.7896	1.1044	1.1903
	0.3846	0.2106	0.2106	0.4092	0.4697
	0.1307			0.1365	0.1747
d	0.3390	0.2373	0.2373	0.3326	0.2838
f	0.7060			0.5990	0.6898

[a]This work. [b]The dcm-variants were optimized with the PBE0 functional.

modifications when optimized in the solid. Actually, it performs much better than the pob-TZVP basis (see Table 5) with the total energy being 0.1 Ha lower. The removal of the outermost *p*-function in the pob basis sets leads to an overall decrease of the exponents of the remaining functions that partly compensates the contribution to the total energy of the missing function. If one includes the outermost *p*-function from the dcm basis set, a further energy lowering of 13 and 17 mE_h is observed for the pob and pob-rev2 basis set, respectively. However, this is not enough to reach the final energy of solid Cl_2 as obtained with the optimized dcm basis set thus showing the crucial role of the outermost *p*-function.

The dcm[NaCl] basis for Cl, optimized in the rocksalt structure, features significantly more contracted exponents, as far as *s*- and *p*-functions are concerned, while the *d* exponent becomes more diffuse. As reported in Table 4, a stronger

Table 4. Gaussian Exponents for Different Na TZVP Basis Sets[b]

	def2	pob[15]	pob-rev2[17]	dcm[Na][a]	dcm[NaCl][a]
s	0.0500	0.6746	0.4246	0.2127	0.3436
	0.0193	0.1006	0.1205	0.0782	0.0828
p	0.4174	0.4009	0.4009	0.4034	0.4023
	0.0910	0.1007	0.1207	0.0851	0.0981
	0.0300				
d	2.6090	1.0463	0.3053	2.6086	2.6074
	0.4300			0.4337	0.4040
	0.1000			0.1115	0.0985

[a]This work. [b]The dcm-variants were optimized with the PBE0 functional.

contraction is observed in exponents of the *s*-type orbitals in going from the molecular def2 to the bulk metal and then the ionic NaCl. In this case we had to remove the most diffuse *p*-function (0.03 au) in order to ensure convergence, but at difference with the pob-TZVP case, we were able to keep all the *d*-functions in.

As shown in Table 5 it can be seen that in all cases dcm-energies are significantly lower than pob- ones, and quite surprisingly the dcm[Cl_2]-TZVP and dcm[Na]-TZVP basis sets seem to perform well also in the ionic case.

Such basis sets effects are also reflected in geometry optimizations. In Table 6 we report the optimized lattice parameters obtained with the different basis sets. It is seen that the dcm-basis sets lead in all cases to an expanded volume with respect to the pob- ones and in the case of Na and NaCl also to a better agreement with experiment at the PBE0 level. In the molecular crystal Cl_2, dispersion effects act as a key role, hence the plain PBE0 leads to an excessively expanded volume when the dcm[Cl_2] basis is used, while the introduction of -D3 dispersion correction restores a more correct description. It is reasonable to assume that the volume expansion associated with the dcm[Cl_2] basis is related to a mitigation of BSSE effects—which usually act as spurious dispersion.

3.3. Use of Large, Extended Basis Sets. Solid LiH is a rather standard benchmark for methods assessment in the solid state. Recently[24,26] lithium hydride has been used as a benchmark for estimating the Hartree−Fock basis set limit compared with results from different approaches.[23,50,51] The case of LiH, similarly as NaCl, poses certain difficulties since standard molecular basis sets are designed for neutral atoms, not ions, hence inapplicable to bulk ionic crystals without modification. We optimized the basis set series def2-SVP/def2-TZVP/def2-QZVP with our BDIIS algorithm, obtaining the

https://dx.doi.org/10.1021/acs.jctc.9b01004
J. Chem. Theory Comput. 2020, 16, 2192−2201

Table 5. Total Energies at the DFT/PBE0 Level for Na, Cl_2, and NaCl as Computed with Different TZVP Basis Sets[b]

E_{TOT}^{PBE0}	pob[15]	pob-rev2[17]	dcm[Na][a]	dcm[Cl_2][a]	dcm[NaCl][a]
Na	−162.202291	−162.198836	**-162.210106**		−162.209707
Cl_2	−1840.065404	−1840.052238		**-1840.186164**	−1840.175452
NaCl	−622.394522	−622.392474	−622.405254		**-622.405810**

[a]This work. [b]Energies in E_h. Energies for the consistently optimized basis sets are reported in bold.

Table 6. Experimental[47−49] and Calculated Lattice Parameters for Solid Na, Cl_2, and NaCl, as Obtained with Different Basis Sets[b]

PBE0		pob[15]	pob-rev2[17]	dcm[Na][a]	dcm[Cl_2][a]	dcm[NaCl][a]	exp
Na	a	4.041 (−0.184)	3.957 (−0.268)	4.258 (0.033)			4.225
	a	6.211 (0.066)			6.634 (0.489)		6.145
Cl_2	b	4.387 (−0.008)			4.683 (0.287)		4.395
	c	8.126 (−0.028)			8.549 (0.395)		8.154
NaCl	a	5.602(−0.038)	5.609(−0.031)			5.644(0.004)	5.640
PBE0-D3		pob[15]	pob-rev2[17]	dcm[Na][a]	dcm[Cl_2][a]	dcm[NaCl][a]	exp
Cl_2	a	6.011 (−0.134)	6.034 (−0.111)		6.175 (0.030)		6.145
	b	4.224 (−0.171)	4.255 (−0.140)		4.307 (−0.088)		4.395
	c	8.013 (−0.140)	8.021 (−0.133)		8.239 (0.085)		8.154

[a]This work. [b]The difference with respect to the experimental reference is reported in round brackets.

corresponding dcm[LiH]-SVP/dcm[LiH]-TZVP/dcm[LiH]-QZVP. The corresponding Hartree−Fock total energy values are −8.059489, −8.063808, and −8.064618 E_h, respectively. In Figure 4 we compare such energies with previous data from the

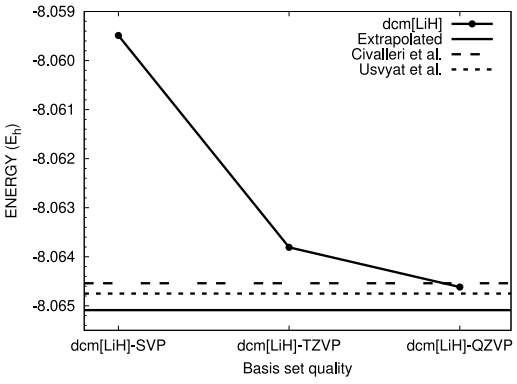

Figure 4. Energy of bulk LiH at the HF level: a comparison of our dcm-XVZP basis set results. Extrapolated CBS limit and literature data (Civalleri et al.[24] and Usvyat et al.[26]).

literature also obtained with the CRYSTAL code. It is seen that with the quadruple basis we reach a value that is very close to that of ref 26 (i.e., −8.06475 E_h), where a much larger basis set was used. This last result was already close to the CBS limit compared to methods employing different basis set types.[26] If the dcm-TZVP and dcm-QZVP total energies are used to estimate the HF complete basis set (CBS) limit by using a two-point extrapolation scheme based on an exponential formula, a value of −8.065089 is attained. Notably, this energy limit is even lower than the one reached by Usvyat and co-workers[26] by 0.3 mE_h. When using the CBS energy for the atoms,[52] the cohesive energy is then −3.60 eV in very good agreement with results from different theoretical approaches.[23,50,51]

Similarly, we have optimized a quadruple-ζ basis for diamond and graphene. The original def2-QZVP basis does not allow convergence in either case, while with the basis sets as reported in Table 7 the energies of −76.165178 and

Table 7. Exponents Comparison of Gaussian Basis Sets[b]

	def2-QZVP	dcm[C_{diam}]-QZVP[a]	dcm[C_{graph}]-QZVP[a]
s	5.2404	6.2060	5.2404
	2.2905	3.3250	2.3278
	0.6967	1.0952	1.0461
	0.2760	0.6304	0.5218
	0.1074	0.3436	0.2004
p	0.4605	0.8740	0.4500
	0.1894	0.5426	0.3287
	0.0760	0.1832	0.1249
d	1.8480	1.9639	1.9130
	0.6490	0.9684	0.8630
	0.2280	0.5478	0.4526
f	1.4190	1.5109	1.4143
	0.4850	0.7423	0.5982
g	1.0110	1.1825	0.9931

[a]This work. [b]Diamond and graphene cases for quadruple-ζ basis sets. Optimization carried out at the PBE level.

−76.174386 E_h are obtained for the two systems at the PBE level. The latter value we believe to be close to basis set completeness. Extrapolation to the CBS limit leads to a value of −76.167396 and −76.177298 E_h, respectively.

In Table 7 we report the reoptimized exponents with respect to def2-QZVP basis sets—all other functions are the same as in the molecular basis set. It is worth noting that *g*-type functions were also included in the basis set as they were recently made available in the development version of the CRYSTAL code.[53]

BSSE effects are reduced much more considerably by the increasing of the basis set quality, rather than by the optimization of the exponents, so that BSSE is quite similar for pob- or dcm- basis sets.

For diamond, we have also calculated the Hartree−Fock CBS limit by using the dcm-TZVP and dcm-QZVP basis sets.

https://dx.doi.org/10.1021/acs.jctc.9b01004
J. Chem. Theory Comput. 2020, 16, 2192−2201

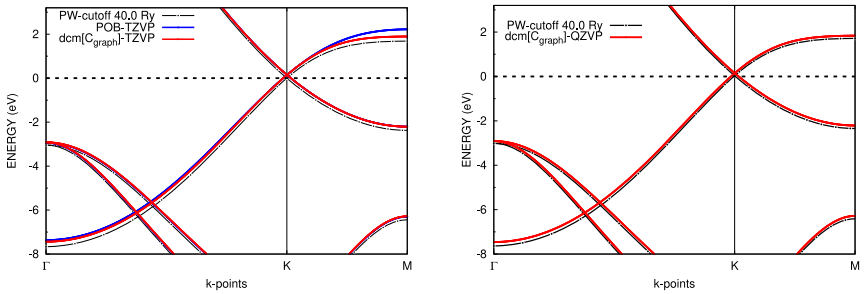

Figure 5. Band structure comparison between plane waves (Quantum Espresso) and CRYSTAL in the graphene case with dcm[C_{graph}] and POB basis sets with PBE as the DFT functional.

Computed total energies are −75.772638 and −75.774752 E_h, respectively. The adopted extrapolation scheme leads to a HF CBS limit of −75.775983 E_h that corresponds to a cohesive energy for diamond[52] of −10.58 eV, very close to a previously reported HF value of −10.56 eV.[54] Interestingly, results show that the basis sets optimized with the PBE functional can also be used for HF even if a tighter setting of the computational parameters is required (see the Supporting Information).

In Figure 5 we compare, for graphene, the electronic band structure computed with Gaussian basis sets with the bands for the same systems as obtained from a plane wave code[55] using a considerably high cutoff. It is evident that the bands at the triple-ζ level are different from the reference ones, specially in the Γ and *M* points of the Brillouin zone. Nevertheless, the dcm[C_{graph}]-TZVP performs better than the pob-TZVP. A considerably better agreement is attained by using the dcm[C_{graph}]-QZVP basis (right panel of Figure 5). We believe this is strong evidence of the possibility of reaching converged results with Gaussian basis sets and the effectiveness of a system-specific optimization scheme.

4. CONCLUSIONS

In the present work, we have developed a basis set optimizer based on the DIIS algorithm that minimizes the total energy of the system constrained to keep the condition number of the overlap matrix as small as possible in a similar approach as proposed by VandeVondele et al.[40] The latter constraint acts as a pivot in the optimization of the basis set and prevents the lowest exponents of the basis set to decrease too much thus reducing the risk of linear dependency and numerical instability. This is particularly important in solid-state calculations where the use of atom-centered diffuse functions is more delicate and sometime useless.

We have then shown that the proposed method is quite effective for solid-state calculations and allows for an easy optimization of basis sets not only of triple-ζ quality but even of quadruple-ζ size. Furthermore, we have demonstrated that the BDIIS method can be used to obtain basis sets for solids of consistent quality as molecules without pruning the original basis sets. Results for simple solids as diamond and graphene for which the definition of an appropriate and system-consistent basis set is uglily difficult are very promising. Also, the possibility of employing basis sets specifically calibrated on a given system allowed us to easily reach the HF complete basis set limit for LiH which has been a long debated issue and for diamond.

While reasonable questions can be raised about the transferability of such optimized basis sets from one method to another, we have seen that a basis set optimized, say, with PBE is very close to convergence when inserted in HF or PBE0. For our diamond test case the energy with such basis was only a few μE_h away from the minimum when transferred from one method to another.

The evidence of the excellent performance of the BDIIS method paves the way for a careful definition of system-specific basis sets, as a viable alternative to all-purpose basis sets. Nevetheless, it could be employed for a more extensive work that would permit the creation of all-purpose basis set families for a larger set of atomic species. Furthermore, the algorithm here described could be very useful to optimize basis sets for post-HF correlation methods[20,56] as well as for response properties.[57−59]

■ ASSOCIATED CONTENT

Supporting Information

The Supporting Information is available free of charge at https://pubs.acs.org/doi/10.1021/acs.jctc.9b01004.

CRYSTAL17 inputs used to obtain reported results (PDF)

■ AUTHOR INFORMATION

Corresponding Author

Lorenzo Maschio − *Dipartimento di Chimica, Università di Torino and NIS (Nanostructured Interfaces and Surfaces) Centre 10125 Torino, Italy;* orcid.org/0000-0002-4657-9439; Email: lorenzo.maschio@unito.it

Authors

Loredana Edith Daga − *Dipartimento di Chimica, Università di Torino and NIS (Nanostructured Interfaces and Surfaces) Centre 10125 Torino, Italy*

Bartolomeo Civalleri − *Dipartimento di Chimica, Università di Torino and NIS (Nanostructured Interfaces and Surfaces) Centre 10125 Torino, Italy;* orcid.org/0000-0003-3198-3161

Complete contact information is available at: https://pubs.acs.org/10.1021/acs.jctc.9b01004

Notes

The authors declare no competing financial interest.

https://dx.doi.org/10.1021/acs.jctc.9b01004
J. Chem. Theory Comput. 2020, 16, 2192−2201

■ ACKNOWLEDGMENTS

The authors thank the anonymous referees for useful suggestions. We acknowledge computational resources from the C3S Centre of the Torino University through the OCCAM computing cluster.[60]

■ REFERENCES

(1) Pisani, C. Quantum-Mechanical Ab-initio Calculation of the Properties of Crystalline Materials; *Lecture Notes in Chemistry Series*; Springer Verlag: Berlin, 1996; Vol. *67*, DOI: 10.1007/978-3-642-61478-1.

(2) Martin, R. M. *Electronic Structure: Basic Theory and Practical Methods*; Cambridge University Press: 2004; DOI: 10.1017/CBO9780511805769.

(3) Dovesi, R.; Civalleri, B.; Orlando, R.; Roetti, C.; Saunders, V. R. Ab initio quantum simulation in solid state chemistry. *Rev. Comp. Chem.* **2005**, *21*, 1.

(4) Boys, S. F. Electronic Wave Functions - I. A General Method of Calculation for the Stationary States of any Molecular System. *Proc. R. Soc. London A* **1950**, *200*, 542−554.

(5) Helgaker, T.; Jorgensen, P.; Olsen, J. *Molecular Electronic Structure Theory*; John Wiley & Sons, Ltd.: 2000.

(6) Kresse, G.; Furthmüller, J. Efficient Iterative Schemes for ab initio Total-Energy Calculations using a Plane-Wave Basis Set. *Phys. Rev. B: Condens. Matter Mater. Phys.* **1996**, *54*, 11169.

(7) Clark, S. J.; Segall, M. D.; Pickard, C. J.; Hasnip, P. J.; Probert, M. I.; Refson, K.; Payne, M. C. First Principles Methods Using CASTEP. *Z. Kristallogr. - Cryst. Mater.* **2005**, *220*, 567−570.

(8) Giannozzi, P.; Baroni, S.; Bonini, N.; Calandra, M.; Car, R.; Cavazzoni, C.; Ceresoli, D.; Chiarotti, G. L.; Cococcioni, M.; Dabo, I.; et al. QUANTUM ESPRESSO: a Modular and Open-Source Software Project for Quantum Simulations of Materials. *J. Phys.: Condens. Matter* **2009**, *21*, 395502.

(9) Dovesi, R.; Erba, A.; Orlando, R.; Zicovich-Wilson, C. M.; Civalleri, B.; Maschio, L.; Rérat; Casassa, S.; Baima, J.; Salustro, S.; et al. Quantum-mechanical Condensed Matter Simulations with CRYSTAL. *WIREs: Comp. Mol. Sci.* **2018**, *8*, e1360.

(10) Lippert, G.; Hutter, J.; Parrinello, M. A Hybrid Gaussian and Plane Wave Density Functional Scheme. *Mol. Phys.* **1997**, *92*, 477−488.

(11) Delley, B. From Molecules to Solids with the DMol^3 Approach. *J. Chem. Phys.* **2000**, *113*, 7756−7764.

(12) Levchenko, S. V.; Ren, X.; Wieferink, J.; Johanni, R.; Rinke, P.; Blum, V.; Scheffler, M. Hybrid Functionals for Large Periodic Systems in an All-Electron, Numeric Atom-Centered Basis Framework. *Comput. Phys. Commun.* **2015**, *192*, 60−69.

(13) Nagy, B.; Jensen, F. Basis Sets in Quantum Chemistry. *Rev. Comp. Chem.* **2017**, *30*, 93−150.

(14) Peterson, K. A.; Hill, J. G. *Annual Reports in Computational Chemistry*; Elsevier: 2018; Vol. *14*, pp 47−74.

(15) Peintinger, M. F.; Oliveira, D. V.; Bredow, T. Consistent Gaussian Basis Sets of Triple-zeta Valence with Polarization Quality for Solid-State Calculations. *J. Comput. Chem.* **2013**, *34*, 451−459.

(16) Laun, J.; Vilela Oliveira, D.; Bredow, T. Consistent gaussian basis sets of double-and triple-zeta valence with polarization quality of the fifth period for solid-state calculations. *J. Comput. Chem.* **2018**, *39*, 1285−1290.

(17) Vilela Oliveira, D.; Laun, J.; Peintinger, M. F.; Bredow, T. BSSE-correction scheme for consistent gaussian basis sets of double- and triple-zeta valence with polarization quality for solid-state calculations. *J. Comput. Chem.* **2019**, *40*, 2364−2376.

(18) Grüneich, A.; Heß, B. A. Choosing GTO Basis Sets for Periodic HF Calculations. *Theor. Chem. Acc.* **1998**, *100*, 253−263.

(19) Jensen, F. Analysis of Energy-Optimized Gaussian Basis Sets for Condensed Phase Density Functional Calculations. *Theor. Chem. Acc.* **2013**, *132*, 1380.

(20) Dunning, T. H., Jr Gaussian Basis Sets for Use in Correlated Molecular Calculations. I. The Atoms Boron Through Neon and Hydrogen. *J. Chem. Phys.* **1989**, *90*, 1007−1023.

(21) Jensen, F. Polarization Consistent Basis Sets: Principles. *J. Chem. Phys.* **2001**, *115*, 9113−9125.

(22) Manby, F.; Alfè, D.; Gillan, M. Extension of Molecular Electronic Structure Methods to the Solid State: Computation of the Cohesive Energy of Lithium Hydride. *Phys. Chem. Chem. Phys.* **2006**, *8*, 5178−5180.

(23) Paier, J.; Diaconu, C. V.; Scuseria, G. E.; Guidon, M.; VandeVondele, J.; Hutter, J. Accurate Hartree-Fock energy of extended systems using large Gaussian basis sets. *Phys. Rev. B: Condens. Matter Mater. Phys.* **2009**, *80*, 174114.

(24) Civalleri, B.; Orlando, R.; Zicovich-Wilson, C. M.; Roetti, C.; Saunders, V. R.; Pisani, C.; Dovesi, R. Comment on "Accurate Hartree-Fock energy of extended systems using large Gaussian basis sets. *Phys. Rev. B: Condens. Matter Mater. Phys.* **2010**, *81*, 106101.

(25) Binnie, S.; Nolan, S.; Drummond, N.; Alfè, D.; Allan, N.; Manby, F.; Gillan, M. Bulk and surface energetics of crystalline lithium hydride: Benchmarks from quantum Monte Carlo and quantum chemistry. *Phys. Rev. B: Condens. Matter Mater. Phys.* **2010**, *82*, 165431.

(26) Usvyat, D.; Civalleri, B.; Maschio, L.; Dovesi, R.; Pisani, C.; Schütz, M. Approaching the theoretical limit in periodic local MP2 calculations with atomic-orbital basis sets: the case of LiH. *J. Chem. Phys.* **2011**, *134*, 214105.

(27) Lehtola, S. Curing basis set overcompleteness with pivoted Cholesky decompositions. *J. Chem. Phys.* **2019**, *151*, 241102.

(28) Kadek, M.; Repisky, M.; Ruud, K. All-electron Fully Relativistic Kohn-Sham Theory for Solids Based on the Dirac-Coulomb Hamiltonian and Gaussian-type Functions. *Phys. Rev. B: Condens. Matter Mater. Phys.* **2019**, *99*, 205103.

(29) Maschio, L.; Kirtman, B. Coupled Perturbation Theory Approach to Dual Basis Sets for Molecules and Solids. I: General Theory and Application to Molecules. *J. Chem. Theory Comput.* **2020**, *16*, 340−353.

(30) Weigend, F.; Ahlrichs, R. Balanced basis sets of split valence, triple zeta valence and quadruple zeta valence quality for H to Rn: Design and assessment of accuracy. *Phys. Chem. Chem. Phys.* **2005**, *7*, 3297−3305.

(31) Weigend, F.; Häser, M.; Patzelt, H.; Ahlrichs, R. RI-MP2: Optimized Auxiliary Basis Sets and Demonstration of Efficiency. *Chem. Phys. Lett.* **1998**, *294*, 143−152.

(32) Schäfer, A.; Huber, C.; Ahlrichs, R. Fully Optimized Contracted Gaussian Basis Sets of Triple Zeta Valence Quality for Atoms Li to Kr. *J. Chem. Phys.* **1994**, *100*, 5829−5835.

(33) Pulay, P. Convergence Acceleration of Iterative Sequences. The Case of SCF Iteration. *Chem. Phys. Lett.* **1980**, *73*, 393−398.

(34) Pulay, P. Improved SCF convergence acceleration. *J. Comput. Chem.* **1982**, *3*, 556−560.

(35) Maschio, L. Direct Inversion of the Iterative Subspace (DIIS) Convergence Accelerator for Crystalline Solids Employing Gaussian Basis Sets. *Theor. Chem. Acc.* **2018**, *137*, 60.

(36) Császár, P.; Pulay, P. Geometry Optimization by Direct Inversion in the Iterative Subspace. *J. Mol. Struct.* **1984**, *114*, 31−34.

(37) Beata, G.; Perego, G.; Civalleri, B. CRYSPLOT: A new Tool to Visualize Physical and Chemical Properties of Molecules, Polymers, Surfaces, and Crystalline Solids. *J. Comput. Chem.* **2019**, *40*, 2329−2338.

(38) Pisani, C.; Dovesi, R.; Roetti, C. *Hartree-Fock Ab Initio Treatment of Crystalline solids*; Lecture Notes in Chemistry Series; Springer Verlag: Berlin, 1988; Vol. *48*, DOI: 10.1007/978-3-642-93385-1.

(39) Saunders, V. R.; Freyria Fava, C.; Dovesi, R.; Salasco, L.; Roetti, C. On the Electrostatic Potential in Crystalline Systems where the Charge Density is Expanded in Gaussian Functions. *Mol. Phys.* **1992**, *77*, 629.

(40) VandeVondele, J.; Hutter, J. Gaussian Basis Sets for Accurate Calculations on Molecular Systems in Gas and Condensed Phases. *J. Chem. Phys.* **2007**, *127*, 114105.
(41) Faegri, K., Jr; Almlof, J. Energy-optimized GTO basis sets for LCAO Calculations. A Gradient Approach. *J. Comput. Chem.* **1986**, *7*, 396−405.
(42) Tonachini, G.; Schlegel, H. B. Hartree−Fock Energy Derivatives with Respect to Basis set Exponents. Integral Derivatives using Rys Polynomials. *J. Chem. Phys.* **1987**, *87*, 514−519.
(43) Perdew, J. P.; Burke, K.; Ernzerhof, M. Generalized Gradient Approximation Made Simple. *Phys. Rev. Lett.* **1996**, *77*, 3865.
(44) Perdew, J. P.; Ruzsinszky, A.; Csonka, G. I.; Vydrov, O. A.; Scuseria, G. E.; Constantin, L. A.; Zhou, X.; Burke, K. Restoring the Density-gradient Expansion for Exchange in Solids and Surfaces. *Phys. Rev. Lett.* **2008**, *100*, 136406.
(45) Adamo, C.; Barone, V. Toward Reliable Density Functional Methods Without Adjustable Parameters: The PBE0Model. *J. Chem. Phys.* **1999**, *110*, 6158.
(46) Jensen, F. The Effect of Different Density Functional Methods on Basis Set Parameters. *Chem. Phys. Lett.* **2005**, *402*, 510−513.
(47) Powell, B.; Heal, K.; Torrie, B. The Temperature Dependence of the Crystal Structures of the Solid Halogens, Bromine and Chlorine. *Mol. Phys.* **1984**, *53*, 929−939.
(48) Walker, D.; Verma, P. K.; Cranswick, L. M.; Jones, R. L.; Clark, S. M.; Buhre, S. Halite-sylvite thermoelasticity. *Am. Mineral.* **2004**, *89*, 204−210.
(49) Barrett, C. X-ray study of the alkali metals at low temperatures. *Acta Crystallogr.* **1956**, *9*, 671−677.
(50) Nolan, S.; Gillan, M.; Alfè, D.; Allan, N.; Manby, F. Calculation of properties of crystalline lithium hydride using correlated wave function theory. *Phys. Rev. B: Condens. Matter Mater. Phys.* **2009**, *80*, 165109.
(51) Marsman, M.; Grüneis, A.; Paier, J.; Kresse, G. Second-order Møller−Plesset Perturbation Theory Applied to Extended Systems. I. Within the Projector-Augmented-wave Formalism Using a Plane Wave Basis Set. *J. Chem. Phys.* **2009**, *130*, 184103.
(52) Reference HF atomic energies for H, Li, and C were computed with an aug-cc-pV5Z basis set.
(53) Desmarais, J. K.; Erba, A.; Dovesi, R. Generalization of the Periodic LCAO Approach in the CRYSTAL Code to g-type Orbitals. *Theor. Chem. Acc.* **2018**, *137*, 28.
(54) Grüneis, A.; Marsman, M.; Kresse, G. Second-order Møller−Plesset Perturbation Theory Applied to Extended Systems. II. Structural and Energetic Properties. *J. Chem. Phys.* **2010**, *133*, 074107.
(55) Giannozzi, P.; Andreussi, O.; Brumme, T.; Bunau, O.; Nardelli, M. B.; Calandra, M.; Car, R.; Cavazzoni, C.; Ceresoli, D.; Cococcioni, M.; et al. Advanced Capabilities for Materials Modelling with Quantum ESPRESSO. *J. Phys.: Condens. Matter* **2017**, *29*, 465901.
(56) Maschio, L. Local MP2 with Density Fitting for Periodic Systems: A Parallel Implementation. *J. Chem. Theory Comput.* **2011**, *7*, 2818−2830.
(57) Sadlej, A. J. Medium-size polarized basis sets for high-level correlated calculations of molecular electric properties. *Collect. Czech. Chem. Commun.* **1988**, *53*, 1995−2016.
(58) Rappoport, D.; Furche, F. Property-Optimized Gaussian Basis Sets for Molecular Response Calculations. *J. Chem. Phys.* **2010**, *133*, 134105.
(59) Kirtman, B.; Maschio, L.; Rérat, M.; Springborg, M. *Frontiers of Quantum Chemistry*; Springer: 2018; pp 87−115, DOI: 10.1007/978-981-10-5651-2_5.
(60) Aldinucci, M.; Bagnasco, S.; Lusso, S.; Pasteris, P.; Rabellino, S.; Vallero, S. OCCAM: a flexible, multi-purpose and extendable HPC cluster. *J. Phys.: Conf. Ser.* **2017**, *898*, 082039.

https://dx.doi.org/10.1021/acs.jctc.9b01004
J. Chem. Theory Comput. 2020, 16, 2192−2201

Supplementary Material for: [Gaussian Basis sets for Crystalline Solids: All-Purpose Basis Set Libraries Vs System–Specific Optimizations]

Loredana Edith Daga, Bartolomeo Civalleri, and Lorenzo Maschio*

Dipartimento di Chimica, Università di Torino and NIS (Nanostructured Interfaces and Surfaces) Centre, Via P. Giuria 5, 10125 Torino, Italy

E-mail: lorenzo.maschio@unito.it

This document explicitly reports most of the CRYSTAL17 inputs used to obtain the results reported in the paper. The basis set in the inputs are the dcm-XZVP obtained by using the BDIIS optimizer. The shells labelled by an asterisk are those that have been optimized.

1 Diamond - triple ζ

```
DIAMOND-TZ-PBE
CRYSTAL
0 0 1
227
3.56679
1
6   0. 0. 0.
END
  6 11
0 0  6  2. 1.
   1.35753496820E+04   2.22458143520E-04
   2.03523336800E+03   1.72327382520E-03
   4.63225623590E+02   8.92557153140E-03
   1.31200195980E+02   3.57279845020E-02
   4.28530158910E+01   1.10762599310E-01
   1.55841857660E+01   2.42956276260E-01
0 0  2  2. 1.
   6.20671385080E+00   4.14402634480E-01
   2.57648965270E+00   2.37449686550E-01
0 0  1  0. 1. *
   2.72877227664E+00   1.00000000000E+00
0 0  1  0. 1. *
   7.08254466129E-01   1.00000000000E+00
0 0  1  0. 1. *
   2.75435053993E-01   1.00000000000E+00
```

```
0 2  4  2. 1.
   3.46972322440E+01   5.33336578050E-03
   7.95826228260E+00   3.58641090920E-02
   2.37808268830E+00   1.42158733290E-01
   8.14332081830E-01   3.42704718450E-01
0 2  1  0. 1. *
   6.18739070583E-01   1.00000000000E+00
0 2  1  0. 1. *
   2.71282775658E-01   1.00000000000E+00
0 3  1  0. 1. *
   2.01143808439E+00   1.00000000000E+00
0 3  1  0. 1. *
   6.26539832528E-01   1.00000000000E+00
0 4  1  0. 1. *
   1.06242225484E+00   1.00000000000E+00
99 0
END
DFT
PBE
END
MAXCYCLE
100
TOLINTEG
8 8 8 12 24
TOLDEE
8
SHRINK
8 8
END
```

2 Diamond - quadruple ζ

```
DIAMOND-QZ-PBE
CRYSTAL
0 0 1
227
3.56679
1
6   0. 0. 0.
END
  6 17
0 0  8  2. 1.
   6.70250710290E+04   3.87363085010E-05
   1.00399865380E+04   3.01079175750E-04
   2.28493169110E+03   1.57879180950E-03
   6.47141221300E+02   6.60870871950E-03
   2.11094723350E+02   2.33671232500E-02
   7.61776438620E+01   7.04207168980E-02
   2.96338391630E+01   1.73603449530E-01
   1.21877850810E+01   3.22923056480E-01
0 0  2  2. 1.
   5.30260062990E+01   7.48974044920E-02
   1.52585027760E+01   7.61362209830E-01
0 0  1  0. 1. *
   6.20602927512E+00   1.00000000000E+00
0 0  1  0. 1. *
   3.32497590179E+00   1.00000000000E+00
0 0  1  0. 1. *
   1.09521378286E+00   1.00000000000E+00
0 0  1  0. 1. *
   6.30358128105E-01   1.00000000000E+00
0 0  1  0. 1. *
   3.43646141101E-01   1.00000000000E+00
```

```
0 2  5  2. 1.
   1.05125550820E+02   8.46475538440E-04
   2.48844610660E+01   6.62740385340E-03
   7.86372308260E+00   3.01203904190E-02
   2.84070018350E+00   9.99514354760E-02
   1.12271373350E+00   2.38262992820E-01
0 2  1  0. 1. *
   8.74041963051E-01   1.00000000000E+00
0 2  1  0. 1. *
   5.42561494412E-01   1.00000000000E+00
0 2  1  0. 1. *
   1.83247854025E-01   1.00000000000E+00
0 3  1  0. 1. *
   1.96394180988E+00   1.00000000000E+00
0 3  1  0. 1. *
   9.68369087225E-01   1.00000000000E+00
0 3  1  0. 1. *
   5.47772457307E-01   1.00000000000E+00
0 4  1  0. 1. *
   1.51085897443E+00   1.00000000000E+00
0 4  1  0. 1. *
   7.42254560983E-01   1.00000000000E+00
0 5  1  0. 1. *
   1.18250314805E+00   1.00000000000E+00
99 0
END
DFT
PBE
END
MAXCYCLE
100
TOLINTEG
8 8 8 12 24
```

```
TOLDEE
8
SHRINK
8 8
NOBIPOLA
END
```

3 Graphene - triple ζ

```
GRAPHENE-TZ-PBE
SLAB
77
2.47
1
6  -0.33333333333 0.33333333333 0.
END
  6 11
0 0  6  2. 1.
   1.35753496820E+04   2.22458143520E-04
   2.03523336800E+03   1.72327382520E-03
   4.63225623590E+02   8.92557153140E-03
   1.31200195980E+02   3.57279845020E-02
   4.28530158910E+01   1.10762599310E-01
   1.55841857660E+01   2.42956276260E-01
0 0  2  2. 1.
   6.20671385080E+00   4.14402634480E-01
   2.57648965270E+00   2.37449686550E-01
0 0  1  0. 1. *
   1.09605489209E+00   1.00000000000E+00
0 0  1  0. 1. *
   5.91106934956E-01   1.00000000000E+00
```

```
0 0  1  0. 1. *
   2.37383807053E-01   1.00000000000E+00
0 2  4  2. 1.
   3.46972322440E+01   5.33336578050E-03
   7.95826228260E+00   3.58641090920E-02
   2.37808268830E+00   1.42158733290E-01
   8.14332081830E-01   3.42704718450E-01
0 2  1  0. 1. *
   3.38693223652E-01   1.00000000000E+00
0 2  1  0. 1. *
   1.59434147140E-01   1.00000000000E+00
0 3  1  0. 1. *
   1.25021363036E+00   1.00000000000E+00
0 3  1  0. 1. *
   7.19402508165E-01   1.00000000000E+00
0 4  1  0. 1. *
   7.06699996366E-01   1.00000000000E+00
99 0
END
DFT
PBE
XLGRID
END
SCFDIR
FMIXING
30
LDREMO
1
MAXCYCLES
100
TOLINTEG
8 8 8 8 16
TOLDEE
```

```
8
SHRINK
64 64
END
```

4 Graphene - quadruple ζ

```
GRAPHENE-QZ-PBE
SLAB
77
2.47
1
6 -0.33333333333 0.33333333333 0.
END
6 17
0 0  8  2. 1.
   6.70250710290E+04   3.87363085010E-05
   1.00399865380E+04   3.01079175750E-04
   2.28493169110E+03   1.57879180950E-03
   6.47141221300E+02   6.60870871950E-03
   2.11094723350E+02   2.33671232500E-02
   7.61776438620E+01   7.04207168980E-02
   2.96338391630E+01   1.73603449530E-01
   1.21877850810E+01   3.22923056480E-01
0 0  2  2. 1.
   5.30260062990E+01   7.48974044920E-02
   1.52585027760E+01   7.61362209830E-01
0 0  1  0. 1. *
   5.24039574640E+00   1.00000000000E+00
0 0  1  0. 1. *
   2.32777405666E+00   1.00000000000E+00
0 0  1  0. 1. *
```

```
   1.04613233770E+00   1.00000000000E+00
0 0  1  0. 1. *
   5.21832251512E-01   1.00000000000E+00
0 0  1  0. 1. *
   2.00431897163E-01   1.00000000000E+00
0 2  5  2. 1.
   1.05125550820E+02   8.46475538440E-04
   2.48844610660E+01   6.62740385340E-03
   7.86372308260E+00   3.01203904190E-02
   2.84070018350E+00   9.99514354760E-02
   1.12271373350E+00   2.38262992820E-01
0 2  1  0. 1. *
   4.50031980659E-01   1.00000000000E+00
0 2  1  0. 1. *
   3.28748485841E-01   1.00000000000E+00
0 2  1  0. 1. *
   1.24896018560E-01   1.00000000000E+00
0 3  1  0. 1. *
   1.91295701725E+00   1.00000000000E+00
0 3  1  0. 1. *
   8.63019243591E-01   1.00000000000E+00
0 3  1  0. 1. *
   4.52624895593E-01   1.00000000000E+00
0 4  1  0. 1. *
   1.41426143665E+00   1.00000000000E+00
0 4  1  0. 1. *
   5.98189433168E-01   1.00000000000E+00
0 5  1  0. 1. *
   9.93072428023E-01   1.00000000000E+00
99 0
END
DFT
PBE
```

```
XLGRID
END
SCFDIR
FMIXING
30
LDREMO
1
MAXCYCLES
100
TOLINTEG
8 8 8 8 16
TOLDEE
8
SHRINK
64 64
END
```

5 Carbyne - triple ζ

```
C_Chain
POLYMER
1
2.56620186
2
6   9.624791798260E-02 -1.258372661974E-18 -4.072637834921E-09
6  -3.962479179826E-01 -2.785734209432E-16  4.072638114753E-09
END
6 11
0 0 6 2. 1.
1.35753496820E+04 2.22458143520E-04
2.03523336800E+03 1.72327382520E-03
4.63225623590E+02 8.92557153140E-03
```

```
1.31200195980E+02 3.57279845020E-02
4.28530158910E+01 1.10762599310E-01
1.55841857660E+01 2.42956276260E-01
0 0 2 2. 1.
6.20671385080E+00 4.14402634480E-01
2.57648965270E+00 2.37449686550E-01
0 0 1 0. 1. *
 1.13833219587E+00   1.00000000000E+00
0 0 1 0. 1. *
 6.55714337901E-01   1.00000000000E+00
0 0 1 0. 1. *
 2.32302377804E-01   1.00000000000E+00
0 2 4 2. 1.
3.46972322440E+01 5.33336578050E-03
7.95826228260E+00 3.58641090920E-02
2.37808268830E+00 1.42158733290E-01
8.14332081830E-01 3.42704718450E-01
0 2 1 0. 1. *
 2.85725969158E-01   1.00000000000E+00
0 2 1 0. 1. *
 9.05806201973E-02   1.00000000000E+00
0 3 1 0. 1. *
 1.30952322712E+00   1.00000000000E+00
0 3 1 0. 1. *
 6.13241389114E-01   1.00000000000E+00
0 4 1 0. 1. *
 1.13300431880E+00   1.00000000000E+00
99 0
END
DFT
PBE
XLGRID
END
```

```
LDREMO
1
SCFDIR
LEVSHIFT
10 1
FMIXING
30
MAXCYCLES
100
TOLINTEG
8 8 8 8 16
TOLDEE
8
SHRINK
64 64
END
```

6 NaCl - triple ζ

```
NaCl_crystal-TZ-PBE0
CRYSTAL
0 0 0
225
5.6402
2
17 0.0 0.0 0.0
11 0.5 0.5 0.5
END
 11 11
0 0  7  2. 1.
   2.60411099270E+04   6.18063428110E-04
   3.90612685480E+03   4.77486044140E-03
```

```
   8.88974549930E+02   2.44716848290E-02
   2.51454979610E+02   9.47553949770E-02
   8.16501435120E+01   2.68674969200E-01
   2.89041584010E+01   4.79254754400E-01
   1.06257829320E+01   3.32485914690E-01
0 0  3  2. 1.
   5.37694101790E+01   1.95277318720E-02
   1.63082430250E+01   9.26480107940E-02
   2.37303841250E+00  -3.99386701720E-01
0 0  2  1. 1.
   9.57307726030E-01   1.64285953910E+00
   4.08064609590E-01   5.56925969660E-01
0 0  1  0. 1. *
   3.43569978393E-01   9.99992062637E-01
0 0  1  0. 1. *
   8.28104267544E-02   9.99700925116E-01
0 2  5  6. 1.
   1.38079799890E+02   5.79518919290E-03
   3.22327003930E+01   4.16208462510E-02
   9.98160753600E+00   1.62819168850E-01
   3.48220339280E+00   3.60117846470E-01
   1.22991346200E+00   4.48589798890E-01
0 2  1  0. 1. *
   4.02257637589E-01   1.00001437874E+00
0 2  1  0. 1. *
   9.81092534535E-02   1.00010780928E+00
0 3  1  0. 1. *
   2.60738659094E+00   1.00000000000E+00
0 3  1  0. 1. *
   4.03951011422E-01   1.00000000000E+00
0 3  1  0. 1. *
   9.84682729829E-02   1.00000000000E+00
 17 13
```

```
0 0  7  2. 1.
   6.95079909450E+04   5.43148974970E-04
   1.04261568800E+04   4.19904639610E-03
   2.37323340610E+03   2.15921416790E-02
   6.71564200710E+02   8.45988500940E-02
   2.18419997900E+02   2.47572497240E-01
   7.75722497140E+01   4.70169302280E-01
   2.88888152770E+01   3.74363707160E-01
0 0  3  2. 1.
   1.27105271850E+02   2.51821666030E-02
   3.93395829610E+01   1.07861124560E-01
   7.67406799890E+00  -2.74088215740E-01
0 0  2  2. 1.
   3.87456276300E+00   1.32138750140E+00
   1.83858325730E+00   6.86369553680E-01
0 0  1  0. 1. *
   5.72362924707E-01   1.00000000308E+00
0 0  1  0. 1. *
   2.31162823985E-01   9.99999997835E-01
0 2  5  6. 1.
   6.66504232840E+02   2.36326638360E-03
   1.57642416900E+02   1.88793003740E-02
   5.02625209780E+01   8.72063412730E-02
   1.85360781050E+01   2.52856129700E-01
   7.29405327770E+00   4.35071548200E-01
0 2  1  5. 1. *
   2.93863280310E+00   1.00000000143E+00
0 2  1  0. 1. *
   1.19026410565E+00   1.00000000000E+00
0 2  1  0. 1. *
   4.69704038156E-01   1.00000000000E+00
0 2  1  0. 1. *
   1.74720163208E-01   1.00000000000E+00
```

```
0 3  2  0. 1.
   4.61000000000E+00   2.00000000000E-01
   1.01100000000E+00   1.00000000000E+00
0 3  1  0. 1. *
   2.83798017576E-01   1.00000000000E+00
0 4  1  0. 1. *
   6.89848600893E-01   1.00000000000E+00
99 0
END
DFT
PBE0
END
TOLINTEG
8 8 8 8 16
TOLDEE
8
SHRINK
8 8
END
```

7 Na - triple ζ

```
Na_crystal-TZ-PBE0
CRYSTAL
0 0 0
229
4.2906
1
11 0. 0. 0.
END
 11 11
0 0  7  2. 1.
```

```
   2.60411099270E+04   6.18063428110E-04
   3.90612685480E+03   4.77486044140E-03
   8.88974549930E+02   2.44716848290E-02
   2.51454979610E+02   9.47553949770E-02
   8.16501435120E+01   2.68674969200E-01
   2.89041584010E+01   4.79254754400E-01
   1.06257829320E+01   3.32485914690E-01
0 0  3  2. 1.
   5.37694101790E+01   1.95277318720E-02
   1.63082430250E+01   9.26480107940E-02
   2.37303841250E+00  -3.99386701720E-01
0 0  2  1. 1.
   9.57307726030E-01   1.64285953910E+00
   4.08064609590E-01   5.56925969660E-01
0 0  1  0. 1. *
   2.12721167582E-01   9.99992062637E-01
0 0  1  0. 1. *
   7.82096876345E-02   9.99700925116E-01
0 2  5  6. 1.
   1.38079799890E+02   5.79518919290E-03
   3.22327003930E+01   4.16208462510E-02
   9.98160753600E+00   1.62819168850E-01
   3.48220339280E+00   3.60117846470E-01
   1.22991346200E+00   4.48589798890E-01
0 2  1  0. 1. *
   4.03415531731E-01   1.00001437874E+00
0 2  1  0. 1. *
   8.50539333916E-02   1.00010780928E+00
0 3  1  0. 1. *
   2.60862497919E+00   1.00000000000E+00
0 3  1  0. 1. *
   4.33739110192E-01   1.00000000000E+00
0 3  1  0. 1. *
```

```
   1.11542851169E-01   1.00000000000E+00
99 0
END
DFT
PBE0
END
TOLINTEG
8 8 8 8 16
TOLDEE
8
SHRINK
8 8
END
```

8 Cl_2 - triple ζ

```
Cl_crystal-TZ-PBE0
CRYSTAL
0 0 0
64
7.77875 4.34941 9.02754
8
17 0            0.40882      0.89848
17 0            0.09118      0.39848
17 0            0.90882      0.60152
17 0            0.59118      0.10152
17 0.50000      0.90882      0.89848
17 0.50000      0.59118      0.39848
17 0.50000      0.40882      0.60152
17 0.50000      0.09118      0.10152
END
 17 13
```

```
0 0  7  2. 1.
   6.95079909450E+04   5.43148974970E-04
   1.04261568800E+04   4.19904639610E-03
   2.37323340610E+03   2.15921416790E-02
   6.71564200710E+02   8.45988500940E-02
   2.18419997900E+02   2.47572497240E-01
   7.75722497140E+01   4.70169302280E-01
   2.88888152770E+01   3.74363707160E-01
0 0  3  2. 1.
   1.27105271850E+02   2.51821666030E-02
   3.93395829610E+01   1.07861124560E-01
   7.67406799890E+00  -2.74088215740E-01
0 0  2  2. 1.
   3.87456276300E+00   1.32138750140E+00
   1.83858325730E+00   6.86369553680E-01
0 0  1  0. 1.
   5.07498154767E-01   1.00000000308E+00
0 0  1  0. 1.
   1.83127456586E-01   9.99999997835E-01
0 2  5  6. 1.
   6.66504232840E+02   2.36326638360E-03
   1.57642416900E+02   1.88793003740E-02
   5.02625209780E+01   8.72063412730E-02
   1.85360781050E+01   2.52856129700E-01
   7.29405327770E+00   4.35071548200E-01
0 2  1  5. 1.
   2.89826632488E+00   1.00000000143E+00
0 2  1  0. 1.
   1.10442102086E+00   1.00000000000E+00
0 2  1  0. 1.
   4.09232170559E-01   1.00000000000E+00
0 2  1  0. 1.
   1.36452167048E-01   1.00000000000E+00
```

```
0 3  2  0. 1.
   4.61000000000E+00   2.00000000000E-01
   1.01100000000E+00   1.00000000000E+00
0 3  1  0. 1.
   3.32581229403E-01   1.00000000000E+00
0 4  1  0. 1.
   5.98970631104E-01   1.00000000000E+00
99 0
END
DFT
PBE0
END
TOLDEE
8
TOLINTEG
8 8 8 8 16
SHRINK
8 8
END
```

9 LiH - SVP

```
LiH-SVP-HF
CRYSTAL
0 0 0
225
4.084
2
3  0.0  0.0  0.0
1  0.5  0.5  0.5
END
  3  5
```

```
0 0  5  2. 1.
   2.66277855160E+02   6.49201503250E-03
   4.00697834470E+01   4.77478632150E-02
   9.05599443890E+00   2.02687961110E-01
   2.45030090510E+00   4.86065748170E-01
   7.22095718550E-01   4.36269779550E-01
0 0  1  1. 1. *
   9.22176144583E-01   1.00000000000E+00
0 0  1  0. 1. *
   3.26710606911E-01   1.00000000000E+00
0 2  2  0. 1.
   1.45000000000E+00   2.58600000000E-01
   3.00000000000E-01   1.00000000000E+00
0 2  1  0. 1. *
   2.44108651001E-01   1.00000000000E+00
  1  3
0 0  3  1. 1.
   1.30107010000E+01   1.96821580000E-02
   1.96225720000E+00   1.37965240000E-01
   4.44537960000E-01   4.78319350000E-01
0 0  1  0. 1. *
   1.12026126213E-01   1.00000000000E+00
0 2  1  0. 1. *
   7.04259338539E-01   1.00000000000E+00
99 0
END
TOLINTEG
8 8 8 15 30
SHRINK
8 8
FMIXING
50
TOLDEE
```

```
10
END
```

10 LiH - triple ζ

```
LiH-TZ-HF
CRYSTAL
0 0 0
225
4.084
2
3  0.0  0.0  0.0
1  0.5  0.5  0.5
END
  3  8
0 0  6  2. 1.
   6.26926280100E+03   2.05409688260E-04
   9.40316124310E+02   1.59165540890E-03
   2.14221075280E+02   8.28698297070E-03
   6.07598401840E+01   3.38563742490E-02
   1.99151520320E+01   1.11032258760E-01
   7.31715097970E+00   2.74493833290E-01
0 0  2  1. 1.
   2.97246742160E+00   2.37924564110E-01
   1.26398523140E+00   3.07654119240E-01
0 0  1  0. 1. *
   7.80051836987E-01   1.00000000000E+00
0 0  1  0. 1. *
   3.56751423380E-01   1.00000000000E+00
0 0  1  0. 1. *
   1.32441081592E-01   1.00000000000E+00
0 2  1  0. 1. *
```

```
   5.32524694781E-01   1.00000000000E+00
0 2  1  0. 1. *
   1.24297352468E-01   1.00000000000E+00
0 2  1  0. 1. *
   3.32168908872E+00   1.00000000000E+00
  1  4
0 0  3  1. 1.
   3.40613410000E+01   6.02519780000E-03
   5.12357460000E+00   4.50210940000E-02
   1.16466260000E+00   2.01897260000E-01
0 0  1  0. 1. *
   7.93610197287E-01   1.00000000000E+00
0 0  1  0. 1. *
   2.38040797833E-01   1.00000000000E+00
0 2  1  0. 1. *
   7.51152930456E-01   1.00000000000E+00
99 0
END
TOLINTEG
10 10 10 15 30
SHRINK
8 8
FMIXING
50
TOLDEE
10
NOBIPOLA
END
```

11 LiH - quadruple ζ

```
LiH-QZ-HF
```

```
CRYSTAL
0 0 0
225
4.084
2
3  0.0  0.0  0.0
1  0.5  0.5  0.5
LATVEC
100000
END
  1 10
0 0  4  1. 1.
   1.90691690000E+02   7.08151670000E-04
   2.86055320000E+01   5.46788270000E-03
   6.50959430000E+00   2.79666050000E-02
   1.84124550000E+00   1.07645380000E-01
0 0  1  0. 1. *
   6.39685855118E-01   1.00000000000E+00
0 0  1  0. 1. *
   2.72584652976E-01   1.00000000000E+00
0 0  1  0. 1. *
   1.44295727123E-01   1.00000000000E+00
0 2  1  0. 1. *
   2.29203807546E+00   1.00000000000E+00
0 2  1  0. 1. *
   8.37965510305E-01   1.00000000000E+00
0 2  1  0. 1. *
   2.95979305342E-01   1.00000000000E+00
0 3  1  0. 1. *
   2.06195543104E+00   1.00000000000E+00
0 3  1  0. 1. *
   6.61486854173E-01   1.00000000000E+00
0 4  1  0. 1. *
```

```
   1.39686108048E+00   1.00000000000E+00
  3 13
0 0  9  2. 1.
   1.48539770850E+04   4.27113888150E-05
   2.22522364770E+03   3.32353108000E-04
   5.04887390080E+02   1.75184366490E-03
   1.42458475480E+02   7.34779958500E-03
   4.63155995800E+01   2.58998376830E-02
   1.66553354740E+01   7.66706824310E-02
   6.43311861990E+00   1.82760757650E-01
   2.60270438580E+00   3.26554340380E-01
   1.08972454050E+00   3.70004298280E-01
0 0  2  1. 1.
   4.42365959710E+00   1.11209879210E-01
   1.23563949900E+00   7.99873358620E-01
0 0  1  0. 1. *
   1.47258539716E+00   1.00000000000E+00
0 0  1  0. 1. *
   9.61687138188E-01   1.00000000000E+00
0 0  1  0. 1. *
   5.44705804681E-01   1.00000000000E+00
0 0  1  0. 1. *
   2.59775255362E-01   1.00000000000E+00
0 2  3  0. 1.
   3.26051092060E+00   8.65047490230E-03
   6.50030431150E-01   4.76141237360E-02
   1.69416710730E-01   2.10011380000E-01
0 2  1  0. 1. *
   3.83906409071E-01   1.00000000000E+00
0 2  1  0. 1. *
   1.98706020944E-01   1.00000000000E+00
0 2  1  0. 1. *
   3.72683460316E+00   1.00000000000E+00
```

```
0 3  1  0. 1. *
   3.33113752884E-01   1.00000000000E+00
0 3  1  0. 1. *
   3.68482801264E-01   1.00000000000E+00
0 4  1  0. 1. *
   1.75294244744E-01   1.00000000000E+00
99 0
END
TOLINTEG
10 10 10 40 160
SHRINK
12 12
NOBIPOLA
LDREMO
1
FMIXING
96
THREDIIS
2
TOLDEE
10
ILASIZE
20000
END
```

12.2 Key Role of Defects in Thermoelectric Performance of TiMSn (M=Ni, Pd, and Pt) Half-Heusler Alloys-Paper Published

THE JOURNAL OF PHYSICAL CHEMISTRY C

pubs.acs.org/JPCC Article

Key Role of Defects in Thermoelectric Performance of TiMSn (M = Ni, Pd, and Pt) Half-Heusler Alloys

Atreyi Dasmahapatra, Loredana Edith Daga, Antti J. Karttunen, Lorenzo Maschio,* and Silvia Casassa*

Cite This: J. Phys. Chem. C 2020, 124, 14997−15006 Read Online

ACCESS | Metrics & More | Article Recommendations | Supporting Information

ABSTRACT: Half-Heusler alloys are thermoelectric materials that enable direct conversion of waste heat to electricity. A systematic study of these alloys has never been attempted using local Gaussian type orbitals (GTOs) and hybrid density functional theory methods within a periodic approach. In this work, we study the thermoelectric properties of TiMSn (M = Ni, Pd, and Pt) alloys with space group $F\bar{4}3m$ using the CRYSTAL code. We, first, set benchmarks for TiNiSn by comparing our data to existing literature values of Seebeck coefficient, power-factor, and thermoelectric figure-of-merit. Our results agree well. We, then, extend these calculations to TiPdSn and TiPtSn, for which consistent previous data are limited. Our computations show that all TiMSn (M = Ni, Pd, and Pt) alloys prefer p-type carriers and exhibit a figure-of-merit of ≈1 at a chosen carrier concentration and temperature. In addition, we aim to explain the low band-gap of TiNiSn by modeling defects in the pure system. Our defect model proves to have a smaller band-gap, and its power-factor is found to be almost twice of the pure TiNiSn.

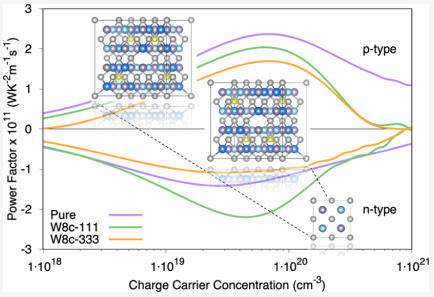

1. INTRODUCTION

The term thermoelectrics (TEs) has sparked huge interest in recent years, as the perspective of turning waste heat into useful electricity grows in the light of renewed attention toward the environment. From electric cars to wearable devices, and thereon up to space exploration, the horizon of reducing energy demands seems to be at hand. Unfortunately, because of their modest efficiency and relatively high cost, currently available devices and materials are not able to deliver this promise.

Compared to other fields of solid-state physics and materials chemistry, the alliance of theoretical modeling, experimental characterization, and synthesis is not prevalent in TEs. Plausible reasons are that for an experimentally synthesized sample, there is a high density of defects (interstitial, substitutional, etc.) that provide a high carrier density. Despite the crystalline nature of the compound, realistic models that integrate these defects are difficult to mimic. Moreover, grain boundaries found in real materials are beneficial to TE properties as they reduce the thermal conductivity of the sample, but these structural defects are also complicated to integrate in a model.

As C. J. Humphreys once quoted: "Crystals are like people: it is the defects in them which tend to make them interesting!".[1] For TEs, this is indeed the case, as the presence of interstitial or substitutional defects not only adds flat bands in the gap but also alters the shape of a large part of the band structure.

Half-Heusler (HH) alloys, intermetallic compounds of the composition ABX, are now actively investigated for their TE performance. These compounds have tunable band gaps which allow the possibility of tailoring TE efficiency and have potential applications in spintronics, solar cells, and data storage.[2−4]

Experimentally, these materials are synthesized using various methods: spark plasma sintering, hot pressing, arc-melting, and microwave-assisted solid-state reactions. These methods are generally followed by prolonged annealing that is targeted to densify the material and heal the sample of defects.[5−8]

On computational side, a recent impetus in the investigation of these alloys is to use machine learning tools to accelerate the discovery of new novel materials.[9−11] The primary focus, however, is doping the parent material to maximize the TE power factor σS^2 and in turn the TE figure of merit ($ZT = S^2\sigma T/k_{total}$, where k_{total} is the material's total thermal conductivity). This approach comes from the general idea that adding impurities (doping or substituting by isoelectronic elements) alters the band gap of the parent material, which in turn enhances the TE properties.[12−17] The changes in the

Received: April 11, 2020
Revised: June 7, 2020
Published: June 22, 2020

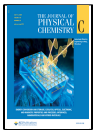

https://dx.doi.org/10.1021/acs.jpcc.0c03243
J. Phys. Chem. C 2020, 124, 14997−15006

atomic bonding in the proximity of the grain boundaries and the consequent covalent bond delocalization can also deeply modify the TEs, thus stimulating the electron transport of the whole system.[18]

In this paper, we investigate three TE compounds, TiNiSn, TiPdSn, and TiPtSn, with the CRYSTAL code,[19] using hybrid density functional methods and basis sets of localized Gaussian orbitals. Such computational setup, if properly tuned, enables the inclusion of exact exchange at a relatively cheap computational cost, allowing for a natural reduction of self-interaction effects. Moreover, it can be more accurate and robust with respect to other density functional theory (DFT) approaches that use Hubbard-U corrected functionals for defects and HH alloys.[20,21] Our work is targeted toward confirming how, contrary to other materials, point defects in HH alloys have a strong impact on the whole band structure and consequently on transport properties. Moreover, we intend to benefit the community that uses Gaussian type orbitals in the study of crystalline materials, by establishing a reliable methodology and providing an integrated tool to compute TE properties within the CRYSTAL code.[22] Among HH alloys, TiNiSn is heralded as a benchmark material and is well investigated in the literature. Thus, naturally, we first compare our data for TiNiSn to the existing literature, validate both the approach and the computational setting, and then extend the same machinery to investigate TiPdSn and TiPtSn.

The paper is arranged as follows: in the following section, the computational setup is described, in particular, the reasoning for our choice of basis-sets and DFT functionals. Results are presented in Section 3, where the variance of the band gap and reproducibility of the band structure depending on the choice of functionals are studied. Thereafter, a discussion of TE properties with appropriate comparison to the existing literature is provided. In the last section, we present a defect model of TiNiSn that shows improved TE performance.

2. METHODS

2.1. Functional and Basis Set. Throughout this work, we apply DFT as implemented in the CRYSTAL code.[19]

While most studies with TEs employ plane-wave based packages and the Perdew−Burke−Ernzerhof (PBE) functional,[23] the local basis in CRYSTAL allows us to introduce a proper amount of 'exact exchange' which is known to improve the accuracy of simulated properties that depend on the extent of electronic delocalization, namely, band gaps, phonon spectra, and magnetic coupling constants.[24]

Nevertheless, atomic basis sets, which allow for an easy use of hybrid functionals, have to be accurately calibrated for periodic systems, and the correct percentage of exact exchange has to be determined.

In order to define a reference setup, which predicts the best compromise of the electronic band gap and lattice parameter for the family of systems under investigation, we perform a comprehensive screening in the choice of the basis sets and on the amount of Hartree−Fock (HF) exchange.

For the basis, we adopt a standard and rather robust procedure to adapt molecular Karlsruhe split-valence polarization basis (def2-SVP) to periodic calculations.[25] A consistent basis set, referred in the following as *P.def2-SVP*, is obtained by cutting off *f* functions, when present, and adjusting the outermost *s* and *p* shells for periodic calculations, also using the BDIIS optimization procedure.[26] For each element included here, the basis set has been used successfully in previous studies. The basis sets and the literature references are reported in Supporting Information.

For the functional, we explore PBE with three different percentages of HF exchange, namely, pure PBE, PBE10 (10% HF exchange) and PBE0 (25% of exact exchange[23,27,28]). On the basis of our results, we resolved to use the hybrid PBE10 for all further computation. It is to be noted here that calculations with PBE are reported for sake of comparison with literature results.

2.2. Computational Parameters. The DFT exchange−correlation contribution is evaluated by numerical integration over the unit cell volume, using a pruned grid with 75 radial and 974 angular points. Integration over the reciprocal space is carried out using Monkhorst−Pack meshes of 8 × 8 × 8. The Coulomb and exchange series, summed in direct space, are truncated using overlap criteria thresholds of [8, 8, 8, 8, 16]. Convergence for the self-consistent field algorithm is achieved up to a threshold of 10^{-9} hartree on the total energy, per unit cell.[29]

Geometry optimization is performed using analytical gradients with respect to atomic coordinates and unit−cell parameters, within a quasi-Newtonian scheme combined with Broyden−Fletcher−Goldfarb−Shanno Hessian updating.[30,31] The default convergence criteria are adopted for both gradient components and nuclear displacements. A full set of vibrational frequencies in Γ is obtained within the harmonic approximation by diagonalizing the mass-weighted Hessian matrix. This matrix is built by numerically differencing the analytical gradient with respect to atomic Cartesian coordinates. The zero-point energy (ZPE) and the thermal contributions to the vibrational energy (E_{vib}) and entropy (S_{vib}) are calculated by considering the vibrational spectrum in Γ and then added to the SCF energy and the pressure x volume term to get all the thermodynamic potential, that is, enthalpy and Gibbs free energy, at any given temperature.

TE properties such as Seebeck coefficient (S) electrical conductivity (σ) and electron contribution to the thermal conductivity (k_{el}) are computed by using the semi-classical Boltzmann transport equation theory and the frozen band approximation, as recently implemented by Sansone et al. in CYRSTAL.[22] We also assume constant relaxation time approximation for carriers and fix it at 10 fs (1×10^{-14} s) for all systems and temperatures. A dense mesh of up to 4000 *k*-points is used in the first Brillouin zone for the calculation of TE parameters. Our computations do not include the effect of spin−orbit coupling as this feature is yet to be implemented in the CRYSTAL code.

Thus, we do our computations within the regime of the CRYSTAL code, using carefully screened localized Gaussian type orbitals and hybrid DFT functionals to describe the chemistry of the HH alloys. Once a reliable computational setting is achieved, features of the code which can then be exploited are (i) calculation of the TE parameters for different carrier-concentrations, at various temperatures and at low computational cost; (ii) chemical insight into the electronic structure because of the atomic nature of the basis set; and (iii) modeling of low concentration of point defects using a supercell approach.

3. RESULTS AND DISCUSSION

3.1. Defect-Free Crystal Structure. The HH pure-phase crystallizes in a MgAgAs-type structure with space group $F\bar{4}3m$

https://dx.doi.org/10.1021/acs.jpcc.0c03243
J. Phys. Chem. C 2020, 124, 14997−15006

(#216). Similar to other ternary HH alloys, Sn, Ni/Pt/Pd, and Ti atoms occupy fused face-centered cubic sublattices at Wyckoff positions of 4*b* [1/4, 1/4, 1/4], 4*c* [1/2, 1/2, 1/2], and 4*a* [0, 0, 0], respectively. A representative model is shown in Figure 1.

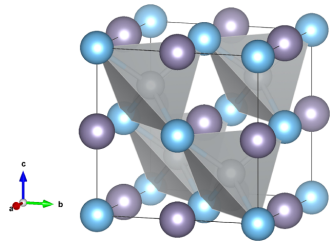

Figure 1. HH structure of TiMSn (M = Ni, Pt, and Pd) alloy with cubic symmetry and space group $F\bar{4}3m$ (#216). Blue spheres are Ti atoms, grey spheres in polyhedra are Ni, Pd, and Pt (for each case), and purple spheres are Sn atoms.

Structural parameters and electron band gap, calculated at the PBE10/*P.def2-SVP* level, are collected in Table 1. The equilibrium Bulk modulus, B_0, elastic constants, c_{11}, c_{12}, c_{44}, Poisson ratio, ν, and Young's modulus, Y, are obtained with CRYSTAL by solving the third-order Birch–Murnaghan isothermal equation of state.[32]

For the lattice parameter, **a**, our finding for TiNiSn deviates from an experiment value of a negligible 0.2%,[33,34] whereas TiPdSn and TiPtSn values are in accordance to those in refs 9 and 35, respectively. Band gaps will be discussed in the next section.

In the case of TiNiSn, the elastic properties are reproduced accurately even though our perfect crystal model is not completely consistent with realistic experimental samples, where local and structural defects are always present. Hence, a good agreement is achieved for Young's modulus, but significant discrepancies are observed for B_0 and the elastic constants.

In the absence of experimental data for TiPdSn and TiPtSn alloys, we compared our calculations with results obtained with a plane-wave approach reported by Kaur[35] and Roy et al.,[36] respectively. As shown in Table 1, the agreement for TiPdNi's B_0 and TiPtSn's c_{44} elastic constant is excellent.

3.2. Defect-Free Electronic Band Structure. For a complete discussion of TE properties of HH compounds, a correct description of the electronic band structure of the material is essential. In Figure 2, we show the band structures of all three ternary compounds computed at the PBE10/*P.def2-SVP* level.

As expected, each compound has an indirect band gap, between the valence-band maximum at the Γ-point and the conduction-band minimum at **X**-point. The percentage of exact exchange in the functionals does affect the numerical value of the band gap. For instance, for TiNiSn, the band-gap varies from 0.48 eV (PBE) to 0.69 eV (PBE10) and finally to 0.98 eV (PBE0). Nevertheless, none of the functionals produce the band gap as low as the experimentally measured value of 0.12 eV.[37] We discuss this anomaly in detail in the following.

For TiPdSn, our computed band gap is 0.76 eV (0.47 eV with PBE) which matches with previous calculations done using the range-separated hybrid HSE06 functionals.[9] TiPtSn has the highest band gap of the three alloys at 1.13 eV (0.72, PBE) which is ≈10% less than the literature value obtained with the HSE06 functional.[9]

For the band structure, the primary difference between the three compounds is at the **X**-point. Going from Ni–Pd–Pt, the splitting between the two lowest energy conduction bands reduces, increasing the band gap. These bands have a pudding mold-like character, which is more pronounced in the case of TiNiSn.

The projected density of states (PDOS) on the atomic orbitals of each element can enlighten more on this important effect. The lowest virtual states of TiNiSn, panel (a) of Figure 3, result as a combination of Ni–Ti AOs and are slightly closer to the Fermi level with respect to the analogous Pd/Pt–Ti states in the other two alloys. This is the primary reason behind why the electronic band gap increases as we go from TiNiSn to TiPtSn because the Sn contribution in the Fermi region is almost negligible for all three compounds.

3.3. Defect-Free TE Properties. We now discuss the Seebeck coefficient (S), the electrical conductivity (σ), and the power factor with respect to the relaxation time (PF = $S^2\sigma/\tau$) for these HH alloys. Because TE materials have high temperature applications, we also present the dependence of these parameters at temperatures, from 300 to 1000 K. We first compute TE properties of TiNiSn and compare it with existing literature, both from computational and experimental studies, to establish a benchmark. Later, we extend the same calculations to TiPdSn and TiPtSn, on which computational data are sparse.

Figure 4 compares S and power-factor for TiNiSn with change in charge carrier concentration (n_c) for both p and n-type carriers adopting the PBE and PBE10 functionals. At low n_c, the Seebeck coefficient differs slightly between PBE and PBE10, but as n_c increases, S quickly converges. For higher temperatures (not shown here) difference between S is almost

Table 1. PBE10/*P.def2-SVP* Results for Three HH Alloys[a]

alloy	*a*	gap	B_0	c_{11}	c_{12}	c_{44}	ν	Y
TiNiSn	5.91	0.69	137.94	235.53	89.98	60.97	0.296	169.62
Ref.	5.92[b]	0.12[c]	124.90[d]	214.90[d]	79.90[d]	67.50[d]	0.271[d]	171.6[d]
TiPdSn	6.17	0.76	131.21	184.96	105.27	58.97	0.330	134.11
Ref.	6.23[e,f]	0.74[e]	135.90[f]					
TiPtSn	6.22	1.13	146.02	206.96	116.85	65.89	0.329	150.42
Ref.	6.25[e]	1.31[e]	67.00[g]					

[a]Lattice parameter **a** in Å. Indirect electronic band gap in eV. Bulk modulus, B_0, elastic contants, c_{11}, c_{12}, c_{44}, Young's modulus, Y, in GPa and Poisson ratio, ν. Literature date ara reported when available. [b]Ref 34, (EXP). [c]Ref 37, (EXP). [d]Ref 38, (EXP). [e]Ref 9, (THEO). [f]Ref 35, (THEO). [g]Ref 36, (THEO).

https://dx.doi.org/10.1021/acs.jpcc.0c03243
J. Phys. Chem. C 2020, 124, 14997–15006

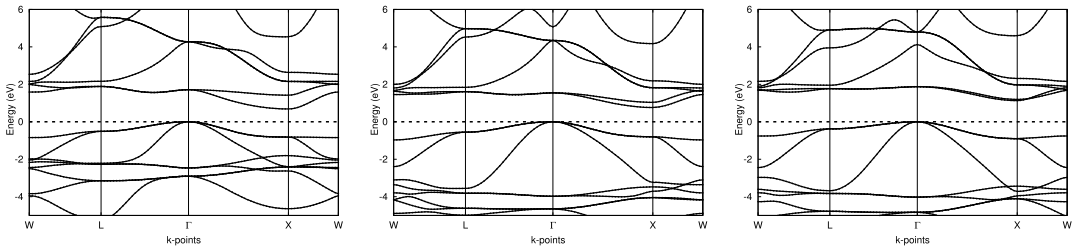

Figure 2. Computed electronic band structures for (a) TiNiSn, (b) TiPdSn, and (c) TiPtSn at the PBE10/*P.def2-SVP* level. Indirect band gaps are 0.69, 0.76, and 1.13 eV (from left to right) between the Γ and **X** point. Dotted line corresponds to the Fermi energy.

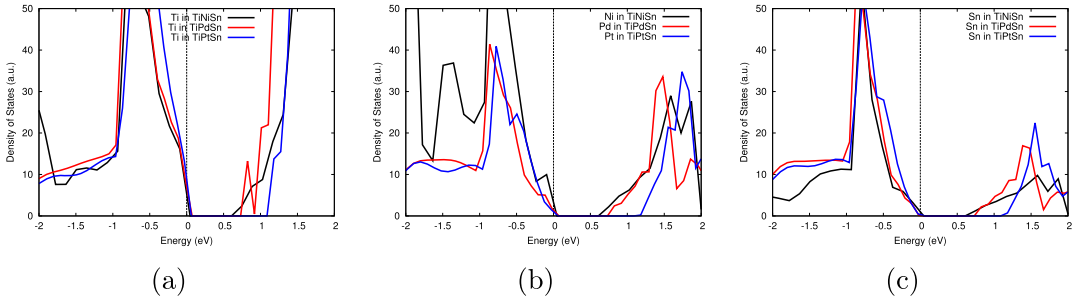

Figure 3. Computed PDOS on the atomic orbitals of (a) Ti, (b) Ni/Pd/Pt, and (c) Sn, at the PBE10/*P.def2-SVP* level. Dotted line corresponds to the Fermi energy.

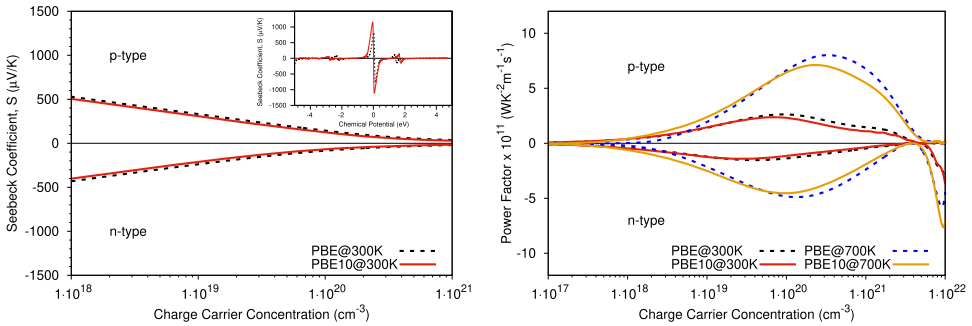

Figure 4. (left) Seebeck coefficient for TiNiSn obtained with PBE10 (solid line, red) and PBE (dotted line, black) for both p-type and n-type doping plotted against carrier concentration at 300 K. Inset: Variance of Seebeck coefficient with change in chemical potential (μ), in eV. (right) Power-factor (PF, $S^2\sigma/\tau$) with respect to relaxation time (τ) of carriers, for p-type and n-type doping with change in n_c at T = 300 K (solid line, red: PBE10 and dotted line, black: PBE) and T = 700 K (solid line, orange: PBE10 and dotted line, blue: PBE). The *x*-axis for the figure on the right is extended to 1×10^{17} for ease of comparison between the functionals. S and PF with n-carriers are plotted on the negative axis for clarity.

negligible. On the contrary, PF is lightly more sensitive to HF percentage at high n_c values, but its main features are the same with the two functionals.

Overall, our computations match the general trend of large Seebeck values for TiNiSn and provide good agreement with existing literature at specified charge carrier concentrations.

In particular, the highest reported value of S for TiNiSn found through computational and experimental studies in literature is ≈−250 μV/K, which we achieve for $n_c \sim 1 \times 10^{19}$ cm^{-3}.[39−41] Scanning at the lower carrier concentration ranges of $n_c \sim 1 \times 10^{18}$ cm^{-3}, we have $S = -400$ μV/K, which corresponds to the work done by Zilber et al.,[42] who reported a value of $S = -425 \pm 50$ μV/K with $n_c \sim 7 \times 10^{18}$ cm^{-3}.

The power-factor dependency on temperature is correctly reproduced because it increases from ≈2 to ≈7 W/ms K^2 × 10^{11} as the temperature increases from 300 to 700 K, in agreement with the results reported by Wang et al.[43]

At 300 K, the maximum value of PF for p-type carriers is 2.2 W/m K^2 × 10^{11} corresponding to $n_c \sim 1 \times 10^{20}$ cm^{-3} and S = +124 μV/K, while for n-type, the highest power-factor is 1.2 W/m K^2 × 10^{11}, with $S = -103$ μV/K, achieved when $n_c \sim 5 \times 10^{19}$ cm^{-3}.

https://dx.doi.org/10.1021/acs.jpcc.0c03243
J. Phys. Chem. C 2020, 124, 14997−15006

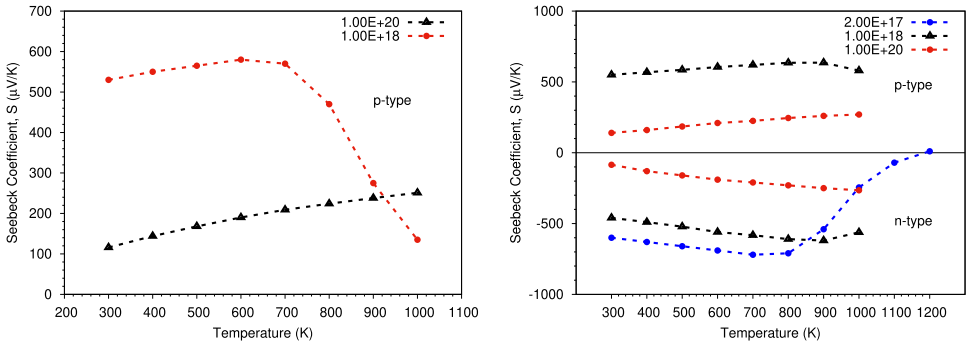

Figure 5. Temperature dependence of Seebeck coefficient. (left) TiPdSn, $n_c = 1 \times 10^{18}$ (red circles) and $n_c = 1 \times 10^{20}$ (black triangles) cm^{-3} for p-type doping. (right) TiPtSn, $n_c = 2 \times 10^{17}$, $n_c = 1 \times 10^{18}$ and $n_c = 1 \times 10^{20}$ cm^{-3} for both p and n-type doping. Calculations performed at the PBE10/*P.def2-SVP* level.

Our computations suggest that p-type doping results in higher TE efficiency in TiNiSn and this is particularly evident at $n_c \sim 1 \times 10^{19}$ cm^{-3}, where PF for p-type is almost double than for n-type, right panel of Figure 4. For most experimental data, TiNiSn is recognized to favor n-type doping. However, as Zilber et al. propose, the electron donor levels arising from grain boundaries in polycrystalline TiNiSn samples can be reduced to single-crystals to attain the p-type TiNiSn TE.[42]

Convinced that our methodology to compute TE parameters yields satisfactory results for HH compounds, we now extend the same setup for the study of TiPdSn and TiPtSn. As mentioned earlier, for these compounds, reliable computational or experimental studies are limited.

In Figure 5, we plot variation of Seebeck coefficient for TiPdSn with temperatures at two values of $n_c \sim 1 \times 10^{18}$ and $n_c \sim 1 \times 10^{20}$ cm^{-3} (left) and for TiPtSn at $n_c \sim 2 \times 10^{17}$, 1×10^{18} and 1×10^{20} cm^{-3} (right).

Maximum power factor in both cases is achieved considering p-type carriers, see Table 2, at $n_c \sim 1 \times 10^{20}$ cm^{-3}.

However, for TiPdSn at 300 K, our value of $S = +116$ μV/K is half of the value suggested by Kaur ($S = +320$ μV/K).[35] We believe that this discrepancy arises from the different lifetime adopted in ref 35 that is 30 times larger compared to our current work. As regards the dependence on temperature of the Seebeck coefficient, the trend change as a function of the carrier concentration, that is, for $n_c \sim 1 \times 10^{18}$ cm^{-3} S, exhibits an increasing with temperature until 700 K and then a steep decrease until 1000 K, whereas at higher n_c (black curve of the left panel, Figure 5), S monotonously rises on increasing the temperature.

In the case of TiPtSn, work reported by Kimura et al.[44] determined the alloy to have an n-type behavior. However, our highest value of the PF graph is for a p-type kind of TE. Thus, we include both p and n transport while reporting the data. With change in temperature, the Seebeck coefficient of TiPtSn shows an increasing trend for p-type and a decreasing trend for n-type carrier, irrespective of the carrier concentration, right panel of Figure 5. At ambient conditions and $n_c \sim 1 \times 10^{20}$, S for p and n carriers is computed to be +140 μV/K and −85 μV/K, respectively, values which are significantly different from the one reported by Kimura et al.,[44] who reported an $S = -500$ μV/K at 300 K and presumably at $n_c \sim 1 \times 10^{22}$ cm^{-3}. If we investigate low carrier concentration, $n_c \sim 1 \times 10^{18}$ cm^{-3}, we find a n-type Seebeck value of −460 μV/K. Furthermore, similar to ref 44, we also notice the transition to p-type behavior at 1200 K (≈1100 K for Kimura et al.) for $n_c \sim 2 \times 10^{17}$ cm^{-3}. However, this is quite unrealistic as low concentration corresponds to a chemical potential of 5−6 eV which is far below the Fermi level of this system.

Table 2. p-Type; Dimensionless TE figure of merit, *ZT*, Evaluated for TiMSn, (M = Ni , Pd, and Pt) Alloys for Specified Carrier Concentration and Temperature[a]

alloy	n (cm^{-3})	T (K)	PF/τ (W/m K^2 × 10^{11})	ZT
TiNiSn	1×10^{18}	300	0.40	0.03
		600	0.50	0.05
	1×10^{19}	300	1.4	0.11
		700	2.4	0.28
	1×10^{20}	300	2.2	0.17
		700	6.4	0.75
TiPdSn	1×10^{18}	300	0.34	0.02
		700	0.45	0.05
	1×10^{19}	300	1.38	0.06
		700	2.20	0.20
	1×10^{20}	300	2.00	0.08
		700	5.80	0.34
TiPtSn	2×10^{17}	300	0.11	0.01
		800	0.14	0.02
	1×10^{18}	300	0.34	0.02
		900	0.52	0.07
	1×10^{20}	300	3.00	0.12
		1000	9.10	0.52

[a]The lattice thermal conductivity k_{ph} is 6 W m^{-1} K^{-1} from refs 37 and 44 and ref 42 for the three systems, respectively, while k_{el} is from our computed data. Relaxation time is fixed at $\tau = 1 \times 10^{-14}$ s or 10 fs.

With our calculated power factors, we can estimate the dimensionless figure of merit for these family of alloys. The figure of merit is described as $ZT = S^2\sigma T/k_{total}$, where k_{total} is the total thermal conductivity, sum of the electronic (el) and phononic (ph) contributions and T is temperature in kelvin. Assuming the phononic thermal conductivity from literature data and using our own calculations for k_{el}, we calculate ZT in chosen carrier concentrations, for p and n-type TEs, respectively, Tables 2 and 3.

The total thermal conductivity of TiNiSn is 4−6 W m^{-1} K^{-1} for 300−700 K taken from experimental measurements as in ref 45. At our peak carrier concentration $n \sim 1 \times 10^{20}$ cm^{-3},

https://dx.doi.org/10.1021/acs.jpcc.0c03243
J. Phys. Chem. C 2020, 124, 14997−15006

Table 3. n-Type; Dimensionless TE Figure of Merit, ZT, Evaluated for TiMSn, (M = Ni, Pd, and Pt) Alloys for Specified Carrier Concentration and Temperature[a]

alloy	n (cm^{-3})	T (K)	PF/τ (W/m K^2 × 10^{11})	ZT
TiNiSn	1×10^{18}	300	0.45	0.03
		600	0.62	0.06
	1×10^{19}	300	1.2	0.09
		700	2.5	0.29
	1×10^{20}	300	1.0	0.08
		700	4.3	0.50
TiPtSn	2×10^{17}	300	0.16	0.01
		800	0.17	0.02
	1×10^{18}	300	0.50	0.02
		700	0.57	0.06
	1×10^{20}	300	1.10	0.04
		900	7.50	0.71

[a]The lattice thermal conductivity k_{ph} is 6 W m^{-1} K^{-1} from refs 37 and 44 and ref 42 for the three systems, respectively, while k_{el} is from our computed data. Relaxation time is fixed at $\tau = 1 \times 10^{-14}$ s or 10 fs.

assuming k_{total} = 6 W m^{-1} K^{-1}, we obtain a ZT of 0.75, which indicates that TiNiSn is likely to be a good p-type TE at 700 K. Assuming an n-type behavior at the same n concentration and T, we arrive at a ZT of 0.50, which is in agreement with most values from literature.[14,46,47]

For TiPdSn, only p-type transport is reported. The highest ZT is 0.34 at $n \sim 1 \times 10^{20}$ cm^{-3} and T = 700 K. This value is not in agreement with ref 35 who report the highest ZT value of 0.74 at 500 K, and discrepancies can possibly be ascribed to a difference in the value of computed band gap in addition to the different value of τ, as already mentioned.

For TiPtSn, similar to that reported by Kimura et al.,[44] we have low values of ZT, irrespective of the T, for $n_c < 1 \times 10^{18}$ cm^{-3}, and then, as n_c rises up to 1×10^{20} cm^{-3}, ZT reaches a maximum value of 0.71 at 900 K.

Summarizing, our calculations confirm large power factors for all three compounds. It is well known that using techniques such as the phonon glass electron crystal, it is possible to moderate the k_{total} and hence increase their ZT and consequently enhance their TE performance.[48,49]

3.4. Modeling Defects in TiNiSn. In this section, we address the disparity in the experimentally measured and computationally attained band gap for TiNiSn HH alloy. While the experimental band gap is at 0.12 eV,[37] this value was never reproduced in computational studies, irrespective of the computational method or DFT functional used.[13,43]

In our work, we compute a band gap of 0.48 eV with PBE functional that is still four times larger than the experimental one. However, there is the possibility that real materials, which contain defects, may have localized states in the density of states (DOS) that lead to a significant decrease in the band gap. This approach, which may explain the discrepancy between DFT and experimentally measured energy gap, was proposed and successfully tested by several authors.[13−15,17] In particular, Colinet et al.[13] and Jund and Berche[14] computed a sensitive drop of the band gap when an interstitial Ni was introduced in the pure HH TiNiSn, and in a recent publication, Kirievsky et al.[17] reproduced the same effect modeling, among the others, composition conserving defects.

We adopted an analogous approach by studying two anti-site composition conserving Ni defects in a 2 × 2 × 2 super-cell of the primitive HH cell (24 atoms) at the PBE10/*P.def2-SVP* level. These defects, which preserve the symmetry of the $F\bar{4}3m$ space group, have the lowest formation energy among those calculated,[17] and it can therefore be assumed that they are quite widespread in the experimental samples.

Thus, a single Ni atom is removed from its HH position [−3/8, 1/8, 1/8] and inserted in one of the two vacant Wyckoff positions 8*c* with fractional coordinates [3/4, 3/4, 3/4] and [1/4, 1/4, 1/4], respectively, obtaining two defect models *W8c-333* and *W8c-111*. Both these sites are occupied in the full-Heusler (FH) $TiNi_2Sn$ crystal structure; thus, essentially, we have only displaced a Ni from its original HH site to a FH site, as can be seen in Figure 1 of Supporting Information.

The formation energy of the defects, ΔE_f, is evaluated according to equation

$$\Delta E_f = E_{el}^{defect} - E_{el}^{perfect} \quad (1)$$

where E_{el} is the electronic energy/per atom of the perfect ordered stoichiometric compound and of the *W8c-333*/*W8c-111* systems. If the atoms in the supercell are not relaxed, we obtain ΔE_f in the order of 0.6 eV, very close to those computed by other authors for similar defects in HH alloys. In particular, Colinet et al.[13] calculated a formation enthalpy at a PBE level (ignoring the much smaller zero-vibration contribution) of 0.77 eV for an interstitial Ni in a 96 atoms supercell of TiNiSn. However, if all the atoms in the supercell are allowed to relax, the formation energies drop off and the two defective structures, *W8c-333* and *W8c-111*, become only 0.081 V and 0.066 eV less stable than the perfect HH.

Formation enthalpies at 0 K, $\Delta H(0)$, which take into account the zero-point vibrational contribution, and Gibbs free energies of formation at room temperature, $\Delta G(298)$, accounting for the thermal phonon terms, are reported in Table 4. As already stated by others,[13,17] all these contributions do not change significantly the magnitude of the formation energies for these defects that remain very low.

Structure relaxation yields to small but significant differences in the electronic structure and in the atomic coordination patterns.

In agreement with the already mentioned results, we observe a narrowing in the band gaps which decrease to 0.187 eV in *W8c-333* and 0.261 eV in *W8c-111*, see Figure 1 in Supporting

Table 4. PBE10/*P.def2-SVP* Results for Defect Models[a]

alloy	a	gap	$\Delta H(0)$	$\Delta G(298)$	B_0	c_{11}	c_{12}	c_{44}	ν	Y
$TiNiSn_{2\times2\times2}$	8.36	0.69			138.02	235.58	90.19	60.67	0.297	169.15
W8c-333	8.35	0.19	0.078	0.070	133.48	194.63	104.83	44.51	0.351	120.67
W8c-111	8.34	0.26	0.064	0.060	133.84	205.21	99.10	59.45	0.315	149.38

[a]Lattice parameter **a** in Å. Indirect electronic band gap in eV. Δ, evaluated according to eq 1, are in eV per atom. Enthalpy and Gibbs free energy are defined as follows: $H(0) = E_{el}$ + ZPE + PV; $G(298) = E_{el}$ + ZPE + $E(T)_{vib}$ + PV − TS_{vib}. Frequencies are computed at Γ point only. Bulk modulus, B_0, elastic constants, c_{11}, c_{12}, c_{44}, Young's modulus, Y, in GPa and Poisson ratio, ν.

https://dx.doi.org/10.1021/acs.jpcc.0c03243
J. Phys. Chem. C 2020, 124, 14997−15006

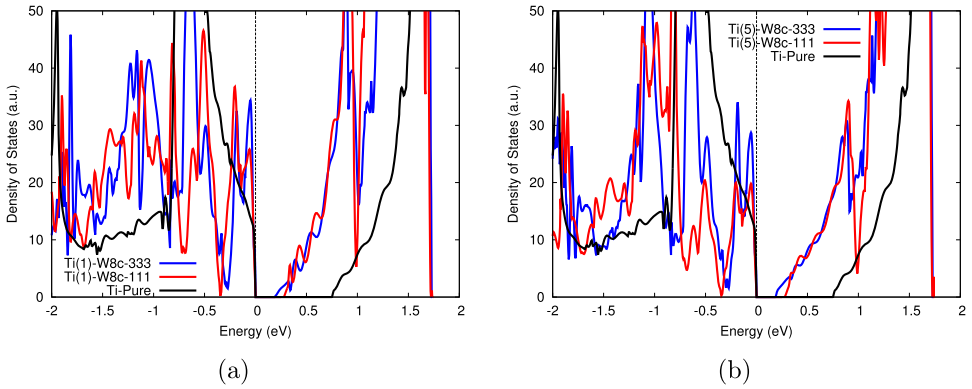

Figure 6. PDOS on the defect TiNiSn alloys; (a) on Ti(1); (b) on Ti(5).

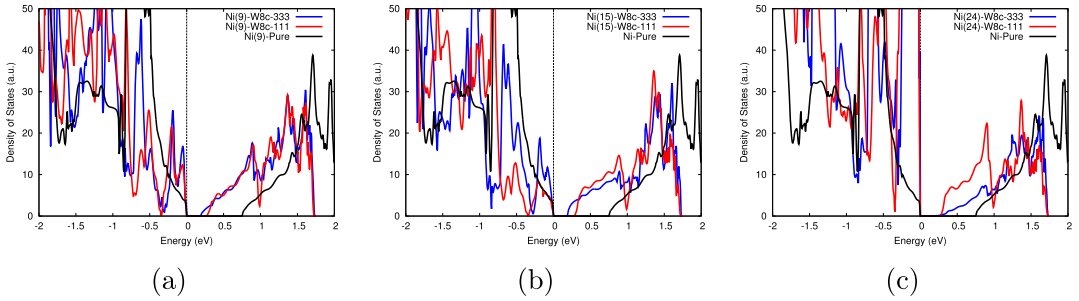

Figure 7. PDOS on the defect TiNiSn alloys; (a) on Ni(9); (b) on Ni(15); and (c) on Ni(24) the displaced atom.

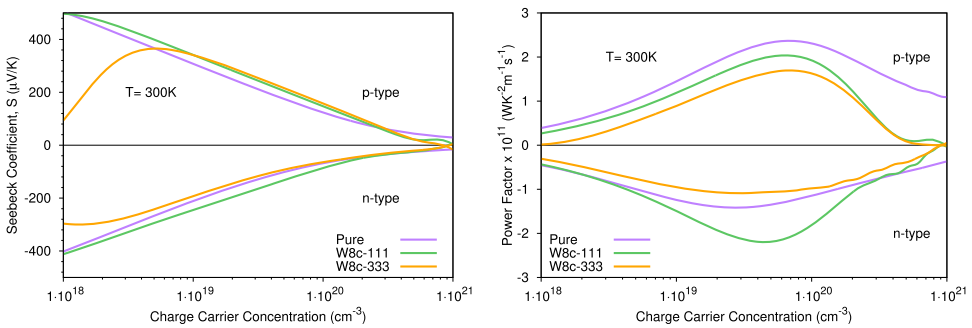

Figure 8. Seebeck coefficient, *S*, and power factor, PF, for perfect TiNiSn, *W8c-333* and *W8c-111* at T = 300 K, as a function of the charge carrier concentration, n_c. PF with n-carriers is plotted on the negative axis for clarity.

Information. The antisite Ni atom leads to a localized level in the vicinity of the Fermi level. In particular, the PDOS reveal the presence of Ti−Ni virtual states within the "forbidden region" of the perfect system, see Figures 6 and 7. The projections onto the AOs of Ti(1)/Ti(5) and Ni(9)/Ni(15) present rather similar features in *W8c-111* and *W8c-333* with a net drop of the lowest virtual states with respect to HH TiNiSn. It is worth to mention that the Ni(24) contribution to the lowest unoccupied bands differentiates the two defect systems as it is significantly more pronounced in *W8c-111* than in *W8c-333*, panel (c) of Figure 7. This difference can account for the different values in some of the TE parameters calculated for the two defect models, as will be shown and discussed in the following.

As the Ni atom is displaced from its HH to a FH position, symmetry related atoms within the 2 × 2 × 2 supercell are no longer equivalent on the basis of different coordination patterns. For example, in *W8c-111*, Ti(1) and Ti(5) have 3 and 5 Ni atoms in the first neighboring shell. while in *W8c-333* Ti(1) and Ti(5), both have four Ni as first neighbors (refer to Tables S1 and S2 of Supporting Information for the adopted notation). Similar behavior is noted for Sn atoms. Interesting

https://dx.doi.org/10.1021/acs.jpcc.0c03243
J. Phys. Chem. C 2020, 124, 14997−15006

enough, after the geometry optimization, both the defect alloys exhibit Ti(1) with three Ni, at a distance of ≈2.57, and the Ti(5) surrounded by five Ni atoms, including the displaced Ni(24). It seems that atomic rearrangement within the supercell is driven by the defective Ni which tends to restore its 4-Ti ⊕ 4-Sn octahedral coordination.

Hirshfield charges, collected in Table S2 of Supporting Information, confirm the loss of chemical equivalence among the atoms in the 2 × 2 × 2 defective supercells and sensitive differences among the two models. For *W8c-111*, the increase in Ti(1) atomic charge is particularly evident and is partially compensated by the charge lost by the displaced Ni(24).

Finally, we compare the Seebeck coefficients of the defect models with respect to the pure HH, Figure 8 right panel. At $n_c = 1 \times 10^{19}$ cm^{-3}, the absolute value of *S* for *W8c-333* is considerably lower than the pure HH or *W8c-111*. When considering only p-type carriers, between $n_c = 1 \times 10^{19}$ and $n_c = 1 \times 10^{20}$ cm^{-3}, the Seebeck coefficient for both defect systems becomes slightly higher than that of the perfect HH. For n-type carriers, *W8c-111* has the highest *S* in the aforementioned range and converges to the same value as the pure HH only at high n_c values of 1×10^{21} cm^{-3}.

In the right panel of Figure 8, we compare the PF of the perfect TiNiSn and the defect systems. *W8c-111* has a power factor almost twice that of the pure system at $n_c \sim 5 \times 10^{19}$ cm^{-3}, for n-type carriers. The electronic contribution to thermal conductivity for this defect system at 300 K is 0.10 W m^{-1} K^{-1}, which is slightly lower than that of the pure TiNiSn (0.15 W m^{-1} K^{-1}). This could explain the enhanced TE properties of *W8c-111* when n-type carriers are considered, and it is consistent with the peculiar antivacant Ni states calculated for this model, see Figure 7.

Hence, by modeling composition conserving Ni defects in TiNiSn, we are able to reproduce rather accurately the expected electronic and TE properties of TiNiSn.

4. CONCLUSIONS

In this work, we used the CRYSTAL code to perform a thorough investigation of the geometry, electronic band structure, and TE properties of three HH alloys: TiNiSn, TiPdSn, and TiPtSn. We described each of these compounds using localized Gaussians and the global hybrid DFT functional PBE10 with 10% HF exchange. Lattice parameters and electronic band structures are correctly reproduced with agreeable band gaps. Next, we computed TE properties—Seebeck coefficient, electrical conductivity, and electronic contribution to the total thermal conductivity within CRYSTAL using a set of basis adapted from the *def2-SVP* and calibrated for periodic calculations.

In TiNiSn, p-type doping shows higher *ZT* as often noticed in computational studies and in contrast to experimental evidence. Moreover, considering the experimental trend of n-type behavior, we were able to reproduce recognized values of the TE figure of merit. For TiPdSn and TiPtSn, we predicted both alloys to favor p-type transport in their pure single-crystal form and have high room temperature values of power factor at carrier concentrations $c_n \sim 1 \times 10^{19}$ and $c_n \sim 1 \times 10^{20}$ cm^{-3}, respectively. Thus, if the lattice thermal conductivity is carefully controlled, the figure of- merit is expected to be high. Last, we presented two defect TiNiSn models which we believe are a better description of the real material. These defect models feature a Ni atom displaced from its original HH crystallographic site to a vacant FH site. Differences in the system response to Ni occupying different interstitial sites were found, which were not expected from pure symmetry considerations. Such differences are seen in the band gap, defect formation free energy, and Seebeck coefficients. The power factor of the defect model *W8c-111* prefers n-type carriers and displays almost twice the value for the same without defects. Thus, we were able to systematically reduce the band gap and increase the power-factor for TiNiSn using a more realistic model. The presence of defects is usually not an undesired feature in TEs because it leads to increased phonon scatterings—which in turn lowers the thermal conductivity of the material—thus increasing the *ZT* value.

■ ASSOCIATED CONTENT

Supporting Information

The Supporting Information is available free of charge at https://pubs.acs.org/doi/10.1021/acs.jpcc.0c03243.

Basis set used for the calculations and further details about the defective models (PDF)

■ AUTHOR INFORMATION

Corresponding Authors

Lorenzo Maschio − *Dipartimento di Chimica, Università di Torino, Turin 10125, Italy;* orcid.org/0000-0002-4657-9439; Email: lorenzo.maschio@unito.it

Silvia Casassa − *Dipartimento di Chimica, Università di Torino, Turin 10125, Italy;* orcid.org/0000-0003-0217-4920; Email: silvia.casassa@unito.it

Authors

Atreyi Dasmahapatra − *Dipartimento di Chimica, Università di Torino, Turin 10125, Italy*

Loredana Edith Daga − *Dipartimento di Chimica, Università di Torino, Turin 10125, Italy*

Antti J. Karttunen − *Department of Chemistry and Materials Science, Aalto University, Espoo 02150, Finland;* orcid.org/0000-0003-4187-5447

Complete contact information is available at: https://pubs.acs.org/10.1021/acs.jpcc.0c03243

Notes

The authors declare no competing financial interest.

■ ACKNOWLEDGMENTS

The work has been performed under the Project HPC-EUROPA3 (INFRAIA-2016-1-730897) with the support of the EC Research Innovation Action under the H2020 Programme. A.J.K. also thanks Academy of Finland for funding (grant no. 317273) and CSC, the Finnish IT Center for Science, for computational resources. A.D., L.E.D., S.C. and L.M. thank University of Turin and Compagnia di Sanpaolo for financial support (project no. CSTO162398).

■ REFERENCES

(1) *Introduction to Analytical Electron Microscopy*; Hren, J. J. J. D., Goldstein, J. I., Eds.; Springer: Boston (MA), 1979.

(2) Xiao, D.; Yao, Y.; Feng, W.; Wen, J.; Zhu, W.; Chen, X.; Stocks, G.; Zhang, Z. Half-Heusler Compounds as a New Class of Three-Dimensional Topological Insulators. *Phys. Rev. Lett.* **2010**, *105*, 096404.

(3) Lin, H.; Wray, L. A.; Xia, Y.; Xu, S.; Jia, S.; Cava, R. J.; Bansil, A.; Hasan, M. Z. Half-Heusler ternary compounds as new multifunctional

experimental platforms for topological quantum phenomena. *Nat. Mater.* **2010**, *9*, 546.
(4) Shi, X.; Chen, L.; Uher, C. Recent advances in high-performance bulk thermoelectric materials. *Int. Mater. Rev.* **2016**, *61*, 379−415.
(5) Birkel, C. S.; Zeier, W. G.; Douglas, J. E.; Lettiere, B. R.; Mills, C. E.; Seward, G.; Birkel, A.; Snedaker, M. L.; Zhang, Y.; Snyder, G. J.; Pollock, T. M.; Seshadri, R.; Stucky, G. D. Rapid Microwave Preparation of Thermoelectric TiNiSn and TiCoSb Half-Heusler Compounds. *Chem. Mater.* **2012**, *24*, 2558−2565.
(6) Jung, D.-y.; Kurosaki, K.; Kim, C.-e.; Muta, H.; Yamanaka, S. Thermal expansion and melting temperature of the half-Heusler compounds: MNiSn (M = Ti, Zr, Hf). *J. Alloys Compd.* **2010**, *489*, 328−331.
(7) Gelbstein, Y.; Tal, N.; Yarmek, A.; Rosenberg, Y.; Dariel, M. P.; Ouardi, S.; Balke, B.; Felser, C.; Köhne, M. Thermoelectric properties of spark plasma sintered composites based on TiNiSn half-Heusler alloys. *J. Mater. Res.* **2011**, *26*, 1919−1924.
(8) Zou, M.; Li, J.-F.; Du, B.; Liu, D.; Kita, T. Fabrication and thermoelectric properties of fine-grained TiNiSn compounds. *J. Solid State Chem.* **2009**, *182*, 3138−3142.
(9) Gautier, R.; Zhang, X.; Hu, L.; Yu, L.; Lin, Y.; Sunde, T. O. L.; Chon, D.; Poeppelmeier, K. R.; Zunger, A. Prediction and accelerated laboratory discovery of previously unknown 18-electron ABX compounds. *Nat. Chem.* **2015**, *7*, 308.
(10) Legrain, F.; Carrete, J.; van Roekeghem, A.; Madsen, G. K. H.; Mingo, N. Materials Screening for the Discovery of New Half-Heuslers: Machine Learning versus ab Initio Methods. *J. Phys. Chem. B* **2018**, *122*, 625−632.
(11) Carrete, J.; Li, W.; Mingo, N.; Wang, S.; Curtarolo, S. Finding Unprecedentedly Low-Thermal-Conductivity Half-Heusler Semiconductors via High-Throughput Materials Modeling. *Phys. Rev. X* **2014**, *4*, 011019.
(12) Hazama, H.; Matsubara, M.; Asahi, R.; Takeuchi, T. Improvement of thermoelectric properties for half-Heusler TiNiSn by interstitial Ni defects. *J. Appl. Phys.* **2011**, *110*, 063710.
(13) Colinet, C.; Jund, P.; Tédenac, J.-C. NiTiSn a Material of Technological Interest: Ab Initio Calculations of Phase Stability and Defects. *Intermetallics* **2014**, *46*, 103−110.
(14) Berche, A.; Jund, P. Fully Ab initio determination of the Thermoelectric properties of Half-Heusler NiTiSn: Crucial role of interstitial Ni Defects. *Materials* **2018**, *11*, 868.
(15) Rittiruam, M.; Yangthaisong, A.; Seetawan, T. Enhancing the Thermoelectric Performance of Self-Defect TiNiSn: A First-Principles Calculation. *J. Electron. Mater.* **2018**, *47*, 7456−7462.
(16) Ren, W.; Zhu, H.; Mao, J.; You, L.; Song, S.; Tong, T.; Bao, J.; Luo, J.; Wang, Z.; Ren, Z. Manipulation of Ni Interstitials for Realizing Large Power Factor in TiNiSn-Based Materials. *Adv. Electron. Mater.* **2019**, *5*, 1900166.
(17) Kirievsky, K.; Fuks, D.; Gelbstein, Y. Composition conserving defects and their influence on the electronic properties of thermoelectric TiNiSn. *Phys. Chem. Chem. Phys.* **2020**, *22*, 8035.
(18) Kirievsky, K.; Shlimovich, M.; Fuks, D.; Gelbstein, Y. An ab initio study of the thermoelectric enhancement potential in nanograined TiNiSn. *Phys. Chem. Chem. Phys.* **2014**, *16*, 20023−20029.
(19) Dovesi, R.; Erba, A.; Orlando, R.; Zicovich-Wilson, C. M.; Civalleri, B.; Maschio, L.; Rérat, M.; Casassa, S.; Baima, J.; et al. Quantum-mechanical condensed matter simulations with CRYSTAL. *Wiley Interdiscip. Rev.: Comput. Mol. Sci.* **2018**, *8*, No. e1360.
(20) Guss, P.; Foster, M. E.; Wong, B. M.; Patrick Doty, F.; Shah, K.; Squillante, M. R.; Shirwadkar, U.; Hawrami, R.; Tower, J.; Yuan, D. Results for aliovalent doping of CeBr3 with Ca2+. *J. Appl. Phys.* **2014**, *115*, 034908.
(21) Mikaeilzadeh, L.; Tavana, A.; Khoeini, F. Electronic structure of the PrNiBi half-Heusler system based on the σ GGA+ U method. *Sci. Rep.* **2019**, *9*, 20075.
(22) Sansone, G.; Ferretti, A.; Maschio, L. Ab initio electronic transport and thermoelectric properties of solids from full and range-separated hybrid functionals. *J. Chem. Phys.* **2017**, *147*, 114101.
(23) Perdew, J. P.; Burke, K.; Ernzerhof, M. Generalized gradient approximation made simple. *Phys. Rev. Lett.* **1996**, *77*, 3865.
(24) Corà, F.; Alfredsson, M.; Mallia, G.; Middlemiss, D.; Mackrodt, W.; Dovesi, R.; Orlando, R. *Principles and Applications of Density Functional Theory in Inorganic Chemistry II*; Springer: Heidelberg, pp 171−232.
(25) Weigend, F.; Ahlrichs, R. Balanced basis sets of split valence, triple zeta valence and quadruple zeta valence quality for H to Rn: Design and assessment of accuracy. *Phys. Chem. Chem. Phys.* **2005**, *7*, 3297−3305.
(26) Daga, L. E.; Civalleri, B.; Maschio, L. Gaussian Basis Sets for Crystalline Solids: All-Purpose Basis Set Libraries vs System-Specific Optimizations. *J. Chem. Theory Comput.* **2020**, *16*, 2192−2201.
(27) Perdew, J. P.; Ernzerhof, M.; Burke, K. Rationale for mixing exact exchange with density functional approximations. *J. Chem. Phys.* **1996**, *105*, 9982−9985.
(28) Adamo, C.; Barone, V. Toward reliable density functional methods without adjustable parameters: The PBE0 model. *J. Chem. Phys.* **1999**, *110*, 6158−6170.
(29) Dovesi, R.; et al. *CRYSTAL17 User's Manual*, 2017.
(30) Shanno, D. F. Conditioning of quasi-Newton methods for function minimization. *Math. Comput.* **1970**, *24*, 647.
(31) Zicovich-Wilson, C. M.; Dovesi, R. On the use of symmetry adapted crystalline orbitals in SCF-LCAO periodic calculations. I. The construction of the symmetrized orbitals. *Int. J. Quantum Chem.* **1998**, *67*, 299.
(32) Erba, A.; Mahmoud, A.; Belmonte, D.; Dovesi, R. High pressure elastic properties of minerals from ab initio simulations: The case of pyrope, grossular and andradite silicate garnets. *J. Chem. Phys.* **2014**, *140*, 124703.
(33) Öğüt, S.; Rabe, K. M. Band gap and stability in the ternary intermetallic compounds NiSnM (M= Ti, Zr, Hf): A first-principles study. *Phys. Rev. B* **1995**, *51*, 10443.
(34) Klimm, D.; Paufler, P. Point defects in GaP single crystals investigated by mechanical damping. *Cryst. Res. Technol.* **1987**, *22*, 1023−1030.
(35) Kaur, K. TiPdSn: A half Heusler compound with high thermoelectric performance. *Europhys. Lett.* **2017**, *117*, 47002.
(36) Roy, A.; Bennett, J. W.; Rabe, K. M.; Vanderbilt, D. Half-Heusler semiconductors as piezoelectrics. *Phys. Rev. Lett.* **2012**, *109*, 037602.
(37) Aliev, F. G.; Kozyrkov, V. V.; Moshchalkov, V. V.; Scolozdra, R. V.; Durczewski, K. Narrow band in the intermetallic compounds MNiSn (M=Ti, Zr, Hf). *Z. Phys. B: Condens. Matter* **1990**, *80*, 353−357.
(38) Rogl, G.; Grytsiv, A.; Gürth, M.; Tavassoli, A.; Ebner, C.; Wünschek, A.; Puchegger, S.; Soprunyuk, V.; Schranz, W.; Bauer, E.; Müller, H.; Zehetbauer, M.; Rogl, P. Mechanical properties of half-Heusler alloys. *Acta Mater.* **2016**, *107*, 178−195.
(39) Bhattacharya, S.; Pope, A. L.; Littleton, R. T.; Tritt, T. M.; Ponnambalam, V.; Xia, Y.; Poon, S. J. Effect of Sb doping on the thermoelectric properties of Ti-based half-Heusler compounds, $TiNiSn_{1-x}Sb_x$. *Appl. Phys. Lett.* **2000**, *77*, 2476−2478.
(40) Kim, K. S.; Kim, Y.-M.; Mun, H.; Kim, J.; Park, J.; Borisevich, A. Y.; Lee, K. H.; Kim, S. W. Direct Observation of Inherent Atomic-Scale Defect Disorders responsible for High-performances $Ti_{1-x}Hf_xNiSn_{1-y}Sb_y$ Half-Heusler Thermoelectric Alloys. *Adv. Mater.* **2017**, *29*, 1702091.
(41) Kimura, Y.; Asami, C.; Chai, Y. W.; Mishima, Y. Thermoelectric Performance of Half-Heusler TiNiSn Alloys Fabricated by Solid-Liquid Reaction Sintering. *Mater. Sci. Forum* **2010**, *654*−*656*, 2795−2798.
(42) Zilber, T.; Cohen, S.; Fuks, D.; Gelbstein, Y. TiNiSn half-Heusler crystals grown from metallic flux for thermoelectric applications. *J. Alloys Compd.* **2019**, *781*, 1132−1138.
(43) Wang, L. L.; Miao, L.; Wang, Z. Y.; Wei, W.; Xiong, R.; Liu, H. J.; Shi, J.; Tang, X. F. Thermoelectric performance of half-Heusler compounds TiNiSn and TiCoSb. *J. Appl. Phys.* **2009**, *105*, 013709.

https://dx.doi.org/10.1021/acs.jpcc.0c03243
J. Phys. Chem. C 2020, 124, 14997−15006

(44) Kimura, Y.; Zama, A.; Mishima, Y. Thermoelectric Properties of P-type Half-Heusler Compounds HfPtSn and ZrPtSn. *25th International Conference on Thermoelectrics*, 2006; pp 115−119.
(45) Aversano, F.; Ferrario, A.; Boldrini, S.; Fanciulli, C.; Baricco, M.; Castellero, A. Thermoelectric Properties of TiNiSn Half Heusler Alloy Obtained by Rapid Solidification and Sintering. *J. Mater. Eng. Perform.* **2018**, *27*, 6306−6313.
(46) Downie, R. A.; Maclaren, D. A.; Bos, J.-W. G. Thermoelectric performance of multiphase XNiSn (X = Ti, Zr, Hf) half-Heusler alloys. *J. Mater. Chem. A* **2014**, *2*, 6107−6114.
(47) Muta, H.; Kanemitsu, T.; Kurosaki, K.; Yamanaka, S. High-temperature thermoelectric properties of Nb-doped MNiSn (M = Ti, Zr) half-Heusler compound. *J. Alloys Compd.* **2009**, *469*, 50−55.
(48) Rowe, D. M. *CRC Handbook of Thermoelectrics*; CRC press, 2010.
(49) Sales, B. C. Electron Crystals and Phonon Glasses: A New Path to Improved Thermoelectric Materials. *MRS Bull.* **1998**, *23*, 15−21.

https://dx.doi.org/10.1021/acs.jpcc.0c03243
J. Phys. Chem. C 2020, 124, 14997−15006

Supplementary Material for:

The Key Role of Defects in Thermoelectric Performance of TiMSn(M = Ni, Pd, Pt) Half-Heusler Alloys

Atreyi Dasmahapatra,[†] Loredana Edith Daga,[†] Antti J. Karttunen,[‡] Lorenzo Maschio,[*,†] and Silvia Casassa[*,†]

[†]*Dipartimento di Chimica, Università di Torino, Italy*

[‡]*Department of Chemistry and Materials Science, Aalto University, Finland*

E-mail: lorenzo.maschio@unito.it; silvia.casassa@unito.it

Modeling Defects in TiNiSn

Geometrical Structure

Neighbors analysis of the defect systems is reported in Table S1

Table S1: Neighbors of the non-equivalent atoms. Distances d are in Å.

	W8c-333				**W8c-111**			
	no opt	d	opt	d	no opt	d	opt	d
Ti(1)	4Ni	2.5665	3Ni	2.5676	3Ni	2.566	3Ni	2.588
Ti(5)	4Ni	2.5665	1Ni	2.6427	5Ni	2.566	1Ni	2.521
			3Ni	2.559			3Ni	2.535
			1Ni	2.602			1Ni	2.585
Sn(16)	3Ni	2.5665	3Ni	2.5921	4Ni	2.566	3Ni	2.586
							1Ni	2.719
Sn(20)	5Ni	2.5665	1Ni	2.5594	4Ni	2.566	3Ni	2.576
			3Ni	2.4895			1Ni	2.577
			1Ni	2.621				

Electronic Structure

In Fig. S2 are reported the band structure of the defect models, compared with the perfect system. Fig. S3 shows the density of state projected onto the AOs of Sn(16) and Sn(20) for TiMSn (M=Ni, Pd, Pt). As already stated, Sn contributions show pretty low intensities in the region close to Fermi level.

In Table S2 the Hirshfeld atomic charges in the pure and defective models are collected.

Table S2: Hirshfeld charges for the irreducible atoms in 24-atoms 2x2x2 supercell. In parenthesis, the multiplicity of each atom.

	Pure	*W8c-333*	*W8c-111*
Ti-1	-0.004 (8)	-0.061 (4)	-0.127 (4)
Ti-5		-0.015 (4)	0.036 (4)
Ni-9	-0.628 (8)	-0.578 (6)	-0.574 (6)
Ni-15		-0.668 (1)	-0.618 (1)
Ni-24		-0.391 (1)	-0.338 (1)
Sn-16	0.632 (8)	0.527 (4)	0.562 (4)
Sn-20		0.681 (4)	0.629 (4)

Basis set *P.def2-SVP*

The hierarchy of atomic orbitals of the *P.def2-SVP* basis-set, adopted in the calculations and obtained by manipulating the molecular *def2-SVP* basis set[1] is listed in Table S3. The Ti,[2] Ni,[3] Pd,[4] Pt,[4] and Sn[5] basis sets adapted for periodic calculations have been described in previous literature. For Sn, Pt and Pd, in order to reduce the computational efforts and to take scalar relativistic effects into account, core electrons are treated with Effective Core Potentials (ECP).

For Titanium, the molecular *def2-SVP* is juxtaposed to show in details the procedure adopted in the manipulation of the basis.

The most diffuse s shell and the outermost f shell are deleted. Then, the exponents of the 4th s and 3rd p shells are doubled, to prevent linear dependency phenomena.

Table S3: [1] D. Andrae, U. Haeussermann, M. Dolg, H. Stoll, H. Preuss, Theor. Chim. Acta 77, 123 (1990). [2] B. Metz, H. Stoll, M. Dolg, J. Chem. Phys. 113, 2563 (2000).

	Ti	Ni	Pd	Pt	Sn
P.def2-SVP	s(6331)	s(6331)	ECP[1]-s(3111)	ECP[1]-s(2111)	ECP[2]-s(621)
	sp(1)	sp(1)	sp(1)	sp(1)	sp(1)
	p(53)	p(53)	p(4)	p(4)	p(411)
	d(41)	d(41	d(41)	d(41)	d(51)

In the following, we list the basis-sets in the CRYSTAL standard input format.

f functions

In order to check the accuracy of our *P.def2-SVP* basis set, we performed a full geometry optimization of the TiPtSn alloy with a basis set for Pt containing an *f* function, *P.def2-SVP-f*. The adopted exponent (0.6681300) is original of the *def2SVP* basis set, as reported in the EMSL exchange database (www.basissetexchange.org). The results, collected in Table S4, and the two band structures, compared in Fig. S4, show that the addition of an *f* exponent does not change significantly the description of the system.

Titanium	*P.def2-SVP*	*def2-SVP*	
22 9		22 9	
0 0 6 2.0 1.0		0 0 6 2.0 1.0	
42961.512185	.39127635355E-02	42961.512185	.39127635355E-02
6450.9759169	.29969820489E-01	6450.9759169	.29969820489E-01
1467.7210915	.14836352707	1467.7210915	.14836352707
414.20997355	.51347285324	414.20997355	.51347285324
134.48715840	1.0335365483	134.48715840	1.0335365483
46.122209796	.77854233930	46.122209796	.77854233930
0 0 3 2.0 1.0		0 0 3 2.0 1.0	
89.447762543	-.28385401259	89.447762543	-.28385401259
10.223346060	1.6772785333	10.223346060	1.6772785333
4.1353774271	1.2411928456	4.1353774271	1.2411928456
0 0 3 2.0 1.0		0 0 3 2.0 1.0	
6.7896181452	-.78399994518E-02	6.7896181452	-.78399994518E-02
1.1106730691	.25495493019E-01	1.1106730691	.25495493019E-01
0.47565975578	.16061172892E-01	0.47565975578	.16061172892E-01
0 0 1 2.0 1.0		0 0 1 2.0 1.0	
0.24	1.0000000000	**0.065986956934**	1.0000000
		0 0 1 0.0 1.0	
		0.025210342250	1.0000000
0 2 5 6.0 1.0		0 2 5 6.0 1.0	
522.03684782	.19754179642E-01	522.03684782	.19754179642E-01
122.68649489	.14460677619	122.68649489	.14460677619
38.572903611	.54669004165	38.572903611	.54669004165
13.672169319	1.0531647540	13.672169319	1.0531647540
5.0118529359	.69111213363	5.0118529359	.69111213363
0 2 3 6.0 1.0		0 2 3 6.0 1.0	
2.4131928282	.75803437136	2.4131928282	.75803437136
0.93252270050	1.3036241399	0.93252270050	1.3036241399
0.35429058390	.53638653300	0.35429058390	.53638653300
0 1 1 0.0 1.0		0 2 1 0.0 1.0	
0.12		**0.1015610**	1.0000000
0 3 4 2.0 1.0		0 3 4 2.0 1.0	
23.465125957	.26536380115E-01	23.465125957	.26536380115E-01
6.3332593832	.13796453963	6.3332593832	.13796453963
2.0766489946	.35312644228	.0766489946	.35312644228
0.69027361954	.48647124166	0.69027361954	.48647124166
0 3 1 0.0 1.0		0 3 1 0.0 1.0	
0.21088738554	.33026314258	0.21088738554	.33026314258
		0 4 1 0.0 1.0	
		0.5620000	1.0000000

Nichel	*P.def2-SVP*
28 9	
0 0 6 2.0 1.0	
71074.803211	.14260386729E-02
10672.020941	.10928236994E-01
2428.1389007	.54212626938E-01
685.53595148	.18874768902
223.10072863	.38324616985
76.842014042	.29550637144
0 0 3 2.0 1.0	
148.71122016	-.11014443059
17.459154987	.64521426988
7.1625280665	.44797838103
0 0 3 2.0 1.0	
12.556137125	-.22645403224
2.0735740488	.72320959286
.85382640602	.44868026476
0 0 1 1.0 1.0	
0.35	1.0000000000
0 1 1 0.0 1.0	
0.14	1.0 1.0
0 2 5 6.0 1.0	
916.73608662	.93439635610E-02
216.06139913	.69737374902E-01
68.383914817	.27073495012
24.593843952	.53078301549
9.1392960204	.34410229438
0 2 3 6.0 1.0	
4.7193371746	.34076082016
1.8161849234	.56580169611
0.6784075072	.23616717361
0 3 4 9.0 1.0	
47.093832108	.28982316948E-01
13.146463975	.15494995950
4.4170548925	.37633115111
1.4771565078	.47365096014
0 3 1 0.0 1.0	
0.4373592179	.31247837833

Palladium	*P.def2-SVP*
246 8	
INPUT	
18. 0 2 2 2 2 0	
12.430000	240.229040 0
6.170759	35.171943 0
11.080000	170.417276 0
5.829554	28.472133 0
9.510000	69.013845 0
4.139781	11.750862 0
13.270000	-31.929554 0
6.630000	-5.398217 0
0 0 3 2.0 1.0	
8.4756400000	1.2392391076
7.1657170000	-1.6563109970
3.1821100000	-.13178619060
0 0 1 0.0 1.0	
1.3973644196	1.0000000000
0 0 1 0.0 1.0	
0.60532955868	1.0000000000
0 0 1 0.0 1.0	
0.29	1.0000000000
0 1 1 0.0 1.0	
0.14	1.0 1.0
0 2 4 6.0 1.0	
4.2460970000	-0.82324104973
3.3925940000	0.87084659933
1.1975891264	0.63512225791
0.52673750585	0.27225338752
0 3 4 10.0 1.0	
7.3613290985	-.17199885828E-01
2.6291037258	.23313745275
1.1292744634	.44536385867
0.44471659896	.39293650406
0 3 1 0.0 1.0	
0.22	1.0

Platinum	*P.def2-SVP*
278 8	
INPUT	
18. 0 2 2 2 1 1	
13.428651	579.223861 0
6.714326	29.669491 0
10.365944	280.860774 0
5.182972	26.745382 0
7.600479	120.396444 0
3.800240	15.810921 0
3.309569	24.314376 0
5.277289	-24.218675 0
0 0 2 2.0 1.0	
16.559563000	-.53808800717
13.892440000	.91402161377
0 0 1 0.0 1.0	
5.8531044732	1.0000000000
0 0 1 0.0 1.0	
1.2498640609	1.0000000000
0 0 1 0.0 1.0	
0.55606439459	1.0000000000
0 1 1 0.0 1.0	
0.13	1.0 1.0
0 2 4 6.0 1.0	
8.1000000000	.72955608128
7.2000000000	-.95441807252
1.5588402917	.57140490320
0.73230402180	.49508234268
0 3 4 10.0 1.0	
4.6299536825	-.87774450596E-01
2.1980241252	.21158360681
0.93629991261	.46533857641
0.37160028160	.41129165525
0 3 1 0.0 1.0	
0.1858001408	1.0

Tin	*P.def2-SVP*
250 9	
INPUT	
22 0 2 4 4 2 0	
17.4204140000000	279.988682000000 0
7.63115500000000	62.3778100000000 0
16.1310240000000	66.1625230000000 0
15.6280770000000	132.174396000000 0
7.32560800000000	16.3394170000000 0
6.94251900000000	32.4889590000000 0
15.5149760000000	36.3874410000000 0
15.1881600000000	54.5078410000000 0
5.45602400000000	8.69682300000000 0
5.36310500000000	12.8402080000000 0
12.2823480000000	-12.5763330000000 0
12.2721500000000	-16.5959440000000 0
0 0 6 2.0 1.0	
375.95156177	0.15224884228E-02
23.661818008	-0.16776065030
19.946281315	0.33989090393
6.8240270454	-0.84441791529
1.8771488722	0.92646952846
0.82033199226	0.53091094490
0 0 2 2.0 1.0	
10.272082089	-0.90331119154E-02
1.3573201180	0.22980877714
0 0 1 0.0 1.0	
0.21345004117	1.0000000000
0 1 1 0.0 1.0	
0.09	1.0 1.0
0 2 4 6.0 1.0	
21.293597748	0.37103218279E-01
8.8171842499	-0.32351709661
1.2347028371	0.83846760898
0.57869142617	0.23294977050
0 2 1 2.0 1.0	
2.5077059216	1.0000000000
0 2 1 0.0 1.0	
0.26647309693	1.0000000000
0 3 5 10.0 1.0	
39.693023177	0.39185734275E-02
20.852179275	-0.68210073667E-02
3.6907832774	0.27938420495
1.5849404530	0.52607409874
0.62772693365	0.36149465348
0 3 1 0.0 1.0	
0.20500000000	1.0000000000

Table S4: Results for TiPtSn with two different basis set at the PBE0 level.

basis set	Mulliken atomic charge (a.u.)	lattice parameter (Å)	band gap (eV)
P.def2-SVP	0.512	6.22	1.13
P.def2-SVP-f	0.527	6.22	1.10

References

(1) Weigend, F.; Ahlrichs, R. Balanced basis sets of split valence, triple zeta valence and quadruple zeta valence quality for H to Rn: Design and assessment of accuracy. *Phys. Chem. Chem. Phys.* **2005**, *7*, 3297–305.

(2) Tanskanen, A.; Karttunen, A. J.; Karppinen, M. Substantially enhanced Raman signal for inorganic-organic nanocomposites by ALD-TiO_2 capping. *RSC Adv.* **2016**, *6*, 41087–41091.

(3) Linnera, J.; Sansone, G.; Maschio, L.; Karttunen, A. J. Thermoelectric Properties of p-Type Cu2O, CuO, and NiO from Hybrid Density Functional Theory. *The Journal of Physical Chemistry C* **2018**, *122*, 15180–15189.

(4) Sergei, I. I.; Artem, V. M.; Karttunen, A. J.; Roman, V. O.; Kraus, F. Reactions of $KBrF_4$ with platinum metals. *Journal of Fluorine Chemistry* **2019**, *218*, 11 – 20.

(5) Karttunen, A. J.; Fässler, T. F.; Linnolahti, M.; Pakkanen, T. A. Structural Principles of Semiconducting Group 14 Clathrate Frameworks. *Inorganic Chemistry* **2011**, *50*, 1733–1742.

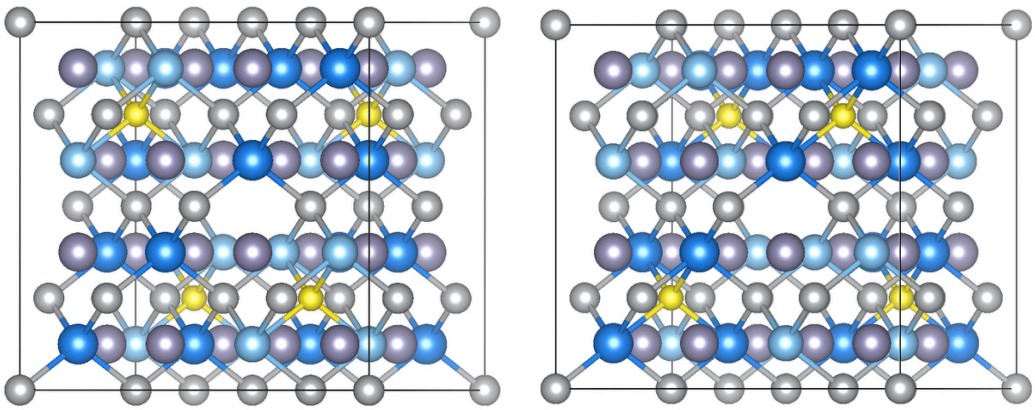

Figure S1: Representative models of the crystallographic cell for *W8c-333* system and *W8c-111* (24 atoms in the unit cell). Blue, grey and purple spheres denote Ti, Ni and Sn atoms respectively. The yellow spheres are Ni(24) positions that were originally unoccupied in the pure system. Light blue are Ti(1) and dark blue are Ti(5).

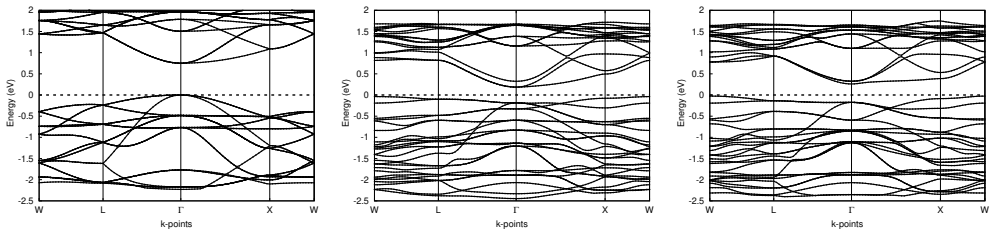

(a) (b) (c)

Figure S2: Computed electronic band structures at PBE10/*P.def2-SVP* level. Dotted line corresponds to Fermi level. (a) Pure system (Band gap: 0.689 eV), (b) *W8c-333* (Band gap: 0.187 eV) and (c) *W8c-111* (Band gap: 0.261 eV).

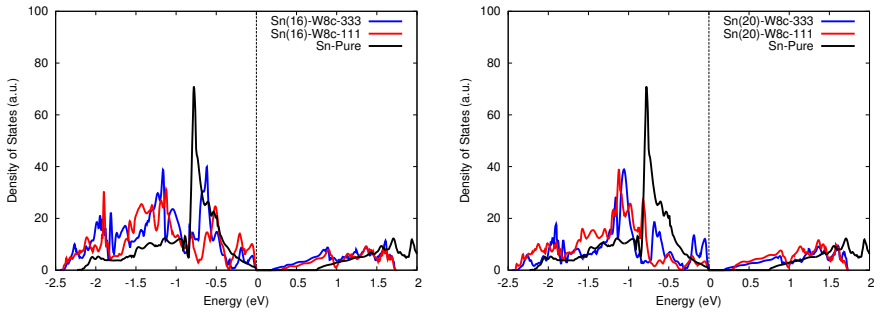

(a) (b)

Figure S3: Density of States of: (a) Sn(16), (b) Sn(20).

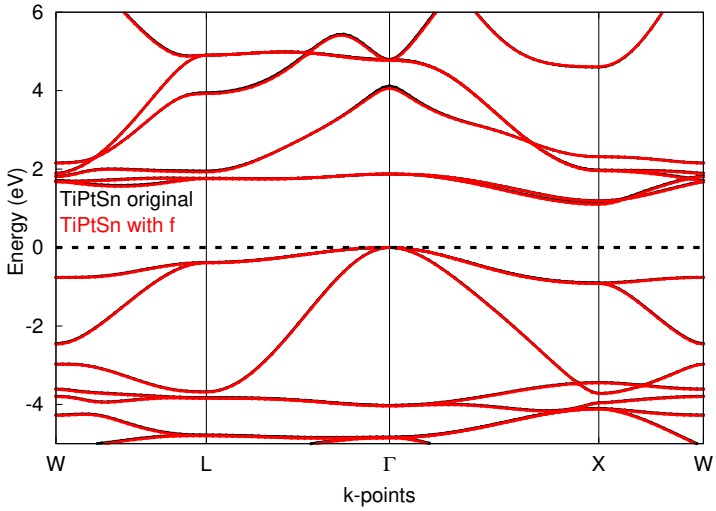

Figure S4: Band structure of TiPtSn at the PBE0 level for *P.def2-SVP* with and without *f* function.

12.3 Electronic Excitations in Crystalline Solids through the Maximum Overlap Method-Paper Submitted

In the following a submitted paper about the Maximum Overlap Method is reported.

Electronic Excitations in Crystalline Solids through the Maximum Overlap Method.

Loredana Edith Daga and Lorenzo Maschio*

Dipartimento di Chimica, Università di Torino and NIS Centre, Via P. Giuria 5, 10125 Torino, Italy

E-mail: lorenzo.maschio@unito.it

Abstract

The Maximum Overlap Method (MOM) emerged in molecular quantum chemistry as a convenient practical procedure for studying excited states. Unlike the Aufbau principle, during the SCF iterations MOM forces orbital occupation to be maximally similar to a reference state. Although still within a single-particle framework, this approach allows for the evaluation of excitation energies (Δ-SCF) and geometry optimization of electronic configurations other than the ground state.

In this work we present an extension of the MOM treatment to periodic crystalline solids, within the framework of an atom-centred Gaussian basis set. Periodic SCF solution techniques involve iterating between direct and reciprocal space. It follows that, in order to preserve translational symmetry, only totalsymmetric excitations are allowed in our treatment: vertical Γ–point excitations or collective excitations in a sphere around Γ. Other types of excitation are accessible through folding of the Brillouin zone subsequent to the creation of a supercell.

The features and performance of the method are presented through its application to prototypical solids such as bulk silicon, diamond and lithium fluoride, and comparing the results to available experimental data. Demonstrative application to nickel oxide

and solid CuI(piperazine) – a luminescent copper halide compound – highlight the promising potential of the MOM method in solid state quantum chemistry.

1 Introduction

Excited states are notoriously much more challenging and costly to be studied through *ab initio methods* than ground states. The most commonly used approaches for this task are many-body methods such as Time-Dependent Density Functional Theory (TD-DFT)[1,2] Configuration-Interaction Singles (CIS),[3,4] and the Green's function Bethe-Salpeter,[5] even though a variety of other methods is available.[6]

Such Post-SCF and/or multiconfigurational methods are however generally demanding, both in terms of computational resources and efforts required for their implementation, and often do not offer many useful tools such as a geometry optimizer or vibrational frequency calculation. Thus, the idea of a simple single-particle approach able to satisfactorily describe excited states by the same methods and tools used for the ground state has a great appeal for routine applications.[7]

In this view, the Maximum Overlap Method (MOM)[8,9] has seen some success despite its simplicity. Given a reference state, the MOM procedure carries out a standard iterative self-consistent procedure, except that instead of setting orbital occupations according to lowest energy ranking, it occupies those orbitals with the largest overlap with respect to a reference configuration. In this way the *aufbau* principle is overridden, and the SCF iterations provide the orbitals of the desired electronic configuration much in the same way as for the ground state, thus allowing for the use of all of the standard algorithms such as atomic gradient calculation. The excitation (or de-excitation) energy can be evaluated simply as the difference between the total energies of the two configurations. (Δ–SCF[10–12]).

The interest toward MOM-related approaches – and beyond – appears to be alive if not rising in recent years and many works have been published on the topic.[13–16]

In this work we present an extension of the MOM method to the case of crystalline solids, treated within periodic boundary conditions using a local atom-centered Gaussian basis set. While such extension might seem trivial at first sight, it poses some conceptual challenges that have to be tackled, which are due to the periodic nature of the crystal and the features of electronic bands. In particular: i) since the unit cell is periodically repeated, performing the excitation in direct space would lead to an unrealistically high density of excitations, thus requiring costly supercell calculations as in Ref. 17; ii) working in reciprocal space allows for a single electron to be excited within the periodic boundary conditions, but how can one tune the concentration of excitations?; iii) evaluation of excitation energies and atomic forces and gradients must properly take into account such concentration. Moreover, if the iterative SCF procedure - as is the case here - involves going back and forth from reciprocal to direct space through the build of a density matrix, only totalsymmetric excitations are allowed in order to preserve the translational symmetry.

In the following we present the simple formalism we developed and discuss its implications in connection to the points listed above through example calculations on simple crystalline systems. We also present demonstrative applications on solid NiO[17] and CuI(piperazine)[18] crystals.

2 Theory

In this section, starting from the basics of the SCF procedure in periodic systems, we will present the details of the periodic MOM method and discuss the consequences of its application to electronic bands. The method has been developed within a local atom-centered (Gaussian) basis set framework[19] but is more generally applicable.

2.1 SCF in Periodic Systems

For a crystalline system, Hartree-Fock/Kohn Sham equations are commonly carried out in reciprocal space, in a number $N_{\mathbf{k}}$ of discrete $\mathbf{k}$-points constituting a uniform sampling of the first Brillouin zone:

$$F(\mathbf{k})C(\mathbf{k}) = S(\mathbf{k})C(\mathbf{k})\epsilon(\mathbf{k}) \tag{1}$$

where, as usual, in each $\mathbf{k}$ point $F(\mathbf{k})$ is the Fock matrix, $S(\mathbf{k})$ is the overlap matrix, $C(\mathbf{k})$ are the coefficients of the crystalline orbitals and $\epsilon(\mathbf{k})$ are the corresponding eigenvalues. The Fock matrix build is, in turn, carried out in direct space, hence at each iteration a direct-space representation of the density matrix P is built from eigenvectors such that

$$P^{\mathbf{g}} = \frac{1}{N_{\mathbf{k}}} \sum_{k} e^{i\mathbf{k}\cdot\mathbf{g}} C^{\dagger}(\mathbf{k}) n(\mathbf{k}) C(\mathbf{k}) \tag{2}$$

where $\mathbf{g}$ is the vector locating a lattice point (cell) in direct space and $n(\mathbf{k})$ is the occupation matrix, a diagonal matrix with non-null elements in correspondence of the occupied orbitals. In the case of a zero-kelvin nonconducting system, which we will assume in this work, such elements are either 1 or 0, and for the ground state occupations are assigned following the Aufbau principle filling in each $\mathbf{k}$ the orbitals having the lowest eigenvalues $\epsilon(\mathbf{k})$. From Eq. (2) it follows that $N_{\mathbf{k}}$ defines the direct space Periodic Boundary Conditions (PBC), that is, the size of the portion of direct space after which the charge density replicates itself: this is called Super Wigner-Seitz Cell (SWSC) and is - to a good approximation - constituted by a number of unit cells equal to $N_{\mathbf{k}}$ (which is strictly true in one-dimensional systems). Hence the definition of the reciprocal space sampling, which is usually in the hands of the user, directly reflects on the characteristics of the periodic boundaries adopted.

2.2 The MOM method for Periodic Systems

The MOM method acts on the definition of the $n(\mathbf{k})$ occupation matrix of Eq. (2). Let us start from a reference solution $C^{ref}(\mathbf{k})$ – which can be either from the converged ground

state, or an initial guess. Once the eigenvectors are sorted by energy, the code overrides the Aufbau principle by forcing a different occupation pattern $n^{ref}(\mathbf{k})$. Technically this can be done in any one – or even more than one – $\mathbf{k}$-points of the Brillouin zone, and in the next subsection we will discuss which choices are physically meaningful.

In subsequent iterations, the overlap between the new coefficients C and C^{ref} ones is evaluated

$$O(\mathbf{k}) = C^{ref\,\dagger}(\mathbf{k})\, S(\mathbf{k})\, C(\mathbf{k}) \tag{3}$$

The projection of the j-th new orbital onto the old occupied space is the expressed by:

$$p_j(\mathbf{k}) = \sum_i^n O_{ij}(\mathbf{k}) = \sum_\nu^N \left[\sum_\mu^N \left(\sum_i^n C_{i\mu}^{ref}(\mathbf{k}) \right)^\dagger S_{\mu\nu}(\mathbf{k})\, C_{\nu j}(\mathbf{k}) \right] \tag{4}$$

For each nonzero diagonal element in $n^{ref}(\mathbf{k})$ the largest corresponding projection $p(\mathbf{k})$ locates the position to be filled in the new $n(\mathbf{k})$.

The evaluation of $O(\mathbf{k})$ as in Eq. (3) is relatively inexpensive, hence the additional cost of the MOM procedure is virtually negligible with respect to that of the corresponding ground-state method (i.e., HF and DFT), even though convergence can turn out to be more difficult. Convergence accelerators such as DIIS[20,21] can normally be used within this framework.

Depending on the definition of $n^{ref}(\mathbf{k})$ MOM can then be used to converge the SCF towards solutions different from the ground state. This will be the use of MOM we will focus on in the following of this work. A further possibility that we do not explore here is to use the method to stabilize the ground state solution, avoiding the intrusion of unphysical states arising from numerical inaccuracies. We also note that the reference state C^{ref} could be kept constant through the SCF, or changed at each iteration shifting the reference to the previous cycle. The latter is the choice we adopted.

2.3 Excitations in Solids through MOM

2.3.1 Excitation from a single k-point to another

It follows from Eq. (2) that the translational invariance of the direct space density matrix has to be granted in the SCF procedure. Subsequently, only excitations that are totally symmetric with respect to the group of lattice translation vectors are possible within our approach. In fact, this property is granted by vertical excitations at the center of the Brillouin zone (Γ-point only excitations), but not by vertical excitation in other **k**- points nor by diagonal excitations. Such excitation can however be accessed through creation of a supercell – as by increasing the size of the periodically repeating unit in the direct space the reciprocal space folds itself into Γ. In Figure 1 the band structure folding is reported for Bulk Silicon, for which we report numeric results in the Results section: excitations E_L and E_X, not accessible through our MOM approach in the primitive unit cell, both become Γ-point excitations in the 2×2×2 supercell (right panel).

Vertical Γ-point excitations result in a new $n^{ref}(\mathbf{\Gamma})$ and hence in a small variation of the density matrix of Eq. (2) leading to a new $P^{\mathbf{g}}_{\uparrow}$. Physically, this is equivalent to having only one single excitation within the periodic boundaries (SWSC). Hence, the excitation is diluted in the whole PBC and since the unit cell total energy is computed, the excitation energy per cell must be evaluated as:

$$E^{exc} = N_{\mathbf{k}} \left(E^{tot}_{\uparrow} - E^{tot}_{ground} \right) \tag{5}$$

where we have denoted as $E^{tot}_{\uparrow}$ the unit cell energy obtained through $P^{\mathbf{g}}_{\uparrow}$. In fact, our reciprocal space MOM approach allows for a diluted excitation using just the small primitive unit cell – hence with a computationally cheap calculation – as opposite to direct-space Δ-SCF as in Ref. 17 that require a more costly supercell calculation also for Γ- point excitations.

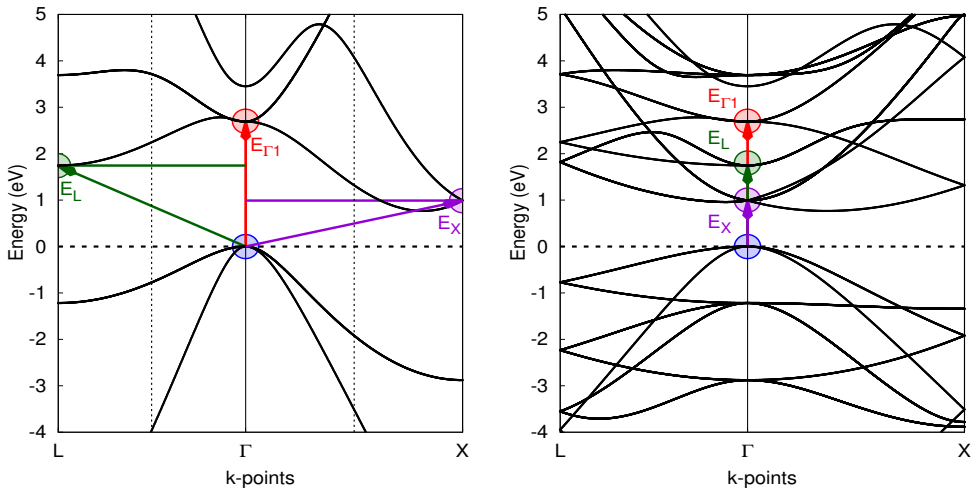

Figure 1: A graphical representation of some possible electronic excitations – labeled as $E_{\Gamma 1}$, E_X, E_L, as computed in Table ref – in the electronic structure of bulk silicon (PBE functional). Left panel: primitive unit cell. Right panel: 2x2x2 supercell. Upon folding of the bands in the supercell creation, the excitations $E_{\Gamma 1}$, E_X, E_L become all Γ–point only excitations. The lines along which the band structure is folded are marked by dashed vertical lines in the left panel.

2.3.2 Tuning the Concentration of Excited Electrons

It follows from the above discussion, that changing the **k**-point sampling also impacts on the concentration of excited electrons in direct space. It is also possible within our approach to consider an excitation involving not only the Γ-point electron, but a portion of the corresponding valence and conduction bands corresponding to a sphere of radius **r** around Γ. This corresponds to a physical process in which a light that is not precisely monochromatic – hence with some frequency broadening – is used to induce the excitation.

As a first thing, when defining the initial reference excited state we need to trace the involved bands across the Brillouin zone, to cope with possible band crossings and degeneracies. Such approach is graphically described in Figure (2): once defined the Γ-point excitation, we evaluate the overlap $O_{\mathbf{k},\mathbf{k}'}$ between the band eigenvectors in two neighboring points **k** and $\mathbf{k}'$, expressed as:

$$O_{\mathbf{k},\mathbf{k}'} = [C(\mathbf{k}')]^{\dagger} S(\mathbf{k}) C(\mathbf{k}) \tag{6}$$

The largest overlap elements allow to trace the bands between $\mathbf{k}$ and $\mathbf{k}'$. Since the space we deal with is – in the general case – a three-dimensional one (although all of our approach works for 2D and 1D periodic systems as well), we follow a path in reciprocal space as depicted in the right panel of Fig. (2), following subsequent rows starting from Γ until completing the whole grid. Once the tracing is completed, a sphere is defined around Γ and only a number of the $n(\mathbf{k})$ corresponding to a number of $N_{\mathbf{k}}^{exc}$ $\mathbf{k}$-points within this sphere. The excitation defined in Γ is then performed also in these points according to the band tracing information. Since the excitation zone is spherical around Γ, the totalsymmetric character of the density $P_{\uparrow}^{bfg}$ is preserved and then it can be effectively represented in direct space. Experimentally, increasing the radius of such sphere corresponds to 1) a broadened (non exactly monochromatic) light triggering the excitation, and 2) a higher density of excited electrons, which are now $N_{\mathbf{k}}/N_{\mathbf{k}}^{exc}$ within the PBC.

The energy of the excitation is then evaluated as:

$$E^{exc} = \frac{N_{\mathbf{k}}}{N_{\mathbf{k}}^{exc}} \left(E_{\uparrow}^{tot} - E_{ground}^{tot} \right) \tag{7}$$

2.4 Energy Gradients and Geometry Optimization

The energy gradients must be computed, in the $\Gamma-$only excitation scheme, by summing back the energy of the ground state to the excitation energy of Eq. (5) (or, eventually, Eq. (7)) and then taking the derivative with respect to atomic displacements

$$\frac{\partial E_{\uparrow}}{\partial \mathcal{R}_a^A} = \frac{\partial E_{\uparrow}^{tot}}{\partial \mathcal{R}_a^A} N_{\mathbf{k}} - \frac{\partial E_{ground}^{tot}}{\partial \mathcal{R}_a^A} \left(N_{\mathbf{k}} - 1 \right) \tag{8}$$

where $\mathcal{R}_a^A$ is the coordinate of atom A along a general cartesian direction a. Analogous

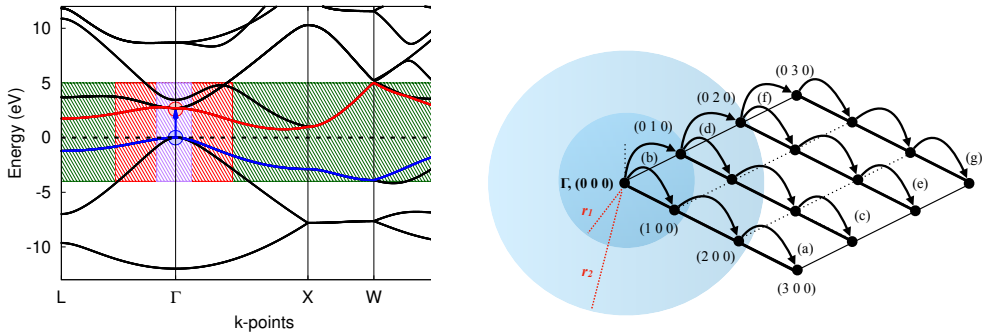

Figure 2: On the left an excitation in Si bulk (PBE functional) in which the radial-sphere approach is graphically represented. On the right the right, the path in a 2D Brillouin zone followed to trace the Γ-point bands and the spheres around Γ are represented.

equations hold for cell gradients, which can always be expressed in form of atomic gradients.[22] Note the distinction between $E_{\uparrow}^{tot}$, the energy that comes as an output to our MOM calculation, and $E_{\uparrow}$, the actual total energy of a unit cell in the excited system.

During a geometry optimization procedure, at each geometry the ground and excited state gradients are required for the evaluation of Eq. (8), thus requiring two SCF procedures.

3 Results

In this section we present some demonstrative calculations using our MOM method, with the purpose to validate the approach and show its capabilities. To this aim we have tested a small group of simple solids (Si, C, LiF) and two cases with more applicative potential, namely NiO and solid CuI-piperazine. All calculations were performed with a development version of the CRYSTAL program.[19]

We have adopted triple-ζ electron basis sets from Peintinger et al.[23] for Si, C, and LiF. We applied the same basis sets for the CuI-piperazine while in the NiO application a dcm-tzvp[24] basis has been used.

In order to validate the method, we begin by considering lowest electronic excitations in a small set of prototypical solids including LiF (ionic crystal), Si (covalent semiconductor),

diamond (covalent insulator). This will allow to compare the MOM excitation energies with experiments, and explore the role of computational parameters.

3.1 Excitation Energies

In Table 1 we report Γ-point excitations as computed with the MOM approach and compare the results with experimental measurements available from the literature. As it is more than well known[25,26] the main impact of the functional choice on the electronic structure is on its band gap, and the amount of exact exchange plays a major role in that. As already reported in literature for the fundamental band gap[27,28] the range-separated HSE06 functional proved to provide a successful balance in that, and this is observed also in our results for covalent crystals, where it consistently leads to excitation energies within 0.1 eV from experimental references for silicon, and diamond. However, for LiF PBE0 seems to represent a better approximation. The difference between the triplet and singlet excited states is always in favor of the latter, which lays in all three cases at a lower energy. The difference is strongly dependent from the amount of exact exchange included, thus suggesting a role of excitonic effects.

The first two columns of Table 1 can be obtained with a primitive cell or a supercell, yielding exactly the same results. The E_X and E_L columns, however, were obtained adopting a 2x2x2 supercell, that allows the bands in X and L points to fold in Γ, as shown in Figures 1 and 3. The reciprocal space grid was reduced to 4x4x4 for consistency.

As discussed in the theory section, the density of excited electrons can be tuned either by changing the **k**-points sampling of the Brillouin zone or by exciting $N_{\mathbf{k}}^{exc}$ **k**-points within a sphere of radius r_s around the Γ point (see Figure 2) The tuning of the number of $N_{\mathbf{k}}$ points and the radius r_s allows to assess any desired exciton density.

In Table 2 we show the combined effect of the two parameters in the case of bulk Silicon:

- Increasing the radius r_s rapidly increases the number of points enclosed in the sphere.

Table 1: Excitation energies (in eV) for simple solids as computed with the MOM approach with different functionals. A primitive cell (no supercell) is used for Γ-point excitations (E_Γ^{sing}, E_Γ^{trip}). A 2x2x2 supercell has been adopted for E_X^{sing} and E_L^{sing}. Available experimental values from the literature are reported for each system.

	Method	E_Γ^{sing}	E_Γ^{trip}	E_X^{sing}	E_L^{sing}
Silicon	Exp.	3.4[29–31] 3.45[32]		1.2[30]	2.0[30]
	PBE	2.691	2.688	0.988	1.743
	HSE06	3.422	3.416	1.577	2.440
	PBE0	4.048	3.993	2.162	3.416
Diamond	Exp.	6.0[33,34] 7.75[31]		5.46-5.6[30]	
	PBE	5.619	5.618	4.795	
	HSE06	7.000	6.988	5.942	
	PBE0	7.677	7.598	6.552	
LiF	Exp.	12.6[35,36]			
	PBE	8.993	8.992		
	HSE06	11.300	11.289		
	PBE0	12.089	11.859		

As a consequence the excitation energy becomes higher due to the increased concentration of excited electrons

- In the second series of data in Table 2 we show that, by changing both parameters simultaneously, we can keep constant $N_{\mathbf{k}}^{exc}$ while increasing the size of the SWSC. The excitation energy decreases until a dilution comparable to the [$N_{\mathbf{k}} = 512$; $r_s = 0.01$] case is reached.

Table 2: Singlet excitation energies (in eV) for bulk Silicon (PBE functional) as a function of the number of points sampling the Brillouin zone ($N_{\mathbf{k}}$) and the radius of the **k**-point sphere around Γ (r_s). $N_{\mathbf{k}}^{exc}$ indicates the number of points enclosed in the sphere having radius r_s.

$N_{\mathbf{k}}$	r_s	$N_{\mathbf{k}}^{exc}$	E^{exc}
512	0.01	1	2.691
512	0.018	9	4.566
512	0.025	15	4.893
512	0.05	21	5.648
512	0.08	47	5.587
512	0.1	53	6.110
512	0.3	247	9.227
512	0.025	15	4.893
1728	0.015	15	2.972
4096	0.010	15	2.794
5832	0.008	15	2.744
13824	0.005	15	2.621

By progressively increasing r_s we can reach a point in which the whole valence band is excited to the whole conduction band, that is, one electron per unit cell is excited. Such a situation is barely physical, specially in covalently bonded semiconductors. The excitation energy becomes, in fact, extremely high. In the case of LiF (not shown here) excitations are localized, and then the penalty due to a high density of excitons is smaller because they interact little one with another.

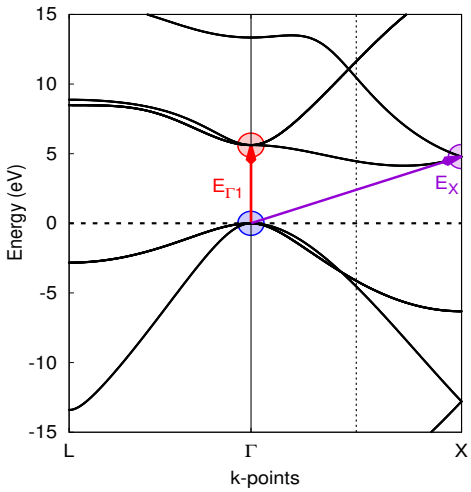

Figure 3: Diamond Band Structure primitive PBE functional

3.2 Geometry Optimization and Luminescence

3.2.1 Nickel Oxide

Even if Nickel Oxide is quite a simple and well known material, its magnetic end electronic properties make it a very interesting system. In a recent work[17] its excited states structure has been studied extensively through Δ-SCF methods within the Crystal code, but with an approach different from MOM. In short, the approach in Ref. 17 consists of forcing an excited state through atomic orbital occupations in the initial guess and eigenvalue shifting. This is in practice a direct space approach, that leads to excitation of entire bands (across the whole BZ) – hence a supercell calculation is mandatory in order to reach a realistic dilution of excitation. Ref. 17 testifies how a detailed analysis of the excitations in NiO must be carried out with great care, given the magnetic phases possible, the number of relevant excited states as well as the delicate role of functional and basis set choice.

Such detailed study goes well beyond the scope of this work. Our aim here is to validate our method on a system that is somewhat more complex than those in Table 1, and to test our excited state optimization algorithm. NiO, in fact, possesses excited states that live long

enough to give rise to observable Stokes shifts. We considered here only the ferromagnetic (FM) phase of NiO, which lends itself well to our purpose because due to its simple structure there are no internal degrees of freedom, so that only the lattice parameter is subject to optimization.

In Figure 4 we present our results. We have considered the three lowest excited states in Γ point – note that NiO has an indirect band gap, so these excitations do not correspond to the band gap - supercells would be needed to reach other parts of the Brillouin zone. Two of such excitations are labeled $\alpha \rightarrow \alpha$ and $\beta \rightarrow \beta$, that is α and β HOMO-LUMO transitions (in our Ferromagnetic phase there are 19 electrons in α bands, and 17 in β ones). The third is the spin-flip excitation from α-HOMO to β-LUMO. These correspond in Figure 4 to green, yellow and red curves, respectively.

For each of the above listed states we have run both a geometry optimization with analytical gradients and a series of single-point calculations. The results clearly shows that our MOM gradients correctly find the right minimum of the excited state curves in all cases, located at 4.45 Å, 4.47 Å and 4.56 Å. The Stokes shifts of 0.44, 0.5 and 1.51 eV reasonably fall within the range of experimental evidences. As said earlier though, out purpose here is mainly of checking internal numerical consistence. As a final note we remark that only a calculation on the primitive unit cell was needed using our MOM approach, while a reciprocal space grid of 8×8×8 points was used, hence describing the excitation of a one electron every 512 unit cells.

3.2.2 Solid CuI(Piperazine)

Among the luminescent copper(I) halides, $[\mathrm{CuI(piperazine)}_{0.5}]_\infty$ is a peculiar compound that exhibits a dual luminescence, a feature that is of potential relevance in technological applications. In recent years, within the framework of a synergic theoretical-experimental study,[18] we have characterized its excitations through *ab initio* post-SCF methods.[37] At that time we were not able to investigate the actual luminescence properties, as we had no tools for

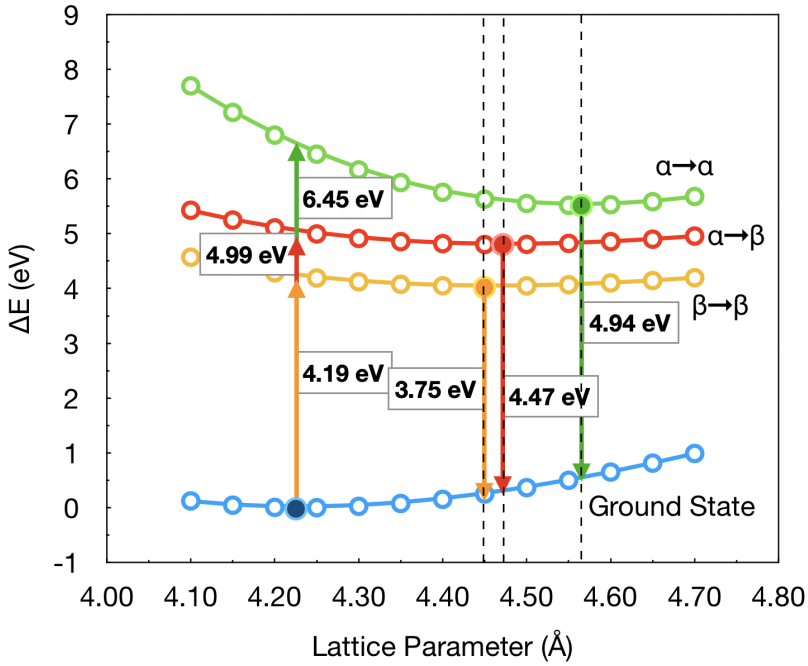

Figure 4: Energy of the ground and first excited states of bulk ferromagnetic NiO as a function of lattice parameter. The ground state minimum is taken as a reference (ΔE=0). B3LYP Functional was used. The full bullets mark the results of the geometry optimizations using analytical gradients as in Eq. (8).

optimizing geometries in the excited state, as we have developed in this work.

We here apply our MOM geometry optimizer to this structure so to analize the structural and electronic changes of the long-lived excited state. As in previous work,[18] we considered two excitations around the Fermi level, namely HOMO→LUMO and HOMO-1→LUMO+1, in Γ-point only. A pob-TZVP basis set was used, along with a hybrid PBE functional with 10% of HF exchange.

The main results of our MOM calculations are reported in Figure 5 and Table 3. From the figures it is seen that the structural relaxation of the excited states leads to mild but significant modifications, mostly seen in the rotation of the organic ring. From Table 3 we also see that the Cu-Cu distance is reduced up to 4% in the highest excitation, and most

notably that the cell parameters undergo quite a change, specially in the HOMO→LUMO excitation which results in a volume expansion. In the HOMO–1→LUMO+1 case the volume does not change so significantly, but a cell distorsion is observed, with an elongation along the c axis.

The effects of the geometry relaxation on the luminescence energies are more pronounced on the highest excitation than on the lowest, with the results of the two corresponding emissions being 3.0 eV and 3.1 eV, respectively. This result is in qualitative agreement with the results of Figure S3 in the supplementary information of Ref. 18, which shows that two excitations exist with markedly different excitation energy but similar emission. Quantitatively, our excitation energies are in reasonable agreement while emission energy are evidently still too large with respect to the experiment. A more detailed study would be needed to clarify this, with a careful analysis of the role of basis sets and functional, which goes beyond the purpose of this paper.

Table 3: Cu-Cu distance and cell parameters (all in Å) for the structures of solid CuI piperazine optimized for the ground and excited states.

	Ground State	HOMO→LUMO	HOMO−1 → LUMO+1
Cu-Cu distance	3.517	3.483	3.384
a,b cell parameters	9.499	9.650	9.503
c cell parameter	6.774	6.805	7.158

4 Conclusions

In this work we have presented a periodic implementation of the Maximum Overlap Method (MOM). It allows to select electronic excitations and optimize geometries of excited states, while keeping a computationally cheap SCF approach as used for the ground state. Due to the iterative transitions from direct to reciprocal space and back, our approach works with excitations that preserve the totalsymmetric nature of the electron density, namely Γ-point excitations or collective excitations in a sphere of k-points around Γ. A calculation

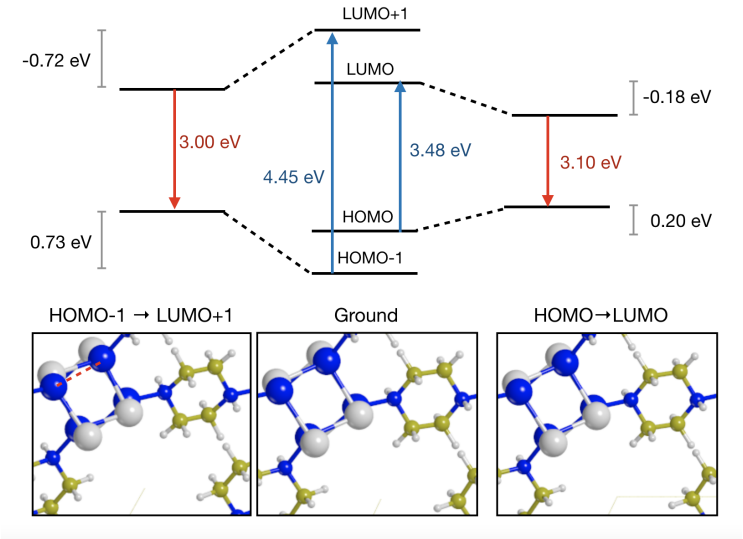

Figure 5: Energy levels and atomic structure of solid CuI-piperazine around the Fermi level at the ground state geometry (center), and at the geometries optimized after an HOMO→LUMO (right) and HOMO-1→LUMO+1 (left) electronic excitation.

using the primitive unit cell allows to describe the excitation of only one electron within the periodic boundary conditions, avoiding costly supercell calculations. Such supercell approach is however needed to access excitations far from the center of the Brillouin Zone.

Through demonstrative applications we have shown how the MOM approach can be easily applied to a variety of crystalline solids, from prototypical simple crystals to complex organic-inorganic frameworks, with full control on the electronic occupations and spins.

As a future perspective we plan to implement vibrational frequencies and representation of electronic densities, which would significantly extend the usefulness and applicability of the approach.

References

(1) Runge, E.; Gross, E. K. Density-functional theory for time-dependent systems. *Phys. Rev. Lett.* **1984**, *52*, 997.

(2) Casida, M. E. *Recent Advances in Density Functional Methods*; pp 155–192.

(3) Foresman, J. B.; Head-Gordon, M.; Pople, J. A.; Frisch, M. J. Toward a systematic molecular orbital theory for excited states. *J. Phys. Chem.* **1992**, *96*, 135–149.

(4) Bene, J. E. D.; Ditchfield, R.; Pople, J. A. Self-Consistent Molecular Orbital Methods. X. Molecular Orbital Studies of Excited States with Minimal and Extended Basis Sets. *J. Chem. Phys.* **1971**, *55*, 2236–2241.

(5) Blase, X.; Duchemin, I.; Jacquemin, D. The Bethe–Salpeter equation in chemistry: relations with TD-DFT, applications and challenges. *Chem. Soc. Rev.* **2018**, *47*, 1022–1043.

(6) Ghosh, S.; Verma, P.; Cramer, C. J.; Gagliardi, L.; Truhlar, D. G. Combining Wave Function Methods with Density Functional Theory for Excited States. *Chem. Rev.* **2018**, *118*, 7249–7292, PMID: 30044618.

(7) Barca, G. M.; Gilbert, A. T.; Gill, P. M. Simple models for difficult electronic excitations. *J. Chem. Theory Comput.* **2018**, *14*, 1501–1509.

(8) Gilbert, A. T.; Besley, N. A.; Gill, P. M. Self-consistent field calculations of excited states using the maximum overlap method (MOM). *J. Phys. Chem. A* **2008**, *112*, 13164–13171.

(9) Besley, N. A.; Gilbert, A. T. B.; Gill, P. M. W. Self-consistent-field calculations of core excited states. *J. Chem. Phys.* **2009**, *130*, 124308.

(10) Jones, R. O.; Gunnarsson, O. The density functional formalism, its applications and prospects. *Rev. Mod. Phys.* **1989**, *61*, 689.

(11) Hellman, A.; Razaznejad, B.; Lundqvist, B. I. Potential-energy surfaces for excited states in extended systems. *J.Chem. Phys.* **2004**, *120*, 4593–4602.

(12) Gavnholt, J.; Olsen, T.; Engelund, M.; Schiøtz, J. Δ self-consistent field method to obtain potential energy surfaces of excited molecules on surfaces. *Phys. Rev. B* **2008**, *78*, 075441.

(13) Ye, H.-Z.; Welborn, M.; Ricke, N. D.; Van Voorhis, T. σ-SCF: A direct energy-targeting method to mean-field excited states. *J. Chem. Phys.* **2017**, *147*, 214104.

(14) Levi, G.; Ivanov, A. V.; Jónsson, H. Variational Density Functional Calculations of Excited States via Direct Optimization. *J. Chem. Theory Comput.* **2020**, *16*, 6968–6982, PMID: 33064484.

(15) Ivanov, A. V.; Levi, G.; Jónsson, E. O.; Jónsson, H. Direct Optimization Method for Variational Excited-State Density Functional Calculations Using Real Space Grid or Plane Waves. 2021.

(16) Hait, D.; Head-Gordon, M. Excited State Orbital Optimization via Minimizing the Square of the Gradient: General Approach and Application to Singly and Doubly Excited States via Density Functional Theory. *J. Chem. Theory Comput.* **2020**, *16*, 1699–1710, PMID: 32017554.

(17) Mackrodt, W. C.; Salustro, S.; Civalleri, B.; Dovesi, R. Low energy excitations in NiO based on a direct Δ-SCF approach. *Journal of Physics: Condensed Matter* **2018**, *30*, 495901.

(18) Maini, L.; Braga, D.; Mazzeo, P.; Maschio, L.; Rérat, M.; Manet, I.; Ventura, B. Dual luminescence in solid CuI (piperazine): hypothesis of an emissive 1-D delocalized excited state. *Dalton Transactions* **2015**, *44*, 13003–13006.

(19) Dovesi, R.; Erba, A.; Orlando, R.; Zicovich-Wilson, C. M.; Civalleri, B.; Maschio, L.; Rérat, M.; Casassa, S.; Baima, J.; Salustro, S.; Kirtman, B. Quantum-mechanical condensed matter simulations with CRYSTAL. *WIRES: Comp. Mol. Sci.* **2018**, *8*, e1360.

(20) Pulay, P. Improved SCF convergence acceleration. *J. Comp. Chem.* **1982**, *3*, 556–560.

(21) Maschio, L. Direct inversion of the iterative subspace (DIIS) convergence accelerator for crystalline solids employing Gaussian basis sets. *Theor. Chem. Acc.* **2018**, *137*, 60.

(22) Doll, K.; Harrison, N. M.; Saunders, V. R. Analytical Hartree-Fock gradients for periodic systems. *Int. J. Quant. Chem.* **2001**, *82*, 1.

(23) Vilela Oliveira, D.; Laun, J.; Peintinger, M. F.; Bredow, T. BSSE-correction scheme for consistent gaussian basis sets of double-and triple-zeta valence with polarization quality for solid-state calculations. *J. Comp. Chem.* **2019**, *40*, 2364–2376.

(24) Daga, L. E.; Civalleri, B.; Maschio, L. Gaussian Basis Sets for Crystalline Solids: All-Purpose Basis Set Libraries vs System-Specific Optimizations. *J. Chem. Theory Comput.* **2020**, *16*, 2192–2201.

(25) Civalleri, B.; Presti, D.; Dovesi, R.; Savin, A. On choosing the best density functional approximation. *Chem. Modell* **2012**, *9*, 168–185.

(26) Medvedev, M. G.; Bushmarinov, I. S.; Sun, J.; Perdew, J. P.; Lyssenko, K. A. Density functional theory is straying from the path toward the exact functional. *Science* **2017**, *355*, 49–52.

(27) Krukau, A. V.; Vydrov, O. A.; Izmaylov, A. F.; Scuseria, G. E. Influence of the exchange screening parameter on the performance of screened hybrid functionals. *J. Chem. Phys.* **2006**, *125*, 224106.

(28) Crowley, J. M.; Tahir-Kheli, J.; Goddard III, W. A. Resolution of the band gap prediction problem for materials design. *J. Phys. Chem. Lett.* **2016**, *7*, 1198–1203.

(29) Lee, I.-H.; Lee, J.; Oh, Y. J.; Kim, S.; Chang, K.-J. Computational search for direct band gap silicon crystals. *Phys. Rev. B* **2014**, *90*, 115209.

(30) Shur, M. S. *Handbook series on semiconductor parameters*; World Scientific, 1996; Vol. 1.

(31) Rohlfing, M.; Krüger, P.; Pollmann, J. Quasiparticle band-structure calculations for C, Si, Ge, GaAs, and SiC using Gaussian-orbital basis sets. *Phys. Rev. B* **1993**, *48*, 17791.

(32) Chelikowsky, J. R.; Cohen, M. L. Nonlocal pseudopotential calculations for the electronic structure of eleven diamond and zinc-blende semiconductors. *Phys. Rev. B* **1976**, *14*, 556.

(33) Persson, C.; Lindefelt, U. Relativistic band structure calculation of cubic and hexagonal SiC polytypes. *J. Appl. Phys.* **1997**, *82*, 5496–5508.

(34) Madelung, O. *Semiconductors: group IV elements and III-V compounds*; Springer Science & Business Media, 2012.

(35) Piacentini, M.; Lynch, D. W.; Olson, C. Thermoreflectance of LiF between 12 and 30 eV. *Phys. Rev. B* **1976**, *13*, 5530.

(36) Roessler, D.; Walker, W. Electronic spectrum of crystalline lithium fluoride. *J. Phys. Chem. Solids* **1967**, *28*, 1507–1515.

(37) Ferrari, A. M.; Orlando, R.; Rérat, M. Ab initio calculation of the ultraviolet–visible (UV-vis) absorption spectrum, electron-loss function, and reflectivity of solids. *J. Chem. Theory Comput.* **2015**, *11*, 3245–3258.

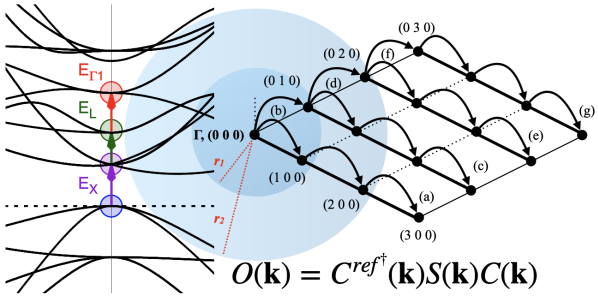

For Table of Contents Only

12.4 Basis Set Optimization Benchmark on Elemental Solids-Paper Draft

In the following drafts of a paper and the relative supplementary material are reported.

Basis Set Optimization Benchmark on Elemental Solids

Loredana Edith Daga, Bartolomeo Civalleri, and Lorenzo Maschio*

Dipartimento di Chimica, Università di Torino and NIS (Nanostructured Interfaces and Surfaces) Centre, Via P. Giuria 5, 10125 Torino, Italy

E-mail: lorenzo.maschio@unito.it

Abstract

In this work we attempt to apply a BDIIS basis set optimization algorithm developed in a previous work[1] to an extended test set based on elementary solids using the CRYSTAL code.[2] In fact, we took inspiration from a paper published in 2016 by Lejaeghere et al.[3] where a systematic work to demonstrate DFT reproducibility is well described. In particular, they calculated equation of states data considering 15 solid state codes, using 40 different potentials or basis set types, to assess the PBE (Perdew-Burke-Ernzerhof) quality for 71 elemental crystals. We tried to reproduce their work for 36 elemental solids, starting from def2-like basis set and optimizing these basis sets by using the BDIIS method. The EOS parameters have been evaluated by fitting 7 energy points around the equilibrium volume. Moreover, we extended the PBE calculation to hybrid functional one, specifically using HSE06 functional.

In quantum mechanical simulations, when dealing with gaussian basis set, the appropriate choice of exponents and coefficients is not a straightforward. The most critical aspect is the sparse availability of basis set database above all for solid states calculations that makes mandatory a proper definition of basis set in this sense. Moreover, molecular basis sets can

not be directly transferred because of their diffuse nature that many times is incompatible with the density of bulk systems and the definition of the basis sets is left to the hands of the user. For this reason, in a previous work we developed a basis set optimizer based on the Direct Inversion of the Iterative Subspace (DIIS)[4,5] to automatically perform the exponents and coefficients optimization in a basis set.[1] We implemented the algorithm in CRYSTAL, which is an ab initio code for quantum mechanical simulation based on gaussian basis functions. In this work we attempt to apply this algorithm to an extended test set based on elementary solids. Taking inspiration from a paper published in 2016 by Lejaeghere et al.[3] where a systematic work to demonstrate DFT reproducibility is well described, we considered 36 elemental solids and starting from def2-like basis set,[6] we optimized these basis sets by using the BDIIS method. The eos parameters have been evaluated as criterion for comparison. Regarding the basis set, they are derived by def2-TZVP, optimizing valence and polarization functions that are the ones relevantly changing in a different chemical environment. In some cases (e.g. noble gases) more extended basis set have been used like def2-QZVP. Behind this, the optimized basis sets are named dcm-TZ or dcm-QZ in the following. As regards geometry and structural parameters they were provided by the Ref.,[3] to which we add the FIXINDEX option of CRYSTAL.[7] In fact, when the geometrical and/or the basis set parameters of the system are changed, maintaining the symmetry and the setting, the truncation criteria of the Coulomb and exchange series, based on overlap can lead to the selection of different numbers of bi-electronic integrals. This may be the origin of numerical noise in the optimization curve. When small changes are made on the lattice parameter or on the Gaussian orbital exponents, the indices of the integrals to be calculated can be selected for a reference geometry (or basis set), "frozen", and used to compute the corresponding integrals with the modified geometry (or basis set). The reference geometry considered corresponds to the most compact structure, thus the one with the smallest volume.

Concerning the functional, as mentioned earlier, PBE functional has been used and an extension to hybrid functional is proposed. In particular, HSE06 functional was adopted.

Other more technical details like energy thresholds and k-mesh grid are reported in the Supplementary Material available in Appendix.

Moreover, as outlined at the beginning, an extensive test set range from Hydrogen to Krypton was used by taking the ground state crystal structures of elemental solids in their most common symmetry geometries.

As mentioned earlier, the benchmark is performed evaluating the equation of states parameters (EOS).

Three are the equations of state (EOS) parameters commonly used for accuracy assessments:

- Volume (V) and the equilibrium volume (V_0)
- Bulk Modulus: resistance to volume changes (B_0). The bulk modulus is closely related to the energy curve $E(V)$ and it is proportional to the curvature of the equation of state at the equilibrium volume. It represents the resistance of the unloaded material to volume change, and hence to uniform pressure (P). Since it is linked to the curvature of the $E(V)$ relation, B_0 is a numerically sensitive quantity. A small deviation at a few data points is already able to change its value noticeably, especially when the bulk modulus is small and a narrow volume range is studied.
- Pressure Derivative of the Bulk Modulus: one order higher effects (B_1). It is a third-order derivative of the energy and hence describes effects that are one order higher even than the bulk modulus. It is related to the volume dependence of the $E(V)$ curvature and it is therefore the most sensitive quantity.

The equations of state (EOS) parameters are usually obtained using a common third-order Birch-Murnaghan relation.[8]

In general, one can extract the equilibrium energy and EOS parameters by fitting few $E(V)$ data points to an empirical equation of state. In this specific work 7 data points were used for the fitting procedure.

In fact, for each elemental solid, 7 different inputs have been prepared, with distinct volume ($0.94 \cdot V$, $0.96 \cdot V$, $0.98 \cdot V$, V, $1.02 \cdot V$, $1.04 \cdot V$ and $1.06 \cdot V$, where V is the volume obtained with the original geometry). In particular, we multiplied the starting lattice parameters by the cubic root of the percentage (e.g. for the 94%, we multiplied the lattice parameters by $\sqrt[3]{0.94} = 0.9796$).

Then we applied the third-order Birch-Murnaghan relation and the fitting procedure described above to get V_0, B_0 and B_1. In particular, for the fitting we used a script provided by Ref.[3]

The comparison between CRYSTAL and the other codes have been performed in terms of Δ gauge. It expresses the root-mean-square difference between the equations of state of two codes a and b, that for each element i is given by the formula:

$$\Delta_i(a,b) = \sqrt{\int_{0.94V_{0,i}}^{1.06V_{0,i}} \frac{(E_{b,i}(V) - E_{a,i}(V))^2}{0.12V_{0,i}} dV} \tag{1}$$

where $V_{0,i}$ is the equilibrium volume, $E_{b,i}(V)$ and $E_{a,i}(V)$ are the energies calculated by performing the 7 equidistant $E(V)$ data points abovementioned.

Even in this case a script has been provided by Ref.[3]

A comparison of Δ_i values allows the expression of EOS differences as a single number, and a small Δ_i automatically implies small deviations between equilibrium volumes, bulk moduli, or any other EOS-derived observables. The overall difference Δ between methods a and b is obtained by averaging Δ_i over all elemental crystals in the benchmark set.

Many tests have been performed and three levels of accuracy have been obtained at the PBE level (see Fig. 1 for EOS comparison):

- *CRYSTAL-TZ*

  Triple-ζ Basis Sets optimized by the BDIIS algorithm are used for all cases. EOS parameters and simulation set up in Table 1 of the Supplementary Material. Comparing our data with WIEN2K results (Ref.[3]), we may observe in the volume comparison a

pretty large divergence in the noble gases (He, Ne, Ar, Kr) which has repercussions above all in the bulk modulus derivative.

- *CRYSTAL-TZ/acc*

  Triple-ζ Basis Sets optimized by the BDIIS algorithm for almost all cases excepting some basis sets that have been handly adjusted. In fact, some diffused functions removed before the basis set optimization, were added a posteriori (e.g. Mg, Si, P, Ga) and in some cases a check on the consistency of the valence exponents with respect to core ones have been performed (e.g. Ca, Cr, Fe, Ge). In two specific cases (Ni, Zn) we resorted to the introduction of sp shells that shown improved results. The Cu case was particularly difficult, so we optimized a different kind of basis set (86-4111(41D) from[9]). In some particular cases (Se, Br, Sc) a full geometry optimization was mandatory to define the reference volume. EOS parameters and simulation set up are reported in Table 2 of the Supplementary Material.

- *CRYSTAL/acc*

  Considering the previous point, we adopted larger basis sets in some critical cases (He, Ne, Na, Al, Ar, Ti, V, Mn, Co, Zn, Ge, As, Kr). EOS parameters and simulation set up are reported in Table 3 of the Supplementary Material. The improvement in this set is rather effective: looking at the Fig. 1 the largest discrepancy in noble gases and some transition metals is reduced, demonstrating that this set can average the oscillations previously seen.

All the basis sets obtained and used for the calculation are listed in the Supplementary Material.

In general, going from V_0 to B_1 we may note an increasing of uncertainty because of the wide range of results available. This implied large error bars (e.g. Fe, Mn) due to the intrinsic formula derivation of the B_0 and B_1. Nevertheless, a good agreement is obtained using the CRYSTAL code with respect with the other code. Special attention has to be

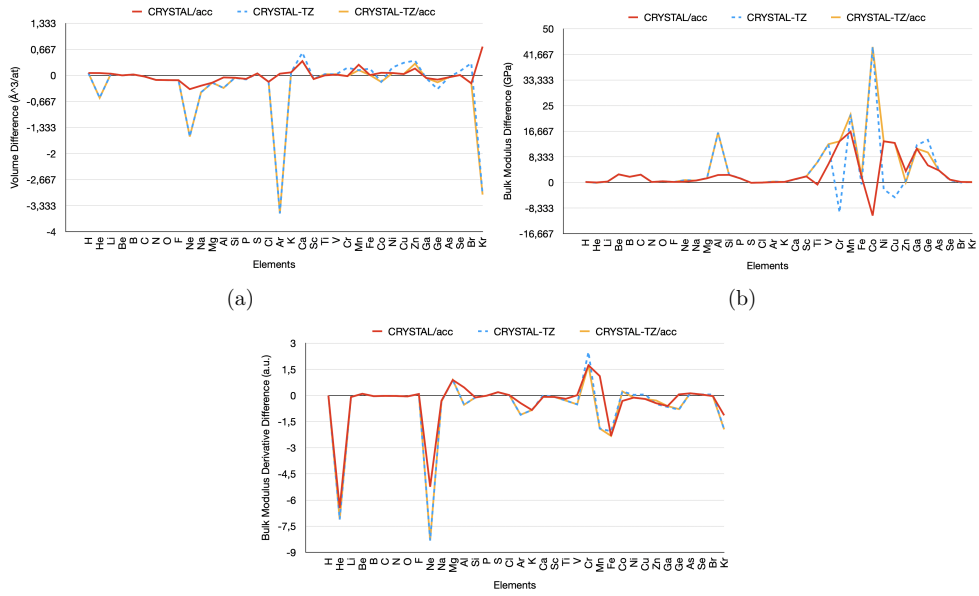

Figure 1: Difference between this work and WIEN2K/acc set reported by Ref.[3] *CRYSTAL-TZ*, *CRYSTAL-TZ/acc* and *CRYSTAL/acc* are shown by blue dotted, yellow and red lines for the EOS parameters: equilibrium volume (a), bulk modulus (b) and bulk modulus derivatives (c).

taken in the case of noble gases because the model adopted enforces these elements in a condensed phase that is not always well described by solid state codes.

Considering the *CRYSTAL/acc* set our Δ gauge values are smaller than 1 with respect to other all electron calculations (see Table 1). This demonstrates that CRYSTAL can reproduce the plane waves results if rather good basis sets are used. An extended comparison with others codes is reported in Table 4 of the Supplementary Material.

Starting from our best set up (*CRYSTAL/acc*), we also extended this work by using Hybrid Functional (HSE06) instead of PBE functional. In fact, with CRYSTAL and in particular with Gaussian Functions, Hybrid Functionals are easy and relatively cheap to be implemented. Moreover, it is well known that hybrids improve accuracy for crystal computations. In Fig. 1 and 2 of the supplementary information EOS parameters evaluated

by using CRYSTAL with PBE and HSE06 functional and other codes with PBE functional are reported graphically for all the elemental solids considered. Relative differences between PBE and HSE06 are reported as well.

Despite of the huge variety of data in particular in the case of the bulk modulus derivative, CRYSTAL can interpolate pretty well the data. In particular, the hybrid functional seems to be a good compromise in some cases, averaging the data dispersion (e.g. Cr, Mn). Looking at the relative differences between functionals, while differences with respect to V_0 and B_1 are less pronounced, in some cases B_0 values deviate more. These problems can be due to the absence of a proper description of noncovalent interactions. This description requires the inclusion of long range electron correlation effects that are missing in DFT methods. In particular, the treatment of the weak London forces can be crucial in some elemental solids (e.g. Cl) because of their attractive and ubiquitous nature.

Table 1: Δ values for comparison between all-electron (AE) DFT methods considered in the Ref. 3 with CRYSTAL code (this work). In green, blue and yellow three different accuracy levels adopted in this work.

		AE									
		E1k	exciting	FHI-aims/tier2	FLEUR	FPLO/T+F+s	RSPt	WIEN2k/acc	CRYSTAL-TZ	CRYSTAL-TZ/acc	CRYSTAL/acc
AE	E1k		0.3	0.3	0.6	1.0	0.9	0.3	2.4	1.5	1.0
	exciting	0.3		0.1	0.5	0.9	0.8	0.2	2.3	1.4	0.9
	FHI-aims/tier2	0.3	0.1		0.5	0.9	0.8	0.2	2.3	1.3	0.9
	FLEUR	0.6	0.5	0.5		0.8	0.6	0.4	2.3	1.5	0.9
	FPLO/T+F+s	1.0	0.9	0.9	0.8		0.9	0.9	2.6	1.7	1.2
	RSPt	0.9	0.8	0.8	0.6	0.9		0.8	2.6	1.8	1.3
	WIEN2k/acc	0.3	0.2	0.2	0.4	0.9	0.8		2.4	1.5	0.9
	CRYSTAL-TZ	2.4	2.3	2.3	2.3	2.6	2.6	2.4			
	CRYSTAL-TZ/acc	1.5	1.4	1.3	1.5	1.7	1.8	1.5			
	CRYSTAL/acc	1.0	0.9	0.9	0.9	1.2	1.3	0.9			

In conclusion, we may state that with gaussian basis functions it is possible to reach the planewaves accuracy, if an appropriate choice of exponents and coefficients is considered. In

particular, the basis set optimizer was a fundamental tool to automatize a calibration that usually is handly performed. Next development will be to enhance even more the overall quality by using different kind of basis sets instead of the def2-like ones and trying to optimize the set up as much as possible.

References

(1) Daga, L. E.; Civalleri, B.; Maschio, L. Gaussian Basis Sets for Crystalline Solids: All-Purpose Basis Set Libraries vs System-Specific Optimizations. *Journal of chemical theory and computation* **2020**, *16*, 2192–2201.

(2) Dovesi, R.; Erba, A.; Orlando, R.; Zicovich-Wilson, C. M.; Civalleri, B.; Maschio, L.; Rérat, M.; Casassa, S.; Baima, J.; Salustro, S., et al. Quantum-mechanical condensed matter simulations with CRYSTAL. *Wiley Interdisciplinary Reviews: Computational Molecular Science* **2018**, *8*, e1360.

(3) Lejaeghere, K.; Bihlmayer, G.; Björkman, T.; Blaha, P.; Blügel, S.; Blum, V.; Caliste, D.; Castelli, I. E.; Clark, S. J.; Dal Corso, A., et al. Reproducibility in density functional theory calculations of solids. *Science* **2016**, *351*.

(4) Pulay, P. Convergence acceleration of iterative sequences. The case of SCF iteration. *Chemical Physics Letters* **1980**, *73*, 393–398.

(5) Pulay, P. Improved SCF convergence acceleration. *Journal of Computational Chemistry* **1982**, *3*, 556–560.

(6) Pritchard, B. P.; Altarawy, D.; Didier, B.; Gibson, T. D.; Windus, T. L. New basis set exchange: An open, up-to-date resource for the molecular sciences community. *Journal of chemical information and modeling* **2019**, *59*, 4814–4820.

(7) Dovesi, R.; Saunders, V.; Roetti, C.; Orlando, R.; Zicovich-Wilson, C.; Pascale, F.; Civalleri, B.; Doll, K.; Harrison, N.; Bush, I., et al. CRYSTAL17. **2017**,

(8) Lejaeghere, K.; Van Speybroeck, V.; Van Oost, G.; Cottenier, S. Error estimates for solid-state density-functional theory predictions: an overview by means of the ground-state elemental crystals. *Critical Reviews in Solid State and Materials Sciences* **2014**, *39*, 1–24.

(9) Doll, K.; Harrison, N. Chlorine adsorption on the Cu (111) surface. *Chemical Physics Letters* **2000**, *317*, 282–289.

Supplementary Material for: [Basis Set Optimization Benchmark on Elemental Solids]

Loredana Edith Daga, Bartolomeo Civalleri, and Lorenzo Maschio*

Dipartimento di Chimica, Università di Torino and NIS (Nanostructured Interfaces and Surfaces) Centre, Via P. Giuria 5, 10125 Torino, Italy

E-mail: lorenzo.maschio@unito.it

1 CRYSTAL calculation settings and results per element

Table 1: **Triple-ζ Basis Sets (CRYSTAL-TZ)**: Equilibrium volume per atom V_0, bulk modulus B_0, pressure derivative of the bulk modulus B_1 per atom are reported. Triple-ζ Basis Sets optimized by the BDIIS algoritm are used for all cases. Bottom: general settings adopted. Functional: PBE.

	Settings	$\mathbf{V_0}$[Å^3/atom]	$\mathbf{B_0}$[GPa]	$\mathbf{B_1}$[-]
H	d	17.44986	10.447010	2.7070
He	d	17.19820	0.7362300	0.5920
Li	d	20.26302	14.138050	3.2490
Be	d	7.911840	125.54068	3.1350
B	d	7.263740	239.13867	3.4300
C	d	11.60751	211.52700	3.5560
N	d	28.76965	54.362750	3.6960
O	d	18.44028	51.762370	3.8430
F	d	19.04538	34.484400	4.0200
Ne	d	22.68457	2.1821900	6.1120
Na	d	37.03582	8.0842500	3.4280
Mg	d	22.74905	37.360660	4.9520
Al	d	16.15990	94.296210	4.0390
Si	d	20.39044	91.083380	4.1920
P	d	21.36948	69.588750	4.3400
S	d	17.23478	83.297990	4.4510
Cl	d	38.72609	19.048840	4.3650
Ar	d	48.85259	1.0365100	6.1500
K	d	73.75765	3.7363800	3.7580
Ca	d	42.78248	18.115170	3.3250
Sc	nd	24.53525	56.432050	3.3400
Ti	d	17.42277	118.82425	3.2890
V	d	13.48150	194.13447	3.2340
Cr	d	11.96955	174.14310	9.6540
Mn	d	11.58163	140.70827	-2.101
Fe	d	11.51764	197.02481	3.7440
Co	d	10.69924	260.62293	4.5960
Ni	d'	11.09556	197.75067	5.0430
Cu	d	12.28056	136.29997	4.9050
Zn	d"	15.57550	75.138260	4.7750
Ga	nd	20.23426	61.376780	4.7250
Ge	d	23.56844	73.010710	4.1740
As	d	22.54166	72.200820	4.3500
Se	d	29.85513	47.794520	4.5030
Br	d	39.76136	22.394070	4.9250
Kr	d	62.60814	0.8459800	7.9120

	SCF convergence	Monkhorst Pack (MP) shrinking factor	Coulomb and Exchange truncation criteria
d	8	8 8	8 8 8 8 16
nd	8	12 24	12 12 12 12 12
d'	10	12 24	10 10 10 20 50
d"	8	24 24	10 10 10 15 20

Table 2: **Triple-ζ Basis Sets - enhancement (CRYSTAL-TZ/acc)**: Equilibrium volume per atom V_0, bulk modulus B_0, pressure derivative of the bulk modulus B_1 per atom are reported. Triple-ζ Basis Sets optimized by the BDIIS algoritm and handly adjusted (mod) are used for all cases. Bottom: general settings adopted. In some cases a full geometry optimization was mandatory to define the reference volume (geom). Functional: PBE.

	Settings	$\mathbf{V_0}$[Å^3/atom]	$\mathbf{B_0}$[GPa]	$\mathbf{B_1}$[-]
H	d	17.44986	10.447010	2.7070
He	d	17.19820	0.7362300	0.5920
Li	d	20.26302	14.138050	3.2490
Be	d	7.911840	125.54068	3.1350
B	d	7.263740	239.13867	3.4300
C	d	11.60751	211.52700	3.5560
N	d	28.76965	54.362750	3.6960
O	d	18.44028	51.762370	3.8430
F	d	19.04538	34.484400	4.0200
Ne	d	22.68457	2.1821900	6.1120
Na	d	37.03582	8.0842500	3.4280
Mg	d-mod	22.75141	37.290830	4.9580
Al	d	16.15990	94.296210	4.0390
Si	d-mod	20.39408	91.015100	4.1930
P	d-mod	21.38203	69.541080	4.3370
S	d	17.23478	83.297990	4.4510
Cl	d	38.72609	19.048840	4.3650
Ar	d	48.85259	1.0365100	6.1500
K	d	73.75765	3.7363800	3.7580
Ca	d-mod	42.56499	18.207790	3.2360
Sc	nd-geom	24.52808	56.359960	3.3370
Ti	d	17.42277	118.82425	3.2890
V	d	13.48150	194.13447	3.2340
Cr	d-mod	11.75456	197.29529	8.8910
Mn	d	11.58163	140.70827	-2.101
Fe	d-mod	11.35441	199.51433	3.4800
Co	d	10.69924	260.62293	4.5960
Ni	d'-mod	10.95258	213.37568	4.8840
Cu	d-mod	11.99283	153.98757	4.6460
Zn	d"-mod	15.49599	74.611400	4.9800
Ga	d-mod	20.24136	60.234630	4.7760
Ge	d-mod	23.73880	68.901330	4.2060
As	d	22.54166	72.200820	4.3500
Se	d-geom	29.75445	47.980380	4.4970
Br	d-geom	39.24538	22.580770	4.8370
Kr	d	62.60814	0.8459800	7.9120

	SCF convergence	Monkhorst Pack (MP) shrinking factor	Coulomb and Exchange truncation criteria
d	8	8 8	8 8 8 8 16
nd	8	12 24	12 12 12 12 12
d'	10	12 24	10 10 10 20 50
d"	8	24 24	10 10 10 15 20

Table 3: **Triple-ζ Basis Sets and larger Basis Sets - enhancement (CRYSTAL/acc)**: Equilibrium volume per atom V_0, bulk modulus B_0, pressure derivative of the bulk modulus B_1 per atom are reported. Triple-ζ Basis Sets and larger basis sets optimized by the BDIIS algoritm and handly adjusted (mod) basis sets are used for all cases. Bottom: general settings adopted. In some cases a full geometry optimization was mandatory to define the reference volume (geom). Functional: PBE.

	Settings	$\mathbf{V_0}$[Å^3/atom]	$\mathbf{B_0}$[GPa]	$\mathbf{B_1}$[-]
H	d	17.44986	10.447010	2.7070
He	d-QZ	17.83233	0.8479900	1.2520
Li	d	20.26302	14.138050	3.2490
Be	d	7.911850	125.53709	3.1350
B	d	7.263740	239.13867	3.4300
C	d	11.60751	211.52700	3.5560
N	d	28.76965	54.362750	3.6960
O	d	18.44028	51.762370	3.8430
F	d	19.04538	34.484400	4.0200
Ne	d-ccpV5z	23.89798	1.6825500	9.1970
Na	d-QZ	37.20596	8.1014900	3.4680
Mg	d-mod	22.75141	37.290830	4.9580
Al	nd-QZ	16.42948	80.505540	5.0330
Si	d-mod	20.39408	91.015100	4.1930
P	d-mod	21.38203	69.541080	4.3370
S	d	17.23478	83.297990	4.4510
Cl	d	38.72609	19.048840	4.3650
Ar	d-QZ	52.42994	0.8346000	6.8180
K	d	73.75765	3.7363800	3.7580
Ca	d-mod	42.56499	18.207790	3.2360
Sc	nd-geom	24.52808	56.359960	3.3370
Ti	d-QZ	17.39161	111.52881	3.3930
V	nd-QZ	13.47247	187.68420	3.7610
Cr	d-mod	11.75456	197.29529	8.8910
Mn	nd-QZ	11.60862	139.61945	0.7240
Fe	d-mod	11.35441	199.51433	3.4800
Co	nd-geom-QZ	10.93250	205.69750	4.0500
Ni	d'-mod	10.95258	213.37568	4.8840
Cu	d-mod	11.99283	153.98757	4.6460
Zn	d"-geom-QZ	15.37220	78.232000	4.8260
Ga	nd-mod	20.24136	60.234630	4.7760
Ge	d-QZ	23.80755	64.708580	5.0520
As	d-QZ	22.54166	72.200820	4.3500
Se	d-geom	29.75445	47.980380	4.4970
Br	d-geom	39.24538	22.580770	4.8370
Kr	d-QZ	66.39630	0.7651800	8.7190

	SCF convergence	Monkhorst Pack (MP) shrinking factor	Coulomb and Exchange truncation criteria
d	8	8 8	8 8 8 8 16
nd	8	12 24	12 12 12 12 12
d'	10	12 24	10 10 10 20 50
d"	8	24 24	10 10 10 15 20

Table 4: Δ values for comparison between the DFT methods considered in the Ref. 1 with CRYSTAL code (this work). In green, blue and yellow three different accuracy levels adopted in this work.

		AE									
		E1k	exciting	FHI-aims/tier2	FLEUR	FPLO/T+F+s	RSPt	WIEN2k/acc	CRYSTAL-TZ	CRYSTAL-TZ/acc	CRYSTAL/acc
AE	E1k		0.3	0.3	0.6	1.0	0.9	0.3	2.4	1.5	1.0
	exciting	0.3		0.1	0.5	0.9	0.8	0.2	2.3	1.4	0.9
	FHI-aims/tier2	0.3	0.1		0.5	0.9	0.8	0.2	2.3	1.3	0.9
	FLEUR	0.6	0.5	0.5		0.8	0.6	0.4	2.3	1.5	0.9
	FPLO/T+F+s	1.0	0.9	0.9	0.8		0.9	0.9	2.6	1.7	1.2
	RSPt	0.9	0.8	0.8	0.6	0.9		0.8	2.6	1.8	1.3
	WIEN2k/acc	0.3	0.2	0.2	0.4	0.9	0.8		2.4	1.5	0.9
	CRYSTAL-TZ	2.4	2.3	2.3	2.3	2.6	2.6	2.4			
	CRYSTAL-TZ/acc	1.5	1.4	1.3	1.5	1.7	1.8	1.5			
	CRYSTAL/acc	1.0	0.9	0.9	0.9	1.2	1.3	0.9			
PAW	GBRV12/ABINIT	0.9	0.8	0.8	0.9	1.3	1.1	0.8	2.9	2.2	1.7
	GPAW09/ABINIT	1.3	1.3	1.3	1.3	1.7	1.5	1.3	2.1	1.9	1.3
	GPAW09/GPAW	1.5	1.5	1.5	1.5	1.8	1.7	1.5	2.2	2.0	1.4
	JTH02/ABINIT	0.6	0.6	0.6	0.6	0.9	0.7	0.5	2.5	1.5	1.0
	PSlib100/QE	0.9	0.8	0.8	0.8	1.3	1.1	0.8	2.8	1.9	1.6
	VASPGW2015/VASP	0.4	0.4	0.4	0.6	1.0	0.8	0.3	2.4	1.5	1.0
USPP	GBRV14/CASTEP	1.1	1.1	1.0	1.0	1.4	1.3	1.0	2.9	2.3	1.8
	GBRV14/QE	1.0	1.0	0.9	1.0	1.4	1.3	1.0	2.8	2.3	1.8
	OTFG9/CASTEP	0.4	0.5	0.5	0.7	1.0	1.0	0.5	2.4	1.5	1.0
	SSSP/QE	0.4	0.3	0.3	0.5	0.9	0.8	0.3	2.6	1.8	1.3
	Vdb2/DACAPO	6.3	6.3	6.3	6.3	6.4	6.5	6.2	6.5	6.8	3.9
NCPP	FHI98pp/ABINIT	13.5	13.4	13.4	13.2	13.0	13.2	13.4	9.5	10.8	10.0
	HGH/ABINIT	2.2	2.2	2.2	2.0	2.3	2.2	2.1	2.8	2.6	1.6
	HGH-NLCC/BigDFT	1.1	1.1	1.1	1.0	1.2	1.1	1.0	2.7	2.0	1.6
	MBK2013/OpenMX	2.1	2.1	2.1	1.9	1.8	1.8	2.0	2.9	2.6	2.0
	ONCVPSP(PD0.1)/ABINIT	0.7	0.7	0.7	0.6	1.0	0.8	0.6	2.3	1.5	1.0
	ONCVPSP(SG15)1/QE	1.4	1.3	1.3	1.3	1.6	1.5	1.3	2.9	2.8	2.0
	ONCVPSP(SG15)2/CASTEP	1.4	1.4	1.4	1.3	1.6	1.5	1.4	2.9	2.8	2.0

2 Hybrid Funcional

In the following a comparison between CRYSTAL/acc with PBE functional and HSE06 hybrid functional.

Table 5: **Triple-ζ Basis Sets and larger Basis Sets - enhancement HSE06 (CRYSTAL/acc HSE06)**: Equilibrium volume per atom V_0, bulk modulus B_0, pressure derivative of the bulk modulus B_1 per atom are reported. Triple-ζ Basis Sets and larger basis sets optimized by the BDIIS algoritm are used for all cases. Bottom: general settings adopted. Functional: HSE06.

	Settings	$\mathbf{V_0}$[Å^3/atom]	$\mathbf{B_0}$[GPa]	$\mathbf{B_1}$[-]
H	d	17.07598	10.933980	2.6330
He	d	18.14868	0.7175000	0.6620
Li	nd	20.52171	13.915170	3.2930
Be	d'	7.889280	126.36884	3.2240
B	nd	7.172230	250.67233	3.3740
C	d	11.37922	226.86298	3.4870
N	d	27.75615	61.100070	3.6080
O	d	17.56863	63.823460	3.8200
F	d	17.67763	42.495510	4.0120
Ne	d	24.13954	1.2869400	10.338
Na	d	37.83911	7.9564800	3.3910
Mg	d	22.66114	38.771100	4.8360
Al	d	16.39101	82.843060	3.4960
Si	d	20.07636	100.22423	4.0710
P	d	20.79507	79.994870	4.2840
S	d	16.50503	98.126070	4.2790
Cl	d	37.45049	21.621890	4.3380
Ar	d	52.50612	0.6937900	7.2140
K	d	75.80466	3.6033600	3.7340
Ca	d	43.90674	17.767720	3.8670
Sc	d	25.23948	61.103850	2.9440
Ti	d	17.21577	129.22367	3.5370
V	d	13.16732	211.95973	2.9210
Cr	d	13.77314	134.91149	3.6970
Mn	d"	15.92248	87.102850	3.5120
Fe	d	12.07484	218.82747	2.2700
Co	nd	10.84894	204.08614	4.6270
Ni	d	10.67155	221.05390	5.4990
Cu	d	12.01562	141.05028	4.8290
Zn	d	15.24572	75.760530	5.2720
Ga	nd	19.72027	70.036730	4.5240
Ge	d	23.07030	76.871350	4.6590
As	d	21.76057	82.098560	4.4760
Se	d	28.71663	55.147710	4.4960
Br	d	37.89302	25.820960	4.8470
Kr	d	88.31656	0.6582000	9.2890

	SCF convergence	Monkhorst Pack (MP) shrinking factor	Coulomb and Exchange truncation criteria
d	8	8 8	8 8 8 12 24
nd	8	12 24	8 8 8 12 24
d'	8	12 24	8 8 8 12 36
d"	8	12 24	10 10 10 20 50

Table 6: Equilibrium volume per atom V_0, bulk modulus B_0, pressure derivative of the bulk modulus B_1 per atom is reported for CRYSTAL/acc PBE and CRYSTAL/acc HSE06. Functional: PBE and HSE06. Differences are reported in the last three columns.

	CRYSTAL/acc PBE			**CRYSTAL/acc HSE06**			**Δ PBE-HSE06**		
	$\mathbf{V_0}$[Å^3/atom]	$\mathbf{B_0}$[GPa]	$\mathbf{B_1}$[-]	$\mathbf{V_0}$[Å^3/atom]	$\mathbf{B_0}$[GPa]	$\mathbf{B_1}$[-]	$\mathbf{V_0}$[Å^3/atom]	$\mathbf{B_0}$[GPa]	$\mathbf{B_1}$[-]
H	17.44986	10.447010	2.7070	17.07598	10.933980	2.6330	0.37	-0.49	0.07
He	17.83233	0.8479900	1.2520	18.14868	0.7175000	0.6620	-0.32	0.13	0.59
Li	20.26302	14.138050	3.2490	20.52171	13.915170	3.2930	-0.26	0.22	-0.04
Be	7.911850	125.53709	3.1350	7.889280	126.36884	3.2240	0.02	-0.83	-0.09
B	7.263740	239.13867	3.4300	7.172230	250.67233	3.3740	0.09	-11.53	0.06
C	11.60751	211.52700	3.5560	11.37922	226.86298	3.4870	0.23	-15.34	0.07
N	28.76965	54.362750	3.6960	27.75615	61.100070	3.6080	1.01	-6.74	0.09
O	18.44028	51.762370	3.8430	17.56863	63.823460	3.8200	0.87	-12.06	0.02
F	19.04538	34.484400	4.0200	17.67763	42.495510	4.0120	1.37	-8.01	0.01
Ne	23.89798	1.6825500	9.1970	24.13954	1.2869400	10.338	-0.24	0.40	-1.14
Na	37.20596	8.1014900	3.4680	37.83911	7.9564800	3.3910	-0.63	0.15	0.08
Mg	22.75141	37.290830	4.9580	22.66114	38.771100	4.8360	0.09	-1.48	0.12
Al	16.42948	80.505540	5.0330	16.39101	82.843060	3.4960	0.04	-2.34	1.54
Si	20.39408	91.015100	4.1930	20.07636	100.22423	4.0710	0.32	-9.21	0.12
P	21.38203	69.541080	4.3370	20.79507	79.994870	4.2840	0.59	-10.45	0.05
S	17.23478	83.297990	4.4510	16.50503	98.126070	4.2790	0.73	-14.83	0.17
Cl	38.72609	19.048840	4.3650	37.45049	21.621890	4.3380	1.28	-2.57	0.03
Ar	52.42994	0.8346000	6.8180	52.50612	0.6937900	7.2140	-0.08	0.14	-0.40
K	73.75765	3.7363800	3.7580	75.80466	3.6033600	3.7340	-2.05	0.13	0.02
Ca	42.56499	18.207790	3.2360	43.90674	17.767720	3.8670	-1.34	0.44	-0.63
Sc	24.52808	56.359960	3.3370	25.23948	61.103850	2.9440	-0.71	-4.74	0.39
Ti	17.39161	111.52881	3.3930	17.21577	129.22367	3.5370	0.18	-17.69	-0.14
V	13.47247	187.68420	3.7610	13.16732	211.95973	2.9210	0.31	-24.28	0.84
Cr	11.75456	197.29529	8.8910	13.77314	134.91149	3.6970	-2.02	62.38	5.19
Mn	11.60862	139.61945	0.7240	15.92248	87.102850	3.5120	-4.31	52.52	-2.79
Fe	11.35441	199.51433	3.4800	12.07484	218.82747	2.2700	-0.72	-19.31	1.21
Co	10.93250	205.6975	4.0500	10.84894	204.08614	4.6270	0.08	1.61	-0.58
Ni	10.95258	213.37568	4.8840	10.67155	221.05390	5.4990	0.28	-7.68	-0.61
Cu	11.99283	153.98757	4.6460	12.01562	141.05028	4.8290	-0.02	12.94	-0.18
Zn	15.37220	78.23200	4.8260	15.24572	75.760530	5.2720	0.13	2.47	-0.45
Ga	20.24136	60.234630	4.7760	19.72027	70.036730	4.5240	0.52	-9.80	0.25
Ge	23.80755	64.708580	5.0520	23.07030	76.871350	4.6590	0.74	-12.16	0.39
As	22.54166	72.200820	4.3500	21.76057	82.098560	4.4760	0.78	-9.90	-0.13
Se	29.75445	47.980380	4.4970	28.71663	55.147710	4.4960	1.04	-7.17	0.00
Br	39.24538	22.580770	4.8370	37.89302	25.820960	4.8470	1.35	-3.24	-0.01
Kr	66.39630	0.765180	8.7190	88.31656	0.6582000	9.2890	-21.92	0.11	-0.57

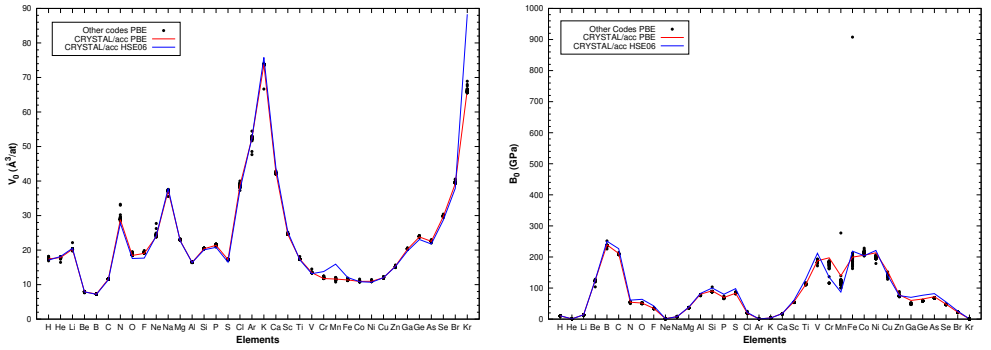

Figure 1: Equilibium volumes (left) and bulk moduli (right) per atoms with the CRYSTAL code/acc (PBE and HSE06 functional) and the DFT methods of other codes (PBE functional).

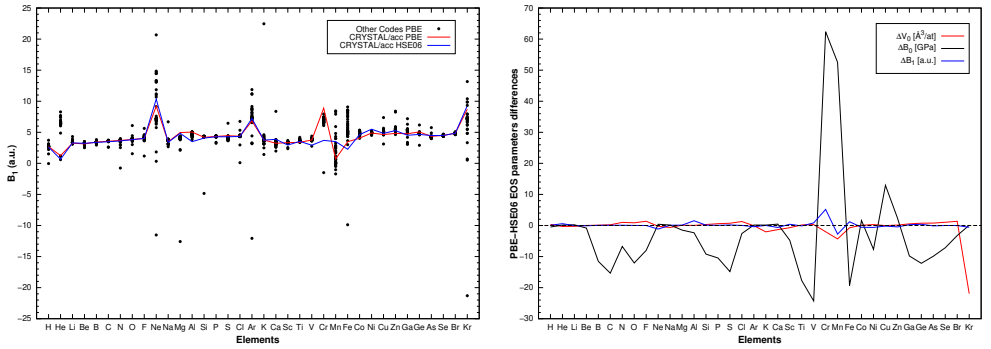

Figure 2: (Left) First order bulk modulus derivatives per atoms with the CRYSTAL code/acc (PBE and HSE06 functional) and the DFT methods of other codes (PBE functional). (Right) EOS parameters differences between CRYSTAL/acc PBE and CRYSTAL/acc HSE06.

The basis sets reported below are the ones obtained by using the optimizer BDIIS and adopted in this work. The shells involved in the optimization are labelled by a star. For more details about the optimization procedure refer to Ref. 2. The *mod* abbreviation is related with the same basis set handly modified.

```
 H - triple ζ

  1  4
0 0  3  1. 1.
   3.40613410000E+01   6.02519780000E-03
   5.12357460000E+00   4.50210940000E-02
   1.16466260000E+00   2.01897260000E-01
0 0  1  0. 1. *
   3.65113151366E-01   1.00000000000E+00
0 0  1  0. 1. *
   1.28206219779E-01   1.00000000000E+00
0 2  1  0. 1. *
   9.69135593351E-01   1.00000000000E+00

 He - triple ζ

  2  4
0 0  3  2. 1.
   9.80783216160E+01   7.58030649670E-03
   1.47644042470E+01   5.48486209370E-02
   3.31858314730E+00   2.20743821860E-01
0 0  1  0. 1. *
   8.57313220271E-01   1.00000000000E+00
0 0  1  0. 1. *
   2.23325230196E-01   1.00000000000E+00
0 2  1  0. 1. *
   9.98010024562E-01   1.00000000000E+00

 He - quadruple ζ

  2 10
0 0  5  2. 1.
   1.14464708090E+03   3.58615786180E-04
   1.71645966670E+02   2.77254344660E-03
   3.90660562540E+01   1.42418922160E-02
   1.10514019890E+01   5.54573522770E-02
   3.57255744730E+00   1.61705118100E-01
0 0  1  0. 1. *
   1.24962646520E+00   1.00000000000E+00
0 0  1  0. 1. *
   4.37747220044E-01   1.00000000000E+00
0 0  1  0. 1. *
   1.42711405402E-01   1.00000000000E+00
0 2  1  0. 1. *
   5.99399783875E+00   1.00000000000E+00
0 2  1  0. 1. *
   1.74498900870E+00   1.00000000000E+00
```

```
0 2  1  0. 1. *
   5.59365043421E-01   1.00000000000E+00
0 3  1  0. 1. *
   4.29901931448E+00   1.00000000000E+00
0 3  1  0. 1. *
   1.22340109576E+00   1.00000000000E+00
0 4  1  0. 1. *
   2.67999999968E+00   1.00000000000E+00

 Li - triple ζ

  3  8
0 0  6  2. 1.
   6.26926280100E+03   2.05409688260E-04
   9.40316124310E+02   1.59165540890E-03
   2.14221075280E+02   8.28698297070E-03
   6.07598401840E+01   3.38563742490E-02
   1.99151520320E+01   1.11032258760E-01
   7.31715097970E+00   2.74493833290E-01
0 0  2  1. 1.
   2.97246742160E+00   2.37924564110E-01
   1.26398523140E+00   3.07654119240E-01
0 0  1  0. 1. *
   5.85479751111E-01   1.00000000000E+00
0 0  1  0. 1. *
   2.45524518689E-01   1.00000000000E+00
0 0  1  0. 1. *
   8.45783348222E-02   1.00000000000E+00
0 2  1  0. 1. *
   5.51558376316E-01   1.00000000000E+00
0 2  1  0. 1. *
   1.00554327699E-01   1.00000000000E+00
0 2  1  0. 1. *
   3.31046385234E+00   1.00000000000E+00

 Be - triple ζ

  4  9
0 0  6  2. 1.
   4.70023656260E+03   2.35843893160E-04
   7.04828456220E+02   1.82437910190E-03
   1.60431104780E+02   9.39661482240E-03
   4.54253473360E+01   3.69089241590E-02
   1.47983341250E+01   1.08975612810E-01
   5.35124525370E+00   2.16942845510E-01
0 0  2  2. 1.
   2.15420448190E+00   4.46954088570E-01
   9.33637444000E-01   2.08669857710E-01
0 0  1  0. 1. *
   9.20293384616E-01   1.00000000000E+00
0 0  1  0. 1. *
   4.89677295049E-01   1.00000000000E+00
0 0  1  0. 1. *
   1.45906555367E-01   1.00000000000E+00
0 2  2  0. 1.
   7.16956943660E-01  -1.68778540320E-01
```

```
   1.95419328600E-01  -5.14034196280E-01
0 2  1  0. 1. *
   3.61410611054E+00   1.00000000000E+00
0 2  1  0. 1. *
   2.01881274143E-01   1.00000000000E+00
0 3  1  0. 1. *
   3.45632242486E-01   1.00000000000E+00

 B - triple ζ

  5 10
0 0  6  2. 1.
   8.56486606870E+03   2.28371981550E-04
   1.28415162630E+03   1.76825764470E-03
   2.92278716040E+02   9.14070805160E-03
   8.27754691760E+01   3.63426389890E-02
   2.70179392690E+01   1.10634584410E-01
   9.81496196600E+00   2.33673443210E-01
0 0  2  2. 1.
   3.93185590590E+00   4.18187779780E-01
   1.65955997120E+00   2.23254737980E-01
0 0  1  0. 1. *
   8.12384664516E-01   1.00000000000E+00
0 0  1  0. 1. *
   5.31944111634E-01   1.00000000000E+00
0 0  1  0. 1. *
   1.70250253491E-01   1.00000000000E+00
0 2  4  1. 1.
   2.24538758030E+01   5.02655751790E-03
   5.10450583300E+00   3.28017389650E-02
   1.49860813440E+00   1.31512307680E-01
   5.09278313150E-01   3.31971677690E-01
0 2  1  0. 1. *
   9.75537780008E-01   1.00000000000E+00
0 2  1  0. 1. *
   1.74196956398E-01   1.00000000000E+00
0 3  1  0. 1. *
   6.90313868442E-01   1.00000000000E+00
0 4  1  0. 1. *
   4.29387241461E-01   1.00000000000E+00

 C - triple ζ

  6 11
0 0  6  2. 1.
   1.35753496820E+04   2.22458143520E-04
   2.03523336800E+03   1.72327382520E-03
   4.63225623590E+02   8.92557153140E-03
   1.31200195980E+02   3.57279845020E-02
   4.28530158910E+01   1.10762599310E-01
   1.55841857660E+01   2.42956276260E-01
0 0  2  2. 1.
   6.20671385080E+00   4.14402634480E-01
   2.57648965270E+00   2.37449686550E-01
0 0  1  0. 1. *
   9.96164942002E-01   1.00000000000E+00
```

```
0 0  1  0. 1. *
   6.38373126590E-01   1.00000000000E+00
0 0  1  0. 1. *
   2.31166652661E-01   1.00000000000E+00
0 2  4  2. 1.
   3.46972322440E+01   5.33336578050E-03
   7.95826228260E+00   3.58641090920E-02
   2.37808268830E+00   1.42158733290E-01
   8.14332081830E-01   3.42704718450E-01
0 2  1  0. 1. *
   3.84832397891E-01   1.00000000000E+00
0 2  1  0. 1. *
   1.87899705316E-01   1.00000000000E+00
0 3  1  0. 1. *
   1.01061584864E+00   1.00000000000E+00
0 3  1  0. 1. *
   6.14506968465E-01   1.00000000000E+00
0 4  1  0. 1. *
   7.55573159273E-01   1.00000000000E+00

 N - triple ζ

  7 11
0 0  6  2. 1.
   1.97308006470E+04   2.18879849910E-04
   2.95789587450E+03   1.69607088030E-03
   6.73221335950E+02   8.79546035380E-03
   1.90682494940E+02   3.53593826050E-02
   6.22954418980E+01   1.10957892170E-01
   2.26541611820E+01   2.49829725520E-01
0 0  2  2. 1.
   8.97914774280E+00   4.06238961480E-01
   3.68630023700E+00   2.43382171760E-01
0 0  1  0. 1. *
   9.84742186051E-01   1.00000000000E+00
0 0  1  0. 1. *
   4.40633028847E-01   1.00000000000E+00
0 0  1  0. 1. *
   1.43374486891E-01   1.00000000000E+00
0 2  4  3. 1.
   4.92003805100E+01   5.55524167510E-03
   1.13467905370E+01   3.80523797230E-02
   3.42739724110E+00   1.49536710290E-01
   1.17855251340E+00   3.49493052300E-01
0 2  1  0. 1. *
   4.05553959640E-01   1.00000000000E+00
0 2  1  0. 1. *
   1.37203509080E-01   1.00000000000E+00
0 3  1  0. 1. *
   1.72557905350E+00   1.00000000000E+00
0 3  1  0. 1. *
   5.60733159589E-01   1.00000000000E+00
0 4  1  0. 1. *
   1.39702995210E+00   1.00000000000E+00

 O - triple ζ
```

```
  8 11
0 0  6  2. 1.
   2.70323826310E+04   2.17263024650E-04
   4.05238713920E+03   1.68386621990E-03
   9.22327227100E+02   8.73956162650E-03
   2.61240709890E+02   3.52399688080E-02
   8.53546413510E+01   1.11535191150E-01
   3.10350352450E+01   2.55889539610E-01
0 0  2  2. 1.
   1.22608607280E+01   3.97687309010E-01
   4.99870760050E+00   2.46278494300E-01
0 0  1  0. 1. *
   1.34152779331E+00   1.00000000000E+00
0 0  1  0. 1. *
   5.74786277552E-01   1.00000000000E+00
0 0  1  0. 1. *
   1.94610904831E-01   1.00000000000E+00
0 2  4  4. 1.
   6.32749548010E+01   6.06851034180E-03
   1.46270493790E+01   4.19125758240E-02
   4.45012234560E+00   1.61538410880E-01
   1.52757996470E+00   3.57069513110E-01
0 2  1  0. 1. *
   5.30270515260E-01   1.00000000000E+00
0 2  1  0. 1. *
   1.80510713838E-01   1.00000000000E+00
0 3  1  0. 1. *
   2.24203061685E+00   1.00000000000E+00
0 3  1  0. 1. *
   6.83126234914E-01   1.00000000000E+00
0 4  1  0. 1. *
   1.50936556890E+00   1.00000000000E+00

 F - triple ζ

  9 11
0 0  6  2. 1.
   3.54791004410E+04   2.15450148880E-04
   5.31847289830E+03   1.67006865270E-03
   1.21048109750E+03   8.67332114760E-03
   3.42855181400E+02   3.50499331750E-02
   1.12019431810E+02   1.11653201330E-01
   4.07147402480E+01   2.59885066470E-01
0 0  2  2. 1.
   1.60396781110E+01   3.94229668800E-01
   6.50381867400E+00   2.49982385510E-01
0 0  1  0. 1. *
   1.66612728857E+00   1.00000000000E+00
0 0  1  0. 1. *
   6.83506515681E-01   1.00000000000E+00
0 0  1  0. 1. *
   2.45202177665E-01   1.00000000000E+00
0 2  4  5. 1.
   8.02339004830E+01   6.36859991340E-03
   1.85940107430E+01   4.43031435300E-02
```

```
   5.68679026530E+00   1.68672487080E-01
   1.95110062940E+00   3.61663462550E-01
0 2  1  0. 1. *
   6.50003554984E-01   1.00000000000E+00
0 2  1  0. 1. *
   2.04092308648E-01   1.00000000000E+00
0 3  1  0. 1. *
   3.09940461539E+00   1.00000000000E+00
0 3  1  0. 1. *
   7.91701663415E-01   1.00000000000E+00
0 4  1  0. 1. *
   1.58659608364E+00   1.00000000000E+00

 Ne - triple ζ

 10 11
0 0  6  2. 1.
   4.50694640220E+04   2.16871551820E-04
   6.75597686560E+03   1.68127367570E-03
   1.53765028640E+03   8.73560627820E-03
   4.35516976670E+02   3.53612669220E-02
   1.42286556380E+02   1.13215214540E-01
   5.16921538040E+01   2.66546531040E-01
0 0  2  2. 1.
   2.03158704900E+01   3.96319599510E-01
   8.20219426460E+00   2.55828112510E-01
0 0  1  0. 1. *
   1.99148453462E+00   1.00000000000E+00
0 0  1  0. 1. *
   7.17861639090E-01   1.00000000000E+00
0 0  1  0. 1. *
   2.30862346114E-01   1.00000000000E+00
0 2  4  6. 1.
   9.97829960320E+01   6.55692341630E-03
   2.31761241010E+01   4.58880091380E-02
   7.11639458720E+00   1.73312878120E-01
   2.44187114350E+00   3.64752675120E-01
0 2  1  0. 1. *
   8.06898037129E-01   1.00000000000E+00
0 2  1  0. 1. *
   2.43088088921E-01   1.00000000000E+00
0 3  1  0. 1. *
   4.01393991301E+00   1.00000000000E+00
0 3  1  0. 1. *
   1.09174509672E+00   1.00000000000E+00
0 4  1  0. 1. *
   2.54397846871E+00   1.00000000000E+00

 Ne - quintuple ζ

 10 20
0 0 10  2. 1.
   2.62700000000E+05   2.60000000000E-05
   3.93500000000E+04   2.00000000000E-04
   8.95500000000E+03   1.05000000000E-03
   2.53800000000E+03   4.40000000000E-03
```

```
   8.29900000000E+02   1.56490000000E-02
   3.01500000000E+02   4.77580000000E-02
   1.19000000000E+02   1.22943000000E-01
   5.00000000000E+01   2.52483000000E-01
   2.19800000000E+01   3.66314000000E-01
   9.89100000000E+00   2.79617000000E-01
0 0 10  2. 1.
   2.62700000000E+05  -6.00000000000E-06
   3.93500000000E+04  -4.70000000000E-05
   8.95500000000E+03  -2.47000000000E-04
   2.53800000000E+03  -1.03800000000E-03
   8.29900000000E+02  -3.71100000000E-03
   3.01500000000E+02  -1.15930000000E-02
   1.19000000000E+02  -3.10860000000E-02
   5.00000000000E+01  -7.09720000000E-02
   2.19800000000E+01  -1.27266000000E-01
   9.89100000000E+00  -1.51231000000E-01
0 0  1  0. 1.
   4.32700000000E+00   1.00000000000E+00
0 0  1  0. 1.
   1.80400000000E+00   1.00000000000E+00
0 0  1  0. 1. *
   7.02052559180E-01   1.00000000000E+00
0 0  1  0. 1. *
   2.62163031170E-01   1.00000000000E+00
0 2  4  6. 1.
   2.99100000000E+02   1.03800000000E-03
   7.07300000000E+01   8.37500000000E-03
   2.24800000000E+01   3.96930000000E-02
   8.24600000000E+00   1.28056000000E-01
0 2  1  0. 1.
   3.26900000000E+00   1.00000000000E+00
0 2  1  0. 1.
   1.31500000000E+00   1.00000000000E+00
0 2  1  0. 1. *
   5.00282036595E-01   1.00000000000E+00
0 2  1  0. 1. *
   1.74006598663E-01   1.00000000000E+00
0 3  1  0. 1. *
   9.83699917449E+00   1.00000000000E+00
0 3  1  0. 1. *
   3.84398728908E+00   1.00000000000E+00
0 3  1  0. 1. *
   1.50191462911E+00   1.00000000000E+00
0 3  1  0. 1. *
   5.85635726905E-01   1.00000000000E+00
0 4  1  0. 1. *
   7.08999976256E+00   1.00000000000E+00
0 4  1  0. 1. *
   2.73799711219E+00   1.00000000000E+00
0 4  1  0. 1. *
   1.05696751482E+00   1.00000000000E+00
0 5  1  0. 1. *
   5.45999998377E+00   1.00000000000E+00
0 5  1  0. 1. *
   1.87999969218E+00   1.00000000000E+00
```

```
 Na - triple ζ

 11 11
0 0  7  2. 1.
   2.60411099270E+04   6.18063428110E-04
   3.90612685480E+03   4.77486044140E-03
   8.88974549930E+02   2.44716848290E-02
   2.51454979610E+02   9.47553949770E-02
   8.16501435120E+01   2.68674969200E-01
   2.89041584010E+01   4.79254754400E-01
   1.06257829320E+01   3.32485914690E-01
0 0  3  2. 1.
   5.37694101790E+01   1.95277318720E-02
   1.63082430250E+01   9.26480107940E-02
   2.37303841250E+00  -3.99386701720E-01
0 0  2  1. 1.
   9.57307726030E-01   1.64285953910E+00
   4.08064609590E-01   5.56925969660E-01
0 0  1  0. 1. *
   2.12721167582E-01   9.99992062637E-01
0 0  1  0. 1. *
   7.82096876345E-02   9.99700925116E-01
0 2  5  6. 1.
   1.38079799890E+02   5.79518919290E-03
   3.22327003930E+01   4.16208462510E-02
   9.98160753600E+00   1.62819168850E-01
   3.48220339280E+00   3.60117846470E-01
   1.22991346200E+00   4.48589798890E-01
0 2  1  0. 1. *
   4.03415531731E-01   1.00001437874E+00
0 2  1  0. 1. *
   8.50539333916E-02   1.00010780928E+00
0 3  1  0. 1. *
   2.60862497919E+00   1.00000000000E+00
0 3  1  0. 1. *
   4.33739110192E-01   1.00000000000E+00
0 3  1  0. 1. *
   1.11542851169E-01   1.00000000000E+00

 Na - quadruple ζ

 11 17
0 0  10  2. 1.
379852.2008100              0.20671384468D-04
  56886.0063780              0.16070466617D-03
  12942.7018380              0.84462905848D-03
   3664.3017904              0.35519026029D-02
   1194.7417499              0.12754034468D-01
    430.98192917             0.39895462742D-01
    167.83169424             0.10720154498
     69.306669040            0.23339516913
     29.951170886            0.36333077287
     13.380791097            0.30544770974
0 0  3  2. 1.
    121.74011283             0.36142427284D-01
```

```
     37.044143387             0.28820961687
     13.995422624             0.79337384869
0 0  1  1. 1.
         5.9827797428            1.0000000
0 0  1  0. 1.
        2.4830455118            1.0000000
0 0  1  0. 1.
     1.0452506187            1.0000000
0 0  1  0. 1. *
    4.94104920953E-01   1.00000000000E+00
0 0  1  0. 1. *
    2.20851632190E-01   1.00000000000E+00
0 0  1  0. 1. *
    8.23456214209E-02   1.00000000000E+00
0 2  8  6. 1.
    690.77627017             0.37478518415D-03
    163.82806121             0.31775441030D-02
     52.876460769            0.16333581338D-01
     19.812270493            0.59754902585D-01
      8.1320378784           0.15879328812
      3.4969068377           0.29049363260
      1.5117244146           0.36368131139
      0.64479294912          0.28195867334
0 2  1  0. 1. *
    8.91735359156E-01   1.00000000000E+00
0 2  1  0. 1. *
    6.36553900328E-01   1.00000000000E+00
0 2  1  0. 1. *
    1.94947306854E-01   1.00000000000E+00
0 2  1  0. 1. *
    9.44419920071E-02   1.00000000000E+00
0 3  1  0. 1.
    2.9000000              1.0000000
0 3  1  0. 1. *
    3.73037855991E-01   1.00000000000E+00
0 3  1  0. 1. *
    1.29784306785E-01   1.00000000000E+00
0 4  1  0. 1. *
    2.40808263966E-01   1.00000000000E+00
```

Mg - triple ζ

```
 12 12
0 0  7  2. 1.
   3.14383495550E+04   6.09123113260E-04
   4.71551533540E+03   4.70661964650E-03
   1.07316292470E+03   2.41358206570E-02
   3.03572387680E+02   9.36289598340E-02
   9.86262510420E+01   2.66467420930E-01
   3.49438084170E+01   4.78909299170E-01
   1.28597851990E+01   3.36984902860E-01
0 0  3  2. 1.
   6.48769130040E+01   1.91808893070E-02
   1.97255207770E+01   9.09137043920E-02
   2.89518043390E+00  -3.95637561250E-01
0 0  2  2. 1.
```

Mg - triple ζ - mod

```
 12 13
0 0  7  2. 1.
   3.14383495550E+04   6.09123113260E-04
   4.71551533540E+03   4.70661964650E-03
   1.07316292470E+03   2.41358206570E-02
   3.03572387680E+02   9.36289598340E-02
   9.86262510420E+01   2.66467420930E-01
   3.49438084170E+01   4.78909299170E-01
   1.28597851990E+01   3.36984902860E-01
0 0  3  2. 1.
   6.48769130040E+01   1.91808893070E-02
   1.97255207770E+01   9.09137043920E-02
   2.89518043390E+00  -3.95637561250E-01
0 0  2  2. 1.
```

```
   1.19604547100E+00   1.68276033730E+00
   5.43294511560E-01   5.21410919540E-01
0 0  1  0. 1. *
   4.09879874002E-01   1.00000000000E+00


 0 0  1  0. 1. *
    9.77945365001E-02   1.00000000000E+00
 0 2  5  6. 1.
   1.79871896120E+02   5.37995490180E-03
   4.21200693760E+01   3.93180140980E-02
   1.31205030320E+01   1.57401294760E-01
   4.62575036090E+00   3.59190941280E-01
   1.66952110160E+00   4.55333793100E-01
 0 2  1  0. 1. *
   5.17378832249E-01   1.00000000000E+00
 0 2  1  0. 1. *
   3.61467900791E-01   1.00000000000E+00
 0 2  1  0. 1. *
   1.21249626127E-01   1.00000000000E+00
 0 3  1  0. 1. *
   3.43299411825E+00   1.00000000000E+00
 0 3  1  0. 1. *
   5.37566209974E-01   1.00000000000E+00
 0 3  1  0. 1. *
   1.57830699502E-01   1.00000000000E+00
```

```
   1.19604547100E+00   1.68276033730E+00
   5.43294511560E-01   5.21410919540E-01
0 0  1  0. 1.
   4.09879874002E-01   1.00000000000E+00
0 0  1  0. 1.
0.2      1.
 0 0  1  0. 1.
    9.77945365001E-02   1.00000000000E+00
 0 2  5  6. 1.
   1.79871896120E+02   5.37995490180E-03
   4.21200693760E+01   3.93180140980E-02
   1.31205030320E+01   1.57401294760E-01
   4.62575036090E+00   3.59190941280E-01
   1.66952110160E+00   4.55333793100E-01
 0 2  1  0. 1.
   5.17378832249E-01   1.00000000000E+00
 0 2  1  0. 1.
   3.61467900791E-01   1.00000000000E+00
 0 2  1  0. 1.
   1.21249626127E-01   1.00000000000E+00
 0 3  1  0. 1.
   3.43299411825E+00   1.00000000000E+00
 0 3  1  0. 1.
   5.37566209974E-01   1.00000000000E+00
 0 3  1  0. 1.
   1.57830699502E-01   1.00000000000E+00
```

```
 Al - triple ζ

 13 12
0 0  7  2. 1.
   3.77925507720E+04   5.70478887090E-04
   5.66806821650E+03   4.40930165380E-03
   1.28985828410E+03   2.26309674110E-02
   3.64865960280E+02   8.80256442950E-02
   1.18576315150E+02   2.52237016120E-01
   4.20248676050E+01   4.59605471690E-01
   1.54995016290E+01   3.32778860140E-01
0 0  3  2. 1.
   7.52080265980E+01   1.92505601900E-02
   2.30314089720E+01   8.79067439520E-02
   3.63487976490E+00  -3.42467045350E-01
0 0  2  2. 1.
   1.60650499570E+00   1.51062660580E+00
   7.61033945810E-01   5.80710164700E-01
0 0  1  0. 1. *
   6.11416028302E-01   1.00000000000E+00
0 0  1  0. 1. *
   1.73483869838E-01   1.00000000000E+00
0 2  5  6. 1.
   4.52523031920E+02   2.31108124660E-03
   1.07081950490E+02   1.85686418230E-02
   3.41310212550E+01   8.72162370350E-02
   1.25870374280E+01   2.69021015230E-01
   4.98119197040E+00   5.21283242720E-01
0 2  1  1. 1. *
```

```
   1.95606775738E+00   1.00000000000E+00
0 2  1  0. 1. *
   7.52775780417E-01   1.00000000000E+00
0 2  1  0. 1. *
   1.68684476735E-01   1.00000000000E+00
0 3  2  0. 1.
   1.57000000000E+00   2.00000000000E-01
   3.33000000000E-01   1.00000000000E+00
0 3  1  0. 1. *
   6.74524566202E-01   1.00000000000E+00
0 4  1  0. 1. *
   2.70290295211E-01   1.00000000000E+00

 Al - quadruple ζ(one p added **)

13 21
0 0  10  2. 1.
 754550.7826500              0.13421335886D-04
 112999.3892200              0.10433210786D-03
  25715.8317590              0.54841772080D-03
   7283.6030283              0.23089081391D-02
   2376.0008796              0.83309974593D-02
    857.65468087             0.26417963653D-01
    334.38922598             0.73443646426D-01
    138.48504731             0.17184039139
     60.150368808            0.31041980030
     27.127610860            0.35669190596
0 0  3  2. 1.
    225.36500065             0.21522039783D-01
     69.341968124            0.18531780493
     26.619335712            0.63533181245
0 0  1  2. 1.
     12.349420671            1.0000000
0 0  1  0. 1.
      4.5878785994           1.0000000
0 0  1  0. 1.
      2.0571338103           1.0000000
0 0  1  0. 1. *
  1.02384436277E+00   1.00000000000E+00
0 0  1  0. 1. *
  3.43681311834E-01   1.00000000000E+00
0 0  1  0. 1. *
  1.93489065577E-01   1.00000000000E+00
0 2  8  6. 1.
   1489.6119522              0.20177122443D-03
    353.01399267             0.17508109203D-02
    114.40764069             0.94424704664D-02
     43.312186111            0.36868004006D-01
     18.027322216            0.10892874007
      7.9675432403           0.23265901004
      3.6090399541           0.34643587076
      1.6456081630           0.33440809866
0 2  2  1. 1.
     34.731187489            0.17823073020D-01
      1.2553083630          -0.59991263926
0 2  1  0. 1. *
```

```
  9.06401118275E-01   1.00000000000E+00
0 2  1  0. 1. *
  4.18778479410E-01   1.00000000000E+00
0 2  1  0. 1. *
  1.91427399866E-01   1.00000000000E+00
0 2  1  0. 1. **
  0.09                1
0 3  1  0. 1.
      1.9700000000            1.0000000
0 3  1  0. 1. *
  9.85958623476E-01   1.00000000000E+00
0 3  1  0. 1. *
  5.74185389508E-01   1.00000000000E+00
0 3  1  0. 1. *
  1.92766506272E-01   1.00000000000E+00
0 4  1  0. 1. *
  1.59524931679E+00   1.00000000000E+00
0 4  1  0. 1. *
  7.26266401604E-01   1.00000000000E+00
0 5  1  0. 1. *
  1.25485470091E+00   1.00000000000E+00
```

Si - triple ζ

```
 14 13
0 0  7  2. 1.
   4.47733580780E+04   5.59147658680E-04
   6.71719921040E+03   4.32060401890E-03
   1.52889603250E+03   2.21870964600E-02
   4.32547465850E+02   8.64892491160E-02
   1.40615052260E+02   2.49398897160E-01
   4.98576367240E+01   4.60171973660E-01
   1.84349748850E+01   3.42502365750E-01
0 0  3  2. 1.
   8.65338861110E+01   2.13000630070E-02
   2.66246068460E+01   9.46761393180E-02
   4.49530571590E+00  -3.26162648590E-01
0 0  2  2. 1.
   2.10350457100E+00   1.39808038500E+00
   1.01060949220E+00   6.38657866990E-01

 0 0  1  0. 1. *
    7.55014937995E-01   1.00000000000E+00
 0 0  1  0. 1. *
    1.98542015743E-01   1.00000000000E+00
 0 2  5  6. 1.
    3.94475036280E+02   2.62856939590E-03
    9.31376831040E+01   2.05562577490E-02
    2.95196087420E+01   9.20702628010E-02
    1.07816637910E+01   2.55658897390E-01
    4.16265747780E+00   4.21117071850E-01
 0 2  1  2. 1. *
    1.60593926612E+00   1.00000000000E+00
 0 2  1  0. 1. *
    6.34982274128E-01   1.00000000000E+00
```

Si - triple ζ - mod

```
 14 14
0 0  7  2. 1.
   4.47733580780E+04   5.59147658680E-04
   6.71719921040E+03   4.32060401890E-03
   1.52889603250E+03   2.21870964600E-02
   4.32547465850E+02   8.64892491160E-02
   1.40615052260E+02   2.49398897160E-01
   4.98576367240E+01   4.60171973660E-01
   1.84349748850E+01   3.42502365750E-01
0 0  3  2. 1.
   8.65338861110E+01   2.13000630070E-02
   2.66246068460E+01   9.46761393180E-02
   4.49530571590E+00  -3.26162648590E-01
0 0  2  2. 1.
   2.10350457100E+00   1.39808038500E+00
   1.01060949220E+00   6.38657866990E-01
0 0  1  0. 1.
0.9    1.
0 0  1  0. 1.
   7.55014937995E-01   1.00000000000E+00
0 0  1  0. 1.
   1.98542015743E-01   1.00000000000E+00
0 2  5  6. 1.
   3.94475036280E+02   2.62856939590E-03
   9.31376831040E+01   2.05562577490E-02
   2.95196087420E+01   9.20702628010E-02
   1.07816637910E+01   2.55658897390E-01
   4.16265747780E+00   4.21117071850E-01
0 2  1  2. 1.
   1.60593926612E+00   1.00000000000E+00
0 2  1  0. 1.
   6.34982274128E-01   1.00000000000E+00
```

```
 0 2  1  0. 1. *
    2.95336224842E-01   1.00000000000E+00
 0 2  1  0. 1. *
    1.01085545700E-01   1.00000000000E+00
 0 3  2  0. 1.
    2.30300000000E+00   2.00000000000E-01
    4.76000000000E-01   1.00000000000E+00
 0 3  1  0. 1. *
    2.62241055556E-01   1.00000000000E+00
 0 4  1  0. 1. *
    3.61111716854E-01   1.00000000000E+00
```

```
 0 2  1  0. 1.
    2.95336224842E-01   1.00000000000E+00
 0 2  1  0. 1.
    1.01085545700E-01   1.00000000000E+00
 0 3  2  0. 1.
    2.30300000000E+00   2.00000000000E-01
    4.76000000000E-01   1.00000000000E+00
 0 3  1  0. 1.
    2.62241055556E-01   1.00000000000E+00
 0 4  1  0. 1.
    3.61111716854E-01   1.00000000000E+00
```

P - triple ζ

```
 15 13
0 0  7  2. 1.
   5.24269992330E+04   5.52071641000E-04
   7.86326605520E+03   4.26785953080E-03
   1.78952273330E+03   2.19315291860E-02
   5.06273001650E+02   8.56671683730E-02
   1.64606985460E+02   2.48406866050E-01
   5.83919187220E+01   4.63367539710E-01
   2.16436632010E+01   3.53505581560E-01
0 0  3  2. 1.
   9.90138376200E+01   2.18956799580E-02
   3.05504398170E+01   9.56504702950E-02
   5.45370876610E+00  -2.94542701860E-01
0 0  2  2. 1.
   2.65033625630E+00   1.32943812000E+00
   1.27266888670E+00   6.61093964730E-01

 0 0  1  0. 1. *
    3.31966459013E-01   1.00000000000E+00
 0 0  1  0. 1. *
    1.36421807855E-01   1.00000000000E+00
 0 2  5  6. 1.
    4.72272192480E+02   2.57106230520E-03
    1.11588827560E+02   2.02502979990E-02
    3.54459364180E+01   9.15807167870E-02
    1.29907768750E+01   2.57494540140E-01
    5.04862216580E+00   4.28628997580E-01
 0 2  1  3. 1. *
    1.97270668835E+00   1.00000000000E+00
 0 2  1  0. 1. *
    7.81937693603E-01   1.00000000000E+00
 0 2  1  0. 1. *
    3.37354535997E-01   1.00000000000E+00
 0 2  1  0. 1. *
    1.27287325416E-01   1.00000000000E+00
 0 3  2  0. 1.
    3.12000000000E+00   2.00000000000E-01
    6.48000000000E-01   1.00000000000E+00
 0 3  1  0. 1. *
    2.27496494415E-01   1.00000000000E+00
 0 4  1  0. 1. *
```

P - triple ζ - mod

```
 15 14
0 0  7  2. 1.
   5.24269992330E+04   5.52071641000E-04
   7.86326605520E+03   4.26785953080E-03
   1.78952273330E+03   2.19315291860E-02
   5.06273001650E+02   8.56671683730E-02
   1.64606985460E+02   2.48406866050E-01
   5.83919187220E+01   4.63367539710E-01
   2.16436632010E+01   3.53505581560E-01
0 0  3  2. 1.
   9.90138376200E+01   2.18956799580E-02
   3.05504398170E+01   9.56504702950E-02
   5.45370876610E+00  -2.94542701860E-01
0 0  2  2. 1.
   2.65033625630E+00   1.32943812000E+00
   1.27266888670E+00   6.61093964730E-01
0 0  1  0. 1.
0.7    1.
 0 0  1  0. 1.
    3.31966459013E-01   1.00000000000E+00
 0 0  1  0. 1.
    1.36421807855E-01   1.00000000000E+00
 0 2  5  6. 1.
    4.72272192480E+02   2.57106230520E-03
    1.11588827560E+02   2.02502979990E-02
    3.54459364180E+01   9.15807167870E-02
    1.29907768750E+01   2.57494540140E-01
    5.04862216580E+00   4.28628997580E-01
 0 2  1  3. 1.
    1.97270668835E+00   1.00000000000E+00
 0 2  1  0. 1.
    7.81937693603E-01   1.00000000000E+00
 0 2  1  0. 1.
    3.37354535997E-01   1.00000000000E+00
 0 2  1  0. 1.
    1.27287325416E-01   1.00000000000E+00
 0 3  2  0. 1.
    3.12000000000E+00   2.00000000000E-01
    6.48000000000E-01   1.00000000000E+00
 0 3  1  0. 1.
    2.27496494415E-01   1.00000000000E+00
 0 4  1  0. 1.
```

```
   4.55790298326E-01   1.00000000000E+00          4.55790298326E-01   1.00000000000E+00

 S - triple ζ

 16 13
0 0  7  2. 1.
   6.07009281040E+04   5.46959442250E-04
   9.10261068540E+03   4.22972245570E-03
   2.07141660090E+03   2.17478241590E-02
   5.86024768210E+02   8.51000535890E-02
   1.90553950210E+02   2.47991284590E-01
   6.76303842600E+01   4.67036404060E-01
   2.51273069050E+01   3.64345875500E-01
0 0  3  2. 1.
   1.12574630100E+02   2.16700402400E-02
   3.47955542170E+01   9.36023017600E-02
   6.51155562150E+00  -2.60680014220E-01
0 0  2  2. 1.
   3.23990322610E+00   1.28420894350E+00
   1.54771608810E+00   6.60364165840E-01
0 0  1  0. 1. *
   4.79267087636E-01   1.00000000000E+00
0 0  1  0. 1. *
   2.10561167562E-01   1.00000000000E+00
0 2  5  6. 1.
   5.64367160270E+02   2.47967963170E-03
   1.33426243790E+02   1.96779302500E-02
   4.24682711890E+01   8.99800082580E-02
   1.56165275800E+01   2.57058805750E-01
   6.10939884690E+00   4.35151672920E-01
0 2  1  4. 1. *
   2.43785034818E+00   1.00000000000E+00
0 2  1  0. 1. *
   1.09182124384E+00   1.00000000000E+00
0 2  1  0. 1. *
   4.31410869933E-01   1.00000000000E+00
0 2  1  0. 1. *
   1.57376926419E-01   1.00000000000E+00
0 3  2  0. 1.
   3.75600000000E+00   2.00000000000E-01
   8.12000000000E-01   1.00000000000E+00
0 3  1  0. 1. *
   2.44218244587E-01   1.00000000000E+00
0 4  1  0. 1. *
   5.38814682974E-01   1.00000000000E+00

 Cl - triple ζ

 17 13
0 0  7  2. 1.
   6.95079909450E+04   5.43148974970E-04
   1.04261568800E+04   4.19904639610E-03
   2.37323340610E+03   2.15921416790E-02
   6.71564200710E+02   8.45988500940E-02
   2.18419997900E+02   2.47572497240E-01
   7.75722497140E+01   4.70169302280E-01
```

```
   2.88888152770E+01   3.74363707160E-01
0 0  3  2. 1.
   1.27105271850E+02   2.51821666030E-02
   3.93395829610E+01   1.07861124560E-01
   7.67406799890E+00  -2.74088215740E-01
0 0  2  2. 1.
   3.87456276300E+00   1.32138750140E+00
   1.83858325730E+00   6.86369553680E-01
0 0  1  0. 1. *
   5.07498154767E-01   1.00000000308E+00
0 0  1  0. 1. *
   1.83127456586E-01   9.99999997835E-01
0 2  5  6. 1.
   6.66504232840E+02   2.36326638360E-03
   1.57642416900E+02   1.88793003740E-02
   5.02625209780E+01   8.72063412730E-02
   1.85360781050E+01   2.52856129700E-01
   7.29405327770E+00   4.35071548200E-01
0 2  1  5. 1. *
   2.89826632488E+00   1.00000000143E+00
0 2  1  0. 1. *
   1.10442102086E+00   1.00000000000E+00
0 2  1  0. 1. *
   4.09232170559E-01   1.00000000000E+00
0 2  1  0. 1. *
   1.36452167048E-01   1.00000000000E+00
0 3  2  0. 1.
   4.61000000000E+00   2.00000000000E-01
   1.01100000000E+00   1.00000000000E+00
0 3  1  0. 1. *
   3.32581229403E-01   1.00000000000E+00
0 4  1  0. 1. *
   5.98970631104E-01   1.00000000000E+00

 Ar - triple ζ

 18 13
0 0  7  2. 1.
   7.91114229980E+04   5.10293250020E-04
   1.18647460090E+04   3.94630369810E-03
   2.70016429730E+03   2.03070739100E-02
   7.63959434850E+02   7.96918252140E-02
   2.48451505610E+02   2.34206238360E-01
   8.82835810000E+01   4.48338494810E-01
   3.29486070690E+01   3.64081674000E-01
0 0  3  2. 1.
   1.42553580000E+02   2.63874070010E-02
   4.41636880090E+01   1.12264339990E-01
   8.95249950000E+00  -2.61789220010E-01
0 0  2  2. 1.
   4.55469209410E+00   1.30024849980E+00
   2.14440790010E+00   6.71972370090E-01
0 0  1  0. 1. *
   6.14874634212E-01   1.00000000000E+00
0 0  1  0. 1. *
   2.17873501799E-01   1.00000000000E+00
```

```
0 2  5  6. 1.
   7.76775419980E+02   2.20280050030E-03
   1.83801070180E+02   1.76941800080E-02
   5.86940031750E+01   8.24312937170E-02
   2.17015916950E+01   2.42072788630E-01
   8.58214896350E+00   4.22635582510E-01
0 2  1  6. 1. *
   3.43108948168E+00   1.00000000000E+00
0 2  1  0. 1. *
   1.29586219954E+00   1.00000000000E+00
0 2  1  0. 1. *
   4.73667526469E-01   1.00000000000E+00
0 2  1  0. 1. *
   1.52964634435E-01   1.00000000000E+00
0 3  2  0. 1.
   5.55100000000E+00   2.00000000000E-01
   1.23500000000E+00   1.00000000000E+00
0 3  1  0. 1. *
   3.68156163751E-01   1.00000000000E+00
0 4  1  0. 1. *
   8.89285192225E-01   1.00000000000E+00

 Ar - quadruple ζ

 18 22
0 0 10  2. 1.
   1.67342194940E+06   1.12459904130E-05
   2.50601753730E+05   8.74281157980E-05
   5.70309121200E+04   4.59616412750E-04
   1.61533039150E+04   1.93638907420E-03
   5.26941092880E+03   6.99940464970E-03
   1.90203155410E+03   2.23120681960E-02
   7.41576771590E+02   6.28080776970E-02
   3.07209019060E+02   1.51011409970E-01
   1.33527862030E+02   2.87136611770E-01
   6.02533812910E+01   3.63854901070E-01
0 0  3  2. 1.
   5.22024262060E+02   1.80713231160E-02
   1.61512904690E+02   1.64492198840E-01
   6.21263694330E+01   6.38973348990E-01
0 0  1  2. 1. *
   2.75924919039E+01   1.00000000000E+00
0 0  1  0. 1. *
   1.11770673532E+01   1.00000000000E+00
0 0  1  0. 1. *
   5.31160209177E+00   1.00000000000E+00
0 0  1  0. 1. *
   2.42316978774E+00   1.00000000000E+00
0 0  1  0. 1. *
   8.67723534175E-01   1.00000000000E+00
0 0  1  0. 1. *
   3.65554120129E-01   1.00000000000E+00
0 0  1  0. 1. *
   1.38659166519E-01   1.00000000000E+00
0 2  8  6. 1.
   2.86845045810E+03   2.40104351210E-04
```

```
   6.79718695900E+02   2.09047886650E-03
   2.20367588240E+02   1.13693168390E-02
   8.36204397340E+01   4.49019773980E-02
   3.49643226570E+01   1.32371567700E-01
   1.55251317840E+01   2.77092776000E-01
   7.09929798060E+00   3.86139796460E-01
   3.30213366020E+00   2.84929253720E-01
0 2  2  6. 1.
   1.28787656670E+02  -3.05094577510E-02
   8.43578679770E+00   6.41016210700E-01
0 2  1  0. 1. *
   1.47872194454E+00   1.00000000000E+00
0 2  1  0. 1. *
   6.10896364502E-01   1.00000000000E+00
0 2  1  0. 1. *
   2.52858406408E-01   1.00000000000E+00
0 2  1  0. 1. *
   9.88483432873E-02   1.00000000000E+00
0 3  1  0. 1. *
   6.31499988581E+00   1.00000000000E+00
0 3  1  0. 1. *
   1.56194566793E+00   1.00000000000E+00
0 3  1  0. 1. *
   7.15288895286E-01   1.00000000000E+00
0 3  1  0. 1. *
   2.89708330278E-01   1.00000000000E+00
0 4  1  0. 1. *
   5.43075106879E-01   1.00000000000E+00
0 4  1  0. 1. *
   1.32501728189E+00   1.00000000000E+00
0 5  1  0. 1. *
   1.00696894667E+00   1.00000000000E+00

 K - triple ζ

 19 13
0 0  8  2. 1.
   1.53976183250E+05   2.36626361070E-04
   2.30824976720E+04   1.83429291370E-03
   5.25323447450E+03   9.53105277690E-03
   1.48695501330E+03   3.86384069800E-02
   4.84063337260E+02   1.24807685020E-01
   1.73566539800E+02   2.92788610090E-01
   6.71163814640E+01   4.06334258600E-01
   2.63395020540E+01   2.00772158600E-01
0 0  4  2. 1.
   1.72876935670E+02  -2.42009609360E-02
   5.30586490630E+01  -1.15530950400E-01
   7.92127539640E+00   5.74555451750E-01
   3.21088804720E+00   5.70231851070E-01
0 0  2  2. 1.
   4.56620708950E+00  -2.26157634660E-01
   7.02099072820E-01   7.55283920450E-01
0 0  1  1. 1. *
   3.40388622730E-01   1.00000000000E+00
0 0  1  0. 1. *
```

```
   1.27244490119E-01   1.00000000000E+00
0 0  1  0. 1. *
   5.62288102535E-02   1.00000000000E+00
0 2  6  6. 1.
   7.28184498730E+02   2.61506897920E-03
   1.72132650610E+02   2.06736308350E-02
   5.48298470750E+01   9.32056038700E-02
   2.01662664940E+01   2.54365182100E-01
   7.86107288060E+00   3.91311328100E-01
   3.11052131320E+00   2.24813459430E-01
0 2  3  6. 1.
   1.17573374920E+01  -2.57772892170E-02
   1.51396174110E+00   5.73594286040E-01
   5.83285917950E-01   1.07983200020E+00
0 2  1  0. 1. *
   2.10909849443E-01   1.00000000000E+00
0 2  1  0. 1. *
   4.78203320068E-02   1.00000000000E+00
0 3  1  0. 1. *
   9.33669696334E-01   1.00000000000E+00
0 3  1  0. 1. *
   2.04046005967E-01   1.00000000000E+00
0 3  1  0. 1. *
   5.25533133715E-02   1.00000000000E+00
```

Ca - triple ζ

```
 20 14
0 0  8  2. 1.
   1.72517326850E+05   2.33175025460E-04
   2.58615192750E+04   1.80765219800E-03
   5.88566186680E+03   9.39438442550E-03
   1.66597300310E+03   3.81084090090E-02
   5.42367181480E+02   1.23312038530E-01
   1.94578034920E+02   2.90044709540E-01
   7.53035976360E+01   4.05871511570E-01
   2.95740625890E+01   2.03984107430E-01
0 0  4  2. 1.
   1.91200746600E+02  -2.44197597590E-02
   5.88402998830E+01  -1.15470274480E-01
   8.96425408450E+00   5.63566367170E-01
   3.68569605410E+00   5.67096827040E-01
0 0  2  2. 1.
   5.24642897260E+00  -2.28253343250E-01
   8.48626215280E-01   7.26252191720E-01
0 0  1  2. 1. *
   4.29267926012E-01   1.00000000000E+00
0 0  1  0. 1. *
   1.58099111851E-01   1.00000000000E+00
0 0  1  0. 1. *
   6.64111683554E-02   1.00000000000E+00
0 2  6  6. 1.
   8.36972620580E+02   2.52583460920E-03
   1.97930401420E+02   2.00765066860E-02
   6.31355580540E+01   9.13029873660E-02
   2.32826871700E+01   2.52470299150E-01
```

Ca - triple ζ - mod

```
 20 14
0 0  8  2. 1.
   1.72517326850E+05   2.33175025460E-04
   2.58615192750E+04   1.80765219800E-03
   5.88566186680E+03   9.39438442550E-03
   1.66597300310E+03   3.81084090090E-02
   5.42367181480E+02   1.23312038530E-01
   1.94578034920E+02   2.90044709540E-01
   7.53035976360E+01   4.05871511570E-01
   2.95740625890E+01   2.03984107430E-01
0 0  4  2. 1.
   1.91200746600E+02  -2.44197597590E-02
   5.88402998830E+01  -1.15470274480E-01
   8.96425408450E+00   5.63566367170E-01
   3.68569605410E+00   5.67096827040E-01
0 0  2  2. 1.
   5.24642897260E+00  -2.28253343250E-01
   8.48626215280E-01   7.26252191720E-01
0 0  1  2. 1.
   4.29267926012E-01   1.00000000000E+00
0 0  1  0. 1.
   1.58099111851E-01   1.00000000000E+00
0 0  1  0. 1.
   6.64111683554E-02   1.00000000000E+00
0 2  6  6. 1.
   8.36972620580E+02   2.52583460920E-03
   1.97930401420E+02   2.00765066860E-02
   6.31355580540E+01   9.13029873660E-02
   2.32826871700E+01   2.52470299150E-01
```

```
   9.11764449320E+00   3.94263263440E-01
   3.63361201390E+00   2.30115594920E-01
0 2  3  6. 1.
   1.34941631200E+01  -2.64950219510E-02
   1.81392597900E+00   5.50881082100E-01
   7.19818260060E-01   1.02806166200E+00
0 2  1  0. 1. *
   5.20419757641E-01   1.00000000000E+00
0 2  1  0. 1. *
   3.08703105774E-01   1.00000000000E+00
0 2  1  0. 1. *
   9.25827750185E-02   1.00000000000E+00
0 3  2  0. 1. *
   5.51680904545E+00   7.37700114330E-02
   1.42468064601E+00   2.60528531690E-01
0 3  1  0. 1. *
   4.03702125099E-01   1.00000000000E+00
0 3  1  0. 1. *
   9.71059836854E-02   1.00000000000E+00
```

```
   9.11764449320E+00   3.94263263440E-01
   3.63361201390E+00   2.30115594920E-01
0 2  3  6. 1.
   1.34941631200E+01  -2.64950219510E-02
   1.81392597900E+00   5.50881082100E-01
   7.19818260060E-01   1.02806166200E+00
0 2  1  0. 1.
0.4   1.
0 2  1  0. 1.
0.2   1.
0 2  1  0. 1.
   9.25827750185E-02   1.00000000000E+00
0 3  2  0. 1.
   5.51680904545E+00   7.37700114330E-02
   1.42468064601E+00   2.60528531690E-01
0 3  1  0. 1.
   4.03702125099E-01   1.00000000000E+00
0 3  1  0. 1.
   9.71059836854E-02   1.00000000000E+00
```

Sc - triple ζ

```
 21 15
0 0  8  2. 1.
      1.91612918740E+05   2.30764759420E-04
      2.87238503630E+04   1.78903299460E-03
      6.53701164900E+03   9.29904011400E-03
      1.85030971710E+03   3.77394380110E-02
      6.02388551560E+02   1.22271483590E-01
      2.16173247660E+02   2.88148214700E-01
      8.37125178800E+01   4.05175430990E-01
      3.29087071890E+01   2.05660196230E-01
0 0  4  2. 1.
      2.11343932340E+02  -2.45279914620E-02
      6.51289201390E+01  -1.15701581420E-01
      1.00343115350E+01   5.59952833170E-01
      4.15968845970E+00   5.60877650730E-01
0 0  2  2. 1.
      6.00090416130E+00  -2.28404943250E-01
      9.82557841500E-01   7.19489703780E-01
0 0  1  2. 1. *
      1.66257260981E+00   1.00000000000E+00
0 0  1  0. 1. *
      4.28283484375E-01   1.00000000000E+00
0 0  1  0. 1. *
      9.11100496971E-02   1.00000000000E+00
0 2  6  6. 1.
      9.47341228230E+02   2.47372087440E-03
      2.24096997320E+02   1.97429670600E-02
      7.15603348820E+01   9.03571475490E-02
      2.64448244900E+01   2.52016025030E-01
      1.03937982850E+01   3.96755359290E-01
      4.16063045590E+00   2.32086245170E-01
0 2  3  6. 1.
      1.55657371350E+01  -2.71294239740E-02
      2.11215448650E+00   5.51092566290E-01
```

```
      8.41847090210E-01   1.00906358060E+00
0 2  1  0. 1. *
      2.99009751549E-01   1.00000000000E+00
0 2  1  0. 1. *
      1.25650387472E-01   1.00000000000E+00
0 3  4  1. 1.
      3.09893909930E+01   1.19028374310E-02
      8.69054650690E+00   6.76558568500E-02
      2.95202563370E+00   2.13325397220E-01
      1.07619107450E+00   3.83910755780E-01
0 3  1  0. 1. *
      1.13800590800E+00   1.00000000000E+00
0 3  1  0. 1. *
      4.15328813342E-01   1.00000000000E+00
0 3  1  0. 1. *
      1.37715918867E-01   1.00000000000E+00
0 4  1  0. 1. *
      4.02932397647E-01   1.00000000000E+00

 Ti - triple ζ

 22 15
0 0  8  2. 1.
      2.11575690250E+05   2.33181510110E-04
      3.17149450580E+04   1.80796908510E-03
      7.21754765430E+03   9.39843113520E-03
      2.04293942470E+03   3.81568536180E-02
      6.65128962080E+02   1.23747571970E-01
      2.38749422640E+02   2.92085511430E-01
      9.25086910010E+01   4.12268008550E-01
      3.64039192090E+01   2.10905340610E-01
0 0  4  2. 1.
      2.32726246070E+02  -2.49201407380E-02
      7.17912097110E+01  -1.17464900870E-01
      1.11585346150E+01   5.65033423180E-01
      4.65481354160E+00   5.62111018120E-01
0 0  2  2. 1.
      6.80346291740E+00  -2.30114255030E-01
      1.12010764030E+00   7.21031867350E-01
0 0  1  2. 1. *
      6.42286938433E-01   1.00000000000E+00
0 0  1  0. 1. *
      3.26579294446E-01   1.00000000000E+00
0 0  1  0. 1. *
      1.61264842584E-01   1.00000000000E+00
0 2  6  6. 1.
      1.06314747320E+03   2.46908393200E-03
      2.51565070610E+02   1.97733455230E-02
      8.04085548540E+01   9.09879766720E-02
      2.97681932690E+01   2.55599004130E-01
      1.17368305560E+01   4.04893867640E-01
      4.71423752300E+00   2.36934025580E-01
0 2  3  6. 1.
      1.77968037040E+01  -2.78786396150E-02
      2.42726986800E+00   5.56729146680E-01
      9.68234455370E-01   1.00554473500E+00
```

```
0 2  1  0. 1. *
      3.25975499934E-01   1.00000000000E+00
0 2  1  0. 1. *
      1.81651058532E-01   1.00000000000E+00
0 3  4  2. 1.
      3.77133847230E+01   1.15138350920E-02
      1.06929311840E+01   6.72463439960E-02
      3.67284469900E+00   2.14842077750E-01
      1.35885903030E+00   3.88908927790E-01
0 3  1  0. 1. *
      7.51072904232E-01   1.00000000000E+00
0 3  1  0. 1. *
      6.21135941037E-01   1.00000000000E+00
0 3  1  0. 1. *
      1.79483221200E-01   1.00000000000E+00
0 4  1  0. 1. *
      5.20291162284E-01   1.00000000000E+00

 Ti - quadruple ζ(one s added**)

  22 25
0 0 11 2 1
3070548.8651000              0.86954016630D-05
 460777.8864300              0.67452737727D-04
 104901.2288900              0.35477293028D-03
  29695.8611990              0.14977525588D-02
   9678.8892688              0.54309912055D-02
   3490.1877912              0.17439360524D-01
   1359.2217621              0.49835634640D-01
    562.42721208             0.12379633943
    244.22296250             0.25057490943
    110.16668710             0.35934609007
     50.881903357            0.27594242664
0 0 4 2 1
    965.95430789             0.41773927781D-02
    299.27072059             0.40277148567D-01
    114.83772939             0.17898686817
     49.477578954            0.31783043543
0 0 1 2 1
     22.982839977            1.0000000
0 0 1 2 1
     10.518305037            1.0000000
0 0 1 0 1
      4.9774390567           1.0000000
0 0 1 0 1
      2.1339846838           1.0000000
0 0 1 0 1 *
   1.12707580031E+00   1.00000000000E+00
0 0 1 0 1 *
   4.72980107853E-01   1.00000000000E+00
0 0 1 0 1 *
   1.70870580664E-01   1.00000000000E+00
0 0 1 0 1 **
      0.10      1.0000000
0 2 9 6 1
   5169.6755427              0.18802523596D-03
```

```
   1225.0961638              0.16473458826D-02
    397.60051934             0.91104554321D-02
    151.36154684             0.36987450926D-01
     63.613321773            0.11376329624
     28.514560307            0.25345208574
     13.248003298            0.38019402704
      6.3048807760           0.30989136346
      2.9493525821           0.87418944007D-01
0 2 5 6 1
     40.738772213            -0.73233793267D-02
     14.062358461            -0.34282591082D-01
      2.7460680961           0.35655009250
      1.2713688141           0.76112035427
      0.57610015545          0.62716743237
0 2 1 0 1 *
   1.14638020999E+00   1.00000000000E+00
0 2 1 0 1 *
   7.34850618789E-01   1.00000000000E+00
0 2 1 0 1 *
   3.56527148967E-01   1.00000000000E+00
0 2 1 0 1 *
   1.65950553993E-01   1.00000000000E+00
0 3 5 2 1
     89.589880075            0.21223030030D-02
     26.591412960            0.15911819913D-01
      9.7739715702           0.62875243121D-01
      3.9625083655           0.17144170807
      1.6890532654           0.30565506624
0 3 1 0 1 *
   1.91682758338E+00   1.00000000000E+00
0 3 1 0 1 *
   9.02577453752E-01   1.00000000000E+00
0 3 1 0 1 *
   4.89592270056E-01   1.00000000000E+00
0 3 1 0 1 *
   1.63162726346E-01   1.00000000000E+00
0 4 1 0 1
      2.0930000              1.0000000
0 4 1 0 1 *
   1.56017293955E+00   1.00000000000E+00
0 4 1 0 1 *
   6.98424123530E-01   1.00000000000E+00
0 5 1 0 1 *
   7.72661233773E-01   1.00000000000E+00

 V - triple ζ

 23 15
0 0  8  2. 1.
      2.32340650582E+05   2.30724100916E-04
      3.48288411698E+04   1.78881789621E-03
      7.92654486906E+03   9.29924901324E-03
      2.24377330458E+03   3.77614633471E-02
      7.30593229434E+02   1.22559096620E-01
      2.62322196310E+02   2.89635088109E-01
      1.01704038050E+02   4.10047029549E-01
```

```
      4.00647846167E+01   2.11136108581E-01
0 0  4  2. 1.
      2.55240149682E+02  -2.44581163379E-02
      7.88046469614E+01  -1.15272053659E-01
      1.23405989460E+01   5.51747494530E-01
      5.17420192185E+00   5.45045284889E-01
0 0  2  2. 1.
      7.65138944692E+00  -2.29676382862E-01
      1.26397598979E+00   7.16837690764E-01
0 0  1  2. 1. *
      6.59290296565E-01   1.00000000000E+00
0 0  1  0. 1. *
      4.16364704888E-01   1.00000000000E+00
0 0  1  0. 1. *
      2.10943638090E-01   1.00000000000E+00
0 2  6  6. 1.
      1.18423691510E+03   2.44498267287E-03
      2.80230751921E+02   1.96434544660E-02
      8.96436271379E+01   9.07969491900E-02
      3.32424112531E+01   2.56507682219E-01
      1.31445144521E+01   4.08153937500E-01
      5.29485341394E+00   2.38603782680E-01
0 2  3  6. 1.
      2.01755868511E+01  -2.82414890230E-02
      2.76058651973E+00   5.55746356193E-01
      1.10089009019E+00   9.93199192700E-01
0 2  1  0. 1. *
      3.74879550513E-01   1.00000000000E+00
0 2  1  0. 1. *
      1.97530908408E-01   1.00000000000E+00
0 3  4  3. 1.
      4.38611348639E+01   1.14871742381E-02
      1.25160218909E+01   6.82471539757E-02
      4.33138549566E+00   2.18377841950E-01
      1.61388557730E+00   3.92452122964E-01
0 3  1  0. 1. *
      6.33418272611E-01   4.26344667860E-01
0 3  1  0. 1. *
      4.58713471836E-01   2.26465626007E-01
0 3  1  0. 1. *
      2.41097777446E-01   1.00000000000E+00
0 4  1  0. 1. *
      8.28001703778E-01   1.00000000000E+00

 V - quadruple ζ

  23 25
0 0 11 2 1
3360380.0382000              0.87027840678D-05
 502646.7317800              0.67786024965D-04
 114247.2286700              0.35699229090D-03
  32321.9726300              0.15075507352D-02
  10532.9472710              0.54664377528D-02
   3798.3004439              0.17547310839D-01
   1479.6094715              0.50106594778D-01
    612.57405507             0.12431296066
```

```
     266.22103326              0.25117026883
     120.21980126              0.35926015903
      55.591180848             0.27505075685
0 0 4 2 1
    1082.4768635               0.39326847695D-02
     334.94462061              0.38298477998D-01
     128.31559026              0.17259908827
      55.311589616             0.31287423870
0 0 1 2 1
      25.108383036             1.0000000
0 0 1 2 1
      11.667553242             1.0000000
0 0 1 0 1
       5.5372073270            1.0000000
0 0 1 0 1
       2.3781007618            1.0000000
0 0 1 0 1
       1.1506947329            1.0000000
0 0 1 0 1
    6.10303786899E-01   1.00000000000E+00
0 0 1 0 1
    3.68604809888E-01   1.00000000000E+00
0 0 1 0 1
    2.20252730219E-01   1.00000000000E+00
0 2 9 6 1
    5782.8035005               0.18344743045D-03
    1369.9392282               0.16095217453D-02
     444.53147129              0.89242268749D-02
     169.25617556              0.36375182379D-01
      71.168730031             0.11246803294
      31.933358374             0.25226107794
      14.865336779             0.38039695005
       7.0921740091            0.31068797325
       3.3281157846            0.88141200458D-01
0 2 5 6 1
      45.842906017             -0.56661391945D-02
      15.940339016             -0.26718979445D-01
       3.1257155025             0.27354632707
       1.4485867558             0.57972883053
       0.65577902825            0.47601110515
0 2 1 0 1
    1.03431288484E+00   1.00000000000E+00
0 2 1 0 1
    7.24363408911E-01   1.00000000000E+00
0 2 1 0 1
    4.04767039950E-01   1.00000000000E+00
0 2 1 0 1
    2.32435177489E-01   1.00000000000E+00
0 3 5 3 1
     103.95047414              0.21007158819D-02
      30.901688665             0.16015244877D-01
      11.420321145             0.64127456940D-01
       4.6573272292            0.17488905695
       1.9963682623            0.31003778048
0 3 1 0 1
    1.64033944306E+00   1.00000000000E+00
```

```
0 3 1 0 1
   8.13028040667E-01   1.00000000000E+00
0 3 1 0 1
   5.64424921068E-01   1.00000000000E+00
0 3 1 0 1
   2.44138615380E-01   1.00000000000E+00
0 4 1 0 1
      2.9330000               1.0000000
0 4 1 0 1
   1.42603160593E+00   1.00000000000E+00
0 4 1 0 1
   7.70965202560E-01   1.00000000000E+00
0 5 1 0 1
   1.18383811217E+00   1.00000000000E+00
```

Cr - triple ζ

```
 24 15
0 0  8  2. 1.
      2.54477807040E+05   2.33869456930E-04
      3.81317970540E+04   1.81426018000E-03
      8.67529306070E+03   9.43639257210E-03
      2.45500998480E+03   3.83436393670E-02
      7.99162177870E+02   1.24591948370E-01
      2.86900214890E+02   2.94896960290E-01
      1.11254132320E+02   4.18461496070E-01
      4.38641526360E+01   2.16337634200E-01
0 0  4  2. 1.
      2.79326691730E+02  -2.34509081110E-02
      8.62747323760E+01  -1.10803700270E-01
      1.35557561130E+01   5.30289658420E-01
      5.69781127510E+00   5.16035169470E-01
0 0  2  2. 1.
      8.56365826150E+00  -3.81095456750E-01
      1.39882967680E+00   1.19915914360E+00
0 0  1  1. 1. *
      8.18694544353E-01   1.00000000000E+00
0 0  1  0. 1. *
      3.56144750597E-01   1.00000000000E+00
0 0  1  0. 1. *
      1.88287334487E-01   1.00000000000E+00
0 2  6  6. 1.
      1.30643988640E+03   2.42773261850E-03
      3.09253114410E+02   1.95440410170E-02
      9.89962739630E+01   9.06517945530E-02
      3.67569164510E+01   2.56992791540E-01
      1.45666570770E+01   4.09355048910E-01
      5.87399374320E+00   2.37293888490E-01
0 2  3  6. 1.
      2.28909996950E+01  -2.81660266130E-02
      3.08550018220E+00   5.60341201480E-01
      1.21323291180E+00   9.81190196500E-01
0 2  1  0. 1. *
      3.89583038656E-01   1.00000000000E+00
0 2  1  0. 1. *
      1.92457015188E-01   1.00000000000E+00
```

Cr - triple ζ - mod

```
 24 15
0 0  8  2. 1.
      2.54477807040E+05   2.33869456930E-04
      3.81317970540E+04   1.81426018000E-03
      8.67529306070E+03   9.43639257210E-03
      2.45500998480E+03   3.83436393670E-02
      7.99162177870E+02   1.24591948370E-01
      2.86900214890E+02   2.94896960290E-01
      1.11254132320E+02   4.18461496070E-01
      4.38641526360E+01   2.16337634200E-01
0 0  4  2. 1.
      2.79326691730E+02  -2.34509081110E-02
      8.62747323760E+01  -1.10803700270E-01
      1.35557561130E+01   5.30289658420E-01
      5.69781127510E+00   5.16035169470E-01
0 0  2  2. 1.
      8.56365826150E+00  -3.81095456750E-01
      1.39882967680E+00   1.19915914360E+00
0 0  1  1. 1.
1.20    1.
0 0  1  0. 1.
      3.56144750597E-01   1.00000000000E+00
0 0  1  0. 1.
      1.88287334487E-01   1.00000000000E+00
0 2  6  6. 1.
      1.30643988640E+03   2.42773261850E-03
      3.09253114410E+02   1.95440410170E-02
      9.89962739630E+01   9.06517945530E-02
      3.67569164510E+01   2.56992791540E-01
      1.45666570770E+01   4.09355048910E-01
      5.87399374320E+00   2.37293888490E-01
0 2  3  6. 1.
      2.28909996950E+01  -2.81660266130E-02
      3.08550018220E+00   5.60341201480E-01
      1.21323291180E+00   9.81190196500E-01
0 2  1  0. 1.
      3.89583038656E-01   1.00000000000E+00
0 2  1  0. 1.
      1.92457015188E-01   1.00000000000E+00
```

```
0 3  4  5. 1.
      4.37200744760E+01   1.36229640260E-02
      1.23912426520E+01   7.89351801330E-02
      4.26394420060E+00   2.38338400000E-01
      1.55252217900E+00   3.95268511220E-01
0 3  1  0. 1. *
      9.08965624952E-01   1.00000000000E+00
0 3  1  0. 1. *
      7.28690080851E-01   1.00000000000E+00
0 3  1  0. 1. *
      2.31872337500E-01   1.00000000000E+00
0 4  1  0. 1. *
      1.10945553242E+00   1.00000000000E+00
```

```
0 3  4  5. 1.
      4.37200744760E+01   1.36229640260E-02
      1.23912426520E+01   7.89351801330E-02
      4.26394420060E+00   2.38338400000E-01
      1.55252217900E+00   3.95268511220E-01
0 3  1  0. 1.
      9.08965624952E-01   1.00000000000E+00
0 3  1  0. 1.
0.5    1.
0 3  1  0. 1.
      2.31872337500E-01   1.00000000000E+00
0 4  1  0. 1.
      1.10945553242E+00   1.00000000000E+00
```

Mn - triple ζ

```
25 15
0 0  8  2. 1.
      2.77185001530E+05   2.28383851330E-04
      4.15507698900E+04   1.77076503750E-03
      9.45597001520E+03   9.20772099940E-03
      2.67652064820E+03   3.74159718250E-02
      8.71466875300E+02   1.21648614260E-01
      3.12983064200E+02   2.88243924990E-01
      1.21444540510E+02   4.10416008470E-01
      4.79225988290E+01   2.13723751450E-01
0 0  4  2. 1.
      3.03667231630E+02  -2.45899261400E-02
      9.38814031870E+01  -1.16026080380E-01
      1.48794212140E+01   5.51120596770E-01
      6.28652007450E+00   5.37075607560E-01
0 0  2  2. 1.
      9.48585913370E+00  -2.28892626950E-01
      1.56987061580E+00   7.11961695870E-01
0 0  1  2. 1. *
      7.35427311231E-01   1.00000000000E+00
0 0  1  0. 1. *
      3.85155147737E-01   1.00000000000E+00
0 0  1  0. 1. *
      2.24416300571E-01   1.00000000000E+00
0 2  6  6. 1.
      1.44479781820E+03   2.39941364550E-03
      3.42065511970E+02   1.93692868640E-02
      1.09584008910E+02   9.02361089880E-02
      4.07479881730E+01   2.57454678510E-01
      1.61886265660E+01   4.12723519580E-01
      6.54845059640E+00   2.40877000070E-01
0 2  3  6. 1.
      2.53570864370E+01  -2.87071740580E-02
      3.48301687820E+00   5.52081007120E-01
      1.38588009060E+00   9.72269013790E-01
0 2  1  0. 1. *
      4.79170174794E-01   1.00000000000E+00
0 2  1  0. 1. *
      2.18219223980E-01   1.00000000000E+00
0 3  4  5. 1.
```

```
      5.65631891190E+01   1.15432452945E-02
      1.62787347110E+01   7.02998459872E-02
      5.69642739140E+00   2.24507708213E-01
      2.14111479420E+00   3.97030654342E-01
0 3  1  0. 1. *
      7.24252926030E-01   4.19410391654E-01
0 3  1  0. 1. *
      5.00606640609E-01   2.18872616727E-01
0 3  1  0. 1. *
      2.73760230337E-01   1.00000000000E+00
0 4  1  0. 1. *
      1.29947345344E+00   1.00000000000E+00

 Mn - quadruple ζ

  25 24
0 0 11 2 1
4289357.6441000              0.79360554972D-05
 636361.0028500              0.62542986761D-04
 143637.2756900              0.33226388724D-03
  40406.3454320              0.14130009568D-02
  13104.3634170              0.51560918319D-02
   4705.0664255              0.16659574919D-01
   1825.7125432              0.47908083403D-01
    753.33816229             0.11994903752
    326.47253285             0.24550296959
    147.10300670             0.35822739571
     67.987226869            0.28295764442
0 0 4 2 1
   1300.7266717              0.76025154141D-02
    402.72027544             0.74365109808D-01
    154.38971348             0.33780474819
     66.443384613            0.62779331746
0 0 1 2 1
     30.975316006            1.0000000
0 0 1 2 1
     14.222980890            1.0000000
0 0 1 0 1
      6.7598265074           1.0000000
0 0 1 0 1
      2.9087083287           1.0000000
0 0 1 0 1 *
    1.37120483174E+00   1.00000000000E+00
0 0 1 0 1 *
    4.77660656030E-01   1.00000000000E+00
0 0 1 0 1 *
    2.30145155128E-01   1.00000000000E+00
0 2 9 6 1
   6483.2629658              0.20479778890D-03
   1556.7134859              0.17525750185D-02
    509.73925460             0.95798802458D-02
    195.28408089             0.38681362983D-01
     82.542547525            0.11832401588
     37.212076731            0.26168459627
     17.425804462            0.38400628821
      8.3691376962           0.29704166759
```

```
      3.9409000444            0.78263290323D-01
0 2 5 6 1
     57.202741010            -0.47749099800D-02
     20.090935947            -0.22989729915D-01
      3.9357553763            0.23197065881
      1.8181984012            0.48435204043
      0.81881535281           0.39159479004
0 2 1 0 1 *
    1.36815980903E+00   1.00000000000E+00
0 2 1 0 1 *
    8.95778742822E-01   1.00000000000E+00
0 2 1 0 1 *
    4.73529149363E-01   1.00000000000E+00
0 2 1 0 1 *
    2.51002092777E-01   1.00000000000E+00
0 3 6 5 1
    200.40254535            0.89549560240D-03
     59.898225773           0.76257630942D-02
     22.810570167           0.34523224226D-01
      9.5874142097          0.10552676975
      4.2933710910          0.22575377683
      1.9537618373          0.32766533667
0 3 1 0 1 *
    1.50805880472E+00   1.00000000000E+00
0 3 1 0 1 *
    9.96546435407E-01   1.00000000000E+00
0 3 1 0 1 *
    4.65264229785E-01   1.00000000000E+00
0 3 1 0 1 *
    2.61516158539E-01   1.00000000000E+00
0 4 1 0 1
      4.3530000             1.0000000
0 4 1 0 1 *
    1.32367190727E+00   1.00000000000E+00
0 4 1 0 1 *
    3.82840001610E-01   1.00000000000E+00
0 5 1 0 1 *
    1.74914727246E+00   1.00000000000E+00
```

Fe - triple ζ

```
 26 15
0 0  8  2. 1.
      3.00784846370E+05   2.28062730960E-04
      4.50889705570E+04   1.76817887610E-03
      1.02625163170E+04   9.19270834900E-03
      2.90528972930E+03   3.73554958070E-02
      9.46114871370E+02   1.21511084260E-01
      3.39878328940E+02   2.88188814680E-01
      1.31944255880E+02   4.11266126770E-01
      5.21114940770E+01   2.15185835730E-01
0 0  4  2. 1.
      3.29488392670E+02  -2.47452164770E-02
      1.01923327390E+02  -1.16830890500E-01
      1.62404627450E+01   5.52936211360E-01
      6.88406758010E+00   5.36016401820E-01
```

Fe - triple ζ - mod

```
 26 15
0 0  8  2. 1.
      3.00784846370E+05   2.28062730960E-04
      4.50889705570E+04   1.76817887610E-03
      1.02625163170E+04   9.19270834900E-03
      2.90528972930E+03   3.73554958070E-02
      9.46114871370E+02   1.21511084260E-01
      3.39878328940E+02   2.88188814680E-01
      1.31944255880E+02   4.11266126770E-01
      5.21114940770E+01   2.15185835730E-01
0 0  4  2. 1.
      3.29488392670E+02  -2.47452164770E-02
      1.01923327390E+02  -1.16830890500E-01
      1.62404627450E+01   5.52936211360E-01
      6.88406758010E+00   5.36016401820E-01
```

```
0 0  2  2. 1.
      1.04706937820E+01  -2.29127085770E-01
      1.73600396480E+00   7.11593199840E-01
0 0  1  2. 1. *
      8.20350892376E-01   1.00000000000E+00
0 0  1  0. 1. *
      4.05524877387E-01   1.00000000000E+00
0 0  1  0. 1. *
      2.21093686651E-01   1.00000000000E+00
0 2  6  6. 1.
      1.58539599700E+03   2.37939601790E-03
      3.75380064990E+02   1.92531547550E-02
      1.20318165010E+02   9.00218365360E-02
      4.47887490310E+01   2.57981723560E-01
      1.78292785840E+01   4.14926497440E-01
      7.22471537860E+00   2.42074747840E-01
0 2  3  6. 1.
      2.81432197560E+01  -2.90417551520E-02
      3.87432414120E+00   5.53122603430E-01
      1.54107522810E+00   9.67711368420E-01
0 2  1  0. 1. *
      5.47919702750E-01   1.00000000000E+00
0 2  1  0. 1. *
      1.91780686138E-01   1.00000000000E+00
0 3  4  6. 1.
      6.19966750340E+01   1.19719722550E-02
      1.78737325520E+01   7.32101354100E-02
      6.27447829340E+00   2.31030943140E-01
      2.35523371750E+00   3.99107064940E-01
0 3  1  0. 1. *
      8.29342770495E-01   1.00000000000E+00
0 3  1  0. 1. *
      5.58837167875E-01   1.00000000000E+00
0 3  1  0. 1. *
      2.80713827067E-01   1.00000000000E+00
0 4  1  0. 1. *
      1.55480311474E+00   1.00000000000E+00
```

```
0 0  2  2. 1.
      1.04706937820E+01  -2.29127085770E-01
      1.73600396480E+00   7.11593199840E-01
0 0  1  2. 1.
1.70   1.
0 0  1  0. 1.
      4.05524877387E-01   1.00000000000E+00
0 0  1  0. 1.
      2.21093686651E-01   1.00000000000E+00
0 2  6  6. 1.
      1.58539599700E+03   2.37939601790E-03
      3.75380064990E+02   1.92531547550E-02
      1.20318165010E+02   9.00218365360E-02
      4.47887490310E+01   2.57981723560E-01
      1.78292785840E+01   4.14926497440E-01
      7.22471537860E+00   2.42074747840E-01
0 2  3  6. 1.
      2.81432197560E+01  -2.90417551520E-02
      3.87432414120E+00   5.53122603430E-01
      1.54107522810E+00   9.67711368420E-01
0 2  1  0. 1.
      5.47919702750E-01   1.00000000000E+00
0 2  1  0. 1.
      1.91780686138E-01   1.00000000000E+00
0 3  4  6. 1.
      6.19966750340E+01   1.19719722550E-02
      1.78737325520E+01   7.32101354100E-02
      6.27447829340E+00   2.31030943140E-01
      2.35523371750E+00   3.99107064940E-01
0 3  1  0. 1.
      8.29342770495E-01   4.13915897650E-01
0 3  1  0. 1.
2.80713827067E-01   1.00000000000E+00
0 3  1  0. 1.
0.25   1.
0 4  1  0. 1.
      1.55480311474E+00   1.00000000000E+00
```

Co - triple ζ

```
  27 15
0 0  8  2. 1.
      3.25817015530E+05   2.25684624840E-04
      4.88396364530E+04   1.74993975330E-03
      1.11149373070E+04   9.10031340970E-03
      3.14616036420E+03   3.69962568370E-02
      1.02443784650E+03   1.20442696210E-01
      3.68025088160E+02   2.85987316490E-01
      1.42912292050E+02   4.09083120040E-01
      5.64826492090E+01   2.15001457390E-01
0 0  4  2. 1.
      3.56402983180E+02  -2.47670596780E-02
      1.10311652150E+02  -1.17021391340E-01
      1.76596348340E+01   5.52155222000E-01
      7.50590304790E+00   5.32468770600E-01
0 0  2  2. 1.
```

```
      1.15018071760E+01  -2.29424700770E-01
      1.90819946060E+00   7.11809335140E-01
0 0  1  2. 1. *
      2.72235165909E+00   1.00000000000E+00
0 0  1  0. 1. *
      7.61625798315E-01   1.00000000000E+00
0 0  1  0. 1. *
      9.03326995733E-02   1.00000000000E+00
0 2  6  6. 1.
      1.73113691440E+03   2.39057676850E-03
      4.09917504380E+02   1.93829999670E-02
      1.31456485780E+02   9.09054485090E-02
      4.89874397140E+01   2.61466815770E-01
      1.95370789920E+01   4.21572645700E-01
      7.92872816340E+00   2.45718135570E-01
0 2  3  6. 1.
      3.10760175840E+01  -2.94380699730E-02
      4.28351806970E+00   5.56155681680E-01
      1.70229215630E+00   9.67721950640E-01
0 2  1  0. 1. *
      7.06469692018E-01   1.00000000000E+00
0 2  1  0. 1. *
      5.68350508120E-01   1.00000000000E+00
0 3  4  7. 1.
      6.81407452390E+01   1.19838453600E-02
      1.96852410190E+01   7.36885404750E-02
      6.93221288250E+00   2.30854967790E-01
      2.60251256940E+00   3.92810592250E-01
0 3  1  0. 1. *
      9.03734406634E-01   1.00000000000E+00
0 3  1  0. 1. *
      4.25767161884E-01   1.00000000000E+00
0 3  1  0. 1. *
      2.75045857572E-01   1.00000000000E+00
0 4  1  0. 1. *
      1.87029415727E+00   1.00000000000E+00

 Co - quadruple ζ

  27 24
0 0 11 2 1
4658206.5032000              0.86609506454D-05
 697560.8745300              0.67336300186D-04
 158759.8712400              0.35399044899D-03
  44969.0993790              0.14926384309D-02
  14670.7142470              0.54053095095D-02
   5295.8947250              0.17335233605D-01
   2065.0581167              0.49486641301D-01
    855.90627750             0.12289351961
    372.48747255             0.24903230028
    168.50576608             0.35838320259
     78.128761566            0.27777974150
0 0 4 2 1
   1534.5149885              0.74464372833D-02
    475.52976096             0.72993601986D-01
    182.54836839             0.33243104986
```

```
     78.916467177            0.61900490005
0 0 1 2 1
     35.500865522            1.0000000
0 0 1 2 1
     16.790414486            1.0000000
0 0 1 0 1
      8.0240232510           1.0000000
0 0 1 0 1
      3.4571682964           1.0000000
0 0 1 0 1
      1.6599835391           1.0000000
0 0 1 0 1
      0.75380022453          1.0000000
0 0 1 0 1 *
    4.28798523787E-01   1.00000000000E+00
0 0 1 0 1 *
    1.59998028373E-01   1.00000000000E+00
0 2 9 6 1
   8425.4331352             0.17491775490D-03
   1995.8758452             0.15378901702D-02
    647.76765681            0.85752453448D-02
    246.88261214            0.35295266911D-01
    104.00952246            0.11050007672
     46.827478138           0.25160924538
     21.934444535           0.38209003019
     10.540499528           0.30947119879
      4.9820419385          0.87436873012D-01
0 2 5 6 1
     69.270787130           -0.61172424428D-02
     24.583977935           -0.29655043898D-01
      4.8562258878          0.29163333190
      2.2480916102          0.60629408335
      1.0114285977          0.49057440018
0 2 1 0 1 *
    8.31203945073E-01   1.00000000000E+00
0 2 1 0 1 *
    6.56155471369E-01   1.00000000000E+00
0 2 1 0 1 *
    2.14050754160E-01   1.00000000000E+00
0 3 6 7 1
    237.58450966            0.97593282671D-03
     71.086896302           0.83432571945D-02
     27.119080683           0.37958471100D-01
     11.448239054           0.11522936171
      5.1391806672          0.23843467913
      2.3323492099          0.33205699955
0 3 1 0 1
    1.0338662062         1.
0 3 1 0 1 *
    7.55474382938E-01   1.00000000000E+00
0 3 1 0 1 *
    3.82471277591E-01   1.00000000000E+00
0 3 1 0 1 *
    2.86571541093E-01   1.00000000000E+00
0 4 1 0 1
      5.9750000             1.0000000
```

```
0 4 1 0 1
      1.9030000               1.0000000
0 4 1 0 1 *
    6.17282432138E-01   1.00000000000E+00
0 5 1 0 1 *
    2.49891040037E+00   1.00000000000E+00
```

Ni - triple ζ

```
 28 15
0 0  8  2. 1.
      3.51535729350E+05   2.25293868840E-04
      5.26958092830E+04   1.74686162230E-03
      1.19924682930E+04   9.08499921360E-03
      3.39457766890E+03   3.69407484470E-02
      1.10535945850E+03   1.20328199500E-01
      3.97146777690E+02   2.85967150570E-01
      1.54275429740E+02   4.09830201960E-01
      6.10187237800E+01   2.16206428510E-01
0 0  4  2. 1.
      3.84455597390E+02  -2.46512792680E-02
      1.19048791990E+02  -1.16585052770E-01
      1.91370122230E+01   5.48641266760E-01
      8.15267185620E+00   5.26400511220E-01
0 0  2  2. 1.
      1.25794086420E+01  -2.27978842930E-01
      2.08708660810E+00   7.07037382150E-01
0 0  1  2. 1. *
      4.13070286139E+00   1.00000000000E+00
0 0  1  0. 1. *
      8.57355806521E-01   1.00000000000E+00
0 0  1  0. 1. *
      1.92795025905E-01   1.00000000000E+00
0 2  6  6. 1.
      1.88309074860E+03   2.37482584430E-03
      4.45951553200E+02   1.92894571720E-02
      1.43084308150E+02   9.07182115070E-02
      5.33729207220E+01   2.61814141170E-01
      2.13219193570E+01   4.23091498320E-01
      8.66435619940E+00   2.46416860150E-01
0 2  3  6. 1.
      3.41442552110E+01  -2.96771291630E-02
      4.71224559210E+00   5.56168240960E-01
      1.87092318450E+00   9.63577664600E-01
0 2  1  0. 1. *
      6.79923475521E-01   1.00000000000E+00
0 2  1  0. 1. *
      1.56834370548E-01   1.00000000000E+00
0 3  4  8. 1.
      7.45916034650E+01   1.20774546720E-02
      2.15906327520E+01   7.46372621540E-02
      7.62461425800E+00   2.32367755020E-01
      2.86322067620E+00   3.90426516800E-01
0 3  1  0. 1. *
      1.00790128764E+00   1.00000000000E+00
0 3  1  0. 1. *
```

Ni - triple ζ - mod

```
 28 13
0 0  8  2. 1.
      3.51535729350E+05   2.25293868840E-04
      5.26958092830E+04   1.74686162230E-03
      1.19924682930E+04   9.08499921360E-03
      3.39457766890E+03   3.69407484470E-02
      1.10535945850E+03   1.20328199500E-01
      3.97146777690E+02   2.85967150570E-01
      1.54275429740E+02   4.09830201960E-01
      6.10187237800E+01   2.16206428510E-01
0 0  4  2. 1.
      3.84455597390E+02  -2.46512792680E-02
      1.19048791990E+02  -1.16585052770E-01
      1.91370122230E+01   5.48641266760E-01
      8.15267185620E+00   5.26400511220E-01
0 0  2  2. 1.
      1.25794086420E+01  -2.27978842930E-01
      2.08708660810E+00   7.07037382150E-01
0 1  1  2. 1.
1.9    1.    1.
 0 1  1  0. 1.
8.57355806521E-01   1.   1.
0 1  1  0. 1.
1.92795025905E-01   1.   1.
0 2  6  6. 1.
      1.88309074860E+03   2.37482584430E-03
      4.45951553200E+02   1.92894571720E-02
      1.43084308150E+02   9.07182115070E-02
      5.33729207220E+01   2.61814141170E-01
      2.13219193570E+01   4.23091498320E-01
      8.66435619940E+00   2.46416860150E-01
0 2  3  6. 1.
      3.41442552110E+01  -2.96771291630E-02
      4.71224559210E+00   5.56168240960E-01
      1.87092318450E+00   9.63577664600E-01
0 3  4  8. 1.
      7.45916034650E+01   1.20774546720E-02
      2.15906327520E+01   7.46372621540E-02
      7.62461425800E+00   2.32367755020E-01
      2.86322067620E+00   3.90426516800E-01
0 3  1  0. 1.
      1.00790128764E+00   1.00000000000E+00
0 3  1  0. 1.
```

```
      6.39433655247E-01   1.00000000000E+00
0 3  1  0. 1. *
      3.00360431319E-01   1.00000000000E+00
0 4  1  0. 1. *
      2.16004241173E+00   1.00000000000E+00
```

Cu - triple ζ

```
 29 15
0 0  8  2. 1.
      3.77518799230E+05   2.28117661280E-04
      5.65899843110E+04   1.76880359310E-03
      1.28787117060E+04   9.19934602270E-03
      3.64537521430E+03   3.74110164340E-02
      1.18700729450E+03   1.21898737370E-01
      4.26464219020E+02   2.89839007140E-01
      1.65706601640E+02   4.15318721740E-01
      6.55989427070E+01   2.19057992870E-01
0 0  4  2. 1.
      4.14412658110E+02  -2.46825250530E-02
      1.28320560390E+02  -1.17168274060E-01
      2.06220897500E+01   5.53013159410E-01
      8.78212260450E+00   5.22427186090E-01
0 0  2  2. 1.
      1.37413720060E+01  -2.27360618210E-01
      2.24312468330E+00   7.17612108730E-01
0 0  1  1. 1. *
      9.62573851032E-01   1.00000000000E+00
0 0  1  0. 1. *
      5.02580555763E-01   1.00000000000E+00
0 0  1  0. 1. *
      1.71670424002E-01   1.00000000000E+00
0 2  6  6. 1.
      2.03475966920E+03   2.35248222980E-03
      4.81904681060E+02   1.91340707510E-02
      1.54674829630E+02   9.01711052780E-02
      5.77405769690E+01   2.60632847350E-01
      2.30990528110E+01   4.20934857700E-01
      9.38824785910E+00   2.43446151210E-01
0 2  3  6. 1.
      3.75961712100E+01  -2.89910945300E-02
      5.12406908100E+00   5.49190838310E-01
      2.01199960850E+00   9.37933304880E-01
0 2  1  0. 1. *
      7.24830098379E-01   1.00000000000E+00
0 2  1  0. 1. *
      1.94161012380E-01   1.00000000000E+00
0 3  4 10. 1.
      7.41294606370E+01   1.43632166760E-02
      2.13598425870E+01   8.66281770960E-02
      7.49952405370E+00   2.56314305410E-01
      2.76013941690E+00   4.03740623680E-01
0 3  1  0. 1. *
      1.06696876154E+00   1.00000000000E+00
0 3  1  0. 1. *
      8.36071589357E-01   1.00000000000E+00
```

```
      6.39433655247E-01   1.00000000000E+00
0 3  1  0. 1.
      3.00360431319E-01   1.00000000000E+00
0 4  1  0. 1.
      2.16004241173E+00   1.00000000000E+00
```

Cu - triple ζ - mod

```
 29  8
0 0  8  2. 1.
      3.98000000000E+05   2.27000000000E-04
      5.66700000000E+04   1.92900000000E-03
      1.20100000000E+04   1.11400000000E-02
      3.13900000000E+03   5.01300000000E-02
      9.47200000000E+02   1.70310000000E-01
      3.27680000000E+02   3.69300000000E-01
      1.28390000000E+02   4.03000000000E-01
      5.36300000000E+01   1.43700000000E-01
0 1  6  8. 1.
      1.02200000000E+03  -4.870E-03   8.500E-03
      2.38900000000E+02  -6.740E-02   6.063E-02
      8.00000000000E+01  -1.242E-01   2.118E-01
      3.18600000000E+01   2.466E-01   3.907E-01
      1.33300000000E+01   6.720E-01   3.964E-01
      4.44200000000E+00   2.890E-01   2.610E-01
0 1  4  8. 1.
      5.47000000000E+01   1.190E-02  -2.880E-02
      2.32600000000E+01  -1.460E-01  -7.410E-02
      9.92000000000E+00  -7.500E-01   1.820E-01
      4.01300000000E+00   1.031E+00   1.280E+00
0 1  1  1. 1. *
      1.61549411866E+00   1.   1.
0 1  1  0. 1. *
      6.50276993901E-01   1.   1.
0 1  1  0. 1. *
      1.61119802401E-01   1.   1.
0 3  4 10. 1.
      4.85400000000E+01   3.10000000000E-02
      1.35500000000E+01   1.62000000000E-01
      4.52000000000E+00   3.78000000000E-01
      1.47000000000E+00   4.59000000000E-01
0 3  1  0. 1. *
      3.89705071297E-01   1.00000000000E+00
```

```
0 3  1  0. 1. *
      2.57419273107E-01   1.00000000000E+00
0 4  1  0. 1. *
      2.22306915419E+00   1.00000000000E+00
```

```
 Zn - triple ζ

 30 16
0 0  8  2. 1.
      4.05924310280E+05   2.24420174830E-04
      6.08469557350E+04   1.74020866260E-03
      1.38473430920E+04   9.05133395650E-03
      3.91961585510E+03   3.68173414450E-02
      1.27635941670E+03   1.20048502560E-01
      4.58672544350E+02   2.85760576210E-01
      1.78287252460E+02   4.10874620620E-01
      7.06121928370E+01   2.18169624560E-01
0 0  4  2. 1.
      4.43880779500E+02  -2.49342749840E-02
      1.37558752670E+02  -1.18179557660E-01
      2.22680834790E+01   5.53673184680E-01
      9.52173106060E+00   5.26289349360E-01
0 0  2  2. 1.
      1.48741140650E+01  -2.29299552540E-01
      2.46475176120E+00   7.11354847420E-01
0 0  1  2. 1. *
      1.07660711961E+00   1.00000000000E+00
0 0  1  0. 1. *
      7.59936967391E-01   1.00000000000E+00
0 0  1  0. 1. *
      1.34083220467E-01   1.00000000000E+00
0 2  6  6. 1.
      2.20535085340E+03   2.33562404480E-03
      5.22353006990E+02   1.90310226340E-02
      1.67730555420E+02   8.99557586750E-02
      6.26700453730E+01   2.61132486310E-01
      2.51097494560E+01   4.23484481730E-01
      1.02251426810E+01   2.46189268850E-01
0 2  3  6. 1.
      4.07134425210E+01  -3.00296675920E-02
      5.62470906960E+00   5.55752548640E-01
      2.22799491160E+00   9.55810134420E-01
0 2  1  0. 1. *
      7.67793092003E-01   1.00000000000E+00
0 2  1  0. 1. *
      5.53471381172E-01   1.00000000000E+00
0 2  1  0. 1. *
      1.63881759413E-01   1.00000000000E+00
0 3  4 10. 1.
      8.85543153110E+01   1.27281700150E-02
      2.57215255570E+01   7.93944998430E-02
      9.12783676240E+00   2.44915068050E-01
      3.43123640640E+00   4.03905264790E-01
0 3  1  0. 1. *
      1.22403302850E+00   1.00000000000E+00
0 3  1  0. 1. *
```

```
 Zn - triple ζ - mod

 30 13
0 0  8  2. 1.
      4.05924310280E+05   2.24420174830E-04
      6.08469557350E+04   1.74020866260E-03
      1.38473430920E+04   9.05133395650E-03
      3.91961585510E+03   3.68173414450E-02
      1.27635941670E+03   1.20048502560E-01
      4.58672544350E+02   2.85760576210E-01
      1.78287252460E+02   4.10874620620E-01
      7.06121928370E+01   2.18169624560E-01
0 0  4  2. 1.
      4.43880779500E+02  -2.49342749840E-02
      1.37558752670E+02  -1.18179557660E-01
      2.22680834790E+01   5.53673184680E-01
      9.52173106060E+00   5.26289349360E-01
0 0  2  2. 1.
      1.48741140650E+01  -2.29299552540E-01
      2.46475176120E+00   7.11354847420E-01
0 1  1  2. 1.
1.6    1.   1.
0 1  1  0. 1.
7.59936967391E-01   1.00000000000E+00    1.
0 1  1  0. 1.
1.34083220467E-01   1.00000000000E+00    1.
0 2  6  6. 1.
      2.20535085340E+03   2.33562404480E-03
      5.22353006990E+02   1.90310226340E-02
      1.67730555420E+02   8.99557586750E-02
      6.26700453730E+01   2.61132486310E-01
      2.51097494560E+01   4.23484481730E-01
      1.02251426810E+01   2.46189268850E-01
0 2  3  6. 1.
      4.07134425210E+01  -3.00296675920E-02
      5.62470906960E+00   5.55752548640E-01
      2.22799491160E+00   9.55810134420E-01
0 3  4 10. 1.
      8.85543153110E+01   1.27281700150E-02
      2.57215255570E+01   7.93944998430E-02
      9.12783676240E+00   2.44915068050E-01
      3.43123640640E+00   4.03905264790E-01
0 3  1  0. 1.
      1.22403302850E+00   1.00000000000E+00
0 3  1  0. 1.
```

```
      4.52228523894E-01   1.00000000000E+00
0 3  1  0. 1. *
      1.88864754578E-01   1.00000000000E+00
0 4  1  0. 1. *
      2.60217014872E+00   1.00000000000E+00
```

```
      4.52228523894E-01   1.00000000000E+00
0 3  1  0. 1.
      1.88864754578E-01   1.00000000000E+00
0 4  1  0. 1.
      2.60217014872E+00   1.00000000000E+00
```

Zn - quadruple ζ

```
  30 25
0 0 11 2 1
5742307.1507000              0.86864381562D-05
 861450.7879000              0.67364668570D-04
 196346.0586600              0.35349715135D-03
  55682.8707370              0.14884153943D-02
  18183.9023940              0.53840916617D-02
   6569.6448019              0.17252738209D-01
   2563.5613276              0.49238679132D-01
   1063.1147176              0.12235812174
    462.89771078             0.24835390245
    209.52821049             0.35830632832
     97.240787991            0.27880259960
0 0 4 2 1
   1929.2689992              0.83077002177D-02
    598.07122307             0.81882590163D-01
    229.69667336             0.37588060221
     99.416819228            0.71067260445
0 0 1 2 1
     44.241101421            1.0000000
0 0 1 2 1
     21.194367113            1.0000000
0 0 1 0 1
     10.158731597            1.0000000
0 0 1 0 1
      4.3746176158           1.0000000
0 0 1 0 1
      2.0901489071           1.0000000
0 0 1 0 1 *
  9.59621063781E-01   1.00000000000E+00
0 0 1 0 1 *
  3.30202931230E-01   1.00000000000E+00
0 0 1 0 1 *
  1.76572210034E-01   1.00000000000E+00
0 2 9 6 1
  10690.4451070              0.17142867222D-03
   2532.3159340              0.15088012830D-02
    821.94295003             0.84368777910D-02
    313.42757800             0.34898103208D-01
    132.18314247             0.10993617353
     59.620554387            0.25207277070
     28.019488868            0.38325657524
     13.511704850            0.30787091255
      6.4053711253           0.86411696761D-01
0 2 5 6 1
     89.981131918            -0.96262847843D-02
     32.241767106            -0.47509407258D-01
      6.3809448581           0.45834100431
```

```
      2.9477928353            0.94473799128
      1.3200854955            0.75923464871
0 2 1 0 1 *
       1. 1.
0 2 1 0 1 *
  8.50011386106E-01   1.00000000000E+00
0 2 1 0 1 *
   0.3   1.
0 2 1 0 1 *
  1.54630798107E-01   1.00000000000E+00
0 3 6 10 1
    305.22298937            0.27359792434D-02
     91.468273202           0.23585229776D-01
     34.986985968           0.10858422440
     14.849415187           0.32843594226
      6.6858545707          0.66180235634
      3.0309412620          0.89165339320
0 3 1 0 1 *
  1.17444930445E+00   1.00000000000E+00
0 3 1 0 1 *
   0.6    1.
0 3 1 0 1 *
   0.4    1.
0 3 1 0 1 *
  2.09255044622E-01   1.00000000000E+00
0 4 1 0 1
      8.0200000             1.0000000
0 4 1 0 1
      2.6140000             1.0000000
0 4 1 0 1 *
  8.29986512749E-01   1.00000000000E+00
0 5 1 0 1 *
  3.61717895240E+00   1.00000000000E+00
```

Ga - triple ζ

```
  31 16
0 0 8 2 1
 435548.6625400           0.23646329650D-03
  65289.5890310           0.18335271776D-02
  14858.7842560           0.95371863081D-02
   4205.9734729           0.38803412468D-01
   1369.6416431           0.12661604848
    492.30348905          0.30175310292
    191.41923233          0.43543934218
     75.840558665         0.23282363780
0 0 4 2 1
    474.30810613          -0.26743707958D-01
    147.10297560          -0.12654657542
     23.982599435          0.58840346839
     10.298230094          0.56324271589
0 0 2 2 1
     16.050381430         -0.24516439508
      2.6988468784         0.74578049593
0 0 1 2 1 *
    1.19037990995E+00   1.00000000000E+00
```

Ga - triple ζ - mod

```
  31 17
0 0 8 2 1
 435548.6625400           0.23646329650D-03
  65289.5890310           0.18335271776D-02
  14858.7842560           0.95371863081D-02
   4205.9734729           0.38803412468D-01
   1369.6416431           0.12661604848
    492.30348905          0.30175310292
    191.41923233          0.43543934218
     75.840558665         0.23282363780
0 0 4 2 1
    474.30810613          -0.26743707958D-01
    147.10297560          -0.12654657542
     23.982599435          0.58840346839
     10.298230094          0.56324271589
0 0 2 2 1
     16.050381430         -0.24516439508
      2.6988468784         0.74578049593
0 0 1 2 1
    1.19037990995E+00   1.00000000000E+00
```

```
0 0 1 0 1 *
   6.16564253310E-01   1.00000000000E+00
0 0 1 0 1 *
   1.54361520209E-01   1.00000000000E+00
0 2 6 6 1
  2432.0171070          0.22434065928D-02
   576.12049582         0.18342265336D-01
   185.11584354         0.87279697167D-01
    69.246572556        0.25684868351
    27.818107777        0.42398378107
    11.420229938        0.25701340043
0 2 3 6 1
    42.819661530       -0.19326519119D-01
     6.3885901000       0.31571386917
     2.6698993326       0.57617792822
0 2 1 1 1 *
   1.06018400680E+00   1.00000000000E+00
0 2 1 0 1 *
   5.97745330763E-01   1.00000000000E+00
0 2 1 0 1 *
   1.59345047474E-01   1.00000000000E+00
0 3 5 10 1
    103.92331829          0.11464613652D-01
     30.371094389         0.73625747383D-01
     10.872078097         0.23505107382
      4.1549137954        0.40318563513
      1.5345659145        0.40824748152
0 3 1 0 1 *
   1.60879809916E+00   1.00000000000E+00
0 3 1 0 1 *
   5.50843627724E-01   1.00000000000E+00
0 3 1 0 1 *
   1.69523212205E-01   1.00000000000E+00
0 4 1 0 1 *
   2.60392252756E+00   1.00000000000E+00
```

```
0 0 1 0 1
   6.16564253310E-01   1.00000000000E+00
0 0 1 0 1
0.3    1.
0 0 1 0 1
   1.54361520209E-01   1.00000000000E+00
0 2 6 6 1
  2432.0171070          0.22434065928D-02
   576.12049582         0.18342265336D-01
   185.11584354         0.87279697167D-01
    69.246572556        0.25684868351
    27.818107777        0.42398378107
    11.420229938        0.25701340043
0 2 3 6 1
    42.819661530       -0.19326519119D-01
     6.3885901000       0.31571386917
     2.6698993326       0.57617792822
0 2 1 1 1
   1.06018400680E+00   1.00000000000E+00
0 2 1 0 1
   5.97745330763E-01   1.00000000000E+00
0 2 1 0 1
   1.59345047474E-01   1.00000000000E+00
0 3 5 10 1
    103.92331829          0.11464613652D-01
     30.371094389         0.73625747383D-01
     10.872078097         0.23505107382
      4.1549137954        0.40318563513
      1.5345659145        0.40824748152
0 3 1 0 1
   1.60879809916E+00   1.00000000000E+00
0 3 1 0 1
   5.50843627724E-01   1.00000000000E+00
0 3 1 0 1
   1.69523212205E-01   1.00000000000E+00
0 4 1 0 1
   2.60392252756E+00   1.00000000000E+00
```

Ge - triple ζ

```
 32 16
0 0  8  2. 1.
      4.66115005920E+05   2.24872646600E-04
      6.98754207620E+04   1.74354267290E-03
      1.59032767160E+04   9.06914822060E-03
      4.50182334530E+03   3.69061746850E-02
      1.46605709240E+03   1.20501679070E-01
      5.27078417280E+02   2.87486417030E-01
      2.05003950740E+02   4.16223218850E-01
      8.12515960650E+01   2.23978456950E-01
0 0  4  2. 1.
      5.05746612820E+02  -2.51846092910E-02
      1.56965937440E+02  -1.18989297210E-01
      2.57614481760E+01   5.49301358700E-01
      1.11066546870E+01   5.29393091290E-01
0 0  2  2. 1.
```

Ge - triple ζ - mod

```
 32 16
0 0  8  2. 1.
      4.66115005920E+05   2.24872646600E-04
      6.98754207620E+04   1.74354267290E-03
      1.59032767160E+04   9.06914822060E-03
      4.50182334530E+03   3.69061746850E-02
      1.46605709240E+03   1.20501679070E-01
      5.27078417280E+02   2.87486417030E-01
      2.05003950740E+02   4.16223218850E-01
      8.12515960650E+01   2.23978456950E-01
0 0  4  2. 1.
      5.05746612820E+02  -2.51846092910E-02
      1.56965937440E+02  -1.18989297210E-01
      2.57614481760E+01   5.49301358700E-01
      1.11066546870E+01   5.29393091290E-01
0 0  2  2. 1.
```

```
      1.72720591040E+01  -2.28545957280E-01
      2.94382890480E+00   6.83779303170E-01
0 0  1  2. 1. *
      1.27865696000E+00   1.00000000000E+00
0 0  1  0. 1. *
      3.39119160320E-01   1.00000000000E+00
0 0  1  0. 1. *
      1.31627163226E-01   1.00000000000E+00
0 2  6  6. 1.
      2.63393462410E+03   2.21439253100E-03
      6.24001616280E+02   1.81408991410E-02
      2.00585284040E+02   8.66321849220E-02
      7.50970815250E+01   2.56490205920E-01
      3.02143884740E+01   4.26586112620E-01
      1.24400875670E+01   2.62005273130E-01
0 2  3  6. 1.
      4.59813160020E+01  -2.03217676780E-02
      6.99456544160E+00   3.20137445270E-01
      2.96860013270E+00   5.90510145550E-01
0 2  1  2. 1. *
      1.20835020190E+00   1.00000000000E+00
0 2  1  0. 1. *
      4.74440968948E-01   1.00000000000E+00
0 2  1  0. 1. *
      1.67787699914E-01   1.00000000000E+00
0 3  5 10. 1.
      1.19448875810E+02   1.05865445210E-02
      3.50629152930E+01   6.96012809450E-02
      1.26369245290E+01   2.28070352870E-01
      4.88886729220E+00   4.03010672200E-01
      1.84531953920E+00   4.13048470150E-01
0 3  1  0. 1. *
      1.99591025098E+00   1.00000000000E+00
0 3  1  0. 1. *
      6.59011400517E-01   1.00000000000E+00
0 3  1  0. 1. *
      1.61065170150E-01   1.00000000000E+00
0 4  1  0. 1. *
      2.83623731395E-01   1.00000000000E+00
```

```
      1.72720591040E+01  -2.28545957280E-01
      2.94382890480E+00   6.83779303170E-01
0 0  1  2. 1.
      1.27865696000E+00   1.00000000000E+00
0 0  1  0. 1.
      3.39119160320E-01   1.00000000000E+00
0 0  1  0. 1.
      1.31627163226E-01   1.00000000000E+00
0 2  6  6. 1.
      2.63393462410E+03   2.21439253100E-03
      6.24001616280E+02   1.81408991410E-02
      2.00585284040E+02   8.66321849220E-02
      7.50970815250E+01   2.56490205920E-01
      3.02143884740E+01   4.26586112620E-01
      1.24400875670E+01   2.62005273130E-01
0 2  3  6. 1.
      4.59813160020E+01  -2.03217676780E-02
      6.99456544160E+00   3.20137445270E-01
      2.96860013270E+00   5.90510145550E-01
0 2  1  2. 1.
      1.20835020190E+00   1.00000000000E+00
0 2  1  0. 1.
      4.74440968948E-01   1.00000000000E+00
0 2  1  0. 1.
      1.67787699914E-01   1.00000000000E+00
0 3  5 10. 1.
      1.19448875810E+02   1.05865445210E-02
      3.50629152930E+01   6.96012809450E-02
      1.26369245290E+01   2.28070352870E-01
      4.88886729220E+00   4.03010672200E-01
      1.84531953920E+00   4.13048470150E-01
0 3  1  0. 1.
      6.59011400517E-01   1.00000000000E+00
0 3  1  0. 1.
      0.35492132          1.
0 3  1  0. 1.
      1.61065170150E-01   1.00000000000E+00
0 4  1  0. 1.
      2.83623731395E-01   1.00000000000E+00
```

```
 Ge - quadruple ζ(one s added**)

32 25
0 0 11 2.0 1.0
7233056.0346000              0.76638751457D-05
1082886.1731000              0.59603601369D-04
 246481.4695900              0.31319088031D-03
  69862.4269550              0.13194051561D-02
  22815.8096620              0.47736099191D-02
   8246.5369297              0.15319250467D-01
   3219.9367257              0.43900870673D-01
   1336.5743706              0.11028573632
    582.87737501             0.22912630489
    264.59511360             0.34779259246
    123.77823320             0.29968722223
0 0 4 2.0 1.0
```

```
   2311.1055804              0.75033084731D-02
    716.27089868             0.74778386626D-01
    275.45330910             0.35092882302
    118.93292565             0.72055989686
0 0 1 2.0 1.0
     58.435699085            1.0000000
0 0 1 2.0 1.0
     26.261575973            1.0000000
0 0 1 0.0 1.0
     12.664880671            1.0000000
0 0 1 0.0 1.0
      5.7269548505           1.0000000
0 0 1 0.0 1.0
      2.7555023203           1.0000000
0 0 1 0.0 1.0
      1.2432886754           1.0000000
0 0 1 0.0 1.0 *
 6.09412279021E-01   1.00000000000E+00
0 0 1 0.0 1.0 *
 1.95548301909E-01   1.00000000000E+00
0 0 1 0.0 1.0 **
      0.09  1.
0 2 9 6.0 1.0
  16555.7110740              0.10199370391D-03
   3914.9903745              0.90504190546D-03
   1269.4766518              0.51558490762D-02
    484.35437789             0.22010335708D-01
    204.64985822             0.73434798827D-01
     92.791032094            0.18608955294
     44.055060255            0.33330981945
     21.601319931            0.36229776246
     10.732169233            0.17765186263
0 2 4 6.0 1.0
      8.0343224115           0.31484763263
      4.5613438333           0.38737744790
      3.1794882223           0.50034353638
      0.92612041457          0.22656707948
0 2 2 2.0 1.0
    100.88933962             -0.11146182144
     36.640254741            -0.52324324314
0 2 1 0.0 1.0
      1.7977040907           1.0000000
0 2 1 0.0 1.0 *
 9.09921700010E-01   1.00000000000E+00
0 2 1 0.0 1.0 *
 4.14457345952E-01   1.00000000000E+00
0 2 1 0.0 1.0 *
 1.35441466557E-01   1.00000000000E+00
0 3 7 10 1.0
    420.99565921             0.78212192196D-03
    126.36209818             0.69560123831D-02
     48.661473548            0.33712188323D-01
     20.880325527            0.10717291194
      9.5418229355           0.23161030141
      4.4353653868           0.33390954301
      2.0285421942           0.33720676378
```

```
0 3 1 0 1.0 *
 7.84734435140E-01   1.00000000000E+00
0 3 1 0 1.0 *
 6.08906904885E-01   1.00000000000E+00
0 3 1 0 1.0 *
 3.09325861217E-01   1.00000000000E+00
0 4 1 0 1.0 *
 5.36350774877E-01   1.00000000000E+00
0 4 1 0 1.0 *
 2.14097848679E-01   1.00000000000E+00
0 5 1 0 1.0 *
 4.41702281401E-01   1.00000000000E+00

 As - triple ζ

 33 16
0 0  8  2. 1.
      4.98032421580E+05   2.27401969000E-04
      7.46568687430E+04   1.76328164130E-03
      1.69909600040E+04   9.17280403810E-03
      4.80962003210E+03   3.73378293440E-02
      1.56628870550E+03   1.21995361170E-01
      5.63213604990E+02   2.91374753240E-01
      2.19111799780E+02   4.23263514790E-01
      8.68660610300E+01   2.29214642780E-01
0 0  4  2. 1.
      5.38195124790E+02  -2.52541972970E-02
      1.67148502240E+02  -1.19154611150E-01
      2.76055171590E+01   5.46284959800E-01
      1.19478585210E+01   5.30015209760E-01
0 0  2  2. 1.
      1.85380231330E+01  -2.34791881360E-01
      3.20189857390E+00   6.91670534280E-01
0 0  1  2. 1. *
      1.45403251228E+00   1.00000000000E+00
0 0  1  0. 1. *
      6.22974277547E-01   1.00000000000E+00
0 0  1  0. 1. *
      2.03491176095E-01   1.00000000000E+00
0 2  6  6. 1.
      2.67894215460E+03   2.33189552870E-03
      6.34617658400E+02   1.90421499770E-02
      2.03939676060E+02   9.02297449130E-02
      7.63238903690E+01   2.61690376930E-01
      3.06641249430E+01   4.18571681550E-01
      1.25050567320E+01   2.34478301900E-01
0 2  4  6. 1.
      4.92562295490E+01  -2.12355398700E-02
      7.72748914660E+00   3.04702066680E-01
      3.54104934760E+00   5.28883731070E-01
      1.69855855010E+00   3.72722509550E-01
0 2  1  3. 1. *
      7.23074504430E-01   1.00000000000E+00
0 2  1  0. 1. *
      3.20532535387E-01   1.00000000000E+00
0 2  1  0. 1. *
```

```
      1.17101493690E-01   1.00000000000E+00
0 3  5 10. 1.
      1.35332893050E+02   9.92911441060E-03
      3.98602127440E+01   6.65688434960E-02
      1.44464283590E+01   2.22757683070E-01
      5.64329003560E+00   4.03092243820E-01
      2.16681886230E+00   4.16716679460E-01
0 3  1  0. 1. *
      6.67956264756E-01   1.00000000000E+00
0 3  1  0. 1. *
      5.14071576787E-01   1.00000000000E+00
0 3  1  0. 1. *
      2.49218364367E-01   1.00000000000E+00
0 4  1  0. 1. *
      3.22333802755E-01   1.00000000000E+00

 As - quadruple ζ

33 25
0 0 11  2. 1.
      8.21748261980E+06   7.05906184220E-06
      1.23050037200E+06   5.48808896110E-05
      2.80225866480E+05   2.88091646980E-04
      7.94825094150E+04   1.21297794640E-03
      2.59637833510E+04   4.39145598800E-03
      9.38140101930E+03   1.41253629610E-02
      3.66049119720E+03   4.06579156180E-02
      1.51823560240E+03   1.03003826330E-01
      6.61800989200E+02   2.17300771010E-01
      3.00586421270E+02   3.39957514120E-01
      1.41111372960E+02   3.10886340770E-01
0 0  4  2. 1.
      2.57708705800E+03   7.07529919800E-03
      7.98078722770E+02   7.13836152560E-02
      3.06575749480E+02   3.42870246340E-01
      1.32275588020E+02   7.43614034130E-01
0 0  1  2. 1.
      6.74487022350E+01   1.00000000000E+00
0 0  1  2. 1.
      2.92091804410E+01   1.00000000000E+00
0 0  1  0. 1.
      1.41565093260E+01   1.00000000000E+00
0 0  1  0. 1.
      6.55615066820E+00   1.00000000000E+00
0 0  1  0. 1.
      3.13928472380E+00   1.00000000000E+00
0 0  1  0. 1.
      1.42946310500E+00   1.00000000000E+00
0 0  1  0. 1. *
      6.77177254855E-01   1.00000000000E+00
0 0  1  0. 1. *
      2.99938309105E-01   1.00000000000E+00
0 0  1  0. 1. *
      1.19396264012E-01   1.00000000000E+00
0 2 10  6. 1.
      2.51985042780E+04   5.47581683720E-05
```

```
      5.97256013810E+03   4.85724624520E-04
      1.94191231830E+03   2.79080856250E-03
      7.43593811040E+02   1.22015059620E-02
      3.15638280520E+02   4.26662851380E-02
      1.43968789250E+02   1.18709191410E-01
      6.90686831640E+01   2.49094070230E-01
      3.42543056290E+01   3.60613569030E-01
      1.73717467590E+01   2.93922418320E-01
      8.76345556280E+00   9.78290573660E-02
0 2  5  6. 1.
      2.28490245820E+02  -2.49001407650E-03
      8.63135554880E+01  -1.94825158430E-02
      3.67513662670E+01  -6.14950710380E-02
      8.53651494640E+00   4.72580650620E-01
      4.19351285990E+00   1.02360650790E+00
0 2  1  3. 1.
      2.04649804170E+00   1.00000000000E+00
0 2  1  0. 1. *
      1.07203779185E+00   1.00000000000E+00
0 2  1  0. 1. *
      5.90412624961E-01   1.00000000000E+00
0 2  1  0. 1. *
      3.39939297171E-01   1.00000000000E+00
0 2  1  0. 1. *
      1.12388419051E-01   1.00000000000E+00
0 3  7 10. 1.
      4.79325996120E+02   7.17228001960E-04
      1.43960648550E+02   6.44192230460E-03
      5.55489092240E+01   3.17764989640E-02
      2.39275810060E+01   1.02762491680E-01
      1.09881941720E+01   2.27109528430E-01
      5.14893562620E+00   3.34774741180E-01
      2.38368108920E+00   3.41759860710E-01
0 3  1  0. 1. *
      1.52041426629E+00   1.00000000000E+00
0 3  1  0. 1. *
      1.19428158287E+00   1.00000000000E+00
0 3  1  0. 1. *
      4.27933068275E-01   1.00000000000E+00
0 4  1  0. 1. *
      9.47824275248E-01   1.00000000000E+00
0 4  1  0. 1. *
      3.92943392968E-01   1.00000000000E+00
0 5  1  0. 1. *
      6.59887506294E-01   1.00000000000E+00

 Se - triple ζ

 34 16
0 0  8  2. 1.
      5.31071666960E+05   2.41089731680E-04
      7.96030441170E+04   1.86964314410E-03
      1.81158442400E+04   9.72716165360E-03
      5.12789231940E+03   3.96047930310E-02
      1.66991308390E+03   1.29488551360E-01
      6.00575345270E+02   3.09594372890E-01
```

```
      2.33700212470E+02   4.51157692160E-01
      9.26724439320E+01   2.45791890330E-01
0 0  4  2. 1.
      5.71575136750E+02  -2.68957078810E-02
      1.77636863750E+02  -1.26709893530E-01
      2.95177670520E+01   5.76990017190E-01
      1.28243997950E+01   5.63690754080E-01
0 0  2  2. 1.
      1.98482358410E+01  -2.51324155340E-01
      3.47440184860E+00   7.29054169800E-01
0 0  1  2. 1. *
      1.58974829107E+00   1.00000000000E+00
0 0  1  0. 1. *
      4.61736708989E-01   1.00000000000E+00
0 0  1  0. 1. *
      1.81399717148E-01   1.00000000000E+00
0 2  6  6. 1.
      2.81535005660E+03   2.55690268540E-03
      6.66925582980E+02   2.08740269010E-02
      2.14342131880E+02   9.87720962500E-02
      8.02466879420E+01   2.84718212210E-01
      3.22510812880E+01   4.50035849340E-01
      1.31064325620E+01   2.44160910550E-01
0 2  4  6. 1.
      5.33661085160E+01  -2.15584562730E-02
      8.18277771950E+00   3.26623106380E-01
      3.62399456720E+00   5.77404993190E-01
      1.63415914010E+00   3.43013208260E-01
0 2  1  4. 1. *
      7.20783886526E-01   1.00000000000E+00
0 2  1  0. 1. *
      2.99622949889E-01   1.00000000000E+00
0 2  1  0. 1. *
      1.03443166373E-01   1.00000000000E+00
0 3  5 10. 1.
      1.51829102790E+02   9.39702769880E-03
      4.48399925230E+01   6.40865039910E-02
      1.63289995100E+01   2.18342380040E-01
      6.43050576120E+00   4.03147896490E-01
      2.50480251690E+00   4.19664914900E-01
0 3  1  0. 1. *
      7.96157680621E-01   1.00000000000E+00
0 3  1  0. 1. *
      5.98438540754E-01   1.00000000000E+00
0 3  1  0. 1. *
      3.14576737908E-01   1.00000000000E+00
0 4  1  0. 1. *
      4.02554512000E-01   1.00000000000E+00

 Br - triple ζ

 35 16
0 0  8  2. 1.
      5.65073252560E+05   2.36603146900E-04
      8.47017231790E+04   1.83483325080E-03
      1.92762719000E+04   9.54658498600E-03
```

```
      5.45642845760E+03   3.88771421530E-02
      1.77695035000E+03   1.27183142310E-01
      6.39193982760E+02   3.04376621910E-01
      2.48788239610E+02   4.44909404970E-01
      9.86783054940E+01   2.43816430580E-01
0 0  4  2. 1.
      6.06078245680E+02  -2.65271587090E-02
      1.88455984840E+02  -1.24845848090E-01
      3.14971445060E+01   5.64686835590E-01
      1.37360083200E+01   5.55552685640E-01
0 0  2  2. 1.
      2.12032127660E+01  -2.49409204930E-01
      3.76164201780E+00   7.12131197430E-01
0 0  1  2. 1. *
      1.75343977436E+00   1.00000000000E+00
0 0  1  0. 1. *
      5.09089234470E-01   1.00000000000E+00
0 0  1  0. 1. *
      1.94973500592E-01   1.00000000000E+00
0 2  6  6. 1.
      3.01969557230E+03   2.49710497980E-03
      7.15354811260E+02   2.04192675960E-02
      2.29983287510E+02   9.68971483090E-02
      8.61678446150E+01   2.80539012520E-01
      3.46678708020E+01   4.46063904730E-01
      1.41138703070E+01   2.44100739230E-01
0 2  4  6. 1.
      5.70856530820E+01  -2.18559507100E-02
      8.81938458400E+00   3.27070753200E-01
      3.93403028720E+00   5.78552295200E-01
      1.79988303840E+00   3.35709876980E-01
0 2  1  5. 1. *
      7.74849635373E-01   1.00000000000E+00
0 2  1  0. 1. *
      3.14209820909E-01   1.00000000000E+00
0 2  1  0. 1. *
      1.13205299852E-01   1.00000000000E+00
0 3  5 10. 1.
      1.68853702570E+02   8.96639819880E-03
      4.99779499190E+01   6.20620593160E-02
      1.82749133380E+01   2.14747323840E-01
      7.24556946310E+00   4.03353367460E-01
      2.85623150250E+00   4.22088130800E-01
0 3  1  0. 1. *
      9.28062896006E-01   1.00000000000E+00
0 3  1  0. 1. *
      7.29226503460E-01   1.00000000000E+00
0 3  1  0. 1. *
      3.30559845991E-01   1.00000000000E+00
0 4  1  0. 1. *
      4.22343575443E-01   1.00000000000E+00

 Kr - triple ζ
 36 16
0 0  8  2. 1.
      6.00250975750E+05   2.37406103990E-04
```

```
      8.99766507810E+04   1.84102405390E-03
      2.04768142250E+04   9.57955806990E-03
      5.79615540780E+03   3.90206504880E-02
      1.88759131960E+03   1.27726456280E-01
      6.79114585190E+02   3.05965213000E-01
      2.64382445110E+02   4.48574744370E-01
      1.04883685740E+02   2.47229573270E-01
0 0  4  2. 1.
      6.41473707640E+02  -2.67452798050E-02
      1.99575248200E+02  -1.25711225670E-01
      3.35454629540E+01   5.64837363900E-01
      1.46839551440E+01   5.59727655390E-01
0 0  2  2. 1.
      2.26031018600E+01  -2.52987718000E-01
      4.06506829910E+00   7.09921599650E-01
0 0  1  2. 1. *
      1.92219601397E+00   1.00000000000E+00
0 0  1  0. 1. *
      5.33811961515E-01   1.00000000000E+00
0 0  1  0. 1. *
      1.98006161430E-01   1.00000000000E+00
0 2  6  6. 1.
      3.23295896140E+03   2.48856079740E-03
      7.65964426940E+02   2.03790074280E-02
      2.46339408100E+02   9.69771885840E-02
      9.23652830410E+01   2.81999609540E-01
      3.71995095510E+01   4.51162543580E-01
      1.51721665340E+01   2.49171314960E-01
0 2  4  6. 1.
      6.09313216980E+01  -2.21736035190E-02
      9.47926006460E+00   3.28384627780E-01
      4.25646863260E+00   5.81249971200E-01
      1.97293137620E+00   3.28635417830E-01
0 2  1  6. 1. *
      8.56378220759E-01   1.00000000000E+00
0 2  1  0. 1. *
      3.42924168394E-01   1.00000000000E+00
0 2  1  0. 1. *
      1.18735766352E-01   1.00000000000E+00
0 3  5 10. 1.
      1.86417609040E+02   8.61202846010E-03
      5.52741243450E+01   6.03944063040E-02
      2.02832191200E+01   2.11813318690E-01
      8.08845369760E+00   4.03662934130E-01
      3.22140338530E+00   4.24028606860E-01
0 3  1  0. 1. *
      1.12352780795E+00   1.00000000000E+00
0 3  1  0. 1. *
      6.85749126033E-01   1.00000000000E+00
0 3  1  0. 1. *
      3.59611504956E-01   1.00000000000E+00
0 4  1  0. 1. *
      6.26853929226E-01   1.00000000000E+00

 Kr - quadruple
```

```
  36 25
0 0 11   2    1
11713823.0080000              0.56915790360D-05
1755253.3979000               0.44214471278D-04
 399717.4192400               0.23227813842D-03
 113285.7926000               0.97973661050D-03
  36977.2052930               0.35537627541D-02
  13355.0365800               0.11468673282D-01
   5210.9012988               0.33241627469D-01
   2162.1137020               0.85620725674D-01
    943.29291023              0.18708766876
    429.20724331              0.31497583326
    202.40720840              0.33406191042
0 0 4   2    1
   3260.4985521               0.73091509287D-02
   1011.1069716               0.74040355445D-01
    392.44359273              0.35414962222
    173.21702132              0.80188286115
0 0 1   2    1
     96.619988467             1.0000000
0 0 1   2    1
     38.158284867             1.0000000
0 0 1   0    1
     18.959517570             1.0000000
0 0 1   0    1
      9.2505996199            1.0000000
0 0 1   0    1
      4.3486517621            1.0000000
0 0 1   0    1
      2.0380324209            1.0000000
0 0 1   0    1 *
   6.65036553434E-01   1.00000000000E+00
0 0 1   0    1 *
   3.29132367931E-01   1.00000000000E+00
0 0 1   0    1 *
   1.34171789744E-01   1.00000000000E+00
0 2 10  6    1
  28609.3357670               0.60526369543D-04
   6773.1236364               0.53786288403D-03
   2199.8011079               0.30935356550D-02
    841.50201590              0.13514318412D-01
    356.92110288              0.47090086910D-01
    162.71174351              0.12960370449
     78.004264994             0.26607435646
     38.682579997             0.36775851233
     19.589158685             0.27406903542
      9.7990863417            0.78773352304D-01
0 2 5   6    1
    261.37786869              -0.16397212361D-02
    100.09932146              -0.12034797573D-01
     44.012139363             -0.34891485263D-01
     10.854010739              0.25212650561
      5.4351930182             0.57400781830
0 2 1   6    1
      2.7062805542             1.0000000
0 2 1   0    1 *
```

```
   1.38393484069E+00   1.00000000000E+00
0 2 1   0   1 *
   5.95803286434E-01   1.00000000000E+00
0 2 1   0   1 *
   2.52417675094E-01   1.00000000000E+00
0 2 1   0   1 *
   9.61569614696E-02   1.00000000000E+00
0 3 7  10   1
    665.35057386            0.59588702935D-03
    200.17995366            0.54594260457D-02
     77.545085570           0.27980992479D-01
     33.677854345           0.94119165910D-01
     15.624928334           0.21825215619
      7.4427867423          0.33739971242
      3.5336073535          0.35141418853
0 3 1   0   1 *
   1.54178368928E+00   2.07567189310E-01
0 3 1   0   1 *
   6.29353174709E-01   1.00000000000E+00
0 3 1   0   1 *
   2.47493605437E-01   1.00000000000E+00
0 4 1   0   1 *
   9.55723793967E-01   1.00000000000E+00
0 4 1   0   1 *
   4.12146433686E-01   1.00000000000E+00
0 5 1   0   1 *
   7.39603984823E-01   1.00000000000E+00
```

References

(1) Lejaeghere, K.; Bihlmayer, G.; Björkman, T.; Blaha, P.; Blügel, S.; Blum, V.; Caliste, D.; Castelli, I. E.; Clark, S. J.; Dal Corso, A., et al. Reproducibility in density functional theory calculations of solids. *Science* **2016**, *351*, aad3000.

(2) Daga, L. E.; Civalleri, B.; Maschio, L. Gaussian Basis Sets for Crystalline Solids: All-Purpose Basis Set Libraries vs System-Specific Optimizations. *Journal of Chemical Theory and Computation* **2020**,

12.5 Ta-Based half Heusler-Basis Sets

Basis sets adopted for the calculations.

```
---Cobalt---
 27 13
0 0 8 2.0 1.0
  325817.01553      .22568462484E-03
  48839.636453      .17499397533E-02
  11114.937307      .91003134097E-02
  3146.1603642      .36996256837E-01
  1024.4378465      .12044269621
  368.02508816      .28598731649
  142.91229205      .40908312004
  56.482649209      .21500145739
0 0 4 2.0 1.0
  356.40298318     -.24767059678E-01
  110.31165215     -.11702139134
  17.659634834      .55215522200
  7.5059030479      .53246877060
0 0 2 2.0 1.0
  11.501807176     -.22942470077
  1.9081994606      .71180933514
0 0 1 1.0 1.0
 0.79396696891      1.0000000000
0 0 1 0.0 1.0
 0.33               1.0000000000
0 1 1 0.0 1.0
 0.14               1.0 1.0
0 2 6 6.0 1.0
  1731.1369144      .23905767685E-02
  409.91750438      .19382999967E-01
  131.45648578      .90905448509E-01
  48.987439714      .26146681577
  19.537078992      .42157264570
  7.9287281634      .24571813557
0 2 3 6.0 1.0
  31.076017584     -.29438069973E-01
  4.2835180697      .55615568168
  1.7022921563      .96772195064
0 2 1 0.0 1.0
 0.64202908602      1.0000000000
0 3 4 8.0 1.0
  68.140745239      .11983845360E-01
  19.685241019      .73688540475E-01
  6.9322128825      .23085496779
  2.6025125694      .39281059225
0 3 1 0.0 1.0
      9.23992055019E-01   4.02034122280E-01
0 3 1 0.0 1.0
      2.83380580890E-01   2.14156067430E-01
0 4 1 0.0 1.0
      1.90233147324E+00   1.00000000000E+00
---Tantalum---
 273 11
INPUT
13. 0 2 2 2 1 1
14.546408 1345.880647 0
7.273204 36.766806 0
9.935565 378.425301 0
4.967782 22.293091 0
6.347377 104.883956 0
3.173688 8.755848 0
2.017881 12.017961 0
3.040330 -11.728933 0
0 0 4 2.0 1.0
  24.473650944      0.20590322488
  18.721372549     -0.74670795514
  11.500000000       3.4071363897
  10.350000000      -2.8175487609
0 0 1 2.0 1.0
  3.8436180089       1.0000000000
0 0 1 0.0 1.0
  1.0202266016       1.0000000000
0 0 1 0.0 1.0
 0.46774781869       1.0000000000
0 0 1 0.0 1.0
 9.00596741452E-02   1.0000000000
```

```
0 2 4 6.0 1.0
  17.000000000      -0.32577305616E-01
  12.008186536       0.10336287365
  5.0278760583      -0.28526521696
  1.1937124184       0.51790141155
0 2 1 0.0 1.0
 0.57889707053       1.0000000000
0 2 1 0.0 1.0
  0.27225198801           1.0000000
0 3 3 3.0 1.0
  3.9738796278      -0.52799310714E-01
  1.4528884813       0.18558319471
  0.61042908544      0.42959071631
0 3 1 0.0 1.0
 1.94462635348E-01   1.00000000000E+00
0 4 1 0.0 1.0
 2.16673293845E-01   1.00000000000E+00
---Tin---
 250 13
INPUT
22   0   2   4   4   2   0
17.4204140000000  279.988682000000  0
7.63115500000000  62.3778100000000  0
16.1310240000000  66.1625230000000  0
15.6280770000000  132.174396000000  0
7.32560800000000  16.3394170000000  0
6.94251900000000  32.4889590000000  0
15.5149760000000  36.3874410000000  0
15.1881600000000  54.5078410000000  0
5.45602400000000  8.69682300000000  0
5.36310500000000  12.8402080000000  0
12.2823480000000 -12.5763330000000  0
12.2721500000000 -16.5959440000000  0
0 0 4 2.0 1.0
  1577.0715931       0.17042767713E-03
  235.26601078       0.81467057272E-03
  38.206330645      -0.39057904293E-02
  13.097031765       0.53245922343
0 0 2 2.0 1.0
  11.673161352        1.5435287275
  5.9463871497       0.76421510041
0 0 1 0.0 1.0
  1.89101828124E+00   1.00000000000E+00
0 0 1 0.0 1.0
  8.80485842761E-01   1.00000000000E+00
0 0 1 0.0 1.0
  1.58075912633E-01   1.00000000000E+00
0 2 3 6.0 1.0
  221.55767496       0.31125177983E-03
  21.084021433       0.31108097016E-01
  8.7600138521      -0.27571560918
0 2 3 2.0 1.0
  2.5902185134       0.45912328666
  1.3409064118       0.49682867217
 0.67241607517       0.18962377821
0 2 1 0.0 1.0
  2.21703584625E-01   1.00000000000E+00
0 3 6 10.0 1.0
  108.33210154       0.46561853277E-03
  23.703936630       0.54063163067E-01
  22.339843906      -0.58928768877E-01
  4.0874834028       0.19588500896
  1.9737354146       0.42301799185
  0.90158257692       0.39252716176
0 3 1 0.0 1.0
  3.65796267659E-01   1.00000000000E+00
0 3 1 0.0 1.0
  1.56348742647E-01   1.00000000000E+00
0 4 1 0.0 1.0
  2.72050278384E-01   1.00000000000E+00
0 4 1 0.0 1.0
  9.93533608529E-01   1.00000000000E+00
---Iridium---
277 11
INPUT
17. 0 2 2 2 1 1
13.652203 732.269200 0
6.826101 26.484721 0
10.279868 299.489474 0
5.139934 26.466234 0
7.349859 124.457595 0
3.674929 14.035995 0
3.034072 21.531031 0
4.808857 -21.607597 0
```

```
0 0 3 2.0 1.0
  30.000000000      0.30797903228
  27.000000000     -0.46726361781
  13.961973911      0.47161003146
0 0 1 2.0 1.0
  5.3956977802       1.0000000000
0 0 1 0.0 1.0
  1.2149128721       1.0000000000
0 0 1 0.0 1.0
 0.55885743756       1.0000000000
0 1 1 0.0 1.0
 0.14097974313       1.0 1.0
0 2 4 6.0 1.0
  15.902664143     -0.16290720099
  14.415830698      0.23483212987
  5.7597608991     -0.30305337176
  1.5008913108      0.55512982069
0 2 1 0.0 1.0
 0.72348035957       1.0000000000
0 3 4 7.0 1.0
  8.6321692504      0.75000099949E-01
  6.5898192302     -0.17326965173
  1.5808379663      0.55065196913
 0.71827834905      0.85273641436
0 3 1 0.0 1.0
  3.04433219672E-01   1.00000000000E+00
0 3 1 0.0 1.0
  1.57796987088E-01   1.00000000000E+00
0 4 1 0.0 1.0
  6.04504862393E-01   1.00000000000E+00
---Rhodium---
245 12
INPUT
17. 0 2 4 4 2 0
  12.194816 225.312054 0
   5.405137  32.441582 0
  11.280755  52.872826 0
  10.927248 105.745526 0
   5.090117   8.619344 0
   4.851832  16.973459 0
   9.136337  25.108501 0
   8.964808  37.695731 0
   3.643612   4.202584 0
   3.636007   6.292790 0
   8.616228  -9.673568 0
   8.629435 -12.899847 0
0 0 2 2 1.0
  17.0000000000     -0.166908031390
  13.9105816940      0.342350016520
0 0 1 2 1.0
  5.2481265288      1.000000000000
0 0 1 0 1.0
  1.2262575928      1.000000000000
0 0 1 0 1.0
  0.60              1.000000000000
0 1 1 0 1.0
  0.30              1.000000000000   1.
0 2 4 6 1.0
  11.7671036310      0.059494859388
  6.74851330830     -0.237358534770
  1.75026798340      0.490193343030
  0.84321166133      0.506239337510
0 2 1 0 1.0
  0.71404324000      1.000000000000
0 2 1 0 1.0
  0.34365143000      1.000000000000
0 3 4 7 1.0
  19.8578301360      0.006696077819
  10.0613781390     -0.021981738213
  2.26195464770      0.379187062360
  0.97098845035      0.672899765920
0 3 1 0 1.0
  0.38353699000      1.000000000000
0 3 1 0 1.0
  0.15000226000      1.000000000000
0 4 1 0 1.0
  1.09499000000      1.000000000000
```

12.6 Ullmannites-Basis Sets

Basis sets adopted for the calculations.

```
---Nichel---
 28 15
0 0  8  2. 1.
      3.51535729350E+05   2.25293868840E-04
      5.26958092830E+04   1.74686162230E-03
      1.19924682930E+04   9.08499921360E-03
      3.39457766890E+03   3.69407484470E-02
      1.10535945850E+03   1.20328199500E-01
      3.97146777690E+02   2.85967150570E-01
      1.54275429740E+02   4.09830201960E-01
      6.10187237800E+01   2.16206428510E-01
0 0  4  2. 1.
      3.84455597390E+02  -2.46512792680E-02
      1.19048791990E+02  -1.16585052770E-01
      1.91370122230E+01   5.48641266760E-01
      8.15267185620E+00   5.26400511220E-01
0 0  2  2. 1.
      1.25794086420E+01  -2.27978842930E-01
      2.08708660810E+00   7.07037382150E-01
0 0  1  2. 1.
      4.13070286139E+00   1.00000000000E+00
0 0  1  0. 1.
      8.57355806521E-01   1.00000000000E+00
0 0  1  0. 1.
      1.92795025905E-01   1.00000000000E+00
0 2  6  6. 1.
      1.88309074860E+03   2.37482584430E-03
      4.45951553200E+02   1.92894571720E-02
      1.43084308150E+02   9.07182115070E-02
      5.33729207220E+01   2.61814141170E-01
      2.13219193570E+01   4.23091498320E-01
      8.66435619940E+00   2.46416860150E-01
0 2  3  6. 1.
      3.41442552110E+01  -2.96771291630E-02
      4.71224559210E+00   5.56168240960E-01
      1.87092318450E+00   9.63577664600E-01
0 2  1  0. 1.
      6.79923475521E-01   1.00000000000E+00
0 2  1  0. 1.
      1.56834370548E-01   1.00000000000E+00
0 3  4  8. 1.
      7.45916034650E+01   1.20774546720E-02
      2.15906327520E+01   7.46372621540E-02
      7.62461425800E+00   2.32367755020E-01
      2.86322067620E+00   3.90426516800E-01
0 3  1  0. 1.
      1.00790128764E+00   1.00000000000E+00
0 3  1  0. 1.
      6.39433655247E-01   1.00000000000E+00
0 3  1  0. 1.
      3.00360431319E-01   1.00000000000E+00
0 4  1  0. 1.
      2.16004241173E+00   1.00000000000E+00
---Antimony---
251 16
INPUT
23. 0 2 4 4 2 0
 16.330865   281.071581   0
 8.556542    61.716604    0
 14.470337   67.457380    0
 13.816194   134.933503   0
 8.424924    14.716344    0
 8.092728    29.518512    0
 14.886331   35.447815    0
 15.146319   53.143466    0
 5.908267    9.179223     0
 5.594322    13.240253    0
 14.444978   -15.366801   0
 14.449295   -20.296138   0
0 0  4  2. 1.
      1.61241999330E+03   2.85403807830E-04
      2.38844520970E+02   1.33937787460E-03
      2.39981188090E+01  -4.93881545740E-02
      1.51931242130E+01   4.33922272540E-01
```

```
0 0  2  2. 1.
      1.17364097330E+01   9.21255199650E-01
      6.52597747940E+00   7.92352802260E-01
0 0  1  0. 1.
      2.06015363274E+00   1.00000000000E+00
0 0  1  0. 1.
      9.87094551814E-01   1.00000000000E+00
0 0  1  0. 1.
      3.06059047204E-01   1.00000000000E+00
0 0  1  0. 1.
      1.38071528035E-01   1.00000000000E+00
0 2  3  6. 1.
      2.15683933540E+02   2.60518232210E-04
      1.63744790880E+01   7.37280001950E-02
      9.72162833450E+00  -2.72300281280E-01
0 2  3  3. 1.
      2.79826431540E+00   4.64726923740E-01
      1.47110450330E+00   5.03642420750E-01
      7.51653853010E-01   1.87066662940E-01
0 2  1  0. 1.
      4.95738271502E-01   1.00000000000E+00
0 2  1  0. 1.
      2.59379082132E-01   1.00000000000E+00
0 2  1  0. 1.
      1.26075565322E-01   1.00000000000E+00
0 3  6 10. 1.
      1.15903122530E+02   5.31409150510E-04
      3.04742337200E+01   5.94111391660E-03
      1.82284182390E+01  -1.05637069470E-02
      4.32914566460E+00   2.03481773410E-01
      2.12948184960E+00   4.27483789280E-01
      9.96826366920E-01   3.85395608090E-01
0 3  1  0. 1.
      4.21224760073E-01   1.00000000000E+00
0 3  1  0. 1.
      1.54857004391E-01   1.00000000000E+00
0 4  1  0. 1.
      1.12025841254E+00   1.00000000000E+00
0 4  1  0. 1.
      2.74140727352E-01   1.00000000000E+00
---Sulphur---
 16 13
0 0  7  2. 1.
   6.07009281040E+04   5.46959442250E-04
   9.10261068540E+03   4.22972245570E-03
   2.07141660090E+03   2.17478241590E-02
   5.86024768210E+02   8.51000535890E-02
   1.90553950210E+02   2.47991284590E-01
   6.76303842600E+01   4.67036404060E-01
   2.51273069050E+01   3.64345875500E-01
0 0  3  2. 1.
   1.12574630100E+02   2.16700402400E-02
   3.47955542170E+01   9.36023017600E-02
   6.51155562150E+00  -2.60680014220E-01
0 0  2  2. 1.
   3.23990322610E+00   1.28420894350E+00
   1.54771608810E+00   6.60364165840E-01
0 0  1  0. 1.
   4.79267087636E-01   1.00000000000E+00
0 0  1  0. 1.
   2.10561167562E-01   1.00000000000E+00
0 2  5  6. 1.
   5.64367160270E+02   2.47967963170E-03
   1.33426243790E+02   1.96779302500E-02
   4.24682711890E+01   8.99800082580E-02
   1.56165275800E+01   2.57058805750E-01
   6.10939884690E+00   4.35151672920E-01
0 2  1  4. 1.
   2.43785034818E+00   1.00000000000E+00
0 2  1  0. 1.
   1.09182124384E+00   1.00000000000E+00
0 2  1  0. 1.
   4.31410869933E-01   1.00000000000E+00
0 2  1  0. 1.
   1.57376926419E-01   1.00000000000E+00
0 3  2  0. 1.
   3.75600000000E+00   2.00000000000E-01
   8.12000000000E-01   1.00000000000E+00
0 3  1  0. 1.
   2.44218244587E-01   1.00000000000E+00
0 4  1  0. 1.
   5.38814682974E-01   1.00000000000E+00
```

```
---Selenium---
 34 16
0 0  8  2. 1.
      5.31071666960E+05   2.41089731680E-04
      7.96030441170E+04   1.86964314410E-03
      1.81158442400E+04   9.72716165360E-03
      5.12789231940E+03   3.96047930310E-02
      1.66991308390E+03   1.29488551360E-01
      6.00575345270E+02   3.09594372890E-01
      2.33700212470E+02   4.51157692160E-01
      9.26724439320E+01   2.45791890330E-01
0 0  4  2. 1.
      5.71575136750E+02  -2.68957078810E-02
      1.77636863750E+02  -1.26709893530E-01
      2.95177670520E+01   5.76990017190E-01
      1.28243997950E+01   5.63690754080E-01
0 0  2  2. 1.
      1.98482358410E+01  -2.51324155340E-01
      3.47440184860E+00   7.29054169800E-01
0 0  1  2. 1.
      1.58974829107E+00   1.00000000000E+00
0 0  1  0. 1.
      4.61736708989E-01   1.00000000000E+00
0 0  1  0. 1.
      1.81399717148E-01   1.00000000000E+00
0 2  6  6. 1.
      2.81535005660E+03   2.55690268540E-03
      6.66925582980E+02   2.08740269010E-02
      2.14342131880E+02   9.87720962500E-02
      8.02466879420E+01   2.84718212210E-01
      3.22510812880E+01   4.50035849340E-01
      1.31064325620E+01   2.44160910550E-01
0 2  4  6. 1.
      5.33661085160E+01  -2.15584562730E-02
      8.18277771950E+00   3.26623106380E-01
      3.62399456720E+00   5.77404993190E-01
      1.63415914010E+00   3.43013208260E-01
0 2  1  4. 1.
      7.20783886526E-01   1.00000000000E+00
0 2  1  0. 1.
      2.99622949889E-01   1.00000000000E+00
0 2  1  0. 1.
      1.03443166373E-01   1.00000000000E+00
0 3  5 10. 1.
      1.51829102790E+02   9.39702769880E-03
      4.48399925230E+01   6.40865039910E-02
      1.63289995100E+01   2.18342380040E-01
      6.43050576120E+00   4.03147896490E-01
      2.50480251690E+00   4.19664914900E-01
0 3  1  0. 1.
      7.96157680621E-01   1.00000000000E+00
0 3  1  0. 1.
      5.98438540754E-01   1.00000000000E+00
0 3  1  0. 1.
      3.14576737908E-01   1.00000000000E+00
0 4  1  0. 1.
      4.02554512000E-01   1.00000000000E+00
---Palladium---
246 14
INPUT
18. 0 2 2 2 2 0
  11.800000   235.245962 0
  5.880000   34.682650 0
  10.820000   170.430396 0
  5.460000   25.301872 0
  9.870000   70.206324 0
  4.500000   14.777436 0
  13.070000 -31.401554 0
  6.530000   -5.298965 0
0 0  2  2. 1.
      1.80000000000E+01  -1.66053885980E-01
      1.46621343080E+01   3.48999550550E-01
0 0  1  2. 1.
      5.51270085981E+00   1.00000000000E+00
0 0  1  0. 1.
      2.04501763798E+00   1.00000000000E+00
0 0  1  0. 1.
      1.17769543373E+00   1.00000000000E+00
0 0  1  0. 1.
      3.48879966389E-01   1.00000000000E+00
0 0  1  0. 1.
      1.69427729703E-01   1.00000000000E+00
```

```
0 2  4  6. 1.
      1.25528993000E+01   6.17289982060E-02
      7.24444963800E+00  -2.41786267530E-01
      1.89059410780E+00   4.94532009150E-01
      9.07371687600E-01   5.04543626260E-01
0 2  1  0. 1.
      8.32687071605E-01   1.00000000000E+00
0 2  1  0. 1.
      5.45343357684E-01   1.00000000000E+00
0 2  1  0. 1.
      1.33096657339E-01   1.00000000000E+00
0 3  4  8. 1.
      2.23574575750E+01   3.95594795460E-03
      1.06825263820E+01  -1.40390116010E-02
      2.48582325500E+00   2.42194767760E-01
      1.07353339030E+00   4.25802832810E-01
0 3  1  0. 1.
      4.40967675265E-01   1.00000000000E+00
0 3  1  0. 1.
      1.53779835739E-01   1.00000000000E+00
0 4  1  0. 1.
      1.21768039162E+00   1.00000000000E+00
```